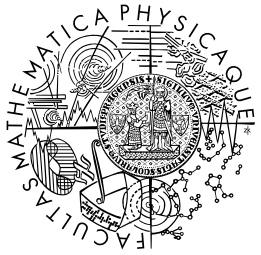

FACULTY
OF MATHEMATICS
AND PHYSICS
Charles University

DOCTORAL THESIS

RNDr. Ing. Libor Kukačka

Urban Ventilation Dependence on Geometric Configuration

Department of Atmospheric Physics

Supervisor of the doctoral thesis:	prof. RNDr. Zbyněk Jaňour, DrSc.
Study programme:	Physics
Study branch:	Meteorology and Climatology

Prague 2018

I declare that I carried out this doctoral thesis independently, and only with the cited sources, literature and other professional sources.

I understand that my work relates to the rights and obligations under the Act No. 121/2000 Sb., the Copyright Act, as amended, in particular the fact that the Charles University has the right to conclude a license agreement on the use of this work as a school work pursuant to Section 60 subsection 1 of the Copyright Act.

In Vrchlabí 14th June 2018 RNDr. Ing. Libor Kukačka

Title: Urban Ventilation Dependence on Geometric Configuration

Author: RNDr. Ing. Libor Kukačka

Department: Department of Atmospheric Physics

Supervisor: prof. RNDr. Zbyněk Jaňour, DrSc., Academy of Sciences of the Czech Republic, Institute of Thermomechanics, v. v. i.

Abstract: The main goal of the thesis is to investigate the impact of urban geometry on the urban ventilation using wind-tunnel modelling. To measure the pollutant transport, both advective and turbulent, within complex urban geometries with a high temporal resolution a special measurement method was developed. At first, the pollution of a simplified urban area was simulated by a ground-level point source and the ventilation of the intersection with respect to four wind directions was studied. Later, the pollution of other simplified and complex urban areas was simulated by a ground-level line source and the ventilation of three different street canyons with respect to wind direction perpendicular and oblique to their along-canyon axis was investigated. The clear impact of urban complexity and wind direction on street canyon ventilation is demonstrated at lateral and top openings of all investigated canyons and the intersection. Whilst the dominance of the pollutant advection is demonstrated at the eaves of pitched roofs, at the roof ridges the turbulent transport clearly dominates irrespective of the urban complexity and wind direction. For turbulent pollution fluxes, coherent structures were identified, and new nomenclature is introduced for assessment of the ventilation. A high correlation with analogical structures known in turbulent momentum flux is demonstrated for all investigated openings. The thesis improves the current knowledge about the characteristics of the flow and dispersion within real urban areas.

Keywords: Air pollution, Atmospheric boundary layer, Wind tunnel modelling, Urban area ventilation, Pollution fluxes, Street canyon, Street intersection

Dedication: At first I would like to thank to my supervisor prof. RNDr. Zbyněk Jaňour, DrSc. for his patient guidance of my work on this thesis. Than I am very grateful to the team of the Laboratory of Environmental Aerodynamics, Institute of Thermomechanis, Czech Academy of Sciences - especially to Ing. Štěpán Nosek, Ph.D. for intensive cooperation and final corrections, than to RNDr. Klára Jurčáková, Ph.D. and Mgr. Radka Kellnerová, Ph.D. Last but not least I am thankful to my wife Mgr. et Bc. Michaela Kukačková and to my parents for their assiduous support and patience.

The study was supported by the Charles University grant GAUK No. 136609 (115-10/259266) and partly by the Ministry of Education, Sports and Youth of the Czech Republic (project AVOZ-20760514 and COST1006 LD 12007); the Czech Science Foundation GAČR (project P101/12/1554 and project GAP15-18964S); the Czech Academy of Sciences (project M100760901); and the Institutional support RVO: 61388998.

Contents

Part I

SUMMARY

Introduction

The air quality within urban areas is the important aspect of the environment for the major part of the world population. After reducing of heavy industry at the end of the 20th century together with decreasing of general emission limits, vehicle emissions became the main pollutant source in large cities (Fenger, 1999; Colvile et al., 2001).

The dispersion of vehicle emissions in street canyons determines a spatial distribution of pollutants and their adverse effects on human health. Short time average concentrations measured especially in lower parts of the street canyons (at the breathing zone of pedestrians) often exceed threshold values. For this reason an improvement of air quality in urban areas is necessary to avoid risk for human health, see e.g. Hoek et al. (2000); Nyberg et al. (2000).

In general, a ventilation of an urban area can be defined as a process of pollutant removal within the urban canopy. Thus, the urban ventilation is directly driven by the horizontal and vertical transport of pollutants from the source (vehicles) to the flow aloft. At the same time, the pollutant transport is driven by two main processes of the flow: the advection and turbulent diffusion.

Because of the geometric complexity of real urban areas which are formed by building blocks of different heights and widths, turbulent flow within these areas is very complex and highly three-dimensional. Current research on urban ventilation has two main approaches: i) to study the urban ventilation with respect to the main units as street canyons and intersections; or ii) to study the urban ventilation as a whole. For the latter approach, ventilation indices as 'city breathability' (e.g. Buccolieri et al. (2015); Ramponi et al. (2015)) were introduced and widely used. This approach, however, neglects inherently those flow structures which govern the pollutant dispersion in urban hotspots (Lo and Ngan, 2015). The former approach has more been focused on the physics of these flow structures and how they are related to the main parameters governing the in-canyon flow such as the street canyon geometry or wind direction. Within this second approach, 2D or 3D but very simplified street canyons or intersections have been studied (e.g. Brixey et al. (2009); Schatzmann and Leitl (2009); Soulhac et al. (2009); Coceal et al. (2014)). Indeed, there are studies on pollutant dispersion within the real urban scenarios (e.g. Xie and Castro (2009); Balogun et al. (2010)) but lack the universality.

Physical modelling of such flows and pollutant dispersion in wind-tunnels promises an ideal and efficient method to solve above-mentioned issues. In a wind-tunnel, neutrally stratified turbulent flow over a scaled model of given complexity with preservation of desired conditions (approach wind speed and direction) might be modelled. Thanks to this advantage we can obtain representative and repeatable data which might be compared with other wind-tunnel or field measurements or with numerical computations, see e.g. Janour (2001). In comparison with field measurements (e.g., Louka et al. (2000); Nelson et al. (2007);

Zajic et al. (2015)), the wind-tunnel modelling is less expensive and able to control input variables (Schatzmann and Leitl, 2011). On the other hand, we are limited by the wind-tunnel dimensions, which determine the scale of models. Due to the similarity constrains, results obtained from a wind-tunnel experiment are mostly valid for windy situations at neutrally stratified conditions and rarely valid for buoyant or stratified flows as simulations of these flows require more sophisticated wind tunnels and experimental apparatus. Nevertheless, a totally calm weather conditions are rare and the thermal stratification affects turbulent flow within urban area during extraordinary and less common events, e.g. (Uehara et al., 2000).

Numerous wind-tunnel studies (see e.g. (Perret and Savory, 2013; Addepalli and Pardyjak, 2015; Carpentieri and Robins, 2015)) have been performed during the last three decades in order to investigate dispersion processes of turbulent flow in the urban canopy. While several wind-tunnel studies, focused on pollutant dispersion within 3D urban-like arrays formed by blocks of uniform (Davidson et al., 1996; Brown et al., 2001; Garbero et al., 2010; Castro et al., 2017) or variable (Hoydysh et al., 1974; Klein et al., 2007; Heist et al., 2009) height, gave relatively deep knowledge about the pollutant dispersion within street networks, there is still lack of systematic studies on pollutant transport within more complex 3D street canyons, e.g. within canyons having different roof heights along their walls. Furthermore, due to the complexity of their measurements only limited wind-tunnel studies investigated the urban ventilation using both mean and turbulent pollution fluxes (Carpentieri et al., 2012). Very recently, Kubilay et al. (2017) demonstrated the very importance of pollution fluxes for the investigation of street canyon ventilation as the air-exchange velocity significantly underestimates the total pollutant exchange.

To our knowledge, there are a few studies (Carpentieri et al., 2012, 2018) which addressed the ventilation of complex 3D urban intersections in the implicit study of street canyons, and no other studies which would systematically investigate the mechanisms of the pollutant transport and diffusion within a 3D urban structure (within the street canyons and intersections of complex 3D geometry). The main goal of the thesis is, therefore, the investigation of the impact of urban geometry on the urban ventilation using both the mean and turbulent pollution fluxes and wind-tunnel techniques. For this a special measurement set-up was developed in order to measure both advective and turbulent part of the pollution flux. At first, basic characteristics of the pollution flux were investigated on a simple model of an urban area together with the experimental set-up and data processing. After that and in order to continue today's knowledge of the topic, an idealised but more complex urban model with a line source simulating traffic emissions was designed. The model was built with several possible geometry configurations concerning roof height non-uniformities and two different approach wind directions. For comparative purposes, additional wind-tunnel experiments were performed on a simple urban model to observe the impact of the urban geometry and wind direction on the urban (street canyon) ventilation.

A. Structure of the thesis

The thesis is compiled from seven papers focused on the influence of the urban geometry on the ventilation processes of street canyons and intersections (see Part II). Three papers have been published in peer-reviewed international journals (The Scientific World Journal, Boundary-Layer Meteorology and Environmental Pollution), two papers were published as chapters of reviewed proceedings of the 31st and 32nd NATO/SPS International Technical Meeting on Air Pollution Modeling and its Application and finally two papers were published in the special issue of The European Physical Journal from contributions of the conferences Experimental Fluid Mechanics 2012 and 2013.

A general approach to the physical modelling of the urban ventilation is discussed in the first paper (Chap. 1). The main focus of the paper is to present the unique experimental set-up for simultaneous measurement of two flow velocity components and tracer gas concentration with a high temporal resolution within an urban canopy. Subsequently, on the basis of the thoroughgoing experimental data analysis, physical quantities characterizing the ventilation – the advective and turbulent scalar fluxes - were selected. The urban geometry is represented by a very simplified model of urban area and the pollution was simulated by a ground-level point source. A basic statistical processing of selected quantities is demonstrated for the ventilation of the urban intersection and five wind directions.

The following two papers (Chap. 2 and Chap. 3) are directly linked to the results of the previous paper. They deal with deeper analysis of the ventilation processes with aim to quantify the role of the turbulent and advective pollution transport within the intersection and to find dominant 'events' of the turbulent transport. Here, the events represent the parts of the vertical momentum flux obtained from the quadrant analysis. The quantification of these events and hence they importance for the intersection ventilation were published in the fourth paper (Chap. 4), whereby we prepared the experimental and physical groundwork for the main goal of the thesis.

In the fifth paper (Chap. 5), a new simplified urban-array model and ground-level line source is presented. The results obtained from the wind tunnel are compared with those obtained from large-eddy simulations (LES) in order to find the representative experimental set-up for the main wind-tunnel experiments.

Finally, key results of this thesis are published in the sixth and seventh paper (Chap. 6 and 7). The impact of the geometric configuration and wind direction on the urban ventilation is studied in detail for two urban models: i) the simple urban-array model (the same used as in previous paper, see Chap. 5) formed by evenly spaced courtyard-type buildings with constant length and width and pitched roofs with constant height; ii) the complex urban-array model having the same layout as the simple model but arbitrarily distributed roof heights along each building wall.

All included papers were prepared in close cooperation with the team of the Laboratory of Environmental Aerodynamics of the Institute of Thermomechanis AS CR under a supervision prof. Zbyněk Jaňour. The author is responsible for the all presented experimental data except the part of additional measurements at the lateral ends of the investigated street canyons, presented in the last paper and performed by Dr. Štěpán Nosek. For the comparison between the wind-tunnel and the numerical data (fifth paper) the later were provided by Dr . Vladimír Fuka. The basic statistical processing of raw data was prepared by the author, whilst the interpretation of the results and additional analysis were prepared together with Dr. Štěpán Nosek. Although all presented texts are based on numerous discussions and close cooperation within the experimental team, the first author of each paper is primarily responsible for the final text.

The used experimental methods including wind tunnel, developed experimental set-up and urban-area models are simply described in the following Chap. B. Obtained data set and its post-processing is introduced in Sect. B.5, key results are synthesized in Chap. C and finally summarised in Conclusions.

B. Methods

B.1 Wind tunnel

All the experiments introduced in the thesis were conducted in the open low-speed wind tunnel of Institute of Institute of Thermomechanics, Czech Academy of Sciences in Nový Knín. Dimensions and the scheme of the tunnel are shown in the Fig. 1.1. The free stream velocity generated within the tunnel was approx. 3 $\mathrm{m.s^{-1}}$ during the measurement of the intersection ventilation, and 6 $\mathrm{m.s^{-1}}$ during the measurement of the street canyon ventilation. Both freestream velocities provided sufficiently high Reynolds number for ($Re_B \geq 20,000$, with respect to the reference height H) to fulfil the Reynolds number independence ($Re_{crit} = 11,000$) recommended by Snyder (1979). Meeting this criterion we obtained a representative data set independent of the approaching stream velocity.

B.2 Measurement techniques

The flow characteristics were measured by two-dimensional optical fibre Laser Doppler Anemometry (LDA), based on DANTEC BSA F-60 burst processor. Tracing particles (glycerine droplets with approximately 1 μm diameter) were produced by a commercial haze generator placed at the beginning of the tunnel development section, about 1 m upstream of the turbulent generators. Data rate about 100-300 Hz was reached nearby the street- canyon bottom and about 1 KHz at the roof top.

The measurements of the concentration of pollutant were realised by Flame Ionisation Detectors (FID). The pollutant was simulated by the ground-level point (the case of the intersection) or by the ground-level line (the case of the street canyons) source. For both sources a passive gas (athane) was released at a constant flow rate (resulting in discharged velocity about 0.01 $\mathrm{m.s^{-1}}$, non-disturbing the flow within the intersection or street canyons). At the beginning of the work (the case of the point source and intersection), the Slow-response Flame Ionisation Detector (SFID, type ROSEMONT NGA 2000) was used. Later and during the key experiments (the line source and street canyons), Fast-response Flame Ionisation Detector (FFID, type Cambustion Ltd. HFR400 Atmospheric Fast FID) was utilised. The FFID was set to acquire data at rate of 1 KHz but the physical response is about 0.5 kHz.

One of the goals of this thesis was to develop and adjust simultaneous velocity and concentration measurement in the Laboratory of Environmental Aerodynamics to obtain synchronised data in a high temporal resolution (approx. 0.5 ms). These data allow detailed analysis of highly turbulent urban canopy flow and dispersion processes.

For the simultaneous measurement, LDA and FFID probes were mounted on 3D traverse system in a way that the measuring volume of the LDA was close

to the intake to the FFID sampling tube. The sampling tube intake was placed 1.5 mm above, 1 mm behind and 1 mm beside the centre of the LDA measuring volume. Several measurement tests with different positions of both probes demonstrated a negligible influence of the tube on the velocity measurement. The configuration of probes is captured in Fig. 1.3. A special sequence of instruments' calibration was designed to validate and verify measured data, see Sect. 1.2.3.

This experimental method for the investigation of pollutant transport was firstly published by Fackrell and Robins (1982), using thermo-anemometry instead of the optical method for velocity measurements. This method was used later, e.g. Bezpalcova (2006) in a dispersion wind-tunnel study. Similar experimental set up of LDA a FFID has been used by Carpentieri et al. (2012) and Carpentieri et al. (2018).

B.3 Boundary layer model

Fully turbulent boundary layer was developed by vertical spires and roughness elements arranged on the floor of the tunnel developing section (Fig. 1.2). The characteristics of the boundary layer developed above urban area models were measured with the LDA system and were in accordance with those parameters recommended for modelling of urban boundary layers (VDI, 2000). That means that for every studied case the boundary-layer measurement was performed for several vertical profiles of longitudinal and vertical velocity upstream of the urban models. Measured data were fitted by the logarithmic and the power law. Mean roughness length z_0, displacement d_0 and friction velocity u_* were obtained from the logarithmic fit. Power exponent α was obtained from the power fit. Further, vertical profiles of turbulence intensities I_u, I_w and mean momentum flux $\langle u'w' \rangle$ were analysed together with spectra of turbulence. For detailed description see e.g. Sects. 1.2.4 and 6.2.3.

B.4 Models of the urban area

Two different urban models were examined in this thesis. At the beginning, with respect to measurement techniques development, we used the simple model of idealised symmetric urban area with apartment houses to investigate the intersection pollution from the ground-level point source (Chaps. 1, 2, 3, 4). For the main experimental campaign the more complex urban model was constructed in order to study the street canyon pollution from traffic (Chaps. 5, 6, 7). Both models were placed on a rotating plate positioned at the centre of the wind-tunnel test section to change the approaching wind direction.

B.4.1 Simple model

This first model is composed from a regular array of courtyard buildings with squared layout and pitched roofs. Thus, this array of buildings forms the perpendicular arrangement of the relatively short street canyons and wide X-shaped intersections (see Fig. 1.2). The model was scaled down to 1:200. The courtyard buildings were made of blocks having 100 mm in height and 50 mm in width. The height of the pitched roof from the eaves to the ridges is 20 mm. A characteristic building height was set to $H = 120$ mm (24 m in full scale) including the pitched roof. The width of the street canyons is $L = 100$ mm. The aspect ratio of the street canyons (the ratio of the building height H to the street width L) is $H/L = 1.2$, see Sect. 1.2.2. The simple point source of the tracer gas simulating a 'pollution hotspot' (the place with higher emission from traffic near by the intersection) was placed at the bottom of the street canyon upstream of studied intersection, see Fig. 1.2.

B.4.2 Complex model

Typical pattern of street canyons in European city centres was used as an initial design of the second and more complex urban model in a scale of 1:400. The model was manufactured for the main experiment. The model represents a part of a regular urban-like array formed by courtyard buildings. The buildings have rectangular layout ($L = 300$ mm in length and $WB = 150$ mm in width) but each of the building has arbitrarily distributed height (0.8H, H or 1.2H, where $H = 62.5$mm is the mean height of the urban model) of pitched roofs along its each wall (see, Fig. 6.1b). For comparison, the second reference urban-array model was designed. This model has the same layout as the complex model but the constant roof height (H) along each building wall (see, Fig. 6.1a). Thus, both models form the street canyons of the same aspect ratio and the same frontal and plane solidity. For more description see Sect. 6.2.1.

For experimental simulation of the urban air pollution from dense traffic, ground-level line sources have been widely used in wind tunnels. A new homogenous ground-level line source of tracer gas was designed and manufactured for the purposes of the thesis according to Meroney et al. (1996). The total length of the line source is $L = 1$ m (400 m at full scale) and the line source ran continuously through the investigated street canyons (Fig. 6.1c). The line source is formed by a line of 504 equally spaced tubes made of stainless steel. The tubes have an inner diameter of 0.3 mm and length of 100 mm. The pressure drop across the tubes ($\Delta p_n = 64.5$ Pa) was sufficiently higher than the highest expected pressure fluctuations (up to 10 Pa) at the bottom of the wind tunnel, thus providing a stable volume flow rate (Meroney et al., 1996). The lateral homogeneity of the line source was verified in several measuring and visualization tests. The standard error of the mean concentration measured along the entire line source placed on the flat floor within the tunnel was lower than 5% (where the concentration measurement error was 4%). For further description see Sect. 6.2.2.

B.5 Data set

Because the ventilation of urban intersections and street canyons is driven by the pollutant removal through their openings, the experimental data were obtained from the measurements at these openings of the studied intersection and street canyons.

Using two-dimensional LDA the longitudinal and vertical (in the case of the vertical openings) or the longitudinal and lateral (in the case of the lateral openings) velocity components were measured. At the same time and at approximately the same position (about 1 mm apart from the LDA measurement volume) the tracer gas was measured by the SFID (the simple case of the intersection) and FFID (the case of the street canyons).

All the measured quantities were calculated to dimensionless values independent on the approach stream velocity and the source strength, see Eq. 1.2 for dimensionless velocity components and Eq. 1.3 or Eq. 5.3 for dimensionless concentration of tracer gas emitted from point or line source, respectively.

The dimensionless values of velocity and concentration were synchronised using author's post-processing routines in Matlab (see Sect. 1.3.4). The author used the same approach for the synchronisation as Contini et al. (2006). Once the data were synchronised, the momentum fluxes, advective pollution fluxes (Eq. 1.3) and turbulent pollution fluxes (Eq. 1.6) were computed, all for the vertical and lateral directions.

C. Summary of results

C.1 Analysis of ventilation processes

As was stated in Introduction, the ventilation of an urban area means a process of removing of polluted air by a fresh air within the urban canopy. This process can be effectively evaluated by the pollution fluxes.

In general, a well-known schema of pollutant transport within 3D street canyon was confirmed by the thesis.. This pollutant transport is driven by a prevailing structure of vertically rotating vortex at the centre of the canyon which drives an intensive upward pollutant transport at the upstream canyon's wall and pollutant re-entry and penetration of clean air at the downstream wall (see Figs. 6.6b and 6.10).

After evaluation of both the advective and the turbulent components of pollution flux, a dominance of the advective pollutant transport below the street canyon roof top was observed. Whilst a relatively small amount of turbulence (relative contribution of the turbulent pollution flux to the total pollution flux was about 20%) acts against this vertical advection below the roof top, at the roof top (more precisely, at the roof ridges) the vertical turbulent pollutant transport dominates, irrespective of the studied canyon and wind direction (see Fig. 6.9d).

In case of the lateral openings, the horizontal transport of pollutants occurs between street canyons and intersections and is enhanced by the oblique winds, and hence better ventilation is achieved for both the intersection and street canyons for these cases of wind directions. For the wind perpendicular to the along-canyon axis (and representing the worse ventilation scenario), the turbulent transport dominates at the lateral openings of the uniform canyon (i.e. having the constant height along each wall), whereas advective transport dominates at the lateral openings of the nonuniform canyons (i.e. having arbitrarily distributed roof heights along each wall). However, if the wind direction is oblique to the along-canyon axis, the advection dominates through the lateral openings due to the well-known helical vortex developed irrespectively within each studied canyon (compare Fig. 7.6 and Fig. 7.7).

Concerning the turbulent transport, a considerable effort was devoted to the investigation which structures of turbulence play a significant role for the street canyon ventilation. First of all, the quadrant analysis was applied to the time series of the measured momentum fluxes (see Sec. 1.3.5). Using this conditional analysis, four events for the transport of momentum were defined: outward interaction, sweep, inward interaction and ejection, see Fig. 1.11. These events are also known as 'coherent structures' and were observed in different canopy flows (Katul et al., 2006; Hertwig et al., 2011; Kellnerova et al., 2014) flow.

Secondly, we used the quadrant analysis between the velocity (vertical or lateral) and concentration fluctuation and introduced a new nomenclature for these events with respect to their physical meaning: venting of polluted air,

polluted air re-entrainment, clean air entrainment and venting of clean air, see Fig. 7.5. Dominance of two events, the 'venting of polluted air' and 'clean air entrainment', was identified already from the preliminary results (Fig. 3.2). The 'venting of polluted air' means a motion of air particle with polluted air from the canyon. Similarly, 'clean air entrainment' means the motion of air particle with less polluted (clean) air into the canyon. This dominance was naturally expected but the key question was whether these events significantly correlate with those events for the momentum transport. The results were summarised in Sect. 6.3.2 and confirm the significant correlation of the events at the roof top, irrespective of the studied model and wind direction (Fig. 6.14), especially at the roof top where the highest intensity of turbulence can be observed (Figs. 6.9d and 6.11).

C.2 Influence of wind direction

The influence of the wind direction on the urban ventilation was investigated since the first performed experiment. We observed significant sensitivity of the velocity and concentration fields within urban area to the approaching wind direction, although the experiments were carried out under required conditions in terms of repeatability and reproducibility.

In the case of the wind approaching the canyons perpendicularly, relatively symmetrical velocity and concentration fields (as was expected) were measured, although a little deviation of the wind direction (about approx. 5○) changed the flow and pollution transport significantly, see Figs. 1.7 and 1.8. However, at the roof level (roof ridges) the ventilation is mainly driven by the vertical turbulent transport in case of this wind direction.

If the wind direction is changed from the perpendicular to an oblique, both the total and the turbulent vertical pollution fluxes are less intensive due to the helical vortex enhancing the lateral transport. The pollutants were mainly transported by the advection along the canyon to the intersections. This mechanism of pollutant transport was observed for the wind directions having at least approx. 15○ from the perpendicular one (see again Fig. 1.7 and Fig. 1.8, for complex model see Figs. 7.2 and 7.2).

A very important result was obtained at the pedestrian level (1.6 m in full scale) along the studied street canyons. Despite the above-mentioned impact of the wind direction on the pollutant dispersion at the canyons' openings, relatively small changes in the pollutant dispersion were observed for the line-averaged concentrations along the canons' walls at the pedestrian level (Fig. 6.8). However, Fig. 6.8 demonstrates that the concentrations at the street canyon upstream walls are approx. 5 times higher than those at the downstream walls, irrespective of the wind direction. This implies that pedestrians at the upstream side of a street canyon are generally more exposed to a serious threat to health than those pedestrians at the downstream side of the canyon. Indeed, for the wind parallel with the along-canyon axis the similar concentrations at both sides of the canyon might be expected.

C.3 Influence of urban geometry

Concerning the urban geometry, the thesis focused on the impact of roof height non-uniformity on the pollutant transport from and into the street canyons. The literature review revealed the knowledge gap about the mechanisms of these pollutant transports (ventilation processes). The main contributions extending the knowledge are presented in Chaps. 6.3 and 7.3.

It was found that the roof height non-uniformity have the insignificant impact on the line-averaged concentrations along the canyon's wall at the pedestrian level (Fig. 6.8). However, there is a strong spatial dependence of the concentration on the roof height non-uniformity as this non-uniformity intensifies the turbulent transport from the canyon to the flow aloft and hence influences locally the contractions at the pedestrian level. This should be kept in mind when one uses only a local or line-averaged concentration for the ventilation assessment.

Changes in the ventilation processes due to the street canyon geometry can be clearly seen from the total and turbulent pollution flux fields (Figs. 6.10 and 6.11). In detail, the intensive total vertical pollution fluxes from the canyon can be found for the fields presented for both investigated heights (z/H = 0.6 and 1 in Fig. 6.10). These total fluxes are enhanced by the highest canyon walls presented upstream which produce so called 'chimney' effect due to the lower walls surrounding those higher and pollutants are transported to the flow aloft. On the other hand, those higher walls caused intensive propagation of the unpolluted air but also the higher retention of the pollutant into the canyon if they are presented upstream. Indeed, in case of the walls lower than the mean canyon (and hence urban) height, the vertical total pollutant transport is rather less intensive as the pollutants were already transported above these roofs aloft and the horizontal (streamwise) total pollution flux together with the vertical turbulent pollution flux dominate at that mean height (see $z/H = 1$ in Fig. 6.11).

Furthermore, the impact of the urban geometry from an integral point of view was investigated as well. In this way, the modelled street canyons were viewed as the averaged step-up or step-down street canyons (averaging of the roof height along the upstream or downstream wall). The spatially averaged results presented in Fig. 6.9 demonstrate the similar behaviour of the ventilation within the whole canyons as was observed in the case of the pollution flux behind individual higher or lower buildings - there was observed more intensive vertical pollution transport in the step-down canyon than in the step-up and more intensive penetration of unpolluted air in the step-up canyon than in the step-down canyon. Although the detailed behaviour of ventilation was completely hidden by the used spatial averaging, from these results can be concluded that particular details of urban geometry significantly influence behaviour of pollution ventilation in whole canyons. Therefore, the street canyon ventilation can also be roughly estimated from these integral calculations.

Conclusions

The presented experimental thesis was compiled from published papers addressing the impact of the urban geometry on the ventilation processes within street canyons and intersections.

First of all, the urban ventilation was studied as the physical process of pollutant removal from urban areas. Due to highly turbulent flows presented in urban environments the mean and turbulent transport of pollutants were studied in detail. To measure the turbulent transport, a special experimental set-up was developed. This comprised simultaneous measurements of instantaneous two velocity components and concentration at a point of interest and subsequent routine for the synchronisation of these velocities with the concentration. Using the quadrant analysis, the ventilation processes were identified for the turbulent pollutant transport and their new nomenclature was introduced. A significant correlation between the ventilation process and coherent structures of turbulence was found.

Then a comprehensive wind-tunnel experiment was performed with simple and complex model configurations to evaluate the impact of urban geometry and wind direction on the urban ventilation. The wind direction together with the roof height non-uniformity was found to have synergic effect on the ventilation processes of the investigated street canyons, even though the highest pollutant concentrations were found at the pedestrian level and at the canyons' upstream walls, irrespective of the studied urban geometry and wind direction. Buildings higher than the averaged canyon height were found to be important for the ventilation. While these buildings cause the intensive vertical pollutant transport from the canyon to the flow aloft if they are located upstream, they cause more intensive penetration of the unpolluted air into the canyon if they located downstream.

In general, the impact of particular details of urban geometry, different roof heights along both street canyon walls, on the ventilation processes within the whole street canyons were proved by the thesis. Integral results obtained as the line-averaged values of pollution fluxes along street canyons implicate the general behaviour of the street-canyon ventilation can be roughly estimated already from the comparisons between the heights averaged along the each canyon wall. There was observed more intensive vertical pollution transport from the 'step-down' canyon than from the 'step-up' and more intensive clean air penetration into the 'step-up' canyon than into the 'step-down'. Without any considerations, the 'step-up' canyon was the best ventilated canyon. This can be a useful knowledge for practical usage in urban planning or emissions managements.

Bibliography

B. Addepalli and E. R. Pardyjak. A study of flow fields in step-down street canyons. *Environmental Fluid Mechanics*, 15(2):439–481, 2015. ISSN 15677419. doi: 10.1007/s10652-014-9366-z.

A. A. Balogun, A. S. Tomlin, C. R. Wood, J. F. Barlow, S. E. Belcher, R. J. Smalley, J. J. N. Lingard, S. J. Arnold, A. Dobre, A. G. Robins, D. Martin, and D. E. Shallcross. In-Street Wind Direction Variability in the Vicinity of a Busy Intersection in Central London. *Boundary-Layer Meteorology*, 136(3): 489–513, sep 2010. ISSN 0006-8314. doi: 10.1007/s10546-010-9515-y. URL `http://link.springer.com/10.1007/s10546-010-9515-y`.

K. Bezpalcova. *Physical Modelling of Flow and Diffusion in Urban Canopy*. PhD thesis, Charles University in Prague, 2006.

L. A. Brixey, D. K. Heist, J. Richmond-Bryant, G. E. Bowker, S. G. Perry, and R. W. Wiener. The effect of a tall tower on flow and dispersion through a model urban neighborhood : Part 2. Pollutant dispersion. *Journal of Environmental Monitoring*, 11(12):2171, dec 2009. ISSN 1464-0325. doi: 10.1039/b907137g. URL `http://xlink.rsc.org/?DOI=b907137g`.

M. Brown, R. Lawson, D. S. DeCroix, and R. Lee. Comparison of centerline velocity measurements obtained around 2D and 3D building arrays in wind tunnel. In *International Society of Environmental Hydraulics Conference*, number December 2001, Tempe, AZ, 2001.

R. Buccolieri, P. Salizzoni, L. Soulhac, V. Garbero, and S. Di Sabatino. The breathability of compact cities. *Urban Climate*, 13:73–93, sep 2015. ISSN 22120955. doi: 10.1016/j.uclim.2015.06.002. URL `http://linkinghub.elsevier.com/retrieve/pii/S2212095515000243`.

M. Carpentieri and A. G. Robins. Influence of urban morphology on air flow over building arrays. *Journal of Wind Engineering and Industrial Aerodynamics*, 145:61–74, 2015. ISSN 01676105. doi: 10.1016/j.jweia.2015.06.001.

M. Carpentieri, P. Hayden, and A. G. Robins. Wind tunnel measurements of pollutant turbulent fluxes in urban intersections. *Atmospheric Environment*, 46: 669–674, jan 2012. ISSN 13522310. doi: 10.1016/j.atmosenv.2011.09.083. URL `http://linkinghub.elsevier.com/retrieve/pii/S1352231011010909`.

M. Carpentieri, A. G. Robins, P. Hayden, and E. Santi. Mean and turbulent mass flux measurements in an idealised street network. *Environmental Pollution*, 234:356–367, mar 2018. ISSN 02697491. doi: 10.1016/

j.envpol.2017.11.069. URL http://linkinghub.elsevier.com/retrieve/pii/S0269749117332335.

I. P. Castro, Z.-T. Xie, V. Fuka, A. G. Robins, M. Carpentieri, P. Hayden, D. Hertwig, and O. Coceal. Measurements and Computations of Flow in an Urban Street System. *Boundary-Layer Meteorology*, 162(2):207–230, feb 2017. ISSN 0006-8314. doi: 10.1007/s10546-016-0200-7. URL http://link.springer.com/10.1007/s10546-016-0200-7.

O. Coceal, E. V. Goulart, S. Branford, T. Glyn Thomas, and S. E. Belcher. Flow structure and near-field dispersion in arrays of building-like obstacles. *Journal of Wind Engineering and Industrial Aerodynamics*, 125:52–68, feb 2014. ISSN 01676105. doi: 10.1016/j.jweia.2013.11.013. URL http://linkinghub.elsevier.com/retrieve/pii/S0167610513002729.

R. Colvile, E. Hutchinson, J. Mindell, and R. Warren. The Transport secotor as a source of air pollution. *Atmospheric Environment*, 35(2001):1537–1565, 2001.

D. Contini, P. Hayden, and A. Robins. Concentration field and turbulent fluxes during the mixing of two buoyant plumes. *Atmospheric Environment*, 40(40):7842–7857, dec 2006. ISSN 13522310. doi: 10.1016/j.atmosenv.2006.07.024. URL http://linkinghub.elsevier.com/retrieve/pii/S1352231006007850.

M. Davidson, W. Snyder, R. Lawson, and J. Hunt. Wind tunnel simulations of plume dispersion through groups of obstacles. *Atmospheric Environment*, 30(22):3715–3731, nov 1996. ISSN 13522310. doi: 10.1016/1352-2310(96)00103-3. URL http://linkinghub.elsevier.com/retrieve/pii/1352231096001033.

J. E. Fackrell and A. G. Robins. The effects of source size on concentration fluctuations in plumes. *Boundary-Layer Meteorology*, 22(3):335–350, mar 1982. ISSN 0006-8314. doi: 10.1007/BF00120014. URL http://link.springer.com/10.1007/BF00120014.

J. Fenger. Urban air quality. *Atmospheric Environment*, 33(29):4877–4900, 1999. ISSN 13522310. doi: 10.1016/S1352-2310(99)00290-3.

V. Garbero, P. Salizzoni, and L. Soulhac. Experimental Study of Pollutant Dispersion Within a Network of Streets. *Boundary-Layer Meteorology*, 136(3):457–487, sep 2010. ISSN 0006-8314. doi: 10.1007/s10546-010-9511-2. URL http://link.springer.com/10.1007/s10546-010-9511-2.

D. K. Heist, L. A. Brixey, J. Richmond-Bryant, G. E. Bowker, S. G. Perry, and R. W. Wiener. The effect of a tall tower on flow and dispersion through a model urban neighborhood : Part 1. Flow characteristics. *Journal of Environmental Monitoring*, 11(12):2163, dec 2009. ISSN 1464-0325. doi: 10.1039/b907135k. URL http://xlink.rsc.org/?DOI=b907135k.

D. Hertwig, B. Leitl, and M. Schatzmann. Organized turbulent structures-Link between experimental data and LES. *Journal of Wind Engineering and Industrial Aerodynamics*, 99(4):296–307, apr 2011. ISSN 01676105. doi: 10.1016/j.jweia.2011.01.002. URL http://linkinghub.elsevier.com/retrieve/pii/S0167610511000043.

G. Hoek, B. Brunekreef, A. Verhoeff, J. V anWijnen, and P. Fischer. Daily mortality and air pollution in the Netherlands. *Journal of the Air and Waste Management Association*, 50(8):1380–1389, aug 2000. ISSN 21622906. doi: 10.1080/10473289.2000.10464182. URL http://www.tandfonline.com/doi/abs/10.1080/10473289.2000.10464182.

W. G. Hoydysh, Y. Ogawa, and R. A. Griffiths. A scale model study of dispersion of pollution in street canyons. In *Annual Meeting of the Air Pollution Control Association, Denver, Colorado*, 1974.

Z. Janour. *Modelovani mezni vrstvy atmosfery*. Karolinum, Prague, 2001.

G. Katul, D. Poggi, D. Cava, and J. Finnigan. The relative importance of ejections and sweeps to momentum transfer in the atmospheric boundary layer. *Boundary-Layer Meteorology*, 120(3):367–375, sep 2006. ISSN 0006-8314. doi: 10.1007/s10546-006-9064-6. URL http://link.springer.com/10.1007/s10546-006-9064-6.

R. Kellnerova, L. Kukacka, S. Nosek, V. Uruba, K. Jurcakova, and Z. Janour. Wavelet analysis of the turbulent flow over the very rough surface. *EPJ Web of Conferences*, 67:02051, mar 2014. ISSN 2100-014X. doi: 10.1051/epjconf/20146702051. URL http://www.epj-conferences.org/articles/epjconf/abs/2014/04/epjconf_efm-13_02051/epjconf_efm-13_02051.html%5Cnhttp://www.epj-conferences.org/10.1051/epjconf/20146702051.

P. Klein, B. Leitl, and M. Schatzmann. Driving physical mechanisms of flow and dispersion in urban canopies. *International Journal of Climatology*, 27(14):1887–1907, 2007. ISSN 08998418. doi: 10.1002/joc.1581.

A. Kubilay, M.-A. Neophytou, S. Matsentides, M. Loizou, and J. Carmeliet. The Pollutant Removal Capacity of an Urban Street Canyon and its Link to the Breathability and Exchange Velocity. *Procedia Engineering*, 180(180):443–451, 2017. ISSN 18777058. doi: 10.1016/j.proeng.2017.04.203. URL http://linkinghub.elsevier.com/retrieve/pii/S1877705817317101.

K. Lo and K. Ngan. Characterising the pollutant ventilation characteristics of street canyons using the tracer age and age spectrum. *Atmospheric Environment*, 122:611–621, dec 2015. ISSN 13522310. doi: 10.1016/j.atmosenv.2015.10.023. URL http://linkinghub.elsevier.com/retrieve/pii/S135223101530443X.

P. Louka, S. E. Belcher, and R. G. Harrison. Coupling between air flow in streets and the well-developed boundary layer aloft. *Atmospheric Environment*, 34 (16):2613–2621, 2000. ISSN 13522310. doi: 10.1016/S1352-2310(99)00477-X.

R. N. Meroney, M. Pavageau, S. Rafailidis, and M. Schatzmann. Study of line source characteristics for 2-D physical modelling of pollutant dispersion in street canyons. *Journal of Wind Engineering and Industrial Aerodynamics*, 62(1):37–56, aug 1996. ISSN 01676105. doi: 10.1016/S0167-6105(96)00057-8. URL http://linkinghub.elsevier.com/retrieve/pii/S0167610596000578.

M. A. Nelson, E. R. Pardyjak, J. C. Klewicki, S. U. Pol, and M. J. Brown. Properties of the wind field within the Oklahoma City Park Avenue Street Canyon. Part I: Mean flow and turbulence statistics. *Journal of Applied Meteorology and Climatology*, 46(12):2038–2054, 2007. ISSN 15588424. doi: 10.1175/2006JAMC1427.1.

F. Nyberg, P. Gustavsson, L. Järup, T. Bellander, N. Berglind, R. Jakobsson, G. Pershagen, and L. Ja. Urban air pollution and lung cancer in Stockholm. *Epidemiology*, 11(5):487–95, 2000. ISSN 1044-3983.

L. Perret and E. Savory. Large-Scale Structures over a Single Street Canyon Immersed in an Urban-Type Boundary Layer. *Boundary-Layer Meteorology*, 148(1):111–131, 2013. ISSN 00068314. doi: 10.1007/s10546-013-9808-z.

R. Ramponi, B. Blocken, L. B. de Coo, and W. D. Janssen. CFD simulation of outdoor ventilation of generic urban configurations with different urban densities and equal and unequal street widths. *Building and Environment*, 92: 152–166, oct 2015. ISSN 03601323. doi: 10.1016/j.buildenv.2015.04.018. URL http://linkinghub.elsevier.com/retrieve/pii/S0360132315001845.

M. Schatzmann and B. Leitl. Evaluation of Numerical Flow and Dispersion Models for Applications in Industrial and Urban Areas. *Chemical Engineering and Technology*, 32(2):241–246, feb 2009. ISSN 09307516. doi: 10.1002/ceat.200800578. URL http://doi.wiley.com/10.1002/ceat.200800578.

M. Schatzmann and B. Leitl. Issues with validation of urban flow and dispersion CFD models. *Journal of Wind Engineering and Industrial Aerodynamics*, 99 (4):169–186, apr 2011. ISSN 01676105. doi: 10.1016/j.jweia.2011.01.005. URL http://linkinghub.elsevier.com/retrieve/pii/S0167610511000079.

W. Snyder. Guideline for fluid modeling of atmospheric diffusion, jun 1979. URL https://www.osti.gov/biblio/5521001.

L. Soulhac, V. Garbero, P. Salizzoni, P. Mejean, and R. J. Perkins. Flow and dispersion in street intersections. *Atmospheric Environment*, 43(18):2981–2996, jun 2009. ISSN 13522310. doi: 10.1016/j.atmosenv.2009.02.061. URL http://linkinghub.elsevier.com/retrieve/pii/S1352231009001186.

K. Uehara, S. Murakami, S. Oikawa, and S. Wakamatsu. Wind tunnel experiments on how thermal stratification affects flow in and above urban street canyons. *Atmospheric Environment*, 34(10):1553–1562, jan 2000. ISSN 13522310. doi: 10.1016/S1352-2310(99)00410-0. URL https://www-sciencedirect-com.ezproxy.is.cuni.cz/science/article/pii/S1352231099004100http://linkinghub.elsevier.com/retrieve/pii/S1352231099004100.

VDI. *Environmental meteorology – Physical modelling of flow and dispersion processes in the atmospheric boundary layer – Application of wind tunnels*. Verein Deutscher Ingenieure, Dusseldorf, Dusseldorf, 2000.

Z.-T. Xie and I. P. Castro. Large-eddy simulation for flow and dispersion in urban streets. *Atmospheric Environment*, 43(13):2174–2185, apr 2009. ISSN 13522310. doi: 10.1016/j.atmosenv.2009.01.016. URL http://linkinghub.elsevier.com/retrieve/pii/S135223100900034X.

D. Zajic, H. J. Fernando, M. J. Brown, and E. R. Pardyjak. On flows in simulated urban canopies. *Environmental Fluid Mechanics*, 15(2):275–303, 2015. ISSN 15677419. doi: 10.1007/s10652-013-9311-6.

Part II

PUBLISHED PAPERS

1. Wind tunnel measurement of turbulent and advective scalar fluxes, case study on an intersection ventilation

The Scientific World Journal, 2012, p. 1-13. Article ID 381357. ISSN 1537-744X. doi: 10.1100/2012/381357.

Libor Kukačka[1,2], Štěpán Nosek[2], Radka Kellnerová[1,2], Klára Jurčáková[2], Zbyněk Jaňour[2]

[1] Charles University in Prague, Faculty of Mathematics and Physics, Prague, Czech Republic
[2] Institute of Thermomechanics, Academy of Sciences of the Czech Republic, Prague, Czech Republic

Abstract
The objective of this study is to determine processes of a pollution ventilation in the X-shaped street intersection in an idealized symmetric urban area for the changing approach flow direction. A unique experimental set-up for simultaneous wind tunnel measurement of the flow velocity and the tracer gas concentration in a high temporal resolution is assembled. Advective horizontal and vertical scalar fluxes are computed from averaged measured velocity and concentration data within the street intersection. Vertical advective and turbulent scalar fluxes are computed from synchronized velocity and concentration signals measured in the plane above the intersection. All the results are obtained for five approach flow directions. The influence of the approach flow to the advective and turbulent fluxes is determined. The contribution of the advective and turbulent flux to the ventilation is discussed. Wind direction with the best dispersive conditions in the area is found. The quadrant analysis is applied to the synchronized signals of velocity and concentration fluctuation to determine events with the dominant contribution to the momentum flux and turbulent scalar flux.

Keywords
Air pollution, Atmospheric boundary layer, Wind tunnel modelling, Contaminant spreading, Scalar fluxes, Street canyon, Street Intersection, Urban area ventilation.

1.1 Introduction

Dispersion of air pollution within urban areas is an important aspect of the environment quality for a significant part of the population. Vehicle emissions represent the main source of pollutants in large cities (Fenger, 1999; Colvile et al., 2001).

The dispersion in street canyons determines a spatial distribution of pollutants and their dangerous impact. Short time average concentrations measured especially in lower parts of the street canyons often reach threshold values. Improvement of air quality in urban areas is necessary to avoid risk for human health (Hoek et al., 2000; Nyberg et al., 2000).

We can define ventilation of an urban area as a process of changing polluted and fresh air within street canyons, which improves the air quality. Ventilation is directly caused by horizontal and vertical transport of pollution out from the area.

Wind tunnel investigations provide an environment where flow and dispersion can be explored in relatively stationary conditions and allow facile changes of model geometry. Several wind tunnel studies focused on concentrations within canyon for a tracer emitted at street level and flow perpendicular to the street (Kastner-Klein and Plate, 1999; Pavageau and Schatzmann, 1999). The transport of pollution to the air above the roof level were estimated from measurements of concentrations in these works.

Wind tunnel and field studies for relatively symmetrical and regular street canyons arrangements express influence of geometry of streets and intersections in pollutant dispersion and hence ventilation in urban areas, see Brown et al. (2004).

Mixing and transport processes in a simple street and its ventilation were elaborated by Belcher (2005). In this work ventilation fluxes were determined for estimation of the mean scalar transport within the urban street network. Barlow and Belcher (2002) focused on studying the ventilation characteristics of a street canyon for the simple case of wind perpendicular to the street. Wind tunnel experiments published by Robins (2008) show that the mass exchange between street canyons may be significantly changed due to a small variations of the building geometry. These results were obtained from computing scalar fluxes determining pollution transport. Results from numerical simulation published by Scaperdas and Colvile (1999) show a very complex behaviour of the flow in an urban area. This work shows configuration of the street canyon and the wind direction when air exchange between alongwind and crosswind streets is reversed. Numerical and wind tunnel simulation of the flow and dispersion near regular and irregular street intersections were studied by Wang and McNamara (2007).

Presented papers demonstrate high sensitivity of flow and dispersion processes to the intersection geometry and wind direction that are naturally connected with ventilation of an urban area. Several publications has been focused on the air quality near street intersection in detail, e.g. Dabberdt et al. (1995). Significantly

higher pollution concentrations have been observed near intersections than along the streets with a continuous traffic, see Claggett et al. (1981). The reason of this observed phenomenon is that vehicles spend longer period of time near junctions, in driving modes that generate more pollutants (decelerating or accelerating), than in relatively steady movement in streets. The review of the traffic pollution modeling was published by Sharma and Khare (2001).

The objective of this study is to determine processes of the traffic pollution transport within the X-shaped intersection in an idealized symmetric urban area for several approach flow directions. Pollutant is emitted into the urban area from the point source simulating "pollution hotspot" - the place with higher emission of traffic pollution situated near a junction (Soulhac et al., 2009; Tomlin et al., 2009).

1.2 Experimental set-up

1.2.1 Wind tunnel

The experiment was conducted in the open low-speed wind tunnel of Institute of Thermomechanics Academy of Sciences of the Czech Republic in Nový Knín. The cross-dimension of the tunnel test section was 1.5 x 1.5 m, the length of the test section was 2 m. The scheme of the tunnel is depicted in Fig. 1.1.

Fully turbulent boundary layer was developed by the 20.5 m long development section of the tunnel. This section was equipped by turbulent generators at the beginning and covered by 50 mm and 100 mm high roughness elements on the floor, see the photo in Fig. 1.2.

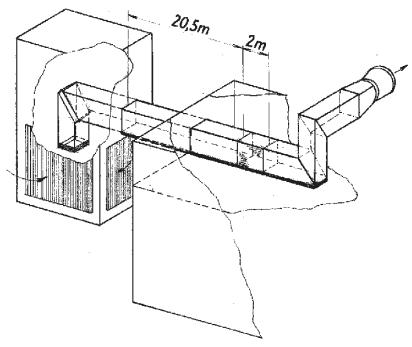

Figure 1.1: The scheme of the open low-speed wind tunnel.

1.2.2 Urban area model

The model of idealised symmetric urban area with apartment houses was designed according to the common Central European inner-city area. Regular blocks of

apartment houses with pitched roofs formed a perpendicular arrangement of the street canyons and X-shaped intersections, see Fig. 1.2.

The model was scaled down to 1:200. The model buildings were formed by the body of height 100 mm and width 50 mm with pitched roof of height 20 mm. We set up the characteristic building height $H = 120$ mm (24 m in full scale) as the height of building body with the roof.

The width of street canyons was $L = 100$ mm. The aspect ratio of the street canyons given by the building height H and the street width S was $H/L = 1.2$.

A point pollution source simulating a "pollution hotspot" (the place with higher emission of traffic pollution situated near a junction) was placed at the bottom of the street canyon in front of the studied intersection, see Fig. 1.2.

Figure 1.2: Scheme of the idealised symmetric urban area model (left), the studied X-shaped intersection (middle) and the photograph of the model placed in the wind tunnel (right).

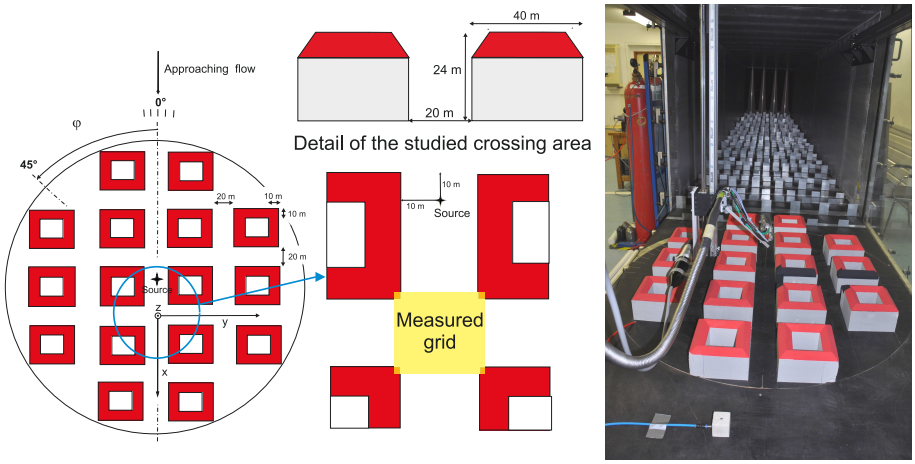

1.2.3 Measurement techniques

The flow characteristics were measured using a two-dimensional optical fibre Laser Doppler Anemometry (LDA), based on DANTEC BSA F-60 burst processor. Tracing particles (glycerine droplets with approximately 1 μm diameter) were produced by a commercial haze generator placed at the beginning of the tunnel generating section, in front of turbulent generators. We got the air flow in the test section equally filled by seeding particles after running the haze generator inside the tunnel for several minutes. Data rate reached about 100 Hz at the bottom levels of street canyons $z \lesssim 0.5H$ and up to 1000 Hz at the roof top level $z \approx H$. The time of recording was 180 s in all the cases.

Point concentration measurements of tracer gas were realised by Slow-response Flame Ionisation Detector (SFID) and Fast-response Flame Ionisation Detector (FFID). We used SFID (type ROSEMONT NGA 2000) for mean concentration measurement within the studied intersection. Simultaneous vertical velocity and

concentration measurement at the roof top level above the intersection was realised using LDA and FFID (type Cambustion Ltd. HFR400 Atmospheric Fast FID). The FFID was set to acquire data at a data rate of 1 KHz. The sampling time was 180 s in all of the cases.

We used ethane as the tracer gas simulating passive pollutants. Ethane is passive and non-reactive gas with its own density $\rho_{Ethane} = 1.24$ kg.m^{-3} close to density of the air $\rho_{Air} = 1.28$ kg.m^{-3}.

SFID and FFID were calibrated approximately every four hours of measurement. The differences in output voltage, reached up to 5% through the measuring campaign. All the concentration values were computed from measured voltage signal using linear interpolated values from two calibrations realised before and after the recorded data set.

We applied a standard three point calibration for the SFID measurement using clean air (air sucked into the wind tunnel from the atmosphere) and two span gases of known hydrocarbons concentrations.

For simultaneous velocity and concentration measurement, the four point FFID calibration using clean air (air sucked into the wind tunnel from the atmosphere), air equally filled by seeding particles and two span gases of known hydrocarbons concentrations were obtained.

As expected, the presence of the seeding particles in the air during simultaneous LDA and FFID measurement influenced FFID output signal. At first we got isolated spikes in the recorded concentration signal probably due to suction of combustible aerosol particles from air into the FFID probe. The problem was mentioned by Hall and Emmott (1991); Contini et al. (2006). Unlike these published results, we got similar count of spikes in time series obtained from measurements in clean air and in air contained seeding particles in most cases. We neglected the influence of spikes on the results because the frequency of isolated spikes was about 0.006% of used sampling data rate.

The second influence of seeding particles on the measured concentration data was an almost constant shift of recorded concentration values caused obviously by sucking seeding particles by FFID probe. This shift reached about 0.5% of the FFID measuring range. The shift was corrected by the calibration sequence mentioned above.

For simultaneous velocity and concentration measurement, LDA and FFID probes were mounted on the traverse system in a way that the measuring volume of the LDA was close to the intake to the FFID sampling tube. The sampling tube intake was placed 1.5 mm above, 1 mm behind and 1 mm beside the centre of the LDA measuring volume. Several test measurements with different positions of both probes demonstrated a negligible influence of FFID sampling tube placed close to the LDA measuring volume on the flow. The configuration of probes is captured in Fig. 1.3.

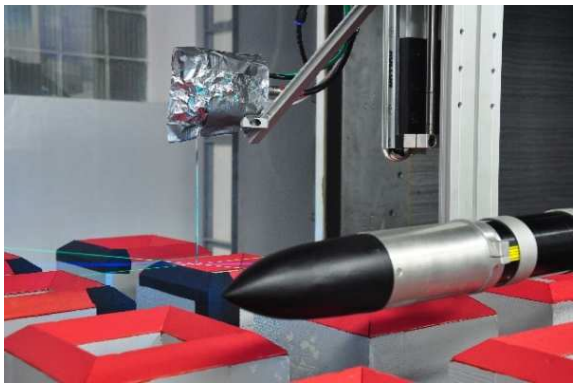

Figure 1.3: The configuration of the FFID (left) and LDA (right) probes mounted on the traverse system in the wind tunnel.

1.2.4 Boundary layer characteristics

Fully turbulent boundary layer was developed by spires and roughness elements placed it the tunnel. The characteristics of the boundary layer above the urban area model were measured with a two-dimensional LDA system in four vertical profiles placed above, upstream and downstream from the studied intersection, see Fig. 1.4.

The vertical profile of mean longitudinal velocity is depicted in Fig. 1.5a, the momentum flux profile can be found in Fig. 1.5b. The vertical profiles of longitudinal and vertical turbulent intensity are plotted in Figures 1.5c and 1.5d. The high above the surface is expressed in full scale.

Vertical profiles of measured turbulent approach flow characteristics were fitted by the logarithmic and the power law. Mean roughness length z_0, displacement d_0 and friction velocity u_* (alias square-root of constant value of Reynolds stress within the inertial sublayer) were obtained from the logarithmic fit. Power exponent α was obtained from the power fit. The parameters are listed in Table 1.1.

Table 1.1: Parameters of modelled boundary layer above the measured area (in full scale).

$z_0\,[m]$	$d_0\,[m]$	$\alpha\,[-]$	$u_*/U_{2H}\,[-]$
0.83	13.40	0.24	0.096

Categories of boundary layer are defined according to classification in VDI (2000). Measured parameters corresponded to a neutrally stratified boundary layer flow above a densely built-up area without much obstacle height variation.

To verify requirements for the Townsend hypothesis, see Townsend (1999), the critical Reynolds building number Re_B was found. This criterion was used by Meroney et al. (1996) and Pavageau and Schatzmann (1999) for the flow

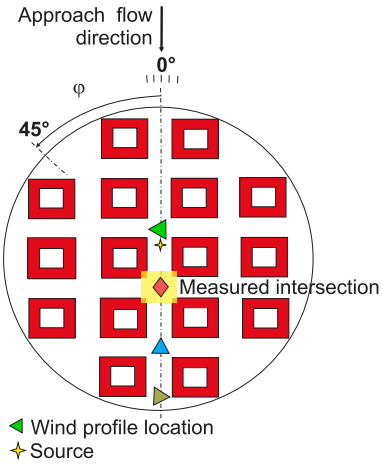

Figure 1.4: Wind profile measurement locations.

within street canyons to be independent of viscous effects. The Reynolds building number modified for our experiment was given by

$$Re_B = \frac{U_{2H} H}{\nu}, \tag{1.1}$$

where ν is kinematic viscosity. The experiment was carried out by $Re_B \approx 21000$ that lies on the lower edge of determined interval for valid Townsend hypothesis. Free stream velocity was approx. 4 ms^{-1}.

1.3 Results

Horizontal velocity of the flow and concentration of the tracer gas was measured in vertical cuts (cross-sections) labelled A, B, C and D. These cuts were placed in the exit planes of the street canyons connected to the studied intersection, see Fig. 1.2. Cuts were placed 5 mm inward to the canyons because of the high gradients of measured quantities and the strongly unstable flow at the exact exit planes of the street canyons.

Furthermore, the vertical velocity and tracer gas concentration were simultaneously measured in a horizontal plane at the roof level $z = H$ above the studied intersection. We used a a reference velocity U_{2H} measured at the reference height $z = 2H$. Results were obtained from five different values of the approach flow angle $\varphi = 0°$, 5°, 15°, 30° and 45°.

In order to get an understandable image of the results, we used a transformation of the measured three-dimensional grid to a horizontal plane, see Fig. 1.6. Vertical cuts of the measured grid were tipped out to the horizontal plane given by the roof level of the intersection. An orientation of horizontal velocity vectors in the vertical cuts was maintained in the transformed horizontal plain image.

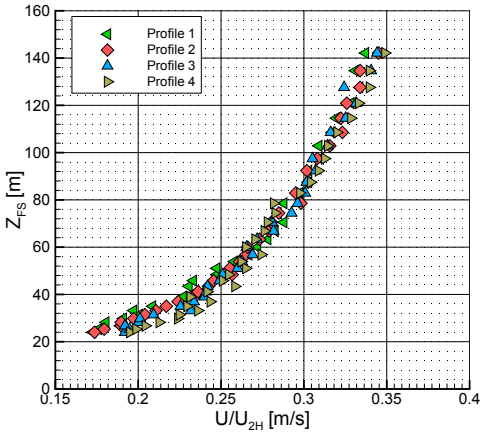

(a) The vertical profiles of mean longitudinal velocity.

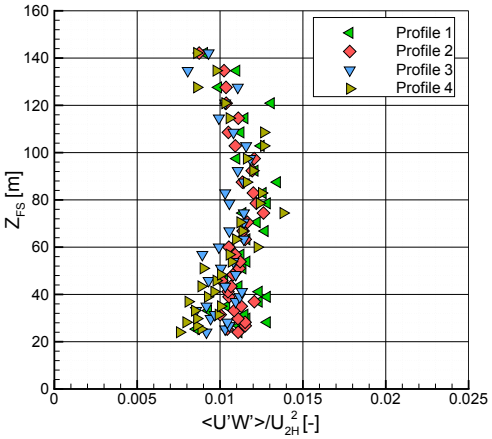

(b) The vertical profiles of mean momentum flux.

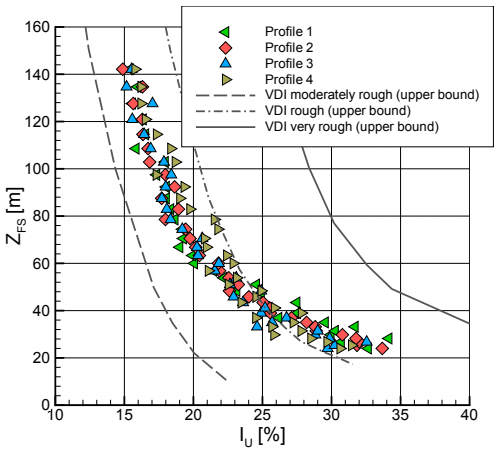

(c) The vertical profiles of longitudinal turbulent intensity.

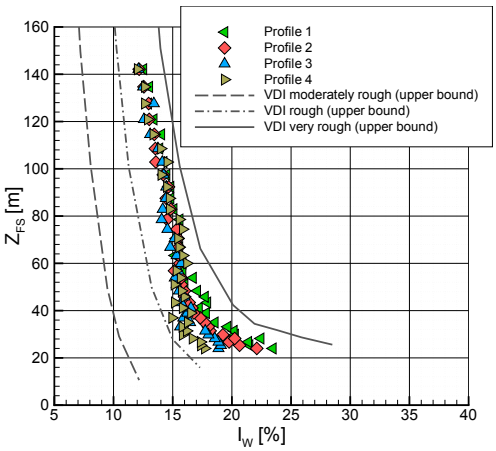

(d) The vertical profiles of vertical turbulent intensity.

Figure 1.5: Boundary layer characteristics above the urban area model.

1.3.1 Mean velocity fields

The flow inside the canopy was strongly three-dimensional and vortices of various scales are formed within and above the canyons and intersections. Measured components of velocity vector are expressed by the dimensionless form given by

$$U/U_{2H}, V/U_{2H}, W/U_{2H}, \tag{1.2}$$

where U and V are the horizontal velocity components measured in vertical cuts placed in the exit planes of the street canyons connected to the studied intersection, W is vertical velocity of the flow measured in the horizontal plane at the roof level $z = H$ above the intersection. U_{2H} means a reference velocity measured at the reference height $z = 2H$.

A contour plots of velocity magnitude were added to the images of the veloc-

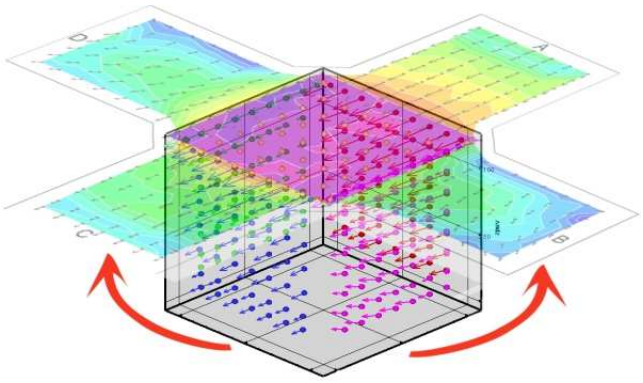

Figure 1.6: The transformation of the measured three-dimensional grid to a horizontal plane.

ity field. The orientation of horizontal velocity components is given by plotted vectors. The orientation of vertical velocity is given by a sign of the scalar values: the positive sign means an upward direction of vertical velocity and the negative sign means a downward direction.

A roughly symmetrical velocity field was formed by $\varphi = 0°$ (Fig. 1.7a). The main stream was situated to a alongwind street parallel with the approach flow (Cut A and C). A vortex with vertical axis was formed within the crosswind streets (Cut B and D). The horizontal velocity decreased in levels towards the bottom of the street canyons (further form the middle of the picture). The vertical velocity on the top of the intersection was negligible in this case.

We observed an obvious change in the velocity field by $\varphi = 5°$ (Fig. 1.7b). The main stream was still situated to a alongwind street, but the horizontal velocity increased in the left transverse street and decreased in the right transverse street. There was a small increase of upwards vertical velocity on the right side. A region with upward vertical velocity was formed near the right leeward corner.

As for the angle $\varphi = 15°$ as well as $\varphi = 30°$ a significant stream was formed within crosswind streets (Fig. 1.7c). The increase in the upwards vertical velocity continued on the right side, however, it was not so important as in comparison with the changes of the vertical velocity.

An almost symmetrical velocity field was formed by $\varphi = 45°$ (Fig. 1.7d). The main stream was divided into the alongwind and left crosswind streets (Cut B and C). Asymmetry of flow was probably caused by minor geometrical deviations of the model in case of approach flow angle $\varphi \approx 0°$.

1.3.2 Mean concentration fields

The dimensionless concentration for a point source was obtained from the formula published in VDI (2000):

$$C^* = \frac{CU_{2H}H^2}{Q} \tag{1.3}$$

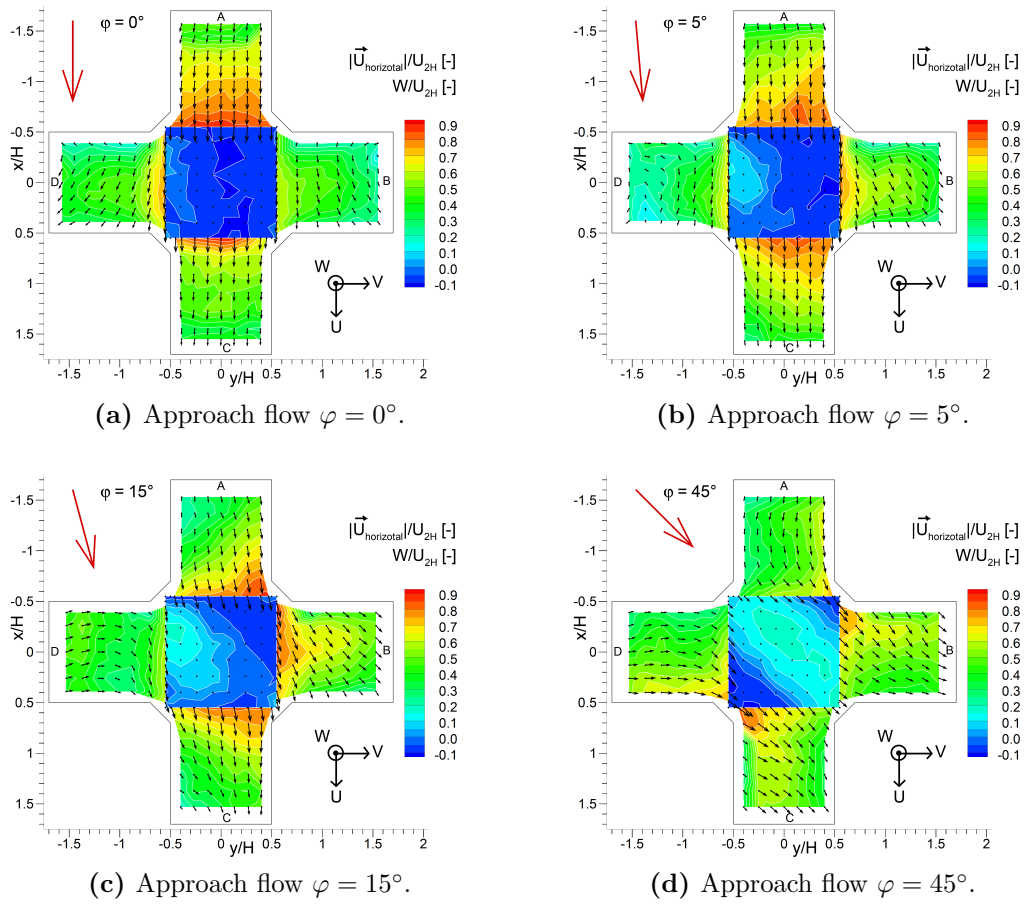

(a) Approach flow $\varphi = 0°$.

(b) Approach flow $\varphi = 5°$.

(c) Approach flow $\varphi = 15°$.

(d) Approach flow $\varphi = 45°$.

Figure 1.7: Dimensionless velocity fields for four angles of the approach flow direction.

where C means the measured concentration in and Q is a source emission volume flow.

Values of computed dimensionless concentration for five angles of the approach flow directions are plotted in Fig. 1.8. A roughly symmetrical concentration field was formed by $\varphi = 0°$ (Fig. 1.8a), but notice slightly higher concentration in alongwind street (cut D) in comparison with the left crosswind street (Cut B). There was almost zero concentration on the top of the intersection, which indicated weaker advective vertical transport of pollution than in the following cases.

We observed that a quite small change of the angle of the approach flow caused a radical change in concentration field by $\varphi = 5°$ (Fig. 1.8b). An obvious deformation of the concentration field is probably caused mainly by street canyon vortices with horizontal axis (Cut A). The decrease in concentration in the right crosswind street (Cut D) was measured.

Transport of the majority of the tracer gas from the alongwind street (Cut A) to the left crosswind street (Cut B) was obvious by $\varphi = 15°$ (Fig. 1.8c).

Consequently there was almost zero concentration in cut D. We measured the lowest concentrations in the intersection area in this case. We got a very similar concentration field for $\varphi = 30°$ (not shown).

We observed an overall increase in concentration by $\varphi = 45°$ (Fig. 1.8d). There was an enhanced transport of the tracer gas to the right crosswind street up the approach wind (Cut C and D) compared with case $\varphi = 15°$. It was probably caused by a small vortex with vertical axis at the leeward wall of this street. There was an area of significant concentration at the top of the intersection.

As we expected, the highest concentrations were measured at the ground levels in all cases and at the leeward wall of the street with the source (Cut A).

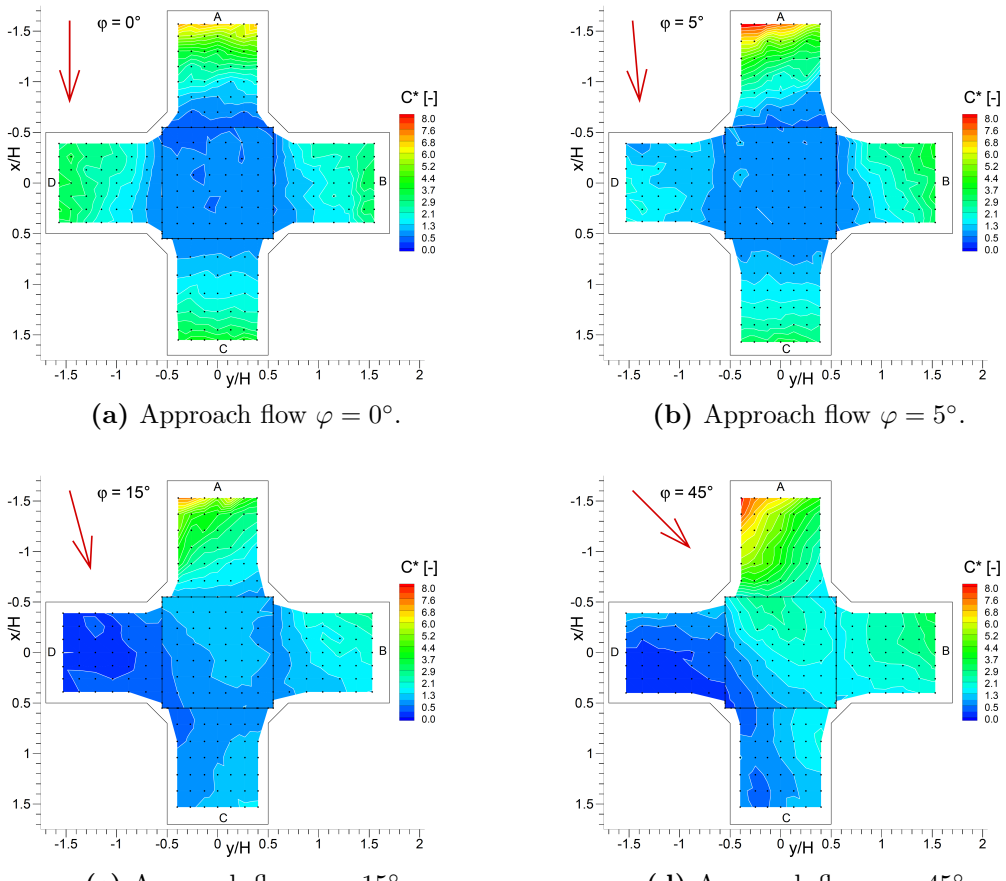

(a) Approach flow $\varphi = 0°$.

(b) Approach flow $\varphi = 5°$.

(c) Approach flow $\varphi = 15°$.

(d) Approach flow $\varphi = 45°$.

Figure 1.8: Dimensionless concentration fields for four angles of the approach flow direction.

1.3.3 Advective scalar flux fields

The dimensionless advective scalar fluxes were computed from the average measured data to quantify advective spreading of pollutants within the studied intersection, see similar approach in Belcher (2005); Robins (2008). We computed

horizontal dimensionless advective fluxes using forms

$$C^*U/U_{2H}, C^*V/U_{2H}, \tag{1.4}$$

where C^* is the mean dimensionless concentration of the tracer gas, U and V are the mean horizontal velocity components of the flow. Vertical dimensionless advective flux given was given by

$$C^*W/U_{2H}, \tag{1.5}$$

where W is the mean vertical velocity of the flow. Results were obtained for all five values of the angle of the approach flow $\varphi = 0°$, 5°, 15°, 30° and 45°.

The dimensionless advective scalar fluxes expressed a rate of emissions spreading through an unit area. Computed fluxes characterized the advective transport of pollution with the following convention of signs: the positive sign means the flux outwards and the negative sign means the flux inwards the studied intersection.

Values of computed fluxes for five angles of the approach flow directions are plotted in Fig. 1.9. We can observe quite an asymmetrical flux field by $\varphi = 0°$ (Fig. 1.9a). There is a higher flux into the right crosswind street (Cut D) than into the left crosswind street (Cut B). As we mentioned this was probably caused by minor geometrical deviations of the model. However, it means very strong sensitivity of scalar fluxes to the geometry of the model and approach flow direction. Notice a negative, i.e. downward, flux at the top.

A roughly reversely spread flux field was formed by $\varphi = 5°$ (Fig. 1.9b) compared to the case of $\varphi = 0°$. We could see a significant transport into the left crosswind street (Cut B).

A noticeable overall decrease in the flux in case of $\varphi = 15°$ was observed (Fig. 1.9c). The lowest fluxes were measured in this case within the studied area. Emissions were transported mainly to the left crosswind street (Cut B). There was an area of the positive flux on the right side at the top of the intersection. We got similar flux field for $\varphi = 30°$ but with higher flux values.

A spreading of emissions mostly to the left side still predominated by $\varphi = 45°$ (Fig. 1.9d). There was an increase in the flux especially in the left crosswind street (Cut B). There was mostly a positive flux at the top of the intersection.

1.3.4 Turbulent scalar flux fields

The dimensionless vertical turbulent scalar fluxes were computed from synchronised vertical velocity and concentration signals using eddy-correlation method (Arya, 1998; Stull, 1988).

The used Matlab post-processing script synchronised simultaneously acquired vertical velocity and concentration data using the maximum of correlation between both signals. The synchronised time series were shifted by an average of 15 ms. This shift expressed the delay between a suck of the sample into the intake

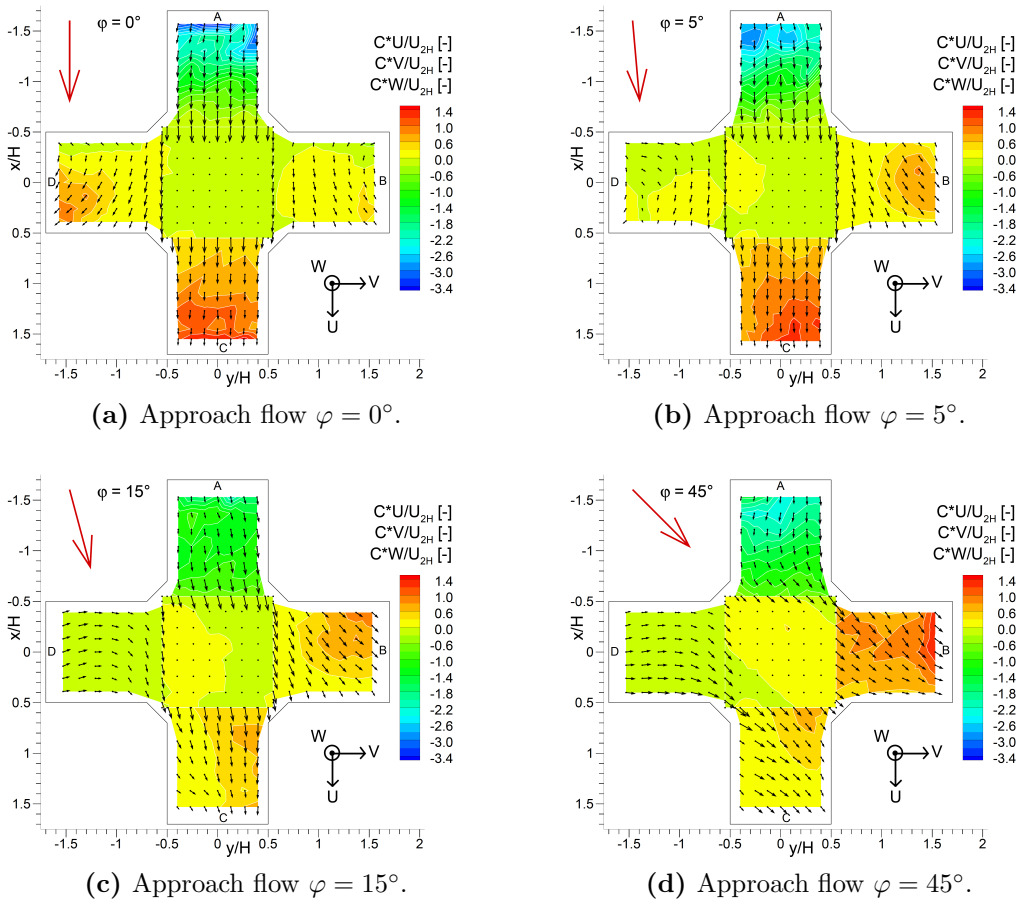

(a) Approach flow $\varphi = 0°$.

(b) Approach flow $\varphi = 5°$.

(c) Approach flow $\varphi = 15°$.

(d) Approach flow $\varphi = 45°$.

Figure 1.9: Horizontal and vertical dimensionless advective flux of passive contaminant with horizontal velocity vectors for four angles of the approach flow direction.

of the FFID probe tube and the moment of the sample analysing in the probe. The value of the shift agrees with very similar experimental set up published by Contini et al. (2006).

The dimensionless vertical turbulent scalar flux is given by

$$\left\langle c^{*\prime} w^{\prime} \right\rangle / U_{2H}, \tag{1.6}$$

where $\langle ... \rangle$ mean a time average, $c^{*\prime}$ and $w^{\prime}$ indicates fluctuations of dimensionless concentration and vertical velocity. Similar approach to turbulent transport computing was published in Jurcakova et al. (2009).

Computed dimensionless vertical turbulent fluxes express a rate of emissions spreading through a unit area by turbulent transport with the same convention as mentioned above.

Values of determined vertical turbulent fluxes for the four approach flow directions are plotted in Fig. 1.10. We measured relatively flat turbulent flux field by

angle $\varphi = 0°$, but, compared with the advective flux, there is a positive turbulent transport of pollution, compare Fig. 1.10a and Fig. 1.9a.

In case $\varphi = 15°$ there are significantly positive values on the upwind side of the area (Fig. 1.10c). The observed phenomenon became stronger by angle $\varphi = 45°$ (Fig. 1.10d).

We estimated a significant turbulent transport of pollution near the leeward side of the buildings, see the upper part of Figures 1.10a and 1.10b. In comparison with the advective transport, the turbulent fluxes are positive in every case. The turbulent fluxes magnitude achieved almost two times the advective fluxes magnitude in the roof top level plane above the studied intersection.

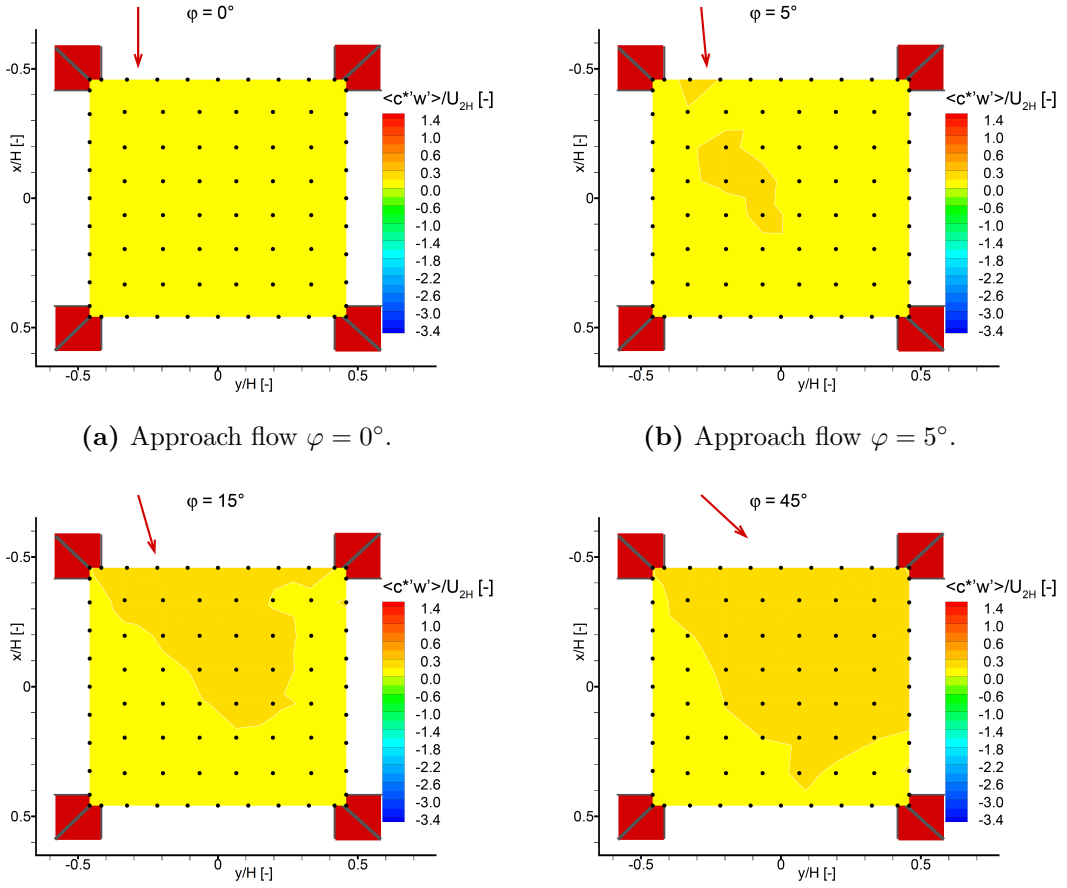

(a) Approach flow $\varphi = 0°$.

(b) Approach flow $\varphi = 5°$.

(c) Approach flow $\varphi = 15°$.

(d) Approach flow $\varphi = 45°$.

Figure 1.10: Vertical dimensionless turbulent scalar flux $\langle c^{*\prime} w^{\prime} \rangle / U_{2H}$ for four angles of the approach flow direction.

1.3.5 Quadrant analysis

We focused on the turbulent flow in vertical direction situated in the horizontal plane at the roof top level above the intersection in this part.

The first step to investigate the turbulent processes in strongly turbulent flow is the quadrant analysis (Kellnerova et al., 2009; Feddersen, 2005). We applied this analysis to the velocity fluctuation time series to obtain contributions of the vertical flux of longitudinal momentum $\langle u'w' \rangle$ from particular quadrants defined as:

1^{st} quadrant "outward interaction" $(u' > 0, w' > 0)$,

2^{nd} quadrant "sweep" $(u' > 0, w' < 0)$,

3^{rd} quadrant "inward interaction" $(u' < 0, w' < 0)$,

4^{th} quadrant "ejection" $(u' < 0, w' > 0)$.

These definitions are illustrated by the Fig. 1.11. The particular contribution

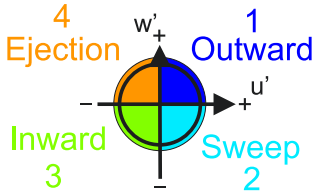

Figure 1.11: The scheme of event definitions used in velocity fluctuation quadrant analysis.

from i^{th} quadrant to the total momentum flux $\langle u'w' \rangle$ is given by

$$S_i = \frac{\langle u'w' \rangle_i N_i}{N_{total}}, \tag{1.7}$$

where $\langle u'w' \rangle_i$ is the average stress and N_i is the number of events in the i^{th} quadrant, number of all measured events is N_{total}.

The relative contribution R of the prevailing event to the total momentum flux is given by

$$R = \frac{S_{max}}{\sum S_i} 100\%, \tag{1.8}$$

where S_{max} is the particular contribution from the dominant event.

Relative contributions R of dominant events for four angles of the approach flow directions are plotted in Fig. 1.12. As you see, ejections and sweeps are the prevailing events. Ejections characterize the upward transport of longitudinal momentum deficit, sweeps correspond to the downward transport of longitudinal momentum excess.

Ejections and sweeps were detected for the approach flow direction $\varphi \lesssim 5°$ with relatively small relative contribution to the mean momentum flux (Figures 1.12a and 1.12b). Large areas of sweeps with high contribution increased for

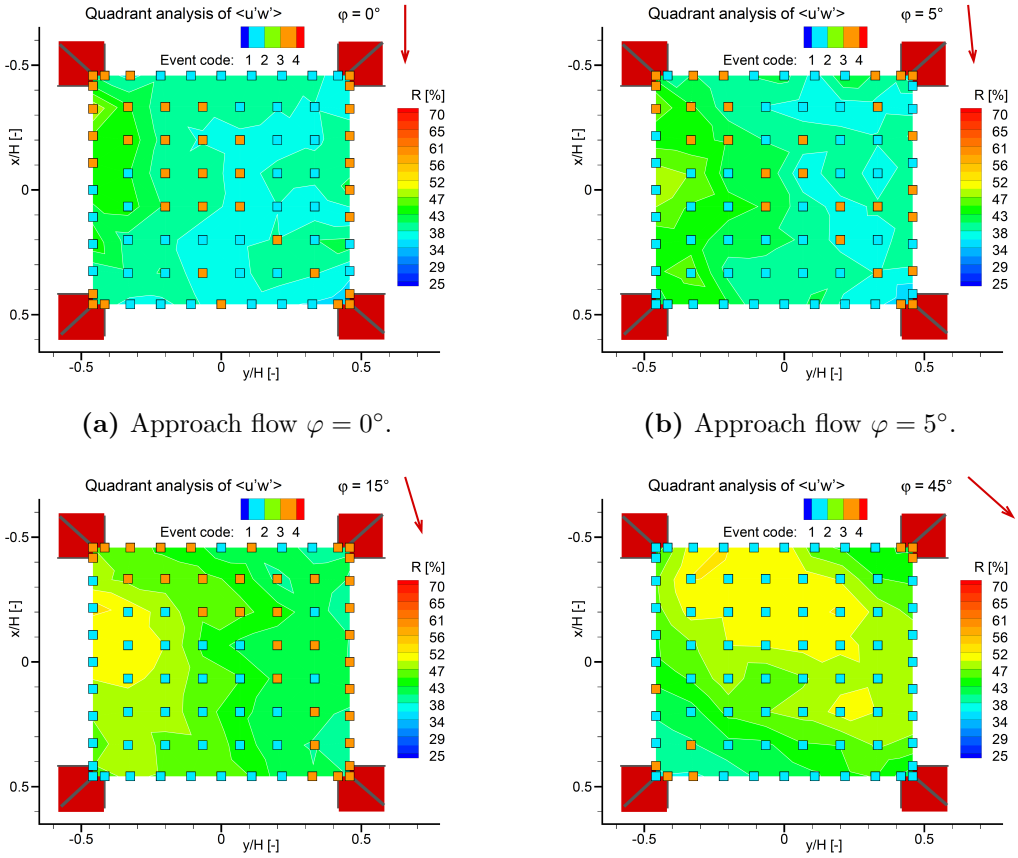

(a) Approach flow $\varphi = 0°$.

(b) Approach flow $\varphi = 5°$.

(c) Approach flow $\varphi = 15°$.

(d) Approach flow $\varphi = 45°$.

Figure 1.12: Relative contributions R of dominant event to the total momentum flux $\langle u'w' \rangle$ for four angles of the approach flow direction.

higher angles $\varphi \gtrsim 15°$ caused probably by increasing magnitude of longitudinal velocity (Figures 1.12c and 1.12d).

We applied described quadrant analysis to the synchronized vertical velocity and concentration signals. In this case, particular quadrants are defined as:

1^{st} quadrant "outward interaction" $(c' > 0, w' > 0)$,

2^{nd} quadrant "sweep" $(c' > 0, w' < 0)$,

3^{rd} quadrant "inward interaction" $(c' < 0, w' < 0)$,

4^{th} quadrant "ejection" $(c' < 0, w' > 0)$.

These definitions are illustrated by the Fig. 1.13.

Relative contributions R of dominant events for four angles of the approach flow directions are plotted in Fig. 1.14. We observed outward interactions as the dominant event with high relative contribution for the approach flow angles $\varphi \sim 0° - 15°$ (Figures 1.14a–1.14c). Inward interaction became dominant in part

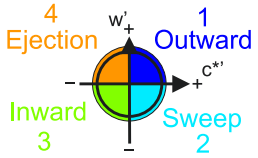

Figure 1.13: The scheme of event definitions used in turbulent flux quadrant analysis.

of the grid for the approach flow angles $\varphi \sim 45°$ but with low relative contribution (Fig. 1.14d).

1.4 Conclusion

The described wind tunnel experiment quantified traffic pollutant dispersion within the X-shaped intersection in an idealized symmetrical urban area depending on the direction of the approach flow. The tracer gas is emitted into the urban area from the point source simulating "pollution hotspot" - the place with higher emission of traffic pollution situated near a junction.

Velocity and concentration measurements were done by the building Reynolds number in the interval of Townsend hypothesis validity. We found out very complex flow and dispersion pattern within street canyons and high sensitivity to the approach flow direction. We determined a significant influence of the street canyon arrangements to the horizontal velocity in lower parts of the canyons at vertical levels of $z \lesssim 0.5H$. The highest concentration of pollution occurred at the bottom levels of streets.

The computed dimensionless advective scalar fluxes of contaminant showed spreading of pollution mostly within the alongwind street for flow almost parallel to the street canyon with pollution source. Spreading of pollution to the crosswind street down the wind was observed for approach flow diverging from orientation of the street canyon with pollution source. We determined the highest advective fluxes at the bottom parts of the street canyons.

A unique experimental set-up for simultaneous measurement of the flow velocity and the tracer gas concentration was designed and assembled, based on Fast-response Flame Ionisation Detector and Laser Doppler Anemometer. Vertical turbulent scalar fluxes of passive contaminant were computed from obtained synchronized signals for a horizontal plane placed above the intersection.

Vertical turbulent fluxes magnitude reached two times higher magnitude of vertical advective fluxes in individual grid points. Determined vertical turbulent fluxes comprised significant and positive contribution to the vertical ventilation of the area. On the other side, horizontal advective fluxes magnitude reached up to four times higher magnitude of vertical turbulent flux, so the contribution of the horizontal advective pollution transport to total ventilation is dominant in all the cases.

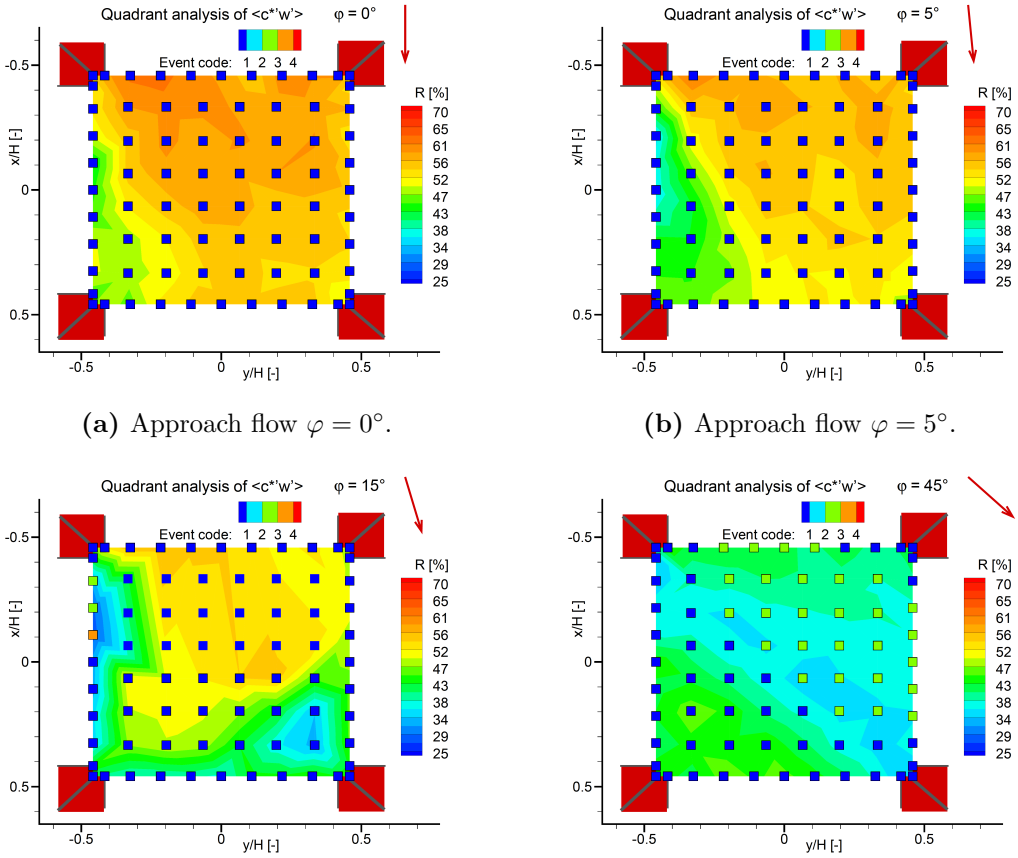

(a) Approach flow $\varphi = 0°$.

(b) Approach flow $\varphi = 5°$.

(c) Approach flow $\varphi = 15°$.

(d) Approach flow $\varphi = 45°$.

Figure 1.14: Relative contributions R of dominant event to the vertical turbulent scalar flux $\langle c^{*\prime} w^{\prime} \rangle / U_{2H}$ for four angles of the approach flow direction.

The best dispersive conditions in the studied intersection were measured for the approach flow angle $\varphi \approx 15°$. In this case we measured generally the lowest concentration in the studied area and the lowest scalar flux from the source to the intersection.

The quadrant analysis was applied to the velocity fluctuation signals determined the sweep as a dominant event in flow above the intersection. The relative contribution of the sweep invents to the momentum flux increased for approach flow diverging from orientation of the street canyon with pollution source.

The quadrant analysis was applied to the synchronized vertical velocity and concentration signals. We determined the outward interaction as a dominant event with high relative contribution to the vertical turbulent flux for flow almost parallel to the street canyon with pollution source. Inward interaction events became dominant for diverging flow but with small relative contribution. The flow in this case is strongly turbulent so that we investigated almost the same contribution to the vertical turbulent flux from all events.

The data set acquired from the experiment in the complex urban structure can

be used for validations of numerical models of flow and dispersion in street scale or for comparisons of results obtained using these models. The data contains unique synchronized flow velocity and pollution concentration fluctuations signals in a high temporal resolution that can be used to verify pollution transport properties.

Acknowledgements
The authors would like to thank the Ministry of Education, Sports and Youth of the Czech Republic (project AVOZ-20760514) and the Academy of Sciences of the Czech Republic (project M100760901) for their financial support.

1.5 References

S. P. Arya. *Air Pollution Meteorology and Dispersion*. Oxford University Press, New York, 1998. ISBN 978-0-19-507398-0. doi: 10.1023/a:1006450618793. URL http://ukcatalogue.oup.com/product/9780195073980.do.

J. F. Barlow and S. E. Belcher. A wind tunnel model for quantifying fluxes in the urban boundary layer. *Boundary-Layer Meteorology*, 104(1):131–150, 2002. ISSN 00068314. doi: 10.1023/A:1015555613672. URL http://link.springer.com/article/10.1023/A:1015555613672.

S. E. Belcher. Mixing and transport in urban areas. *Philosophical Transactions of the Royal Society A: Mathematical, Physical and Engineering Sciences*, 363(1837):2947–2968, 2005. ISSN 1364-503X. doi: 10.1098/rsta.2005.1673. URL http://rsta.royalsocietypublishing.org/cgi/doi/10.1098/rsta.2005.1673.

M. Brown, H. Khalsa, M. Nelson, and D. Boswell. Street canyon flow patterns in a horizontal plane: measurements from the Joint URBAN 2003 field experiment. *... AMS Symp. on the Urban ...*, 2004. URL https://ams.confex.com/ams/pdfpapers/80299.pdf.

M. Claggett, J. Shrock, and K. E. Noll. Carbon monoxide near an urban intersection. *Atmospheric Environment (1967)*, 15(9):1633–1642, 1981. ISSN 00046981. doi: 10.1016/0004-6981(81)90148-7.

R. Colvile, E. Hutchinson, J. Mindell, and R. Warren. The Transport secotor as a source of air pollution. *Atmospheric Environment*, 35(2001):1537–1565, 2001.

D. Contini, P. Hayden, and A. Robins. Concentration field and turbulent fluxes during the mixing of two buoyant plumes. *Atmospheric Environment*, 40(40):7842–7857, dec 2006. ISSN 13522310. doi: 10.1016/j.atmosenv.2006.07.024. URL http://linkinghub.elsevier.com/retrieve/pii/S1352231006007850.

W. Dabberdt, W. Hoydysh, M. Schorling, F. Yang, and O. Holynskyj. Dispersion modeling at urban intersections. *The Science of the total environment*, 169:93–102, 1995. URL http://www.sciencedirect.com/science/article/pii/004896979504637G.

B. Feddersen. *Wind tunnel modelling of turbulence and dispersion above tall and highly dense urban roughness*. PhD thesis, ETH Zurich, 2005. URL http://scholar.google.com/scholar?hl=en&btnG=Search&q=intitle:Wind+tunnel+modelling+of+turbulence+and+dispersion+above+tall+and+highly+dense+urban+roughness#0.

J. Fenger. Urban air quality. *Atmospheric Environment*, 33(29):4877–4900, 1999. ISSN 13522310. doi: 10.1016/S1352-2310(99)00290-3.

D. J. Hall and M. A. Emmott. Avoiding aerosol sampling problems in fast response flame ionisation detectors. *Experiments in Fluids*, 10(4):237–240, 1991. ISSN 07234864. doi: 10.1007/BF00190394. URL http://link.springer.com/article/10.1007/BF00190394.

G. Hoek, B. Brunekreef, A. Verhoeff, J. V anWijnen, and P. Fischer. Daily mortality and air pollution in the Netherlands. *Journal of the Air and Waste Management Association*, 50(8):1380–1389, aug 2000. ISSN 21622906. doi: 10.1080/10473289.2000.10464182. URL http://www.tandfonline.com/doi/abs/10.1080/10473289.2000.10464182.

K. Jurcakova, O. Massaki, and Z. Janour. Contribution of advective and turbulent mass transfers to the ventialtion of urban canopy. In *The seventh Asia-Pacific Conference on Wind Engineering*, Taipei, Taiwan, 2009. ISBN 9866717437.

P. Kastner-Klein and E. J. Plate. Wind-tunnel study of concentration fields in street canyons. *Atmospheric Environment*, 33(24-25):3973–3979, 1999. ISSN 13522310. doi: 10.1016/S1352-2310(99)00139-9.

R. Kellnerova, L. Kukacka, and Z. Janour. Quadrant analysis of boundary layer above pitched and flat roofs. *Acta Technica CSAV (Ceskoslovensk Akademie Ved)*, 54(4):401–413, 2009. ISSN 00017043.

R. N. Meroney, M. Pavageau, S. Rafailidis, and M. Schatzmann. Study of line source characteristics for 2-D physical modelling of pollutant dispersion in street canyons. *Journal of Wind Engineering and Industrial Aerodynamics*, 62(1):37–56, aug 1996. ISSN 01676105. doi: 10.1016/S0167-6105(96)00057-8. URL http://linkinghub.elsevier.com/retrieve/pii/S0167610596000578.

F. Nyberg, P. Gustavsson, L. Järup, T. Bellander, N. Berglind, R. Jakobsson, G. Pershagen, and L. Ja. Urban air pollution and lung cancer in Stockholm. *Epidemiology*, 11(5):487–95, 2000. ISSN 1044-3983.

M. Pavageau and M. Schatzmann. Wind tunnel measurements of concentration fluctuations in an urban street canyon. *Atmospheric Environment*, 33:3961–3971, 1999. ISSN 13522310. doi: Doi10.1016/S1352-2310(99)00138-7.

A. Robins. DAPPLE (dispersion of air pollution and its penetration into the local environment) experiments and modelling. *HPA Chemical Hazards and Poisons Report*, 13(September):24–28, 2008.

A. Scaperdas and R. N. Colvile. Assessing the representativeness of monitoring data from an urban intersection site in central London, UK. *Atmospheric Environment*, 33(4):661–674, 1999. ISSN 13522310. doi: 10.1016/S1352-2310(98)00096-X.

P. Sharma and M. Khare. Modelling of vehicular exhausts - A review. *Transportation Research Part D: Transport and Environment*, 6(3):179–198, may 2001. ISSN 13619209. doi: 10.1016/S1361-9209(00)00022-5. URL `http://linkinghub.elsevier.com/retrieve/pii/S1361920900000225`.

L. Soulhac, V. Garbero, P. Salizzoni, P. Mejean, and R. J. Perkins. Flow and dispersion in street intersections. *Atmospheric Environment*, 43(18):2981–2996, jun 2009. ISSN 13522310. doi: 10.1016/j.atmosenv.2009.02.061. URL `http://linkinghub.elsevier.com/retrieve/pii/S1352231009001186`.

R. B. Stull. *An Introduction to Boundary Layer Meteorology*. Kluwer Aademic Publishers, Dordrecht, 1988. ISBN 978-90-277-2769-5. doi: 10.1007/978-94-009-3027-8. URL `http://link.springer.com/10.1007/978-94-009-3027-8`.

A. S. Tomlin, R. J. Smalley, J. E. Tate, J. F. Barlow, S. E. Belcher, and S. J. Arnold. A field study of factors influencing the concentrations of a traffic related pollutant in the vicinity of a complex urban junction. *Atmos. Env.*, 43:5027–5037, 2009.

A. A. Townsend. *The Structure of Turbulent Shear Flow*. Cambridge University Press, New York, 1999. ISBN 0 521 20710.

VDI. *Environmental meteorology – Physical modelling of flow and dispersion processes in the atmospheric boundary layer – Application of wind tunnels*. Verein Deutscher Ingenieure, Dusseldorf, Dusseldorf, 2000.

X. Wang and K. F. McNamara. Effects of street orientation on dispersion at or near urban street intersections. *Journal of Wind Engineering and Industrial Aerodynamics*, 95(9-11):1526–1540, oct 2007. ISSN 01676105. doi: 10.1016/j.jweia.2007.02.021. URL `http://linkinghub.elsevier.com/retrieve/pii/S0167610507000621`.

2. Analysis of scalar fluxes and flow within modelled intersection depending on the approach flow direction

In D. G. Steyn and S. T. Castelli, editors, *Proceeding of the 31st NATO/SPS International technical meeting on air pollution modelling and its application, Air Pollution Modeling and its Application XXI*, chapter Analysis of scalar fluxes and flow within modelled intersection depending on the approach flow direction, pages 113–118. Springer, Dordrecht, Netherlands, 2011. ISBN 978-94-007-1361-1.

Libor Kukačka[1,2], Štěpán Nosek[2], Radka Kellnerová[1,2], Klára Jurčáková[2], Zbyněk Jaňour[2]

[1] Charles University in Prague, Faculty of Mathematics and Physics, Prague, Czech Republic
[2] Institute of Thermomechanics, Academy of Sciences of the Czech Republic, Prague, Czech Republic

Abstract
The influence of the approach flow direction on contaminant spreading and ventilation within an intersection in an idealised symmetrical urban area was investigated in this study. Advective horizontal and vertical scalar fluxes are computed from measured data for five flow directions. The highest advective contaminant fluxes are measured in the bottom parts of street-canyons. The important role of the vertical turbulent scalar flux in ventilation of intersection is expected. Quadrant analysis of vertical flux of longitudinal momentum is used to determine a domination of sweep or ejection events above the intersection.

Keywords
Air pollution, Boundary layer, Wind tunnel modelling, Contaminant spreading, Scalar fluxes, Street canyon, Intersection.

2.1 Introduction

Vehicle traffic pollutants emitted directly to street-canyons represent the serious health hazard for people in large cities. As shown in Robins et al. (2002) and Wang and McNamara (2007), geometry of street intersections plays an important

role in pollutant dispersion and ventilation in urban areas. The objective of this study is to investigate the influence of the approach flow direction on contaminant spreading and ventilation within an intersection in an idealised urban area.

2.2 Experimental set-up

The model of idealised urban area with apartment houses was designed after the common European inner-city area. Regular blocks of apartment houses with pitched roofs form a perpendicular arrangement of street canyons and intersections, see Fig. 2.1. Wind tunnel model has been scaled down to 1 : 200. We consider characteristic obstacle high H = 20 m as a height of building walls to the bottom edge of the roofs. The experiment was conducted in low-speed aerodynamic tunnel of Institute of Thermomechanics in Nový Knín. Fully turbulent boundary layer was developed by spires and roughness elements. 2-D Laser Doppler Anemometry (LDA) was used for flow measurements. Concentration was measured by slow-response Flame Ionisation Detector (FID). Tracer gas ethane was emitted from a point source placed in the street canyon in front of the intersection, see Fig. 2.1. Vertical profile of measured turbulent approach flow characteristics data was fitted by the logarithmic and the power law with following parameters: roughness length $z_0 = 0.53$ m, displacement $d_0 = 14.4$ m and power law exponent $\alpha = 0.25$ in full scale. This corresponds according to Britter and Hanna (2003) to parameters for neutrally stratified boundary layer flow above a densely built-up area without much obstacle height variation. Validity of the Towsend hypothesis Townsend (1999) was verified during the experiment. Free stream velocity was 3 m/s.

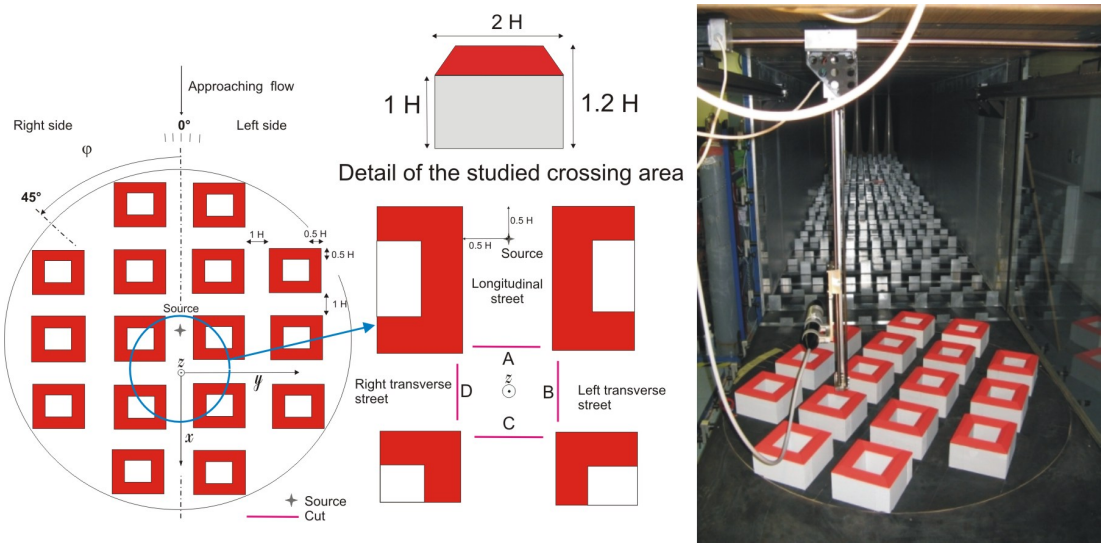

Figure 2.1: Scheme of the built-up area model, the studied X-shaped intersection and the photograph of the model placed in the wind tunnel.

2.3 Results

We determined dimensionless quantities to quantify spreading of pollutants within the studied intersection: concentration of tracer gas C^*, horizontal velocity of flow U^* in vertical cross-sections placed at outfalls street canyons connected to the intersection and vertical velocity W^* of flow in a horizontal cross-section at roof level ($z = 1.2H$) above the intersection. Results were obtained for 5 values of the approach flow angle $\varphi = 0°, 5°, 15°, 30°$ and $45°$.

A relative dimensionless flux of passive contaminant F^* was computed by $F^* = U^*C^*$, see similar approach in Belcher (2005) and Robins (2009). For getting an information about absolute values of dimensionless flux of passive contaminant in different parts of studied area we computed an absolute dimensionless flux of passive contaminant F_A^* by $F_A^* = A^*U^*C^*$, where A^* is dimensionless area.

The relative flux and absolute flux expresses a rate of emissions spreading through an unit area and area A^*, respectively. Computed fluxes characterize advective transfer with following convention of signs: the positive sign means flux outwards and the negative sign means flux inwards the intersection. Values of computed fluxes for three approach flow directions are plotted in Fig. 2.2.

The quadrant analysis was applied to the velocity fluctuation time series to obtain contributions of vertical flux of longitudinal momentum $\langle u'w' \rangle$ from particular quadrants defined as:

1^{st} quadrant "outward interaction" $(u' > 0, w' > 0)$,

2^{nd} quadrant "sweep" $(u' > 0, w' < 0)$,

3^{rd} quadrant "inward interaction" $(u' < 0, w' < 0)$,

4^{th} quadrant "ejection" $(u' < 0, w' > 0)$.

The particular contribution from i^{th} quadrant to the total momentum flux $\langle u'w' \rangle$ is given by $S_i = \langle u'w' \rangle_i N_i / N_{total}$, where $\langle u'w' \rangle_i$ is the average stress and N_i is the number of events in the i^{th} quadrant, number of all measured events is N_{total}, see Kellnerova et al. (2009).

The relative contributions from ejections S_4 and sweeps S_2 to the total momentum flux dominated the other two interactions. The difference $\Delta S = S_4 - S_2$ indicates prevailing mechanism of vertical momentum transport in the area, see Fig. 2.3. Ejections characterize the upward transport of longitudinal momentum deficit ($\Delta S > 0$), sweeps correspond to the downward transport of longitudinal momentum excess ($\Delta S < 0$). Ejections and sweeps are approx. of the same magnitude for the approach flow direction $\varphi \sim 0°$, see Fig. 2.3a. Large areas of sweeps increase for directions $\varphi \geq 15°$, see Fig. 2.3b and 2.3c.

2.4 Conclusions

The described wind tunnel experiment quantified traffic pollutant dispersion within the X-shaped intersection in an idealised symmetric urban area depending

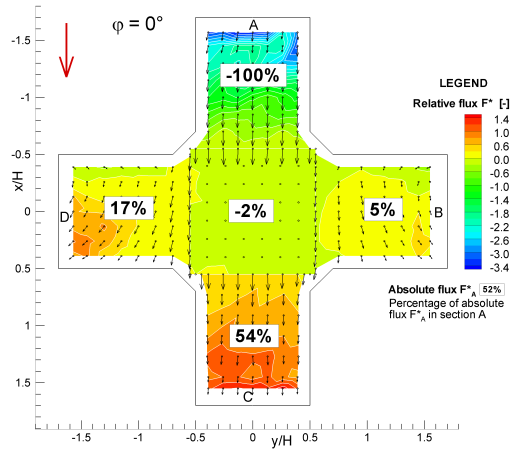

(a) Approach flow $\varphi = 0°$.

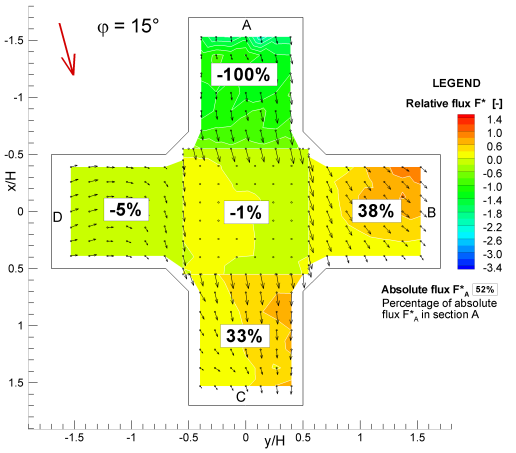

(b) Approach flow $\varphi = 15°$.

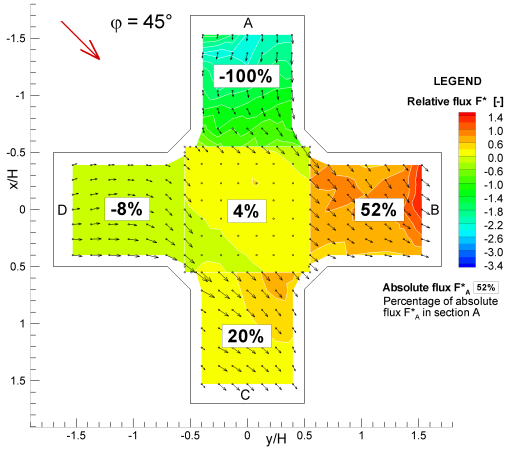

(c) Approach flow $\varphi = 15°$.

Figure 2.2: Relative and absolute dimensionless flux of passive contaminant fields for 3 approach flow directions in the intersection with horizontal velocity vectors. Numbers in the white boxes mean the absolute flux in each cross-section as a percentage of the absolute flux in section A.

on the approach flow direction. Computed scalar fluxes of contaminant showed spreading of pollution mostly within the longitudinal street for the approach flow angles $\varphi \leq 5°$ and to the transverse street by angles $\varphi \geq 15°$. We determined the highest absolute fluxes in bottom parts of street canyons. Significant vertical turbulent ventilation is expected because of non-zero sum of all measured fluxes within the intersection. Quadrant analysis determined dominating sweeps events by angles $\varphi \geq 15°$ that probably extensively influences ventilation of the area by transporting clean air from free stream downwards.

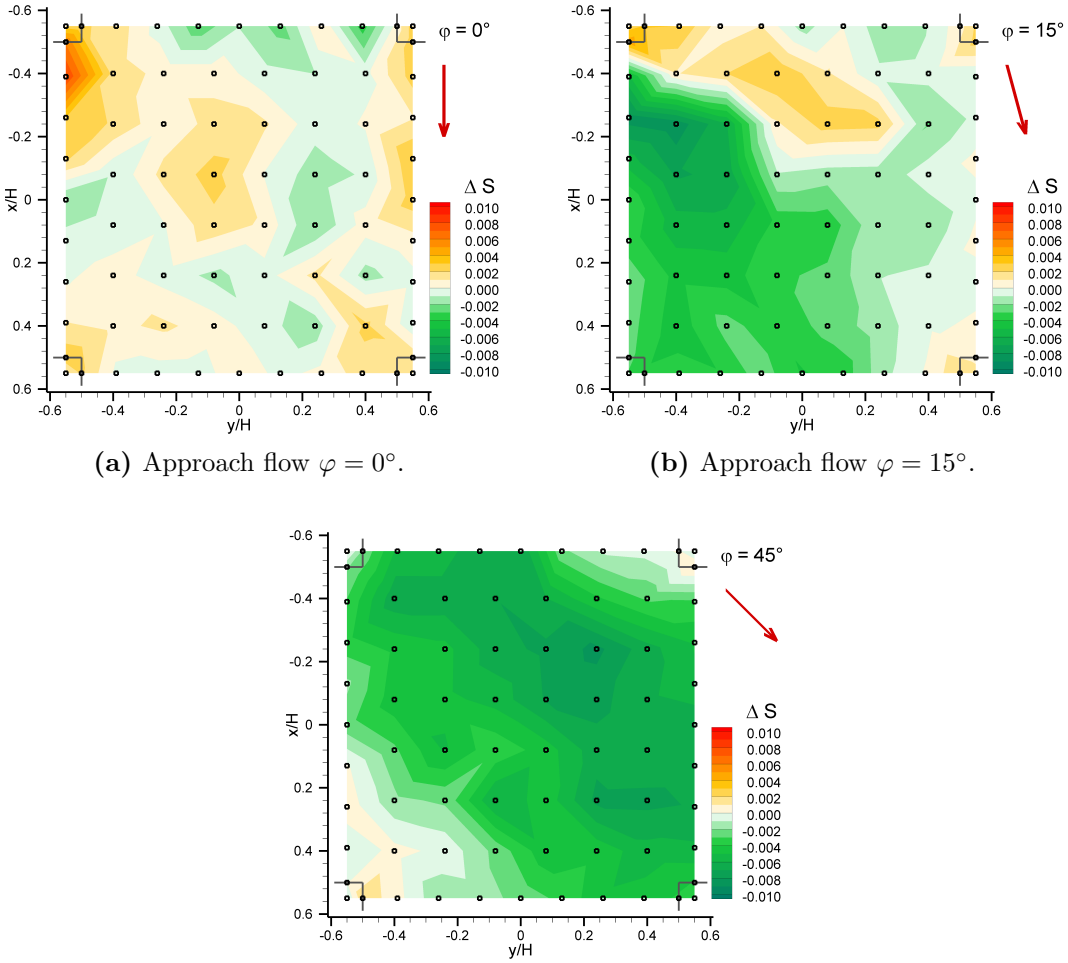

(a) Approach flow $\varphi = 0°$.

(b) Approach flow $\varphi = 15°$.

(c) Approach flow $\varphi = 15°$.

Figure 2.3: Difference ΔS between sweeps and ejection events in vertical momentum flux distribution in a horizontal plane at roof level above the studied intersection for 3 approach flow directions.

Acknowledgements

Authors kindly thank Charles University for support by grant GAUK No. 136609 (115-10/259266), the Ministry of Education, Sports and Youth of the Czech Republic for support by AVOZ20760514 and support of the Academy of Sciences of the Czech Republic.

2.5 References

S. E. Belcher. Mixing and transport in urban areas. *Philosophical Transactions of the Royal Society A: Mathematical, Physical and Engineering Sciences*, 363(1837):2947–2968, 2005. ISSN 1364-503X. doi: 10.1098/rsta.2005.1673.

URL http://rsta.royalsocietypublishing.org/cgi/doi/10.1098/rsta.2005.1673.

R. E. Britter and S. R. Hanna. Flow and Dispersion in Urban Areas. *Annual Review of Fluid Mechanics*, 35(1):469–496, jan 2003. ISSN 0066-4189. doi: 10.1146/annurev.fluid.35.101101.161147. URL http://www.annualreviews.org/doi/10.1146/annurev.fluid.35.101101.161147.

R. Kellnerova, L. Kukacka, and Z. Janour. Quadrant analysis of boundary layer above pitched and flat roofs. *Acta Technica CSAV (Ceskoslovensk Akademie Ved)*, 54(4):401–413, 2009. ISSN 00017043.

A. Robins, A. Scaperdas, E. Savory, E. Savory, D. Grigoriadis, A. Scaperdas, A. Robins, and D. Grigoriadis. Spatial variability and source-receptor relations at a street intersection. *Water, Air, and Soil Pollution: Focus*, 2(5):381–393, 2002. ISSN 1567-7230. doi: 10.1023/A:1021360007010. URL http://dx.doi.org/10.1023/A:1021360007010.

A. G. Robins. Short range dispersion in urban areas. Technical report, NCAS Urban Meteorology Workshop, Reading, 2009.

A. A. Townsend. *The Structure of Turbulent Shear Flow*. Cambridge University Press, New York, 1999. ISBN 0 521 20710.

X. Wang and K. F. McNamara. Effects of street orientation on dispersion at or near urban street intersections. *Journal of Wind Engineering and Industrial Aerodynamics*, 95(9-11):1526–1540, oct 2007. ISSN 01676105. doi: 10.1016/j.jweia.2007.02.021. URL http://linkinghub.elsevier.com/retrieve/pii/S0167610507000621.

3. Contribution of advective and turbulent contaminant transport to the intersection ventilation

In D. G. Steyn and S. T. Castelli, editors, *Proceeding of the 32nd NATO/SPS International technical meeting on air pollution modelling and its application, Air pollution modelling and its application XXII*, chapter Contribution of advective and turbulent contaminant transport to the intersection ventilation, pages 665–668. Springer, Dordrecht, Netherlands, 2014. ISBN 978-94-007-5576-5.

Libor Kukačka[1,2], Štěpán Nosek[2], Radka Kellnerová[1,2], Klára Jurčáková[2], Zbyněk Jaňour[2]

[1] Charles University in Prague, Faculty of Mathematics and Physics, Prague, Czech Republic
[2] Institute of Thermomechanics, Academy of Sciences of the Czech Republic, Prague, Czech Republic

Abstract
The objective of this experimental study is to determine processes of a pollution ventilation above the X-shaped street intersection in an idealised symmetric urban area for several approach flow directions. A unique experimental set-up for simultaneous measurement of the flow velocity and the tracer gas concentration in a high temporal resolution is assembled. Advective and turbulent vertical scalar fluxes are computed from the measured data in a horizontal plane above the street intersection. Vertical turbulent pollution transport was found to be a significant and positive contribution to the total vertical transport of pollutants form the intersection. Prevailing events in vertical scalar and momentum fluxes were determined using quadrant analysis.

Keywords
Air pollution, Boundary layer, Wind tunnel modelling, Contaminant transport, Pollution fluxes, Street canyon intersection.

3.1 Introduction

Dispersion of air pollution within urban areas is an important aspect of the environment quality for a significant part of the population. Traffic in street canyons is often a dominant source of pollutants in large cities, see Fenger (1999). Im-

provement of air quality in urban areas is necessary to avoid risk for human health, see Hoek et al. (2000). We can define ventilation of built-up areas as a process of changing polluted with a fresh air, which improves the air quality. Street intersections are very important in the redistribution of pollutants between streets and in the air exchanges between streets and the atmosphere. Characteristics of the transport pollution within the street intersection can be found in recent works (Carpentieri and Robins, 2010; Carpentieri et al., 2012; Soulhac et al., 2009). We focused on vertical ventilation processes in a complex and highly three-dimensional flow and concentration fields above the idealised street intersection. This study relates to former work published in Kukacka et al. (2011).

3.2 Experimental set-up

The experiment was conducted in the open low-speed wind tunnel of Institute of Thermomechanics Academy of Sciences of the Czech Republic in Nový Knín. According to the standard criteria, modeled boundary layer corresponded to a neutrally stratified boundary layer flow above a densely built-up area without much obstacle height variation. The model of an idealised symmetric urban area formed by apartment houses was designed according to common Central European inner-city areas. The model was scaled down to 1 : 200, the characteristic building height was $H = 120$ mm (24 m in full scale).

The turbulent momentum and mass transport was detected by simultaneous velocity and concentration measurement in a high temporal resolution using two-dimensional optical fibre Laser Doppler Anemometry (LDA) and Fast-response Flame Ionisation Detector (FFID). A point pollution source simulating a "pollution hotspot" (the place with higher emission of traffic pollution situated near a junction) was placed at the bottom of the street canyon in front of the studied street intersection.

3.3 Results

The vertical and longitudinal velocity with concentration of tracer gas were simultaneously measured in a horizontal plane at the roof-top level $z = H$ above the studied intersection. Results were obtained for five approach flow directions $\varphi = 0°, 5°, 15°, 30°$ and 45°. The dimensionless advective scalar fluxes were computed by C^*W/U_{2H}, where C^* means dimensionless pollutant concentration, W is the mean vertical velocity of the flow and U_{2H} means reference velocity measured at the reference height $z = 2H$, see Belcher (2005); Robins (2008); Carpentieri and Robins (2010). Dimensionless vertical turbulent scalar fluxes were computed from synchronised vertical velocity and concentration signals using eddy-correlation method. The turbulent scalar flux is given by $\langle c^{*\prime} w' \rangle / U_{2H}$, where $\langle\rangle$ is a time average, $c^{*\prime}$ and w' indicate fluctuations of dimensionless con-

centration and vertical velocity, respectively (see similar approach in Carpentieri et al. (2012)). The positive sign means the flux outwards and the negative sign means the flux inwards the street intersection. A contribution of the turbulent flux to the total flux was computed by $|\langle c^{*\prime} w^{\prime} \rangle| / (|\langle c^{*\prime} w^{\prime} \rangle| + |C^{*} W|)$, see Fig. 3.1.

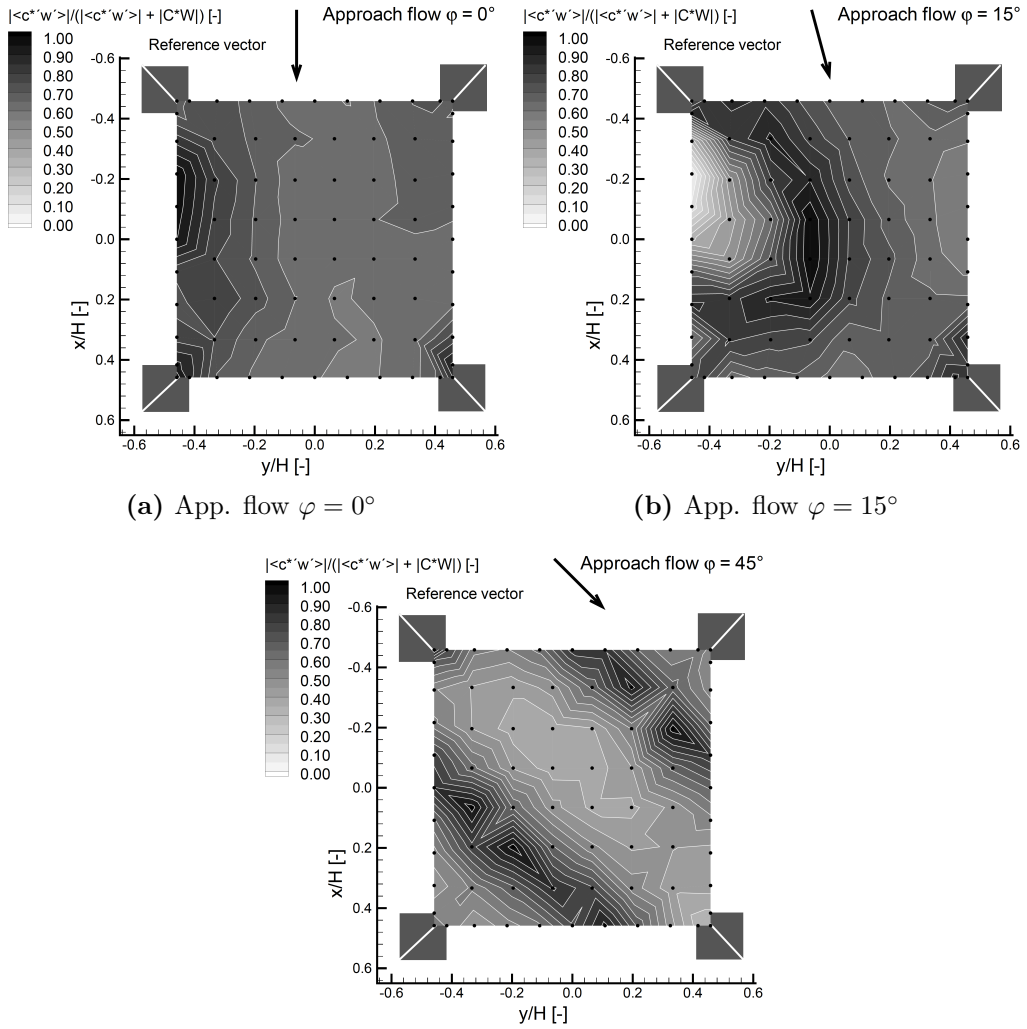

(a) App. flow $\varphi = 0°$

(b) App. flow $\varphi = 15°$

(c) App. flow $\varphi = 45°$

Figure 3.1: Contribution of the vertical turbulent pollution flux to the total vertical pollution flux at the roof top level above the street intersection (view from the top).

The quadrant analysis was applied to the velocity and concentration fluctuation time series. We used usual nomenclature published in Willmarth and Lu (1975):

"outward interaction" $(x^{\prime} > 0, w^{\prime} > 0)$,

"sweep" $(x^{\prime} > 0, w^{\prime} < 0)$,

"inward interaction" $(x' < 0, w' < 0)$,

"ejection" $(x' < 0, w' > 0)$,

where x' represents longitudinal velocity fluctuation u' or concentration fluctuation c'. The particular contribution from i^{th} quadrant to the total turbulent flux is given by $S_i = \langle x'w' \rangle_i \, N_i/N_{total}$, where N_i is the number of events in the i^{th} quadrant, number of all measured events is N_{total}. The relative contribution of the prevailing event S_{max} to the total momentum flux is given by $|S_{max}|/\sum |S_i| \cdot 100\%$, see Fig. 3.2.

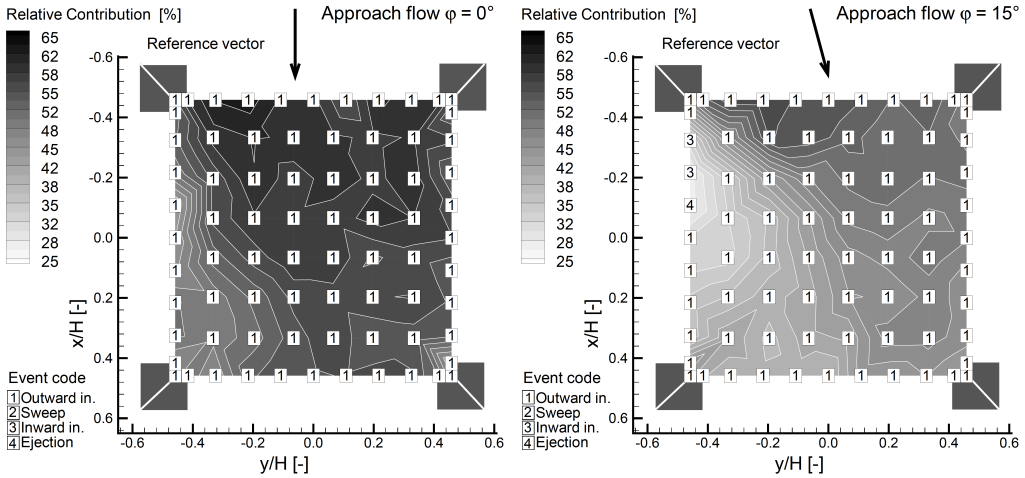

(a) App. flow $\varphi = 0°$

(b) App. flow $\varphi = 15°$

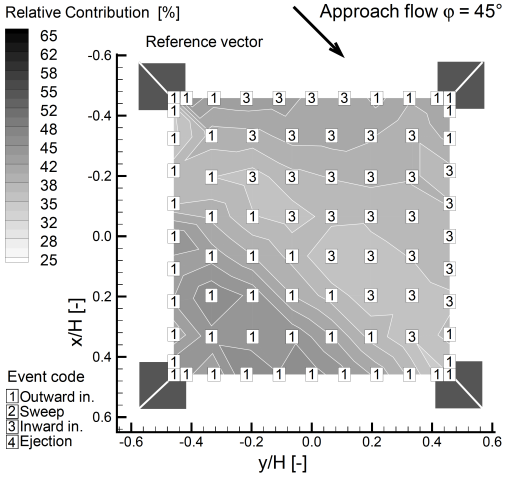

(c) App. flow $\varphi = 45°$

Figure 3.2: Relative contributions of the dominant event to the total turbulent flux of the passive contaminant at the roof top level above the street intersection (view from the top).

3.4 Conclusions

Vertical advective and turbulent fluxes of pollution were measured above the modeled X-shaped street intersection in an idealized symmetrical urban area. Determined vertical turbulent flux comprised significant and positive contribution to the ventilation of the area. The quadrant analysis was applied to the synchronized velocity and concentration signals. In the area of the significant advective pollution transport, sweeps were found to be events with the dominant contribution to the vertical momentum flux. We determined the outward interaction and to a lesser extent inward interaction as a dominant event in the vertical turbulent pollution flux.

Acknowledgements
The authors thank the Ministry of Education, Sports and Youth of the Czech Republic (projects AVOZ-20760514 and COST1006 LD 12007), the Czech Science Foundation GACR (project P101/12/1554) and the Charles University in Prague (project GAUK No. 535412) for their financial support.

3.5 References

S. E. Belcher. Mixing and transport in urban areas. *Philosophical Transactions of the Royal Society A: Mathematical, Physical and Engineering Sciences*, 363(1837):2947–2968, 2005. ISSN 1364-503X. doi: 10.1098/rsta.2005.1673. URL `http://rsta.royalsocietypublishing.org/cgi/doi/10.1098/rsta.2005.1673`.

M. Carpentieri and A. G. Robins. Tracer flux balance at an urban canyon intersection. *Boundary-Layer Meteorology*, 135(2):229–242, feb 2010. ISSN 00068314. doi: 10.1007/s10546-010-9471-6. URL `http://link.springer.com/10.1007/s10546-010-9471-6`.

M. Carpentieri, P. Hayden, and A. G. Robins. Wind tunnel measurements of pollutant turbulent fluxes in urban intersections. *Atmospheric Environment*, 46: 669–674, jan 2012. ISSN 13522310. doi: 10.1016/j.atmosenv.2011.09.083. URL `http://linkinghub.elsevier.com/retrieve/pii/S1352231011010909`.

J. Fenger. Urban air quality. *Atmospheric Environment*, 33(29):4877–4900, 1999. ISSN 13522310. doi: 10.1016/S1352-2310(99)00290-3.

G. Hoek, B. Brunekreef, A. Verhoeff, J. V anWijnen, and P. Fischer. Daily mortality and air pollution in the Netherlands. *Journal of the Air and Waste Management Association*, 50(8):1380–1389, aug 2000. ISSN 21622906. doi: 10.1080/10473289.2000.10464182. URL `http://www.tandfonline.com/doi/abs/10.1080/10473289.2000.10464182`.

L. Kukacka, R. Kellnerova, K. Jurcakova, and J. Zbynek. Analysis of scalar fluxes and flow within modelled intersection depending on the approach flow direction. In D. G. Steyn and S. T. Castelli, editors, *Proceeding of the 31st NATO/SPS International technical meeting on air pollution modelling and its application Air Pollution Modeling and its Application XXI*, pages 113–118. Springer, Dordrecht, Netherlands, 2011. ISBN 978-94-007-1361-1.

A. Robins. DAPPLE (dispersion of air pollution and its penetration into the local environment) experiments and modelling. *HPA Chemical Hazards and Poisons Report*, 13(September):24–28, 2008.

L. Soulhac, V. Garbero, P. Salizzoni, P. Mejean, and R. J. Perkins. Flow and dispersion in street intersections. *Atmospheric Environment*, 43(18):2981–2996, jun 2009. ISSN 13522310. doi: 10.1016/j.atmosenv.2009.02.061. URL `http://linkinghub.elsevier.com/retrieve/pii/S1352231009001186`.

W. W. Willmarth and S. S. Lu. Structure of the reynolds stress and the occurrence of bursts in the turbulent boundary layer. *Advances in Geophysics*, 18(PA): 287–314, 1975. ISSN 00652687. doi: 10.1016/S0065-2687(08)60467-7.

4. Quadrant analysis of turbulent pollution flux above the modelled street intersection

The European Physical Journal, 2013, Volume 45, p. 1-13. Article ID 01053. ISSN 2100-014X. doi: 10.1051/epjconf/20134501053

Libor Kukačka[1,2], Štěpán Nosek[2], Radka Kellnerová[1,2], Klára Jurčáková[2], Zbyněk Jaňour[2]

[1] Charles University in Prague, Faculty of Mathematics and Physics, Prague, Czech Republic
[2] Institute of Thermomechanics, Academy of Sciences of the Czech Republic, Prague, Czech Republic

Abstract
The objective of this experimental study is to determine processes of a vertical turbulent pollution transport above the X-shaped street intersection in an idealised symmetric urban area for several approach flow directions. An experimental set-up for simultaneous measurement of the flow velocity and the tracer gas concentration in a high temporal resolution is assembled. Vertical turbulent scalar fluxes are computed from the measured data in a horizontal plane above the street intersection. The quadrant analysis was applied to the vertical turbulent pollution fluxes data. Events with dominant contribution to vertical turbulent pollution flux were detected. The mean duration, repetition frequency and the duration percentage were computed for these events. A strong influence of the approach flow direction on the the type of dominant events and their characteristics was resolved.

4.1 Introduction

Dispersion of air pollution within urban areas is an important aspect of the environment quality for a significant part of the population. Traffic in street canyons is often a dominant source of pollutants in large cities (Fenger, 1999). Improvement of air quality in urban areas is necessary to avoid risk for human health (Hoek et al., 2000). We focused on vertical turbulent pollution transport in a complex and highly three-dimensional flow and concentration fields above the idealised street intersection. This study relates to former published work (Kukacka et al., 2012).

Street intersections are very important in the redistribution of pollutants between streets and in the air exchanges between streets and flow above the canopy layer. Characteristics of the transport pollution within the street intersection can be found in recent works (Carpentieri and Robins, 2010; Carpentieri et al., 2012; Soulhac et al., 2009). Understanding processes of pollution transport in complex urban areas is important for estimation of ventilation intensity in the polluted street canyons, for finding suitable configuration of built-up areas and for developing local scale dispersion models.

The quadrant analysis is usually the first step to investigate the turbulent processes in strongly turbulent flow. It is usually applied to the turbulent momentum flux (Kellnerova et al., 2009; Feddersen, 2005). Using this analysis, the prevailing events in the flow can be detected. There have been only several studies using quadrant analysis for turbulent scalar flux investigation, but only in the flow above relatively homogeneous surface, e.g. (Katul et al., 1997; Raupach, 1981). The quadrant analysis is applied newly to the turbulent scalar flux in highly turbulent a tree dimensional flow in this work.

4.2 Experimental set-up

4.2.1 Wind tunnel

The experiment was conducted in the open low-speed wind tunnel of Institute of Thermomechanics Academy of Sciences of the Czech Republic in Nový Knín. The cross-dimension of the tunnel test section was 1.5×1.5 m, the length of the test section was 2 m. The scheme of the tunnel is depicted in figure 4.1.

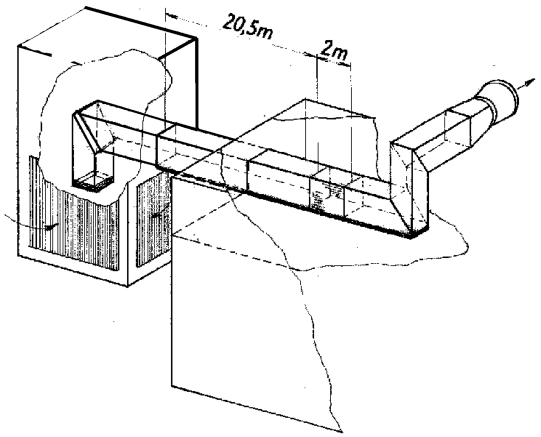

Figure 4.1: The scheme of the open low-speed wind tunnel.

Fully turbulent boundary layer was developed by the 20.5 m long development section of the tunnel. This section was equipped by turbulent generators at the beginning and covered by 50 mm and 100 mm high roughness elements on the floor, see the photo in figure 4.2.

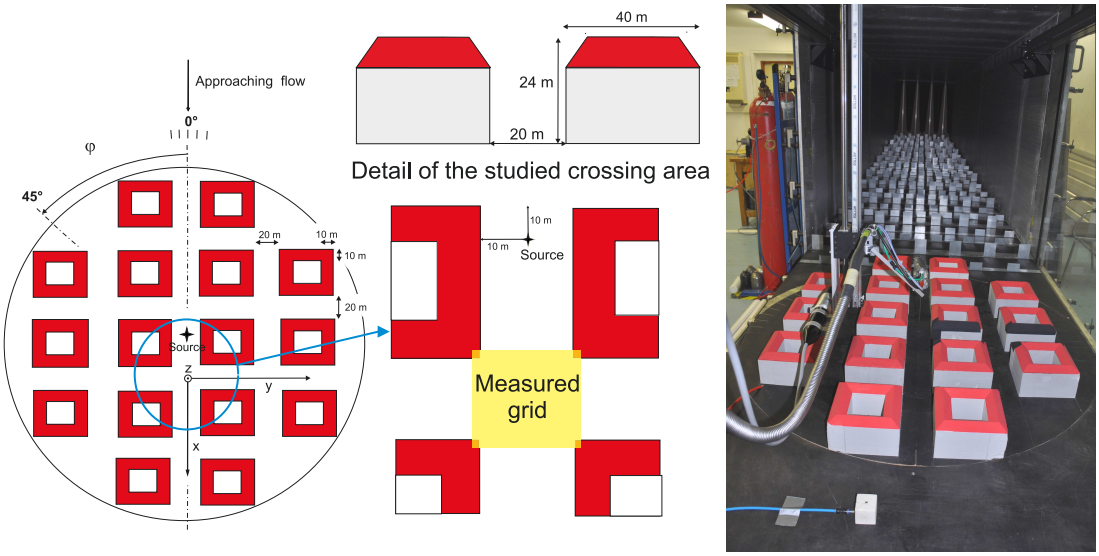

Figure 4.2: Scheme of the idealised symmetric urban area model (left), the studied X-shaped intersection (middle) and the photograph of the model placed in the wind tunnel (right).

4.2.2 Urban area model

The model of idealised symmetric urban area with apartment houses was designed according to the common Central European inner-city area. Regular blocks of apartment houses with pitched roofs formed a perpendicular arrangement of the street canyons and X-shaped intersections, see figure 4.2.

The model was scaled down to 1 : 200. The model buildings were formed by the body of height 100 mm and width 50 mm with pitched roof of height 20 mm. We set up the characteristic building height $H = 120$ mm (24 m in full scale) as the height of building body with the roof.

The width of street canyons was $L = 100$ mm. The aspect ratio of the street canyons given by the building height H and the street width S was $H/L = 1.2$.

A point tracer gas source simulating a "pollution hot spot" (the place with higher emission of traffic pollution situated near a junction) was placed at the bottom of the street canyon in front of the studied intersection, see the scheme in figure 4.2.

4.2.3 Measurement techniques

The flow characteristics were measured by a two-dimensional optical fibre Laser Doppler Anemometry based on DANTEC BSA F-60 burst processor (LDA). Tracing particles (glycerine droplets with approximately 1 μm diameter) were produced by a commercial haze generator placed at the beginning of the tunnel generating section, in front of turbulent generators. We got the air flow in the test section equally filled by seeding particles after running the haze generator

inside the tunnel for several minutes. Data rate reached about 100 Hz at the bottom levels of street canyons $z \lesssim 0.5H$ and up to 1000 Hz at the roof top level $z \approx H$. The time of recording was 180 s in all the cases.

Point concentration measurements of tracer gas were realised by Fast-response Flame Ionisation Detector HFR-400 Atmospheric Fast FID (FFID) made by Cambustion Ltd. The detector was set to acquire data at a data rate of 1 KHz. The sampling time was 180 s in all of the cases. We used ethane as the tracer gas simulating passive pollutants. Ethane is passive and non-reactive gas with its own density $\rho_{Ethane} = 1.24$ kg m^{-3} close to density of the air $\rho_{Air} = 1.28$ kg m^{-3}.

Simultaneous vertical velocity and concentration measurement at the roof top level above the intersection was realised using LDA and FFID. LDA and FFID probes were mounted on the traverse system in a way that the measuring volume of the LDA was close to the intake to the FFID sampling tube. The sampling tube intake was placed 1.5 mm above, 1 mm behind and 1 mm beside the centre of the LDA measuring volume, see figure 4.3.

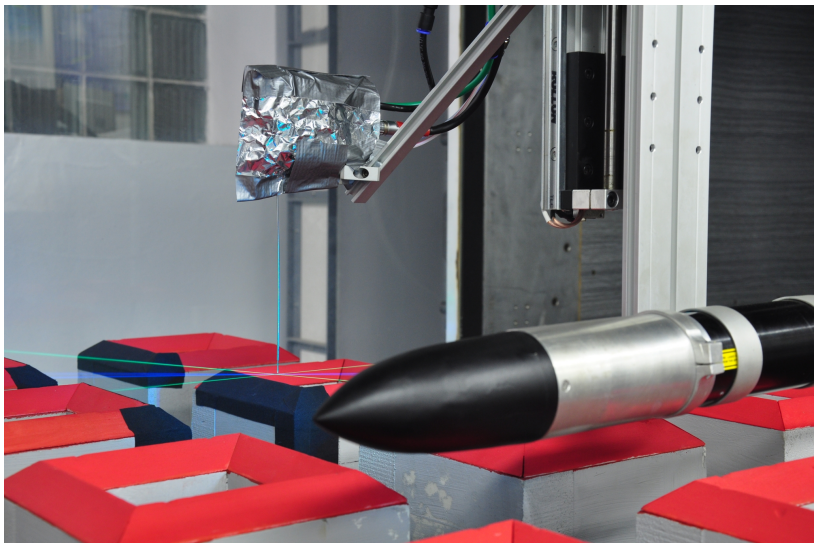

Figure 4.3: The configuration of the FFID (left) and LDA (right) probes mounted on the traverse system in the wind tunnel.

As expected, the presence of the seeding particles in the air during simultaneous LDA and FFID measurement influenced FFID output signal. We got isolated spikes in the recorded concentration signal probably due to suction of combustible aerosol particles into the FFID probe, see Hall and Emmott (1991); Contini et al. (2006). We got similar count of spikes in time series obtained from measurements in clean air and in air contained seeding particles in most cases unlike these published results. We neglected the influence of spikes on the results because the frequency of isolated spikes was about 0.006% of used sampling data rate.

The second influence of seeding particles on the measured concentration data was an almost constant shift of recorded concentration values caused obviously

by sucking seeding particles by FFID probe. This shift reached about 0.5% of the FFID measuring range. The shift was corrected by the calibration sequence.

4.2.4 Boundary layer characteristics

Fully turbulent boundary layer was developed by spires and roughness elements placed it the tunnel. The characteristics of the boundary layer above the urban area model were measured with a two-dimensional LDA system in four vertical profiles placed above, upstream and downstream from the studied intersection, see figure 4.4.

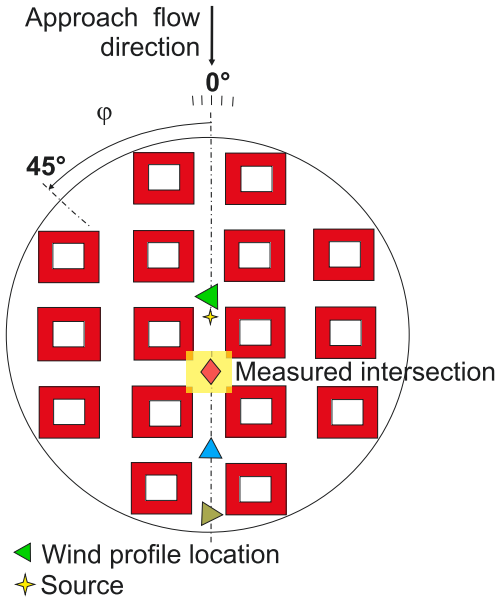

Figure 4.4: Wind profile measurement locations.

The vertical profile of mean longitudinal velocity is depicted in figure 4.5a, the momentum flux profile can be found in figure 4.5b. The vertical profiles of longitudinal and vertical turbulent intensity are plotted in figures 4.5c and 4.5d. The high above the surface is expressed in full scale.

Vertical profiles of measured turbulent approach flow characteristics were fitted by the logarithmic and the power law. Mean roughness length z_0, displacement d_0 and friction velocity u_* (alias square-root of constant Rey-nolds stress within the inertial sublayer) were obtained from the log wind profile fitting. Power exponent α was obtained from the power wind profile fitting. The parameters are listed in table 4.1. Measured parameters corresponded to a neutrally stratified boundary layer flow above a densely built-up area without much obstacle height variation. We used boundary layer classification according VDI (2000).

To verify requirements for the Townsend hypothesis Townsend (1999) the critical Reynolds building number Re_B was found. For our experiment, the modified

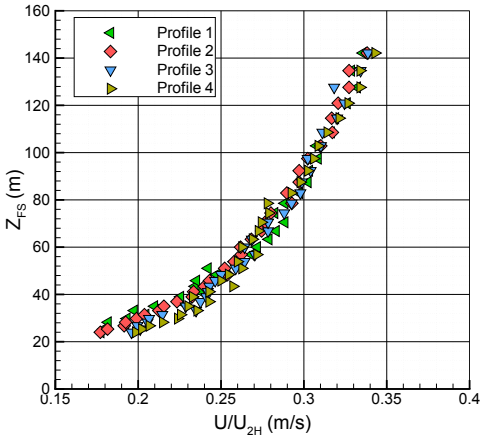

(a) The vertical profiles of mean longitudinal velocity.

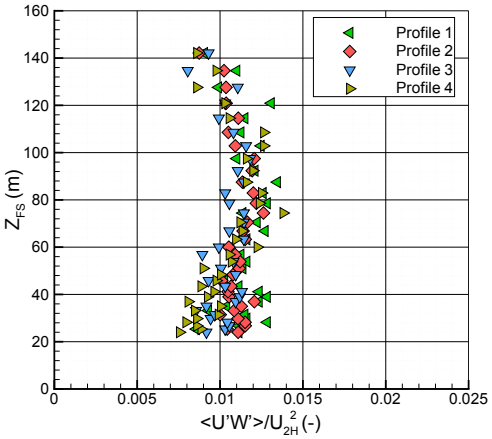

(b) The vertical profiles of mean momentum flux.

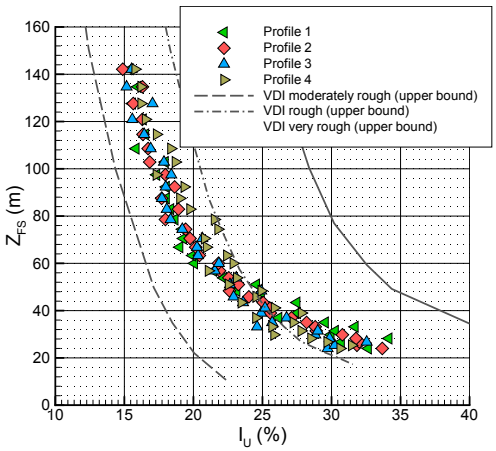

(c) The vertical profiles of longitudinal turbulent intensity.

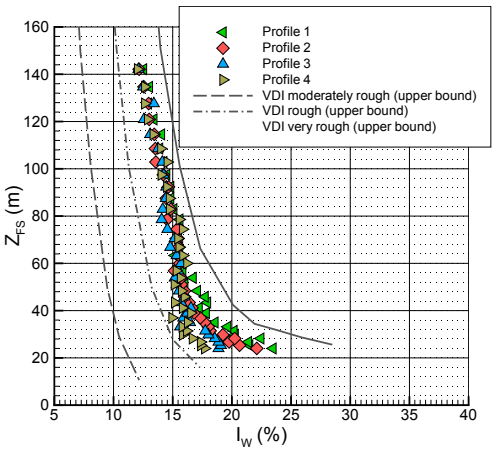

(d) The vertical profiles of vertical turbulent intensity.

Figure 4.5: Boundary layer characteristics above the urban area model.

Table 4.1: Parameters of modelled boundary layer above the measured area (in full scale).

$z_0\,(m)$	$d_0\,(m)$	$\alpha\,(-)$	$u_*/U_{2H}\,(-)$
0.83	13.40	0.24	0.096

Reynolds building number was given by

$$Re_B = \frac{U_{2H}H}{\nu}, \tag{4.1}$$

where U_{2H} is reference longitudinal velocity measured at a height of $z = 2H$ and ν is kinematic viscosity. This criterion is used for the flow within street canyons to be independent of viscous effects Meroney et al. (1996); Pavageau and

Schatzmann (1999). The experiment was carried out by $Re_B \approx 21000$ that lies on the lower edge of determined interval for valid Towsend hypothesis. Free stream velocity was approximately 4 m s^{-1}.

4.3 Results

4.3.1 Turbulent scalar flux fields

The vertical and longitudinal velocity with concentration of tracer gas were simultaneously measured in a horizontal plane at the roof-top level $z = H$ above the studied intersection. Results were obtained for five approach flow angles $\varphi = 0°, 5°, 15°, 30°$ and $45°$.

The used Matlab post-processing script for synchronising simultaneously acquired vertical velocity and concentration data using the maximum of correlation between both signals. The synchronised time series were shifted by an average of 15 ms. This shift expressed the delay between a suck of the sample into the intake of the FFID probe tube and the moment of the sample analysing in the probe. The value of the shift agrees with very similar experimental set up published by Contini et al. (2006).

The dimensionless vertical turbulent scalar fluxes were computed from synchronised vertical velocity and concentration signals using eddy-correlation method Arya (1998); Stull (1988) using

$$\left\langle c^{*\prime} w^{\prime} \right\rangle \frac{1}{U_{2H}}, \tag{4.2}$$

where $\langle\rangle$ is the time average, $c^{*\prime}$ and $w^{\prime}$ indicate fluctuations of dimensionless concentration and vertical velocity, respectively (see similar approach in Carpentieri et al. (2012)). These computed fluxes express a rate of emissions spreading through a unit area by turbulent transport. The positive sign means the flux outwards and the negative sign means the flux inwards the street intersection.

Values of determined vertical turbulent fluxes for the four approach flow directions are plotted in figure 4.6. We measured relatively flat turbulent flux field with small and positive values by angle 0°, see figure 4.6a. In case 15° there are significantly positive values on the upwind side of the area, see figure 4.6c. This phenomenon became stronger by angle 45°, see figure 4.6d. We estimated a significant turbulent transport of pollution near the leeward side of the buildings, see the upper part of figures 4.6a and 4.6b.

4.3.2 Quadrant analysis

The quadrant analysis was applied to the synchronised velocity and concentration fluctuation time series. We used usual nomenclature published in Willmarth and Lu (1975):

1^{st} quadrant "outward interaction" $(x^{\prime} > 0, w^{\prime} > 0)$,

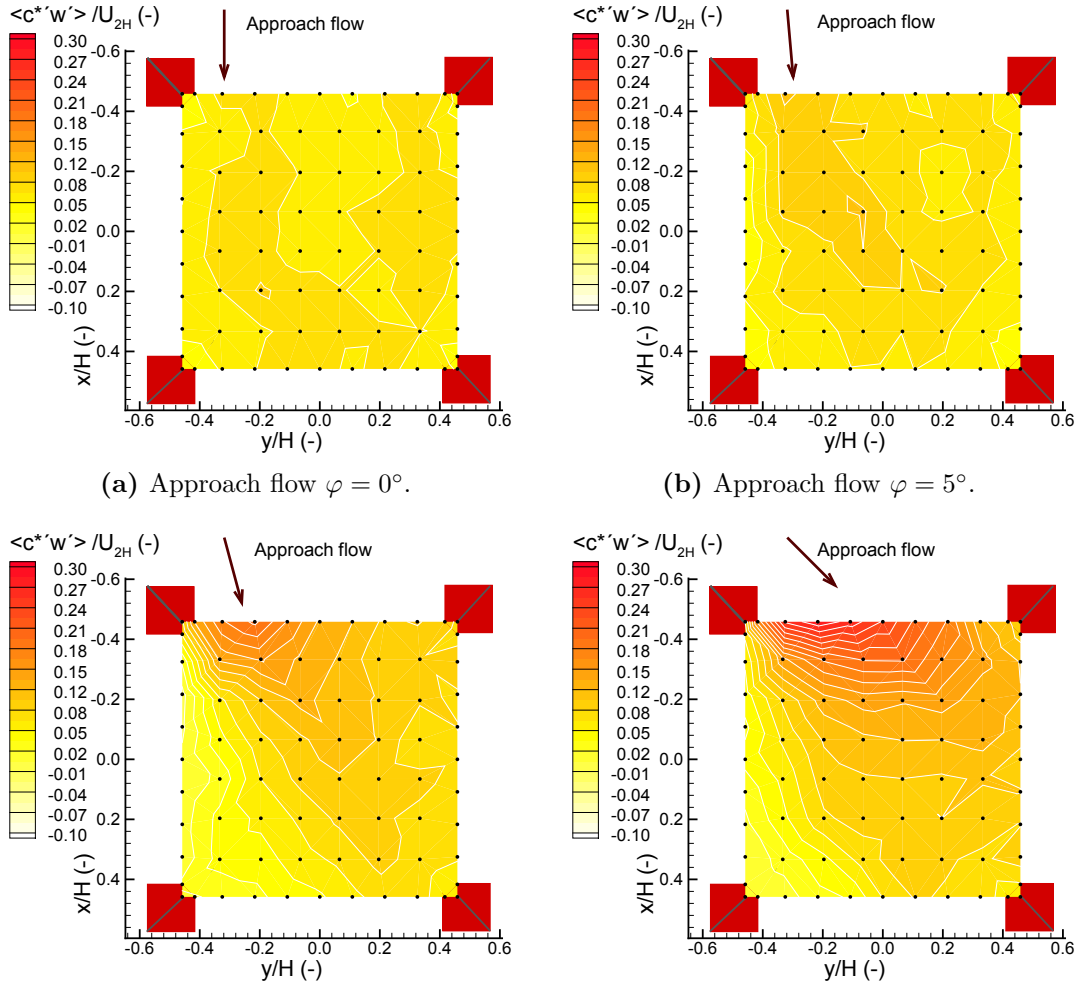

(a) Approach flow $\varphi = 0°$.

(b) Approach flow $\varphi = 5°$.

(c) Approach flow $\varphi = 15°$.

(d) Approach flow $\varphi = 45°$.

Figure 4.6: Vertical dimensionless turbulent scalar flux $\langle c^{*\prime} w^{\prime} \rangle / U_{2H}$ for four angles of the approach flow direction.

2^{st} quadrant "sweep" $(x^{\prime} > 0, w^{\prime} < 0)$,

3^{st} quadrant "inward interaction" $(x^{\prime} < 0, w^{\prime} < 0)$,

4^{st} quadrant "ejection" $(x^{\prime} < 0, w^{\prime} > 0)$,

where $x^{\prime}$ represents dimensionless concentration fluctuation $c^{*\prime}$. These definitions are illustrated in figure 4.7 bellow. The threshold time and value was used to identify individual events in fluctuation signals. The threshold time was set to 2 ms as a duration of two consecutive time steps in measured signal. The threshold value was used 0.0005 (-) as a minimum value that can be resolved from an electric noise in the signals.

The particular contribution from i^{th} quadrant to the total turbulent pollution

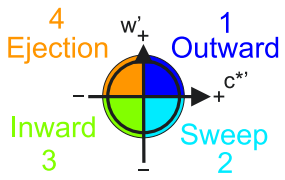

Figure 4.7: The scheme of event definitions used in quadrant analysis of turbulent pollution flux.

flux $\langle c^{*\prime} w^{\prime} \rangle / U_{2H}$ is given by

$$S_i = \frac{\langle c^* w^{\prime} \rangle_i N_i}{N_{total}}, \tag{4.3}$$

where N_i is the number of events in the i^{th} quadrant and N_{total} is number of all measured events.

The relative contribution of the prevailing event to the total scalar flux was computed as

$$\frac{S_{max}}{\sum S_i} 100\%, \tag{4.4}$$

where S_{max} is the particular contribution from the dominant event. These contributions of the prevailing events are plotted in figure 4.8 for four approach flow directions. As you see in figures 4.8a, 4.8b and 4.8c, outward interactions dominated in the area for smaller approach wind directions. It means, that particles of air with a positive fluctuation of the vertical velocity and concentration were transported upwards from the intersection. There is a large area with domination of inward interaction for approach flow angle $\varphi = 45°$, see figure 4.8d. The positive vertical turbulent flux is formed mostly by downwards moving particles of fresh air in this area.

The mean dimensionless duration was computed for the dominant events as

$$\langle t_i \rangle_{S_{max}} \frac{U_{2H}}{H}, \tag{4.5}$$

where t_j is the measured duration of the dominant event. Values of mean durations are depicted in figure 4.9 for four approach flow angles.

The mean dimensionless repetition frequency was computed for dominant events using

$$\left\langle \frac{1}{\tau_j} \right\rangle_{S_{max}} \frac{H}{U_{2H}}, \tag{4.6}$$

where τ_j is the measured duration between two dominant events. Computed repetition frequencies are plotted in figure 4.10 for the four approach flow directions.

We can compare figures 4.6, 4.9 and 4.10 now. It is obvious that the outward interactions with low repetition frequencies and relatively long durations dominated in a low and positive vertical turbulent transport for lower approach flow angles 0° and 5°; compare figures 4.9a and 4.10a, figures 4.9b and 4.10b. The

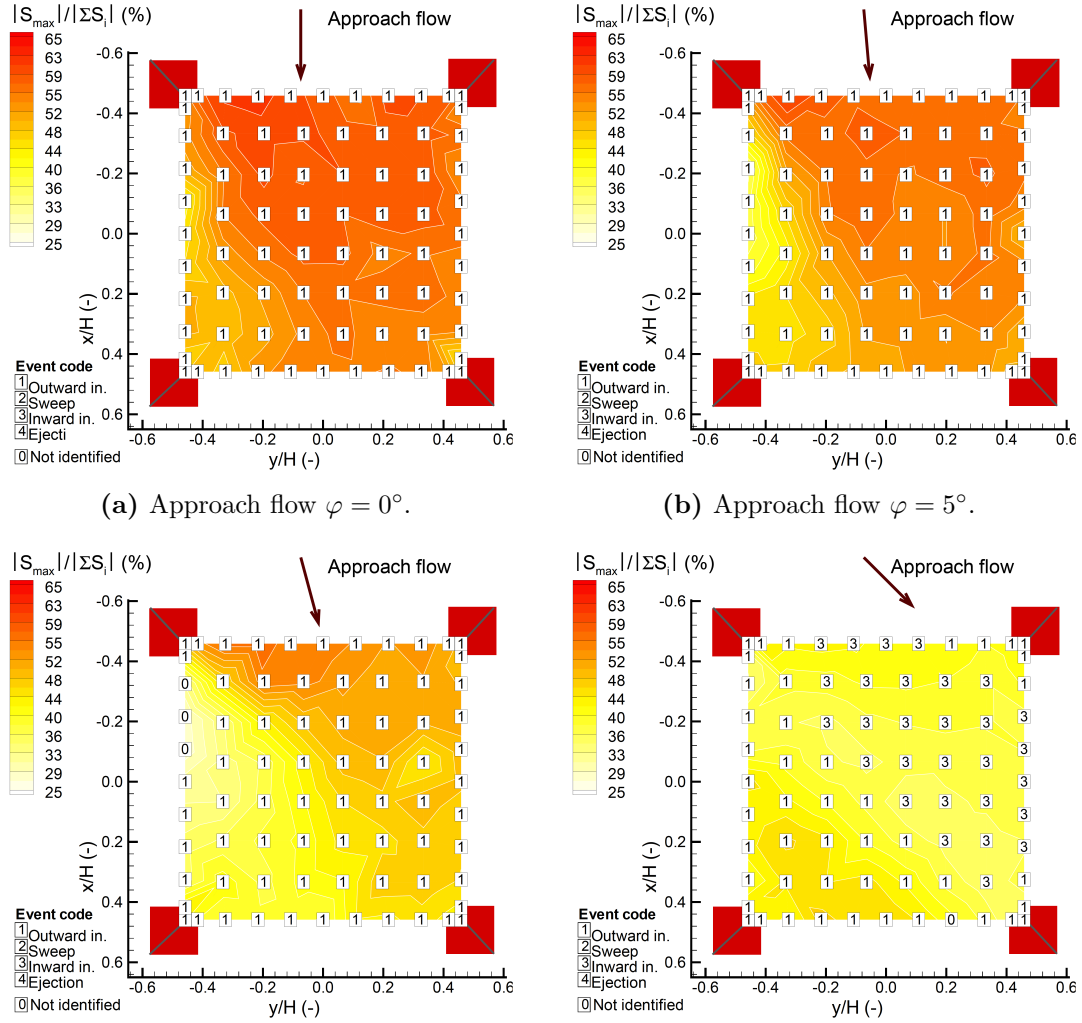

(a) Approach flow $\varphi = 0°$.

(b) Approach flow $\varphi = 5°$.

(c) Approach flow $\varphi = 15°$.

(d) Approach flow $\varphi = 45°$.

Figure 4.8: The relative contribution of the prevailing event to the total scalar flux $S_{max}/\sum S_i 100\%$.

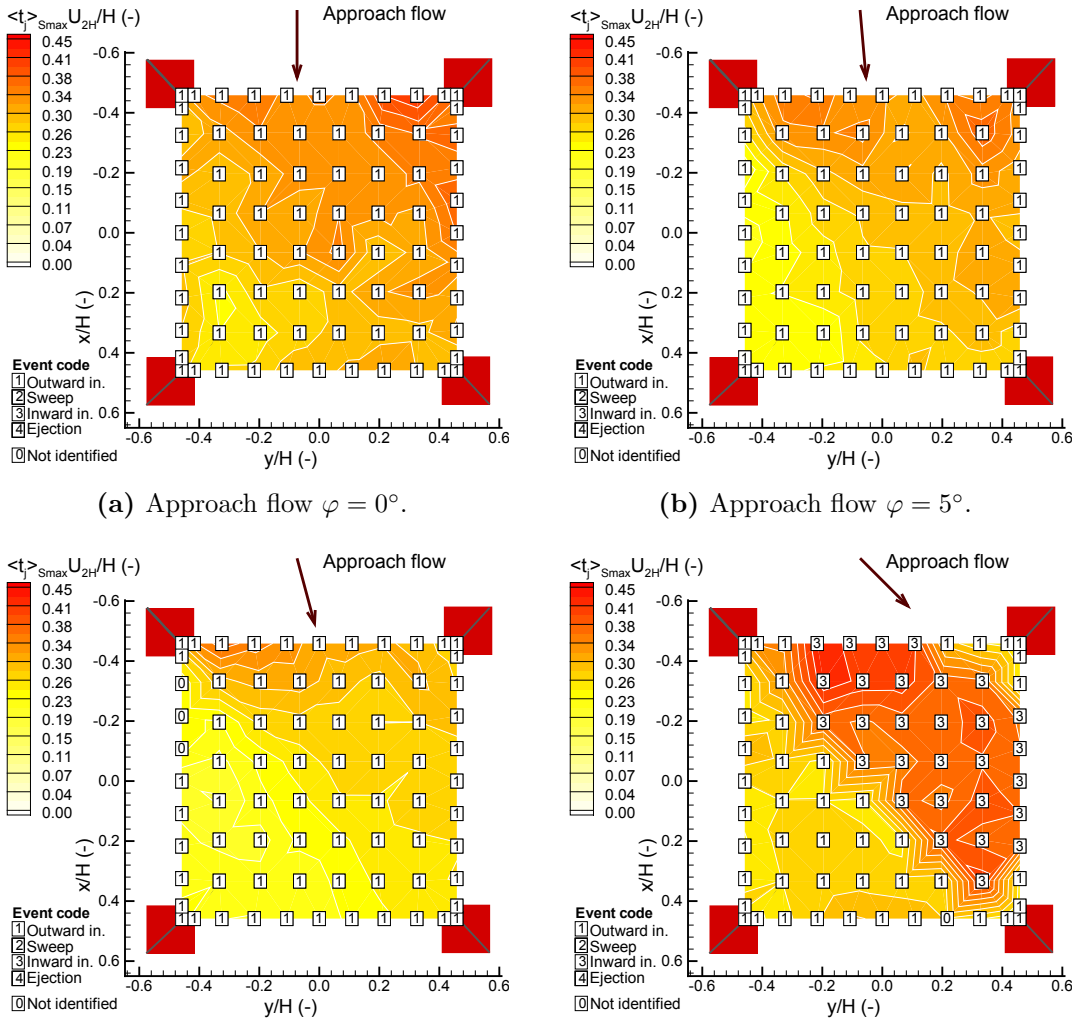

(a) Approach flow $\varphi = 0°$.

(b) Approach flow $\varphi = 5°$.

(c) Approach flow $\varphi = 15°$.

(d) Approach flow $\varphi = 45°$.

Figure 4.9: The mean dimensionless duration of the dominant events $\langle t_j \rangle_{S_{max}} U_{2H}/H$.

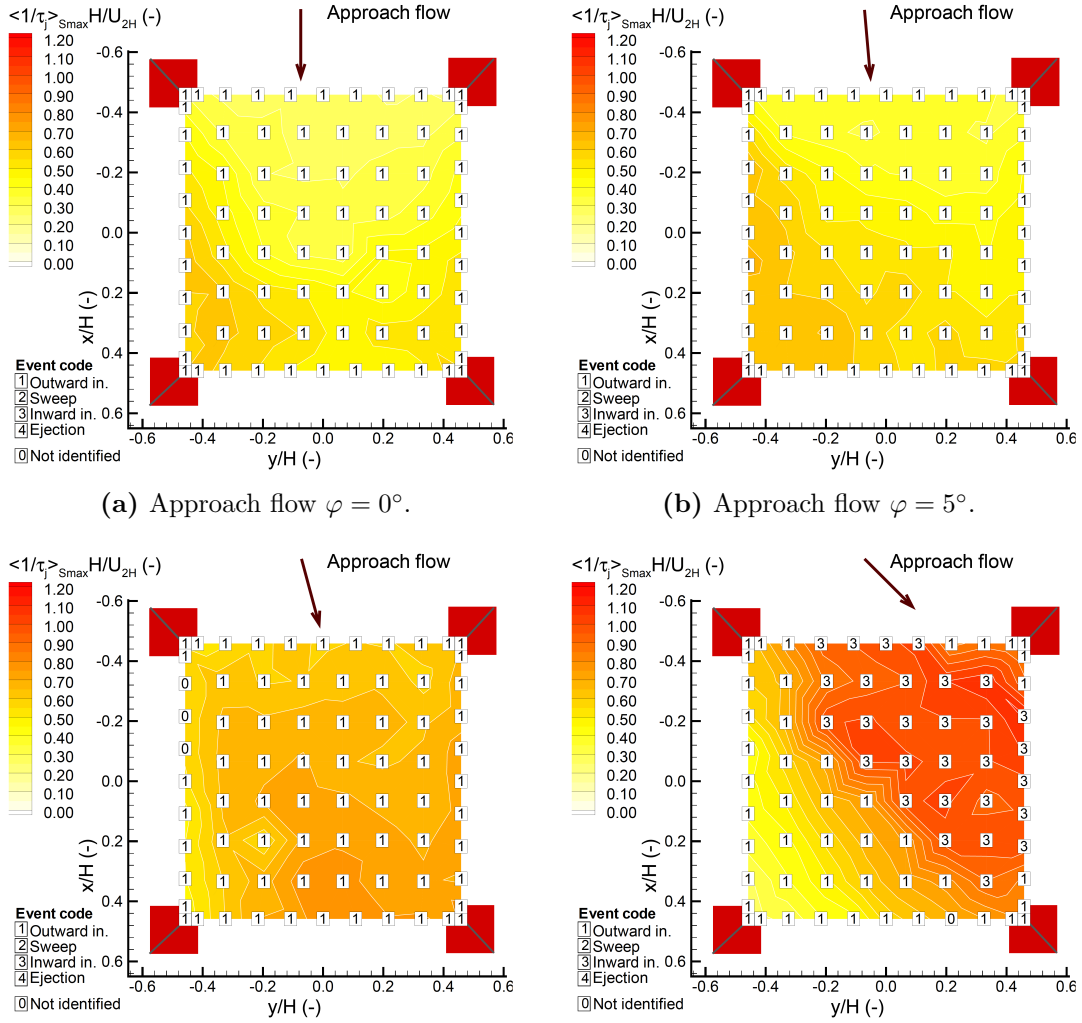

(a) Approach flow $\varphi = 0°$.

(b) Approach flow $\varphi = 5°$.

(c) Approach flow $\varphi = 15°$.

(d) Approach flow $\varphi = 45°$.

Figure 4.10: The mean dimensionless repetition frequency of the dominant events $\langle 1/\tau_j \rangle_{S_{max}} H/U_{2H}$.

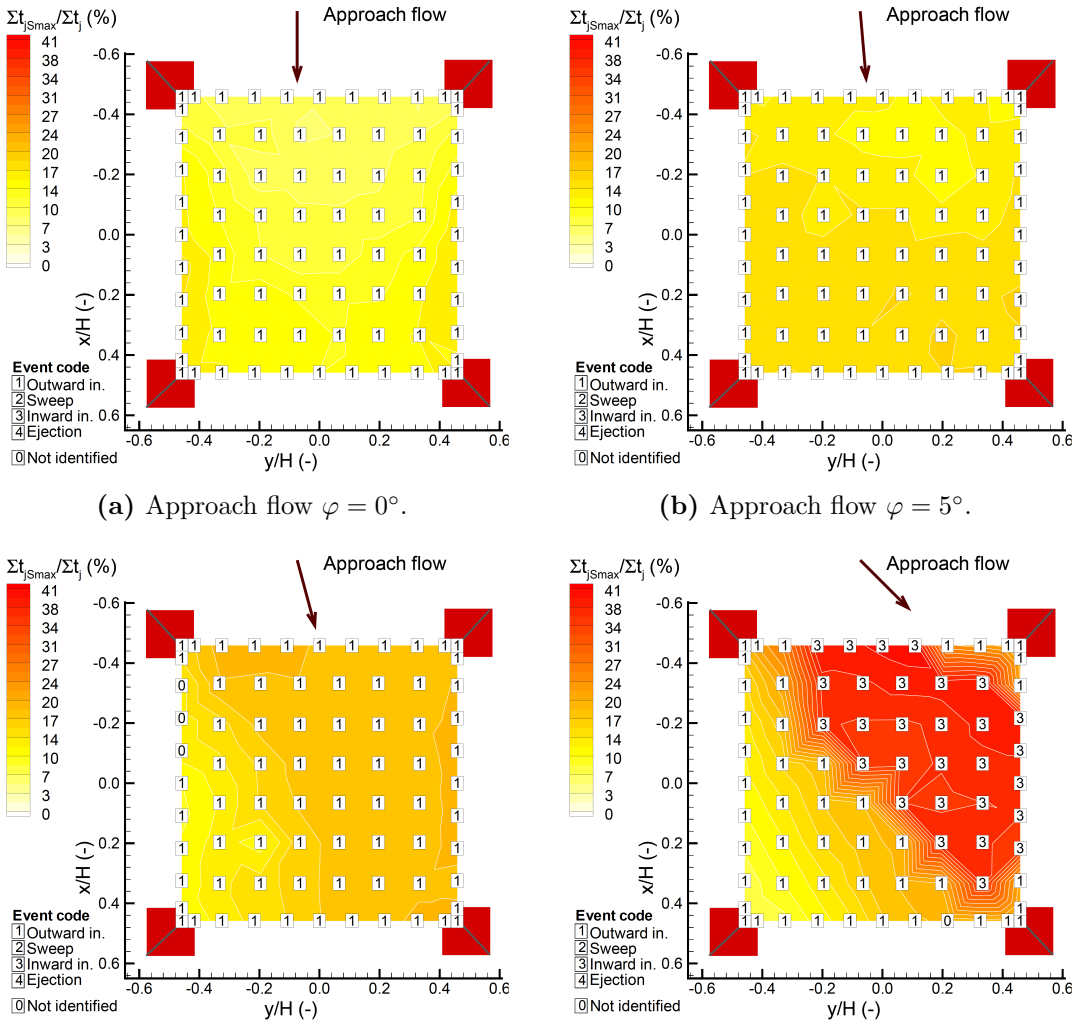

(a) Approach flow $\varphi = 0°$.

(b) Approach flow $\varphi = 5°$.

(c) Approach flow $\varphi = 15°$.

(d) Approach flow $\varphi = 45°$.

Figure 4.11: The duration percentage of the dominant events $\Sigma t_{jS_{max}}/\Sigma t_j 100\%$.

repetition frequency increased and duration slightly decrease in case of angle 15°, compare figures 4.9c and 4.10c. This can be observed by angle 30°, as well (not shown). The inward interactions with high frequencies and long durations dominated in the intensive positive turbulent flux in the last situation by approach flow angle 45°, see figures 4.9d and 4.10d.

Measured values of the mean dimensionless duration of dominant events between 0.20–0.45 correspond to durations around 1.6–3.6 s in a real symmetric urban area with $H = 24$ m and $U_{2H} = 3$ m s^{-1}. In case of repetition frequencies, measured values 0.5–1.2 correspond to 0.06–0.15 Hz. It means that periods of events reach values around 6.5–16.0 s.

The duration percentage of the dominant events was computed as the last quantity by

$$\frac{\Sigma t_{jS_{max}}}{\Sigma t_j} 100\%, \tag{4.7}$$

where $t_{jS_{max}}$ is the duration of the dominant event and t_i is duration of every detected event. The duration percentage is shown in figure 4.11 for the four approach flow directions. The dominate outward interactions influenced the vertical pollution turbulent flux for a relatively short time in lower approach flow angles 0° and 5°, see figures 4.11a and 4.11b. The duration percentage of outward interaction obviously increase with increasing angle, see figure 4.11c. The dominant inward interaction were detected in up to 40% of measured period in case of angle 45°, see figure 4.11d.

4.4 Conclusions

Vertical turbulent pollution fluxes were measured in a horizontal plane above the modeled X-shaped street intersection in an idealized symmetrical urban area for five wind directions. An experimental set-up for simultaneous measurement of the flow velocity and the tracer gas concentration was designed and assembled, based on Fast-response Flame Ionisation Detector and Laser Doppler Anemometer.

The influence of the approach flow direction on the vertical turbulent pollution fluxes were determined. The increasing vertical turbulent pollution flux was observed with diverging approach flow direction from the street with pollution source.

The quadrant analysis was applied to the vertical turbulent pollution fluxes data. We determined that the vertical turbulent pollution flux is caused by transport of polluted air particles upward from the intersection (outward interactions) in case of approach flow almost parallel to the street canyon with the pollution source. The turbulent pollution flux reach low magnitude in these cases. Outward interactions reached low repetition frequencies and relatively long durations. In general, the outward interactions influenced the vertical pollution turbulent flux for a relatively short time compared with the total duration of all detected events.

Transport of fresh air downward into the street intersection (inward interaction) dominated in the vertical turbulent flux for diverging approach flow from

the street with the pollution source. These dominate events reached high repetition frequencies and long durations. The outward interactions were present in almost half of the total duration of all detected events.

Acknowledgements
The authors kindly thank the Ministry of Education, Sports and Youth of the Czech Republic (project AVOZ-20760514), Charles University in Prague (projekt GAUK No. 535412) and the Czech Science Foundation GACR (project GAP101/12/1554) for their financial support.

4.5 References

S. P. Arya. *Air Pollution Meteorology and Dispersion*. Oxford University Press, New York, 1998. ISBN 978-0-19-507398-0. doi: 10.1023/a:1006450618793. URL http://ukcatalogue.oup.com/product/9780195073980.do.

M. Carpentieri and A. G. Robins. Tracer flux balance at an urban canyon intersection. *Boundary-Layer Meteorology*, 135(2):229–242, feb 2010. ISSN 00068314. doi: 10.1007/s10546-010-9471-6. URL http://link.springer.com/10.1007/s10546-010-9471-6.

M. Carpentieri, P. Hayden, and A. G. Robins. Wind tunnel measurements of pollutant turbulent fluxes in urban intersections. *Atmospheric Environment*, 46: 669–674, jan 2012. ISSN 13522310. doi: 10.1016/j.atmosenv.2011.09.083. URL http://linkinghub.elsevier.com/retrieve/pii/S1352231011010909.

D. Contini, P. Hayden, and A. Robins. Concentration field and turbulent fluxes during the mixing of two buoyant plumes. *Atmospheric Environment*, 40(40):7842–7857, dec 2006. ISSN 13522310. doi: 10.1016/j.atmosenv.2006.07.024. URL http://linkinghub.elsevier.com/retrieve/pii/S1352231006007850.

B. Feddersen. *Wind tunnel modelling of turbulence and dispersion above tall and highly dense urban roughness*. PhD thesis, ETH Zurich, 2005. URL http://scholar.google.com/scholar?hl=en&btnG=Search&q=intitle:Wind+tunnel+modelling+of+turbulence+and+dispersion+above+tall+and+highly+dense+urban+roughness#0.

J. Fenger. Urban air quality. *Atmospheric Environment*, 33(29):4877–4900, 1999. ISSN 13522310. doi: 10.1016/S1352-2310(99)00290-3.

D. J. Hall and M. A. Emmott. Avoiding aerosol sampling problems in fast response flame ionisation detectors. *Experiments in Fluids*, 10(4):237–240, 1991. ISSN 07234864. doi: 10.1007/BF00190394. URL http://link.springer.com/article/10.1007/BF00190394.

G. Hoek, B. Brunekreef, A. Verhoeff, J. V anWijnen, and P. Fischer. Daily mortality and air pollution in the Netherlands. *Journal of the Air and Waste Management Association*, 50(8):1380–1389, aug 2000. ISSN 21622906. doi: 10.1080/10473289.2000.10464182. URL http://www.tandfonline.com/doi/abs/10.1080/10473289.2000.10464182.

G. Katul, G. Kuhn, J. Schieldge, and C.-I. Hsieh. THE EJECTION-SWEEP CHARACTER OF SCALAR FLUXES IN THE UNSTABLE SURFACE LAYER. *Boundary-Layer Meteorology*, 83(1):1–26, apr 1997. ISSN 0006-8314. doi: 10.1023/A:1000293516830. URL http://link.springer.com/10.1023/A:1000293516830.

R. Kellnerova, L. Kukacka, and Z. Janour. Quadrant analysis of boundary layer above pitched and flat roofs. *Acta Technica CSAV (Ceskoslovensk Akademie Ved)*, 54(4):401–413, 2009. ISSN 00017043.

L. Kukacka, S. Nosek, R. Kellnerova, K. Jurcakova, and Z. Janour. Wind Tunnel Measurement of Turbulent and Advective Scalar Fluxes: A Case Study on Intersection Ventilation. *The Scientific World Journal*, 2012:1–13, 2012. ISSN 1537-744X. doi: 10.1100/2012/381357. URL http://www.hindawi.com/journals/tswj/2012/381357/.

R. N. Meroney, M. Pavageau, S. Rafailidis, and M. Schatzmann. Study of line source characteristics for 2-D physical modelling of pollutant dispersion in street canyons. *Journal of Wind Engineering and Industrial Aerodynamics*, 62(1):37–56, aug 1996. ISSN 01676105. doi: 10.1016/S0167-6105(96)00057-8. URL http://linkinghub.elsevier.com/retrieve/pii/S0167610596000578.

M. Pavageau and M. Schatzmann. Wind tunnel measurements of concentration fluctuations in an urban street canyon. *Atmospheric Environment*, 33:3961–3971, 1999. ISSN 13522310. doi: Doi10.1016/S1352-2310(99)00138-7.

M. R. Raupach. Conditional statistics of Reynolds stress in rough-wall and smooth- wall turbulent boundary layers. *Journal of Fluid Mechanics*, 108: 363–382, 1981.

L. Soulhac, V. Garbero, P. Salizzoni, P. Mejean, and R. J. Perkins. Flow and dispersion in street intersections. *Atmospheric Environment*, 43(18):2981–2996, jun 2009. ISSN 13522310. doi: 10.1016/j.atmosenv.2009.02.061. URL http://linkinghub.elsevier.com/retrieve/pii/S1352231009001186.

R. B. Stull. *An Introduction to Boundary Layer Meteorology*. Kluwer Aademic Publishers, Dordrecht, 1988. ISBN 978-90-277-2769-5. doi: 10.1007/978-94-009-3027-8. URL http://link.springer.com/10.1007/978-94-009-3027-8.

A. A. Townsend. *The Structure of Turbulent Shear Flow*. Cambridge University Press, New York, 1999. ISBN 0 521 20710.

VDI. *Environmental meteorology – Physical modelling of flow and dispersion processes in the atmospheric boundary layer – Application of wind tunnels*. Verein Deutscher Ingenieure, Dusseldorf, Dusseldorf, 2000.

W. W. Willmarth and S. S. Lu. Structure of the reynolds stress and the occurrence of bursts in the turbulent boundary layer. *Advances in Geophysics*, 18(PA): 287–314, 1975. ISSN 00652687. doi: 10.1016/S0065-2687(08)60467-7.

5. Ventilation of idealised urban area, LES and wind tunnel experiment

The European Physical Journal, 2014, Volume 67, p. 1-10. Article ID 02062. ISSN 2100-014X. doi: 10.1051/epjconf/20146702062

Libor Kukačka[1,2], Vladimír Fuka[1], Štěpán Nosek[2], Radka Kellnerová[1,2], Klára Jurčáková[2], Zbyněk Jaňour[2]

[1] Charles University in Prague, Faculty of Mathematics and Physics, Prague, Czech Republic
[2] Institute of Thermomechanics, Academy of Sciences of the Czech Republic, Prague, Czech Republic

Abstract
In order to estimate the ventilation of vehicle pollution within street canyons, a wind tunnel experiment and a large eddy simulation (LES) was performed. A model of an idealised urban area with apartment houses arranged to courtyards was designed according to common Central European cities. In the wind tunnel, we assembled a set-up for simultaneous measurement of vertical velocity and tracer gas concentration. Due to the vehicle traffic emissions modelling, a new line source of tracer gas was designed and built into the model. As a computational model, the LES model solving the incompressible Navier-Stokes equations was used. In this paper, we focused on the street canyon with the line source situated perpendicular to an approach flow. Vertical and longitudinal velocity components of the flow with the pollutant concentration were obtained from two horizontal grids placed in different heights above the street canyon. Vertical advective and turbulent pollution fluxes were computed from the measured data as ventilation characteristics. Wind tunnel and LES data were qualitatively compared. A domination of advective pollution transport within the street canyon was determined. However, the turbulent transport with an opposite direction to the advective played a significant role within and above the street canyon.

5.1 Introduction

Vehicle traffic became often a dominant pollution source in large cities all over the world (Fenger, 1999). Air quality improvement in urban areas is necessary to avoid risk for human health (Hoek et al., 2000). The problem of the pollu-

tion transport within the built-up areas were summarised in several recent works (Kastner-Klein et al., 2004; Ahmad et al., 2005; Carpentieri, 2013). A mass exchange between street canyon and external atmospheric flow and the influence of the external turbulence intensity on the scalar transfer from the canyon was investigated in Soulhac et al. (2009). A pollution transfer within a model of a real street intersection in Central London (DAPPLE series of projects) was balanced in Carpentieri and Robins (2010). Finally, the investigation of advective and turbulent fluxes within street intersections in a complex urban area was presented in Carpentieri et al. (2012). We used similar experimental method in the present paper. A significant role of a building geometry influence on the flow patterns and pollutant dispersion was proved in Xie et al. (2005). Highly three-dimensional flow and an important role of a turbulent pollution exchange at roof level above the street intersections was demonstrated in Carpentieri et al. (2012); Kukacka et al. (2012). Mechanisms of the turbulent mass transport above the street intersection were subsequently analysed in Kukacka et al. (2013).

In this study, we have followed our recent research described in Kukacka et al. (2012) and Kukacka et al. (2013). We present a part of the complex project that aims to investigate the influence of the building height variation and the ground arrangement on the ventilation intensity. Presented experiment and numerical simulation are focused on vertical advective and turbulent pollution transport above a finite street canyon within the one type of an idealised built-up area. Understanding processes of pollution transport in complex urban areas could enable better estimation of the ventilation intensity within street canyons. Consequently, this could provide opportunities for designing suitable configuration of built-up areas and effective development of local scale dispersion models.

5.2 Experimental set-up

5.2.1 Urban area model

The model was designed according to an idealised urban area formed by apartment houses with pitched roofs arranged in courtyards that can be found in central Prague. The model was manufactured in scale 1 : 400, see figure 5.1.

The height of model buildings with pitched roof was $H = 62.5$ mm (25 m in full scale). The width of street canyons was $S = 50$ mm (20 m in full scale). The aspect ratio of the street canyons was $H/S = 1.25$.

5.2.2 Wind tunnel experiment

Wind tunnel

The physical experiment was performed in the open low-speed wind tunnel of Institute of Thermomechanics Academy of Sciences of the Czech Republic in Nový Knín. The cross dimension of the tunnel was 1.5 x 1.5 m. The development

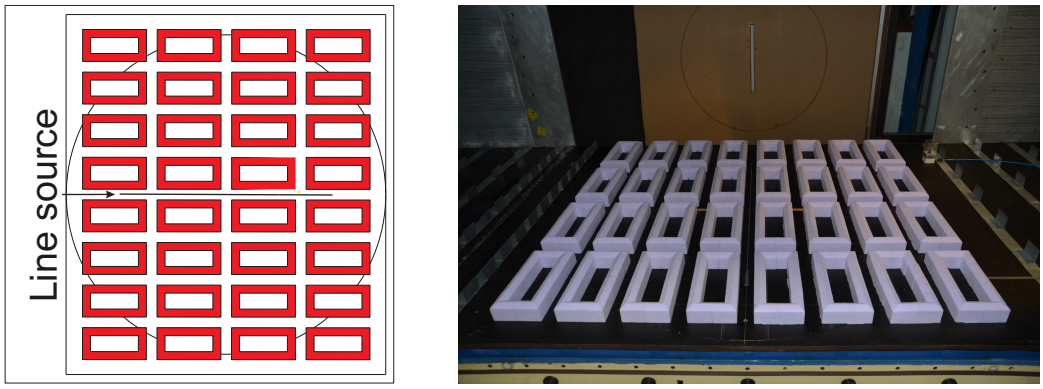

(a) (b)

Figure 5.1: Scheme of the idealised symmetric urban area model (a) and the photograph of the model placed in the wind tunnel (b).

section of the tunnel was 20.5 m long and the length of the test section was 2 m. The scheme of the tunnel is depicted in figure 5.2.

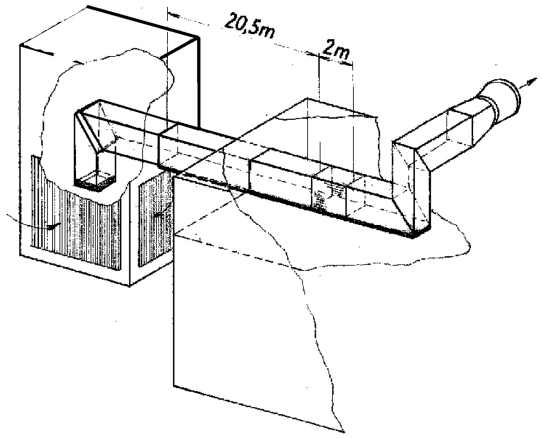

Figure 5.2: The scheme of the open low-speed wind tunnel.

Line source of tracer gas

A new line source of a tracer gas was designed and manufactured for the urban area model according to the vehicle traffic pollution simulation. The total length of the line source was $L = 1$ m (400 m in full scale). The 1 m long line source was formed by four independent units. In every 250 mm long unit, a line of 126 equally spaced needles was built in. Needles with inner diameter 0.3 mm were 100 mm long. The pressure drop across the needles exceeded the stagnation pressure in the wind tunnel of 130 Pa. That was sufficiently high value in comparison with expected pressure fluctuations on the tunnel floor (up to 10 Pa). The line source homogeneity was successfully verified before measurement.

Measurement techniques

A simultaneous point measurement of hydrocarbon concentration together with longitudinal and vertical velocity components was realised by Fast-response Flame Ionisation Detector (FFID) with two-dimensional optical fibre Laser Doppler Anemometry (LDA). LDA and FFID probes were mounted on the traverse system in a way that the measuring volume of the LDA was close to the intake to the FFID sampling tube, see Figure 5.3. A detailed description of the measurement can be found in Kukacka et al. (2013).

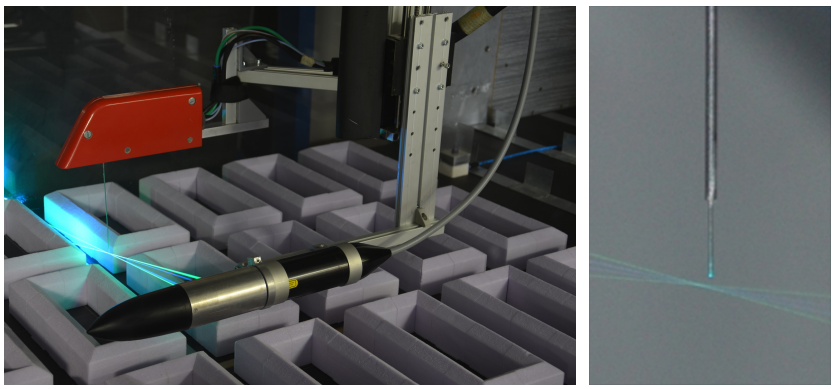

(a) **(b)**

Figure 5.3: The configuration of the FFID (red) and LDA (black and silver) probes mounted on the traverse system in the wind tunnel (a). The detail of the measuring volume of LDA with FFID sampling tube intake (b).

We used ethane as the tracer gas simulating passive pollutants emitted by vehicle traffic. A data rate of LDA reached about 200 Hz in a measured area; the FFID detector was set to acquire data at the data rate of 1 KHz. A free-stream velocity of the flow in the tunnel was measured using Prandtl tube fixed in the centre of tunnel cross-section 4 m upwind from the test section.

We applied Matlab post-processing script to synchronise the simultaneously acquired vertical velocity and concentration data finding a maximum correlation between signals. The synchronised data were shifted by an average of 12 ms. This shift expressed the delay between the suck of the sample into the intake of the FFID probe tube and the moment of the sample analysing in the probe. The value of the shift agrees with very similar experimental set published in recent works (Kukacka et al., 2013; Contini et al., 2006).

5.2.3 Large eddy simulation

Numerical model

A numerical part of this work was computed by CLMM model (Charles University Large-eddy Microscale Model), for further details see Fuka and Brechler (2011).

The model utilised large eddy simulation (LES) for the turbulent flow. Navier-Stokes equations were solved in incompressible form by the fractional step method in the model. Equations are discretized using the third order Runge-Kutta and the semi-implicit Crank-Nicolson methods.

The finite volume method on a uniform Cartesian grid was used in space. The spatial discretization of the fluxes was the second order central except. The momentum advection and scalar advection that were solved by the fourth order central and the third order positive method (Hundsdorfer et al., 1995), respectively. The nonlinear terms are filtered with filter width equal to two cell widths Vasilyev et al. (1998). The sigma subgrid model Nicoud et al. (2011) is utilised in subfilter (subgrid) scales computations.

Boundary conditions

The above described simulation was carried out with the model at the scale of 1:400 and finite line source according to the wind tunnel experiment. The boundary conditions were set-up periodic on horizontal domain boundaries. The flow was driven by a constant pressure gradient. The top boundary was a zero stress (free-slip) wall.

5.2.4 Boundary layer characteristics

A fully turbulent boundary layer (BL) was formed by development section of the tunnel. At the beginning of this section, three triangular turbulent generators were placed there. The floor of the section was covered by roughness elements of dimensions 50 x 50 mm.

The turbulent characteristics of the BL were measured with a two-dimensional LDA system in four vertical profiles placed in different positions among roughness elements around 330 mm upwind from the model, see the scheme in figure 5.4.

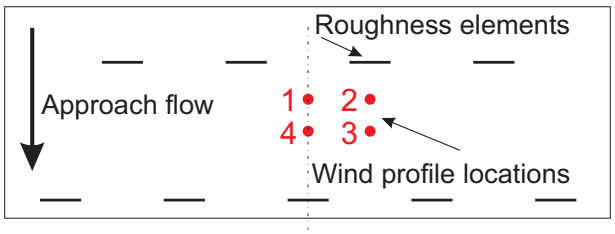

Figure 5.4: Wind profile measurement locations.

The vertical profile of mean longitudinal velocity is depicted in figure 5.5a, the momentum flux profile can be found in figure 5.5b. The vertical profiles of longitudinal and vertical turbulent intensity are plotted in figures 5.5c and 5.5d. The height above the surface is expressed in full scale.

A representative vertical profile of longitudinal mean velocity no. 4 was fitted by the logarithmic and the power law. Mean roughness length z_0, displacement d_0

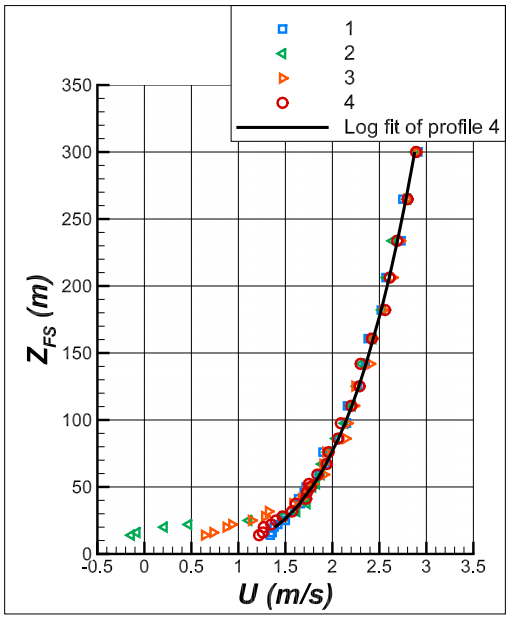

(a) The vertical profiles of mean longitudinal velocity.

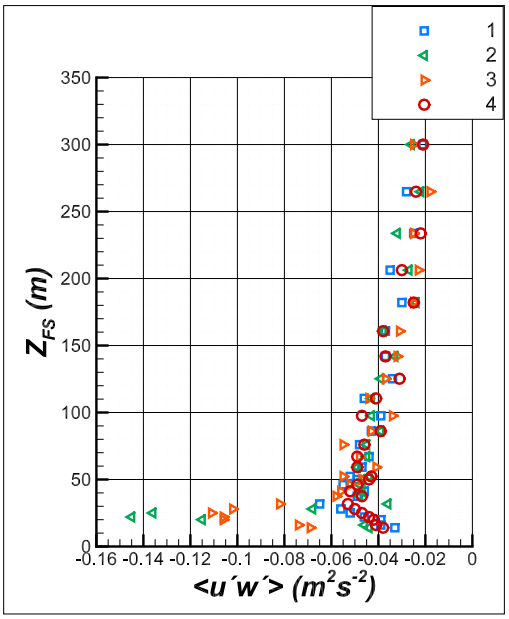

(b) The vertical profiles of mean momentum flux.

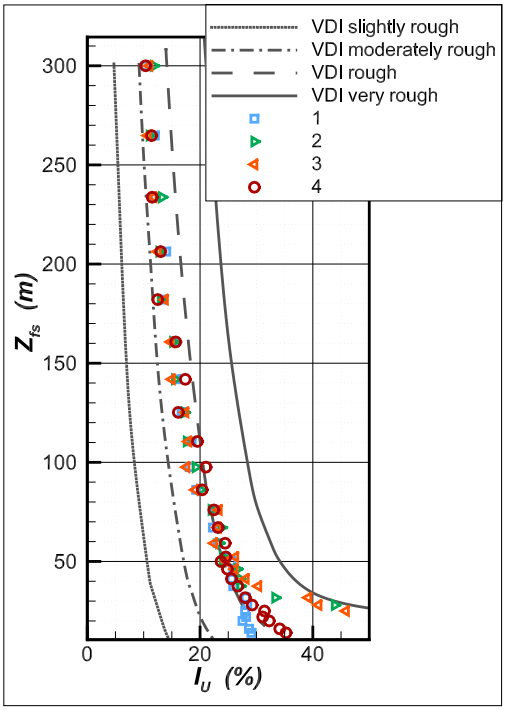

(c) The vertical profiles of longitudinal turbulent intensity with upper bounds of VDI profiles for various roughness classes (VDI, 2000).

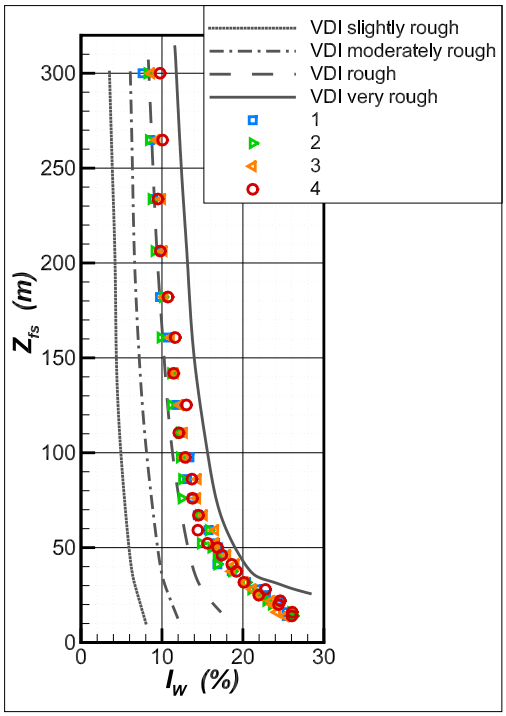

(d) The vertical profiles of vertical turbulent intensity with upper bounds of VDI profiles for various roughness classes (VDI, 2000).

Figure 5.5: Characteristics of the approach boundary layer in the wind tunnel.

and friction velocity u_* (alias square-root of constant Reynolds stress within the inertial sublayer) were obtained from the log wind profile fitting. Power exponent α was obtained from the power wind profile fitting. The BL parameters are listed in table 5.1.

Table 5.1: Parameters of the wind tunnel boundary layer (in full scale).

$z_0\,(m)$	$d_0\,(m)$	$\alpha\,(-)$	$u_*/U_{FreeStream}\,(-)$
1.87	2.96	0.27	0.07

According to VDI guideline VDI (2000), modelled BL met the requirements of the flow above densely built-up inner-city area with a small building height variation. The vertical wind profile no. 4 was used as a starting condition of the flow in the LES.

To verify requirements for the Towsend hypothesis (Townsend, 1999), an independency on Reynolds building number Re_B was verified for measured quantities. In our experiment, the modified Reynolds building number was given by

$$Re_B = \frac{U_{2H} H}{\nu}, \tag{5.1}$$

where U_{2H} is reference longitudinal velocity measured at a height of $z = 2H$ and ν is kinematic viscosity. This criterion is usually used for the flow within street canyons to be independent of viscous effects, see (Meroney et al., 1996; Pavageau and Schatzmann, 1999).

The experiment was carried out by $Re_B \approx 9000$ that lied on a lower edge of the determined interval for valid Townsend hypothesis and corresponded to the free stream velocity $U_{FreeStream} \approx 3.5$ m s^{-1} and to the reference velocity $U_{2H} \approx 2.0$ m s^{-1}.

5.3 Results

5.3.1 Area of the results

In the wind tunnel, the data were measured in two horizontal planes at the level z/H = 0.8 (at eaves height) and z/H = 1.2H (above the roof) above the street canyon with the line source, see the scheme in Figure 5.6. This street canyon was oriented perpendicular to the approach flow.

For LES simulation, a computational domain was situated in a windward half of the model. The domain, containing 161 x 281 x 101 grid points, was set-up with the resolution of 5 mm (2 m in full scale). Simulation results are displayed for a middle part of the domain, see Figure 5.7.

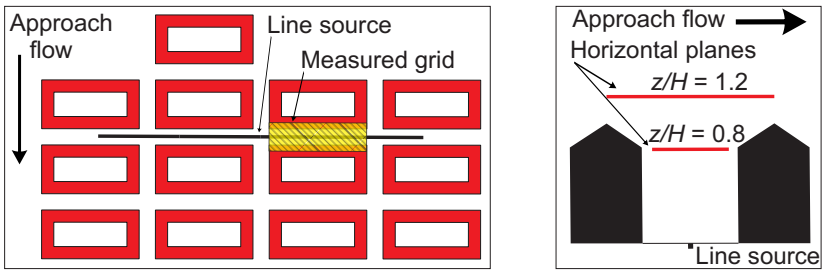

Figure 5.6: Location of measured grids above the street canyon: top view (a) and side view (b).

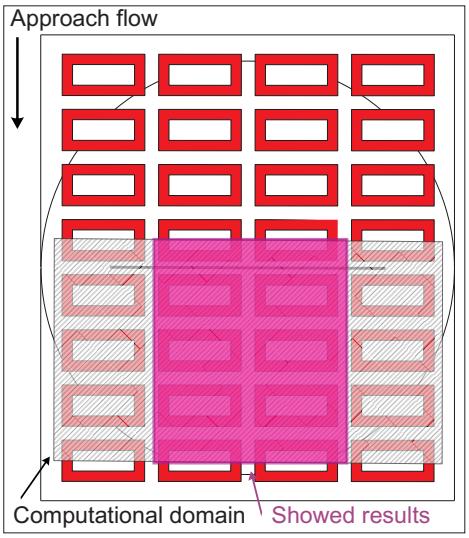

Figure 5.7: The scheme of the computational domain of LES simulation (hatched) and results area (coloured).

5.3.2 Quantities definition

The data from the wind tunnel experiment and the LES simulation were transformed to dimensionless quantities using following formulas. Longitudinal U and vertical W velocity components were converted to dimensionless form as

$$\frac{U}{U_{2H}}, \frac{W}{U_{2H}}, \tag{5.2}$$

where U_{2H} is is the reference longitudinal velocity measured at the height of $z = 2H$ above the middle of the model.

The dimensionless concentration of the tracer gas C^* was given as

$$\frac{CU_{2H}HL}{Q}, \tag{5.3}$$

where C means the measured volume concentration, L is the line source length

and Q is the source emission volume flow (VDI, 2000). We computed the dimensionless vertical advective pollution flux as

$$\frac{C^* W}{U_{2H}} \tag{5.4}$$

The dimensionless vertical turbulent pollution flux was defined as

$$\frac{c^{*\prime} w^{\prime}}{U_{2H}}, \tag{5.5}$$

where $\langle\rangle$ is the time average, $c^{*\prime}$ is the dimensionless concentration fluctuation and $w^{\prime}$ indicated the fluctuation of the vertical velocity e.g. (Kukacka et al., 2013; Carpentieri et al., 2012)).

In a vertical direction, the positive and negative signs mean the movement outwards and inwards the street canyon, respectively.

5.3.3 Velocity fields

Approximately symmetrically distributed data of the dimensionless longitudinal and vertical velocities were measured in both horizontal planes above the street canyon, see figures 5.8a–5.9b.

At the height $z/H = 0.8$, we determined a significant acceleration of the longitudinal flow along the left and right edge of the focused street canyon (figure 5.8a). These areas were situated near the street intersection with the street oriented as the approach flow. The channeling effect arose there. In case of the vertical velocity, we detected an area of significant descending and ascending flow along windward and leeward walls, respectively (figure 5.9a). This structure of flow was caused by the horizontal vortex formed within the street canyon. At the level $z/H = 1.2$, higher longitudinal velocity was measured above the street canyons oriented in parallel with the approach flow (figure 5.8b). The vertical velocity was not significantly influenced by buildings at that height unlike the longitudinal component (figure 5.9b).

The LES corresponded well with the wind tunnel results of velocity, compare right parts of the figures 5.8a–5.9b. In case of the vertical velocity at the height $z/H = 0.8$, a slightly different structure with underestimated magnitudes was observed in LES results (figure 5.9a).

5.3.4 Concentration fields

Values of dimensionless concentration were also distributed approximately symmetrically at both heights, see figures 5.10a and 5.10b. Significant values were obtained only within the focused street canyon and its close surrounding.

Maximum of concentration was found along the leeward wall of the focused street canyon at the height $z/H = 0.8$ (figure 5.10a). A marked decrease of

pollutant concentration was observed at height $z/H = 1.2$ compared to the previous case. Above the street canyon, the contaminant was detected mainly in the middle part above the roof of the windward building (figure 5.10a).

At the level $z/H = 0.8$, LES significantly overestimated pollution concentration in the focused street canyon. In comparison of magnitudes, values computed by LES exceeded results from the wind tunnel twice. In case of level $z/H = 1.2$, LES and wind tunnel gave similar values.

5.3.5 Advective scalar flux fields

Considering the advective pollution transport in vertical direction, strong upward pollution transport was found along the leeward wall of the focused street canyon at the lower level $z/H = 0.8$. Along the windward wall, fresh air flowed into the canyon (figure 5.11a). It is obvious that the advective pollution transport is mainly driven by the horizontal vortex formed within the street canyon.

We measured negligible negative flux at plane $z/H = 1.2$. This was caused by the low vertical velocities and concentrations in this area (figure 5.11b).

The LES and the wind tunnel experiment provided very similar magnitudes and distributions of the vertical pollution flux above the focused street canyon. A slight difference in LES results can be observed along the leeward wall. This was caused by underestimated vertical velocities and overestimated concentrations.

5.3.6 Turbulent scalar flux fields

At the level $z/H = 1.2$, vertical turbulent fluxes were detected negligible or slightly positive (figure 5.12b). The maximum of the turbulent flux was situated, as in case of concentrations, in the middle part above the roof of the windward canyon wall.

At $z/H = 0.8$, an intensive upward turbulent pollution transport was found along the windward wall of the street canyon. The fresh air propagated into the canyon along leeward wall (figure figure 5.12a). Compared with the advective flux, the turbulent pollution transport was opposite to the advective within and above the canyon, compare plots in figures 5.11a) and 5.12a). This phenomenon was also described in Bezpalcova et al. (2009). However, the magnitude of the turbulent flux was significantly lower then the advective.

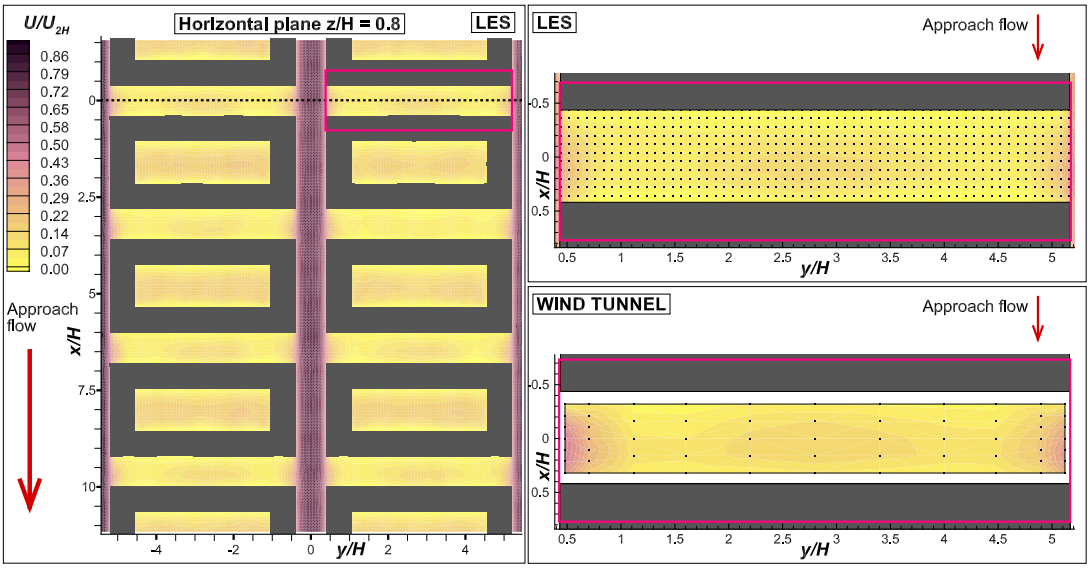

(a) U/U_{2H} at height $z/H = 0.8$.

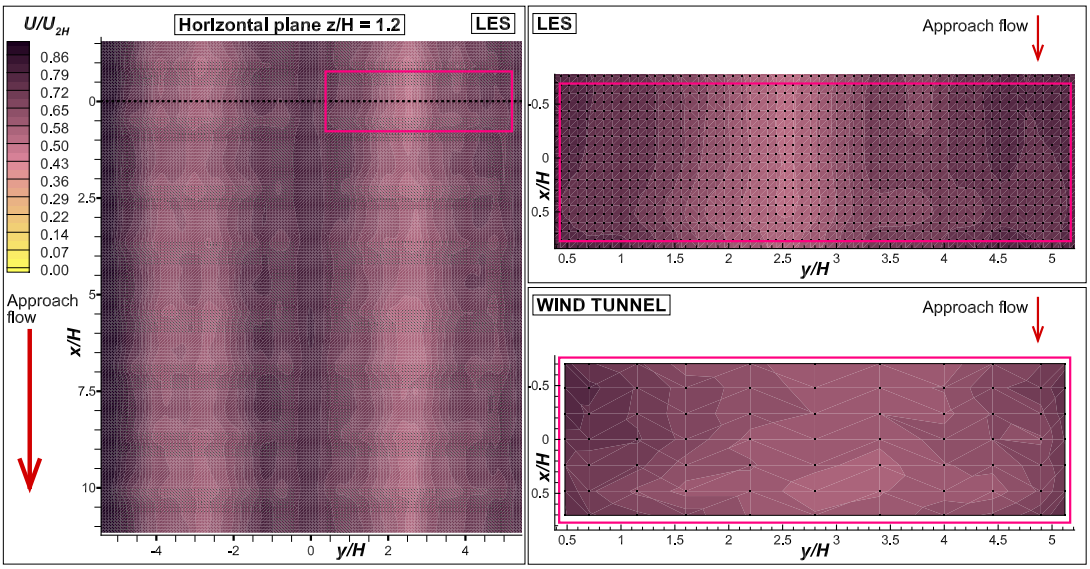

(b) U/U_{2H} at height $z/h = 1.2$.

Figure 5.8: Mean dimensionless longitudinal velocity U/U_{2H} at heights $z/H = 0.8$ and $z/h = 1.2$.

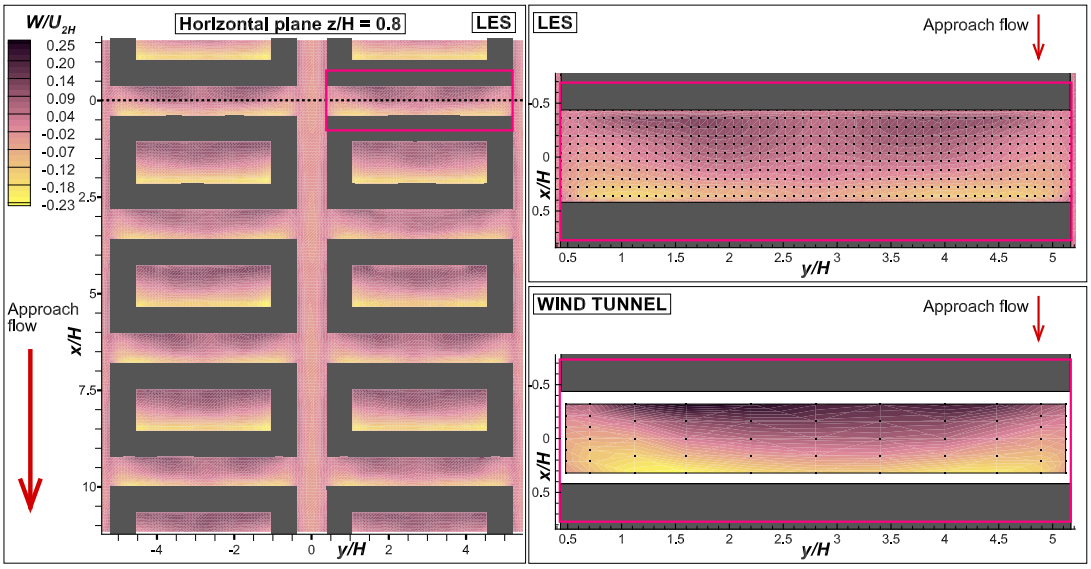

(a) W/U_{2H} at height $z/H = 0.8$

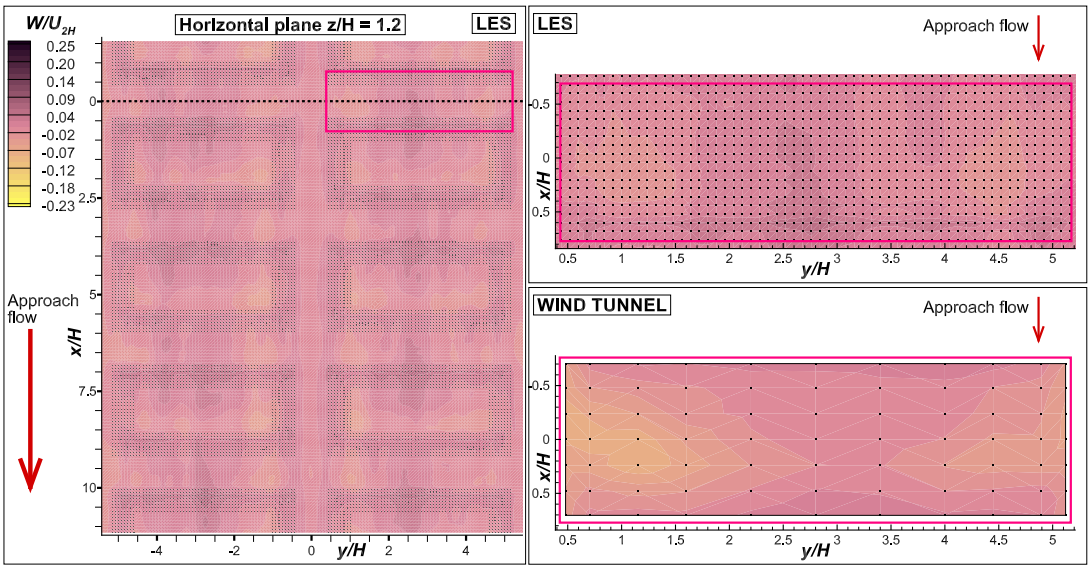

(b) W/U_{2H} at height $z/H = 1.2$

Figure 5.9: Mean dimensionless vertical velocity W/U_{2H} at heights $z/H = 0.8$ and $z/H = 1.2$.

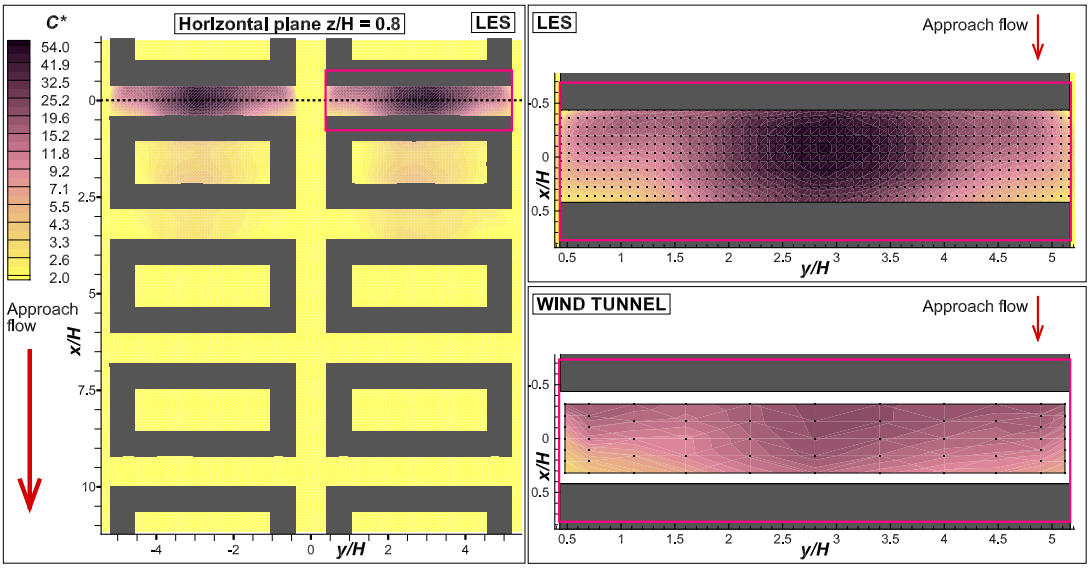

(a) C^* at height $z/H = 0.8$.

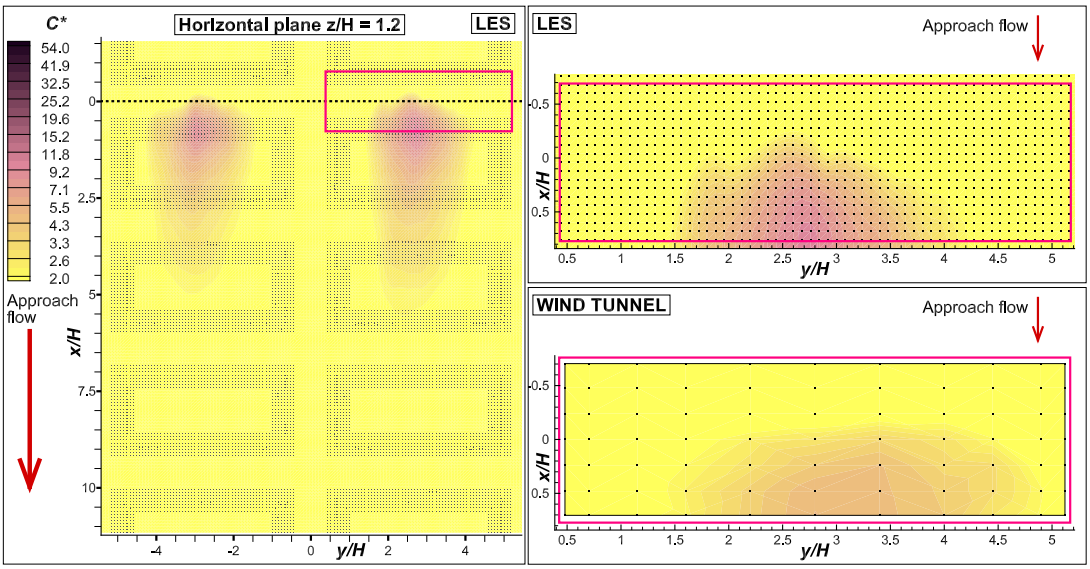

(b) C^* at height $z/H = 1.2$.

Figure 5.10: Mean dimensionless concentration C^* at heights $z/H = 0.8$ and $z/H = 1.2$.

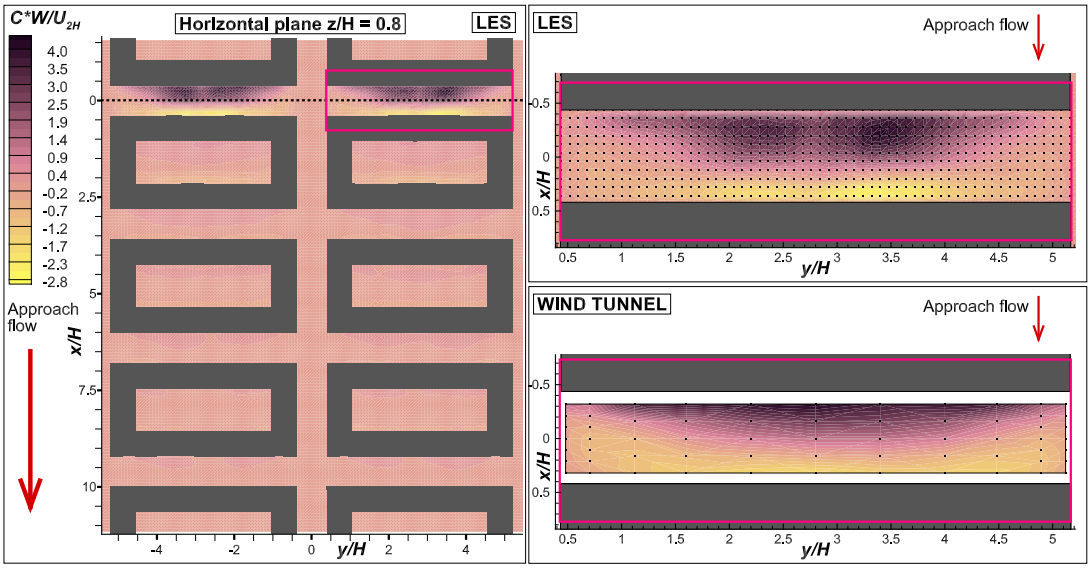

(a) C^*W at height $z/H = 0.8$

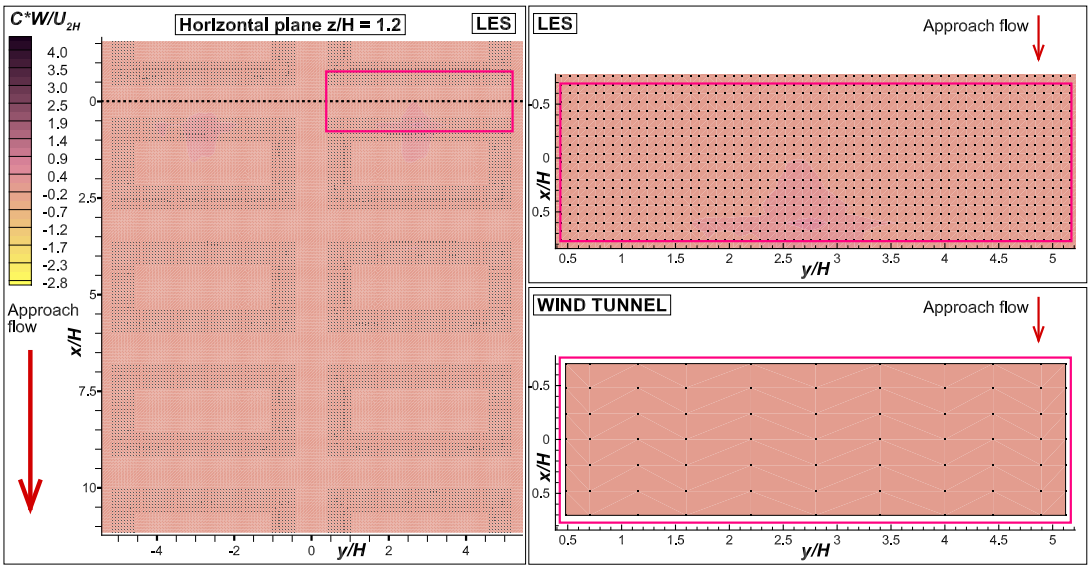

(b) C^*W at height $z/H = 1.2$

Figure 5.11: Vertical dimensionless pollution flux C^*W at heights $z/H = 0.8$ and $z/H = 1.2$.

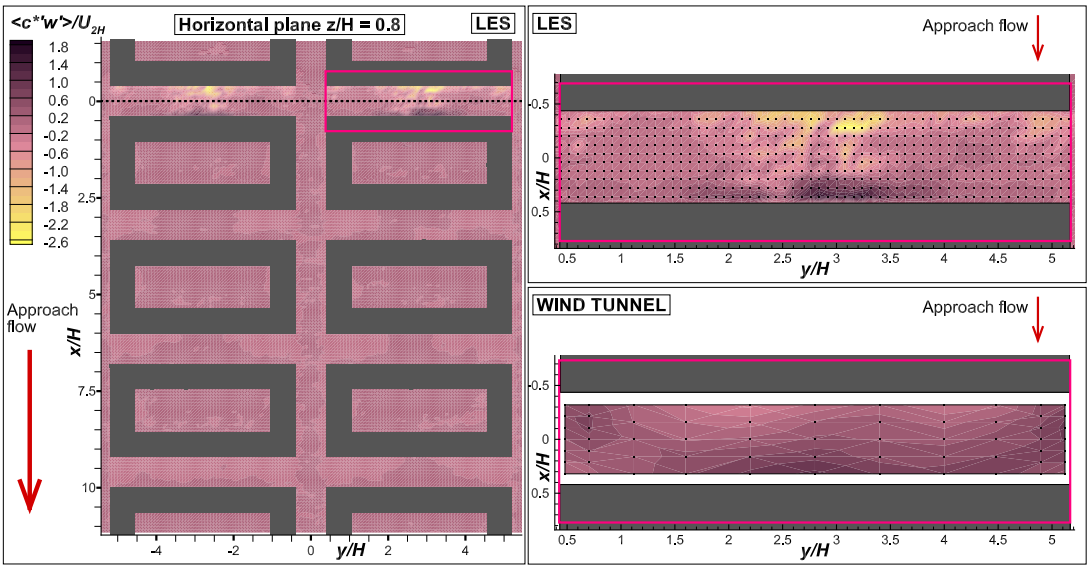

(a) $c^{*'}w'$ at height $z/H = 0.8$.

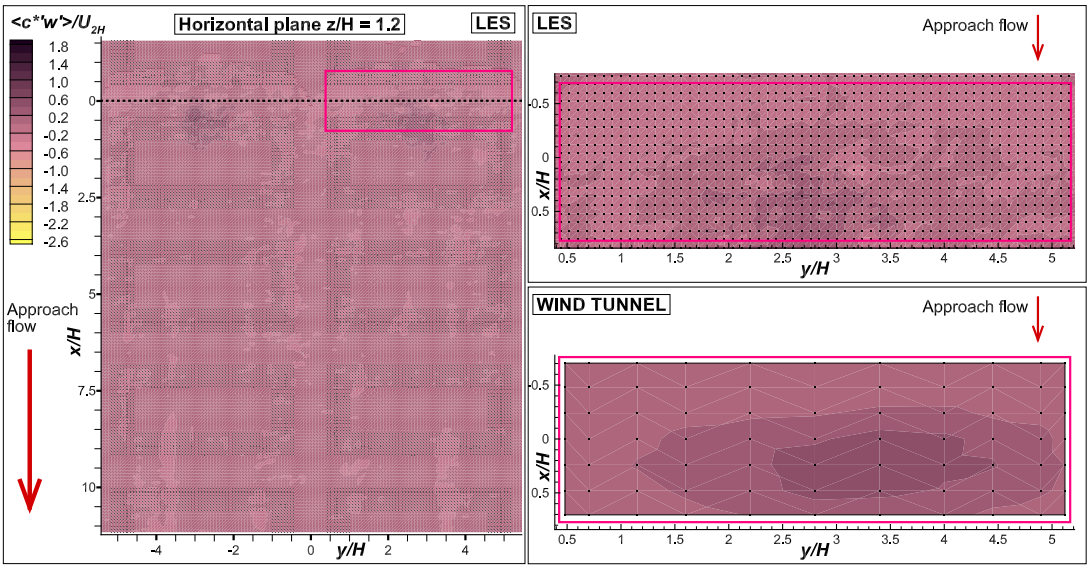

(b) $c^{*'}w'$ at height $z/H = 1.2$.

Figure 5.12: Vertical dimensionless turbulent flux $c^{*'}w'$ at heights $z/H = 0.8$ and $z/H = 1.2$.

5.4 Conclusions

This paper summarizes the ventilation intensity of the street canyon at different heights and compares the wind tunnel experiment with the large eddy simulation.

The model of the idealised urban-area was designed according to the typical Central-European urban buildings arranged into courtyards. For the wind tunnel experiment, we assembled the experimental set-up for simultaneous measurement of the flow velocity and the tracer gas concentration. This set-up was based on Fast-response Flame Ionisation Detector and Laser Doppler Anemometry. The new line source of tracer gas simulating vehicle emissions was designed and built into the model. The large eddy simulation (LES) of the flow and dispersion was realised in the urban-area model to get complex tree dimensional data from the area. The LES and the wind tunnel data were compared in selected grids.

In the study, we focused mainly on the finite street canyon with the line source situated perpendicular to the approach flow. Longitudinal and vertical velocity components and concentration of the tracer gas were obtained from two horizontal planes at different heights above the canyon (at the eaves level and above the roof). Advective and turbulent pollution fluxes were computed from the results.

Within the street canyon, the velocity and concentration data confirmed a well-known behaviour of the flow and dispersion, which is mainly caused by a large horizontal vortex. An intensive advective pollution flux was detected in the lower measured plane. As we expected, the maximum and minimum of the advective flux vas oriented along the leeward wall and windward wall, respectively.

The turbulent pollution transport was smaller compared to the advective one. On the other hand, it still played a significant role in the pollution transport. In both planes, the turbulent pollution transport was opposite to the advective and reached approximately the same magnitudes.

The wind tunnel data corresponded well with the LES above the buildings, however, the results slightly differed within the canyon. We got a different pattern in the vertical velocity field with smaller magnitudes. In the matter of concentration, the LES overestimated the concentration maxima. Nonetheless, the mentioned differences reached acceptable rate, and flow and dispersion were satisfactorily comparable.

In the future, we will investigate the impact of building geometry and orientation on pollution ventilation using both the LES and the wind the wind tunnel modelling.

Acknowledgements
The authors kindly thank the Charles University in Prague (project GAUK No. 535412) and the Czech Science Foundation (project GAP101/12/1554) for financing this project. This work was also carried out with institutional support RVO: 61388998.

5.5 References

K. Ahmad, M. Khare, and K. K. Chaudhry. Wind tunnel simulation studies on dispersion at urban street canyons and intersections - A review. *Journal of Wind Engineering and Industrial Aerodynamics*, 93(9):697–717, sep 2005. ISSN 01676105. doi: 10.1016/j.jweia.2005.04.002. URL http://linkinghub.elsevier.com/retrieve/pii/S0167610505000504.

K. Bezpalcova, M. Ohba, and Z. Janour. Influence of building packing density and building height distribution on vertical mass transport. *ICUC-7, Yokohama, Japan, A5-4*, (July):3–6, 2009. URL http://www.ide.titech.ac.jp/$\sim$icuc7/extended_abstracts/pdf/376194-1-090519004918-002.pdf.

M. Carpentieri. Pollutant dispersion in the urban environment. *Reviews in Environmental Science and Biotechnology*, 12(1):5–8, 2013. ISSN 15691705. doi: 10.1007/s11157-012-9305-8. URL http://link.springer.com/article/10.1007/s11157-012-9305-8.

M. Carpentieri and A. G. Robins. Tracer flux balance at an urban canyon intersection. *Boundary-Layer Meteorology*, 135(2):229–242, feb 2010. ISSN 00068314. doi: 10.1007/s10546-010-9471-6. URL http://link.springer.com/10.1007/s10546-010-9471-6.

M. Carpentieri, P. Hayden, and A. G. Robins. Wind tunnel measurements of pollutant turbulent fluxes in urban intersections. *Atmospheric Environment*, 46:669–674, jan 2012. ISSN 13522310. doi: 10.1016/j.atmosenv.2011.09.083. URL http://linkinghub.elsevier.com/retrieve/pii/S1352231011010909.

D. Contini, P. Hayden, and A. Robins. Concentration field and turbulent fluxes during the mixing of two buoyant plumes. *Atmospheric Environment*, 40(40):7842–7857, dec 2006. ISSN 13522310. doi: 10.1016/j.atmosenv.2006.07.024. URL http://linkinghub.elsevier.com/retrieve/pii/S1352231006007850.

J. Fenger. Urban air quality. *Atmospheric Environment*, 33(29):4877–4900, 1999. ISSN 13522310. doi: 10.1016/S1352-2310(99)00290-3.

V. Fuka and J. Brechler. Large Eddy Simulation of the Stable Boundary Layer. *Finite Volumes for Complex Applications VI - Problems and Perspectives*, pages 485–493, 2011. doi: 10.1007/978-3-642-20671-9_51. URL http://link.springer.com/10.1007/978-3-642-20671-9_51.

G. Hoek, B. Brunekreef, A. Verhoeff, J. V anWijnen, and P. Fischer. Daily mortality and air pollution in the Netherlands. *Journal of the Air and Waste Management Association*, 50(8):1380–1389, aug 2000. ISSN 21622906. doi: 10.1080/10473289.2000.10464182. URL http://www.tandfonline.com/doi/abs/10.1080/10473289.2000.10464182.

W. Hundsdorfer, B. Koren, M. Van Loon, and J. G. Verwer. A positive finite-difference advection scheme. *Journal of Computational Physics*, 117(1):35–46, mar 1995. ISSN 00219991. doi: 10.1006/jcph.1995.1042. URL http://linkinghub.elsevier.com/retrieve/pii/S002199918571042Xhttp://dx.doi.org/10.1006/jcph.1995.1042.

P. Kastner-Klein, R. Berkowicz, and R. Britter. The influence of street architecture on flow and dispersion in street canyons. *Meteorology and Atmospheric Physics*, 87(1-3):121–131, jun 2004. ISSN 01777971. doi: 10.1007/s00703-003-0065-4. URL http://link.springer.com/10.1007/s00703-003-0065-4.

L. Kukacka, S. Nosek, R. Kellnerova, K. Jurcakova, and Z. Janour. Wind Tunnel Measurement of Turbulent and Advective Scalar Fluxes: A Case Study on Intersection Ventilation. *The Scientific World Journal*, 2012:1–13, 2012. ISSN 1537-744X. doi: 10.1100/2012/381357. URL http://www.hindawi.com/journals/tswj/2012/381357/.

L. Kukacka, S. Nosek, R. Kellnerova, K. Jurcakova, and Z. Janour. Quadrant analysis of turbulent pollution flux above the modelled street intersection. *EPJ Web of Conferences*, 45:01053, apr 2013. ISSN 2100-014X. doi: 10.1051/epjconf/20134501053. URL http://www.epj-conferences.org/articles/epjconf/abs/2013/06/epjconf_efm2013_01053/epjconf_efm2013_01053.htmlhttp://www.epj-conferences.org/10.1051/epjconf/20134501053.

R. N. Meroney, M. Pavageau, S. Rafailidis, and M. Schatzmann. Study of line source characteristics for 2-D physical modelling of pollutant dispersion in street canyons. *Journal of Wind Engineering and Industrial Aerodynamics*, 62(1):37–56, aug 1996. ISSN 01676105. doi: 10.1016/S0167-6105(96)00057-8. URL http://linkinghub.elsevier.com/retrieve/pii/S0167610596000578.

F. Nicoud, H. B. Toda, O. Cabrit, S. Bose, and J. Lee. Using singular values to build a subgrid-scale model for large eddy simulations. *Physics of Fluids*, 23 (8):085106, aug 2011. ISSN 10706631. doi: 10.1063/1.3623274. URL http://link.aip.org/link/?PHFLE6/23/085106/1.

M. Pavageau and M. Schatzmann. Wind tunnel measurements of concentration fluctuations in an urban street canyon. *Atmospheric Environment*, 33:3961–3971, 1999. ISSN 13522310. doi: Doi10.1016/S1352-2310(99)00138-7.

L. Soulhac, V. Garbero, P. Salizzoni, P. Mejean, and R. J. Perkins. Flow and dispersion in street intersections. *Atmospheric Environment*, 43(18):2981–2996, jun 2009. ISSN 13522310. doi: 10.1016/j.atmosenv.2009.02.061. URL http://linkinghub.elsevier.com/retrieve/pii/S1352231009001186.

A. A. Townsend. *The Structure of Turbulent Shear Flow*. Cambridge University Press, New York, 1999. ISBN 0 521 20710.

O. V. Vasilyev, T. S. Lund, and P. Moin. A General Class of Commutative Filters for LES in Complex Geometries. *Journal of Computational Physics*, 146(1):82–104, oct 1998. ISSN 00219991. doi: 10.1006/jcph.1998.6060. URL `http://dx.doi.org/10.1006/jcph.1998.6060`.

VDI. *Environmental meteorology – Physical modelling of flow and dispersion processes in the atmospheric boundary layer – Application of wind tunnels*. Verein Deutscher Ingenieure, Dusseldorf, Dusseldorf, 2000.

X. Xie, Z. Huang, and J.-s. Wang. Impact of building configuration on air quality in street canyon. *Atmospheric Environment*, 39(25):4519–4530, aug 2005. ISSN 13522310. doi: 10.1016/j.atmosenv.2005.03.043. URL `http://linkinghub.elsevier.com/retrieve/pii/S1352231005003596`.

6. Ventilation processes in a three-dimensional street canyon

Boundary-Layer Meteorology, 2016, Volume 159, p. 259-284. ISSN 0006-8314. doi: 10.1007/s10546-016-0132-2

Štěpán Nosek[2], Libor Kukačka[1,2], Radka Kellnerová[1,2], Klára Jurčáková[2], Zbyněk Jaňour[2]

[1] Charles University in Prague, Faculty of Mathematics and Physics, Prague, Czech Republic
[2] Institute of Thermomechanics, Academy of Sciences of the Czech Republic, Prague, Czech Republic

Abstract
The ventilation processes in three different street canyons of variable roof geometry were investigated in a wind tunnel using ground-level line source. All three street canyons were part of an urban-type array formed by courtyard-type buildings with pitched roofs. A constant roof height was used in the first case, while a variable roof height along the leeward or windward walls was simulated in the two other cases. All street-canyon models were exposed to a neutrally stratified flow with two approaching wind directions, perpendicular and oblique. The complexity of the flow and dispersion within the canyons of variable roof height was demonstrated for both wind directions. The relative pollutant removals and spatially-averaged concentrations within the canyons revealed that the model with constant roof height has higher re-emissions than models with variable roof heights. The nomenclature for the ventilation processes according to quadrant analysis of the pollutant flux was introduced. The venting of polluted air (positive fluctuations of both concentration and velocity) from the canyon increased when the wind direction changed from perpendicular to oblique, irrespective of the studied canyon model. Strong correlations (> 0.5) between coherent structures and ventilation processes were found at roof level, irrespective of the canyon model and wind direction. This supports the idea that sweep and ejection events of momentum bring clean air in and detrain the polluted air from the street canyon, respectively.

Keywords
Coherent structures, Line source, Pollution flux measurements, Street canyon, Wind tunnel.

6.1 Introduction

Street canyons are of research interest because they have the highest concentrations of pollutants in cities. Because of the geometric complexity of buildings and transitional meteorological conditions, dispersion processes within street canyons are complex. Extensive wind-tunnel (e.g., Meroney et al. (1996); Rafailidis (1997); Kastner-Klein et al. (2004); Perret and Savory (2013); Addepalli and Pardyjak (2015); Carpentieri and Robins (2015)) and computational fluid dynamics (CFD) studies (e.g., Leitl and Meroney (1997); Baik and Kim (2002); Xie et al. (2005); Madalozzo et al. (2014); dong Huang et al. (2015)) have been performed over the last three decades to clarify these dispersion processes. Compared with field measurements (e.g., Louka et al. (2000); Nelson et al. (2007); Zajic et al. (2015)), physical modelling using a wind tunnel is more favourable in terms of the cost and ability to control input variables (Schatzmann and Leitl, 2011). Despite the increasing use of CFD simulation for the prediction of flow and pollutant dispersion within the urban canopy layer, there is still the need to validate such simulation with experimental data (Blocken, 2015).

The ideally modelled street canyon is a two-dimensional (2D) rectangular cavity exposed to fully turbulent flow. If the flow is perpendicular to a canyon having an aspect ratio of near unity (H/B, where H is the building height and B is the canyon width), a strong shear layer develops across the top of the cavity (Perret and Savory, 2013; Savory et al., 2013). Owing to the unstable flow condition, the shear layer intermittently flaps up and down and is affected by fluxes of turbulent kinetic energy from the external flow as observed by Salizzoni et al. (2011). The phenomena of these unstable dynamics were also observed by Louka et al. (2000) in a field experiment performed between two long bars with pitched roofs. Inside the cavity there develops a vortex that has a rotation axis parallel to the street and is neither steady nor symmetric (Britter and Hanna, 2003) and is sensitive to changes in the structure of the external flow (Salizzoni et al., 2011). A strong channel effect arises for airflow that is parallel with the canyon, where the pollutants are transported predominantly by horizontal advection. A helical vortex along the canyon dominates for the oblique wind direction (Belcher, 2005).

However, the real street canyon is part of a city street network with intersections, and three-dimensional (3D) street canyons of finite length incorporated in an urban-like array are thus more appropriate to model (Klein et al., 2007; Carpentieri and Robins, 2015). The morphology of a real street canyon usually comprises uneven roof heights along one or both sides of the canyon (i.e., the so-called non-uniform street canyon, as introduced by Gu et al. (2011)). This morphology provides additional openings for flow aloft to penetrate the canyon and to produce structures that are more complex than the along-canyon vortex, which typically forms for idealized quasi two-dimensional uniform street canyons. Both wind-tunnel (Klein et al., 2007) and field (Nelson et al., 2007) studies have demonstrated the importance of building height variability along both street sides on canyon-flow dynamics and pollutant dispersion. More recently, a CFD study

(Gu et al., 2011) employing a large-eddy simulation (LES) model was conducted for simplified variations of non-uniform street canyons and revealed new flow features, such as the tilting of flow streamlines and the horizontal divergence and convergence of airflow inside and just above the canyon. The simulation of pollutant concentrations using a line source at the centre of the canyon revealed that uneven building heights enhance pollutant dispersion through large-scale exchange of air mass inside and above such non-uniform canyons.

Perret and Savory (2013) and more recently Carpentieri and Robins (2015) highlighted two main approaches used in previous wind-tunnel studies to observe the effects of urban morphology on flow and dispersion in cities. The first approach (e.g., Dabberdt and Hoydysh (1991); Kastner-Klein and Plate (1999); Baik et al. (2000); Robins et al. (2002); Perret and Savory (2013); Addepalli and Pardyjak (2015)) concerns directly the flow characteristics inside the street canyon and is mainly based on local canyon geometric parameters, such as the building and canyon aspect ratios (H/B and H/L, respectively, where L is the canyon length). The second approach (e.g., Grimmond and Oke (1999); Cheng and Castro (2002); Takimoto et al. (2013); Blackman et al. (2015)) is related to boundary layer parameters (i.e., aerodynamic roughness length, z_0, friction velocity, u_*) or larger-scale geometrical characteristics of the urban models, such as the mean building height (h_m) or the plan-area index ($\lambda_p = A_b/A_t$, where A_b is the area occupied by the buildings and A_t is the total ground area) or the frontal area index ($\lambda_f = A_f/A_t$, where A_f is the frontal area of the buildings viewed from the approach direction of flow). While the second approach might be sufficient for the parametrization of the flow inside the canyon to some extent, local geometrical features affect local wind profiles within the canyons more strongly (especially in 3D cases) than larger-scale geometrical characteristics (Carpentieri and Robins, 2015). Hence, the present study takes the first approach in examining the effect of the aforementioned building height non-uniformity on local pollutant dispersion within the 3D street canyon under neutral stability. The following review is of wind-tunnel studies that have taken the first approach, except where stated otherwise.

Since the 1970s, 3D street-canyon arrangements, including a line source, have been investigated in many wind-tunnel studies with respect to the mean velocity and concentration fields and neutrally-stratified conditions. Hoydysh et al. (1974) pointed out that a high-density configuration of uniformly sized buildings generally increases pollutant concentrations, whereas a configuration with varying building heights allows pollutants to escape. Another important conclusion of that work was that the pair of vertical vortices emerging at street corners transports less polluted air into the street compared with the case for 2D street canyons. The leeward concentration in the middle of the canyon thus increases with increasing canyon length.

Hoydysh and Daeberdt (1988) studied the effects of different set-ups of asymmetric street canyons (with the upwind building having a different height than the downwind building, but both having constant height along the canyon length)

and wind direction (varying from 0 to ±90 deg in 10 deg increments) on the street-canyon concentration. For step-up street-canyon types ($H_U < H_D$, where H_U and H_D are the heights of the upwind and downwind buildings, respectively), the concentration levels at the leeward wall were at least twice those at the windward wall. The opposite phenomenon occurred for a step-down ($H_U > H_D$) configuration; i.e., the concentration at the windward wall was slightly higher than that at the leeward wall. Generally, the concentrations in a step-up canyon were half those in a symmetric or step-down canyon. The detailed flow patterns inside quasi-2D asymmetric canyons having three different building aspect ratios were studied by Baik et al. (2000) in a water channel. The magnitudes of the updraft and downdraft were almost independent of the aspect ratio (H/B). One vortex was observed within the canyon in the case of a step-up building arrangement while two counter-rotating vortices were observed within the canyon for a step-down building arrangement.

Theurer (1999) summarized results from several wind-tunnel studies and discovered that the local concentration within the street canyon is a function of the wind direction, the vehicle-induced turbulence and the local building arrangement, providing neutral atmospheric stability. Here, the building arrangement refers to the building and canyon aspect ratios (H/B and L/H, respectively), the distance from the centre of the vehicle lanes to the building walls (assumed to be $B/2$ for a symmetric arrangement of the vehicle lanes), roof types and surroundings. Despite the different input conditions, such as the approach flow, scale, dimensions and position of the source, each study showed that the concentration increases with increasing H/B. The same was found for the canyon length, confirming the results of the previously mentioned Hoydysh et al. (1974). The roof shape had a weaker but still important effect on the pollutant concentration in street canyons. For $H/B = 1$, the concentration at the leeward side of canyons with pitched roofs was approximately 30% lower than those with flat roofs (Rafailidis and Shatzmann, 1995). Later, Rafailidis (1997) suggested that altering the roof shape might have a stronger beneficial effect than increasing the spacing between buildings on urban air quality.

A systematic wind-tunnel study of parameter (L/H, B/H, upwind building presence, roof shape and wind direction) variations affecting the mean concentration profiles along leeward and windward two-dimensional street canyon walls was performed by Kastner-Klein and Plate (1999). Vehicle emissions were simulated as two ground-level line sources positioned equidistantly from the centre of the investigated street canyon. In good agreement with the results of previous studies, the reduction of L/H led to a 3D flow pattern that decreased the mean concentration; the presence of additional upwind buildings increased the mean concentration inside the canyon; and the mean concentration decreased with the wind direction changing from perpendicular to oblique. In a later study, Kastner-Klein et al. (2004) demonstrated for a detailed reconstructed urban landscape model (of central Nantes, France) the important effect of the roof shape on flow and dispersion within the canyon. The main conclusion was that it is

necessary to model a real array of buildings to obtain results that are realistic.

To better understand street canyon ventilation processes, pollution flux exchanges have studied experimentally (Barlow et al., 2004; Carpentieri et al., 2012; Kukacka et al., 2013) but foremost numerically (e.g., Baik and Kim (2002); Liu et al. (2005); Yang and Shao (2008); Cai et al. (2008); Liu et al. (2013)) owing to difficulties in simultaneously measuring velocity and the pollutant concentration. CFD studies have mainly focused on quasi 2D canyons, where scalar exchange rates provide a mass flux equilibrium between the canyon cavity and free surface layer above the canyon that is simpler than that observed in more complex 3D cases (Nozu and Tamura, 2012; Michioka et al., 2014; Moon et al., 2014). While simplified, the numerical simulation of these 2D cases gave important answers to problems of ventilation and pollutant removal processes with respect to different street-canyon aspect ratios and morphologies of roof shapes or canyon-height asymmetry. The pollutant removal from a 2D canyon at roof level is mainly driven by the turbulent transport mechanism and the mean flow aids the pollutants to reenter the street canyon cavity (Baik and Kim, 2002). Liu et al. (2005) showed that a cavity having a unity aspect ratio ($H/B = 1$) has a higher pollutant exchange rate (defined as the ratio of the turbulent vertical pollution flux to the rate of pollutant emission from the source) than a cavity having $H/B = 0.5$ or 2. His main conclusion was that complex turbulent transport cannot be represented by a simple gradient diffusion model. More recently, Liu et al. (2013) demonstrated for 2D canyons having different hypothetical building morphologies that, whereas the air exchange rate of the canyons had a strong linear relationship with the square root of the friction factor for all tested building morphologies, the turbulent pollutant flux correlated loosely. They pointed out that additional LES and experimental studies are needed to examine the detailed flow physics and pollutant removal mechanism over 3D urban areas.

To our knowledge, since the work of Carpentieri et al. (2012) addressed street intersections in the implicit study of street canyons, there has been only one wind-tunnel study (Kukacka et al., 2014) on both advective and turbulent pollution transport within a 3D street canyon. That study concluded that a strong recirculation vortex brought about intensive advective pollution flux at the mid-height of the street canyon ($H/B = 1.25$, $L/H = 4.8$, formed by courtyard buildings with a pitched roof), whereas at roof level, a higher contribution of the turbulent pollution flux to the total was observed. The turbulent pollution transport was opposite to advective at the mid-height of the canyon, but at roof level both transport mechanism had the same (upward) direction. Similar phenomena were observed by Michioka et al. (2014) using an LES model for 3D street canyons with almost the same aspect ratios ($H/B = 1$, $L/H = 4$) and a ground-level line source.

Interestingly, there has been a lack of systematic wind-tunnel studies on pollutant transport within 3D street canyons, where the upwind or downwind buildings (or both upwind and downwind buildings) have a variable roof height along the canyon spanwise direction. The flow within the street canyon is mainly affected

by the architecture and arrangement of buildings, and the spatial variability of the roof height and shape should be of primary concern, as was demonstrated in the aforementioned studies. For a better understanding of the effects of the 3D non-uniformity of a street canyon on ventilation processes, and to provide additional experimental data for CFD models, we present an extension of our previous work (Kukacka et al., 2014) here. The extension principally refers to the effects of two parameters, the approach wind direction and pitched-roof height non-uniformity in all directions (thus considering a 3D street canyon), on pollutant transport within a 3D street canyon. This requires not only the mean flow and concentration fields but also the vertical pollution fluxes (turbulent and mean) and coherent structure analysis in two horizontal planes, namely at the mid-height of the canyon and at roof level.

6.2 Methods

6.2.1 Street canyon models

Typical patterns of street canyons in the centres of Central European cities were used as the initial designs of three types of 3D street-canyon models having a scale of 1:400 (Fig. 6.1). All designed canyon models (labelled M1, M2 and M3) were a part of an urban-like array with a constant street width ($B = 50$ mm) formed by 8×4 courtyard-type buildings of constant length ($L = 300$ mm) and width ($B_B = 150$ mm) (Fig. 6.1c).

The first canyon model (M1), considered as the reference model, was part of an urban-like array (A1) with courtyard-type buildings having the same roof height $H = 62.5$ mm (Fig. 6.1d). Model M1 therefore has constant building and canyon aspect ratios ($H/B = 1.25$ and $L/H = 4.8$, respectively). To check the similarity of flow, we examined two M1 models, where $M1_R$ and $M1_L$ were positioned on the right and left of the streamwise avenue, respectively, and in the fourth row (in the streamwise direction) of the urban array (Fig. 6.1c). This position has been shown to be representative with respect to flow regime independence in many wind-tunnel studies (e.g., Bezpalcova (2006)).

For the examination of fully 3D street-canyon ventilation processes, we designed the second urban model (A2) according to the same plan dimensions of model A1 (corresponding to the same plan area index, $\lambda_{pA1} = \lambda_{pA2} = 0.43$), but with arbitrarily varying roof heights along each canyon wall in the spanwise direction. However, the mean height of the urban-like array A2, h_{A2}, corresponded to the mean height of the urban-like array A1, h_{A1}, and hence $h_{A2} = h_{A1} = H$. The second (M2) and third (M3) canyon models were situated at the same positions as models $M1_R$ and $M1_L$, respectively (Fig. 6.1c). While street-canyon model M2 represents locally two step-up and two equally high roof configurations, model M3 represents two step-downs, one step-up and one equally high roof configuration (Fig. 6.1b). The local configurations for both canyon models were distributed randomly.

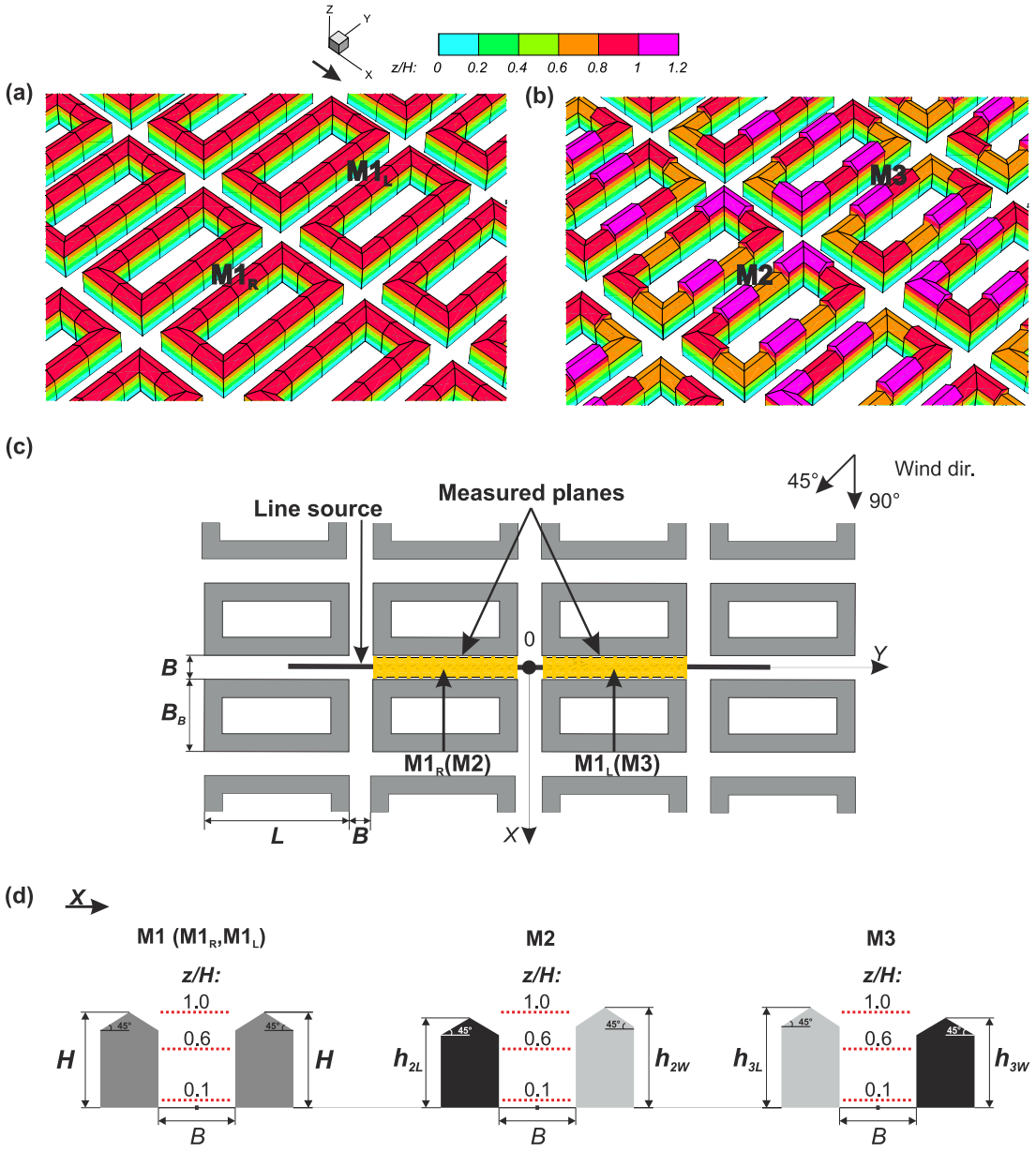

Figure 6.1: Schemas of the models with respect to wind-tunnel coordinates x, y, z: isometric view of the urban-like array (**a**) A1, incorporating the street-canyon models $\mathrm{M1}_R$ and $\mathrm{M1}_L$, and (**b**) A2, incorporating the street-canyon models M2 and M3; (**c**) top view of the horizontal cross-sections of the two urban models (A1 and A2) at dimensionless height $z/H = 0.6$ with the measured horizontal planes (yellow rectangles) and origin of the coordinates; (**d**) side view of the measured horizontal planes (z/H) within the street-canyon models M1, M2 and M3 (where, for canyons M2 and M3, the projections of the mean building heights along the leeward (h_L) and windward (h_W) canyon walls are used).

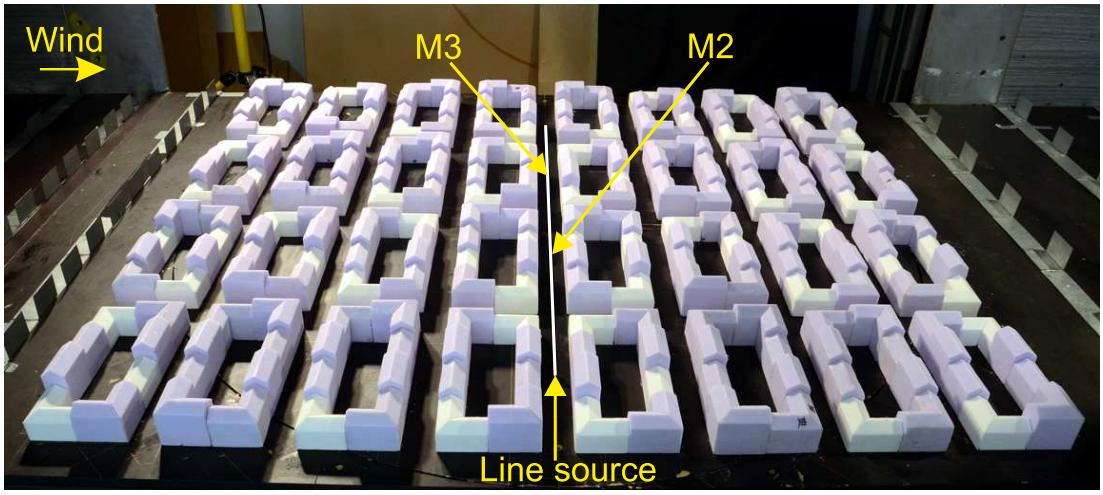

Figure 6.2: Photograph of the urban-like array model A2 positioned at the bottom of the wind tunnel for the perpendicular wind direction. The flow is from left to right and the line source is positioned in the middle of the model and investigated street canyons M2 and M3.

Because of the roof height non-uniformity along the each side of the modelled canyons, we introduced the mean building aspect ratio of the canyon; e.g., $h_{2L}/B = 1.18$ and $h_{2W}/B = 1.31$ are the ratios of the mean building heights along the leeward and windward walls to the canyon width of the model M2, respectively. Similarly, for model M3, $h_{3L}/B = 1.31$ and $h_{3W}/B = 1.18$ (Fig. 6.1d). Hence, from an integral point of view, canyon model M2 can be classified as a step-up canyon and model M3 as a step-down canyon.

We simulated two approach wind directions for both urban-array models. The first direction was perpendicular to the street canyons while the second was oblique (45°) to the street canyons (Fig. 6.1c). We did not observe any appreciable wind-tunnel side effects on the flow above the investigated street canyons for either simulated direction in lateral flow homogeneity tests at three different heights ($z/H = 2$, 4 and 6). The standard error of the mean streamwise velocity component was lower than 1.7% for all investigated points (where the velocity measurement error was 1%). As one example from four wind-tunnel runs, a photograph of the urban array model A2 positioned at the bottom of the wind tunnel for the perpendicular wind direction is presented in Fig. 6.2.

6.2.2 Line source model

To simulate the pollution emitted by dense traffic within the street canyon, we designed a homogenous ground-level line source of a passive tracer gas (ethane in our case) according to Meroney et al. (1996). The total length of the line source was $L = 1$ m (400 m at full scale) and the line source ran continuously through the investigated street canyons (Fig. 6.1c). The line source was formed by a line of 504 equally spaced tubes made of stainless steel. The tubes had an

inner diameter of 0.3 mm and length of 100 mm. The pressure drop across the tubes ($\Delta p_n = 64.5$ Pa) was sufficiently higher than the highest expected pressure fluctuations (up to 10 Pa) at the bottom of the wind tunnel, thus providing a stable volume flow rate (Meroney et al., 1996).

The lateral homogeneity of the line source was verified in several measuring and visualization tests. The standard error of the mean concentration measured along the entire source length at dimensionless downstream position $x/H = 1$ from the source (without the model) was lower than 5% (where the concentration measurement error was 4%). The ethane volume rate of flow from the line source was established in flow-rate independence tests for $Q = 18$ ml.s^{-1}, at a wind-tunnel free stream velocity $U_0 = 6.2$ m.s^{-1}. The computed velocity magnitude of the trace gas discharge from the line source was 0.28 m.s^{-1}, which was significantly lower than the friction velocity ($u_* = 0.43$ m.s^{-1}) of the canyons.

6.2.3 Experimental set-up

Wind tunnel

We used the open low-speed environmental wind tunnel of the Institute of Thermomechanics of the Czech Academy of Sciences in Nový Knín. The cross-sectional dimensions of the wind tunnel were 1.5 m × 1.5 m and the lengths of the development and test sections were 20.5 and 2 m, respectively. Throughout the measuring campaign, the wind-tunnel free stream velocity was maintained at $U_0 \approx 6.2$ m.s^{-1} and measured using a Prandtl tube at a fixed position in the centre of the wind tunnel, 4 m upwind from the test section. The free stream velocity provides a Reynolds number for buildings that is sufficiently high ($Re_B \approx 24,400$, with respect to the reference height H) to fulfil the Reynolds number independence ($Re_{crit} = 11,000$) recommended by Snyder (1979).

A fully turbulent boundary layer formed at the bottom of the development section owing to turbulence generators and roughness elements at the beginning and along the remaining part of the development section, respectively. The approach boundary-layer characteristics were obtained employing two-dimensional laser Doppler anemometry (LDA), using a DANTEC BSA F-60 burst processor, at four positions between the roughness elements upwind from the model. The positions are described in detail in Fig. 6.3. Vertical profiles of the mean dimensionless longitudinal velocity component (U/U_0), longitudinal and vertical turbulent intensity (I_u and I_w, respectively) and dimensionless momentum flux ($\overline{u'w'}/U_0^2$) for all measurement positions are depicted in Fig. 6.4a, b, c, and d, respectively. The best fit for all simulated boundary-layer parameters, as required by VDI (2000) guidelines for very rough terrain, is attained using vertical profiles from position 4 (circles in Fig. 6.4). Other profiles show higher discrepancy at full-scale heights $z_{FS} < 50$ m because they are close to the roughness elements (Fig. 6.3). Representative parameters of the mean longitudinal velocity vertical profile (Fig. 6.4a) are presented at full scale in table 6.1 in comparison with those recommended by VDI (2000) for very rough terrain. The mean roughness length

Table 6.1: Boundary-layer parameters (where h is the mean height of buildings)

	z_0 (m)	d_0/h	α
Exp	1.87	0.12	0.27
VDI	0.5 – 2.0	0.75	0.24 – 0.40

z_0 and displacement d_0 were fitted by a logarithmic law and the power exponent α by a power law. All parameters, except d_0, are within the limits recommended by VDI (2000) guidelines for the atmospheric boundary layer above very rough terrain. The displacement d_0 corresponds more to moderately rough terrain, which is more typical for suburban areas and might be acceptable for the presented urban-like array models. The same can be stated for the longitudinal turbulent intensity, I_u, at full-scale height $z_{FS} > 100$ m (Fig. 6.4b). However, below this level, where the street canyons are presented, I_u is within the limits for very rough terrain. The vertical turbulent intensity profiles of position 4, I_w (circles in Fig. 6.4c), are within the bounds recommended by VDI for the entire boundary-layer depth ($\delta_{FS} = 300$ m). The profiles of the dimensionless momentum flux $\overline{u'w'}/U_0^2$ have almost constant values with respect to height for $50 < z_{FS} < 100$ m (Fig. 6.4d).

The integral length scales of the streamwise velocity component, L_{ux}, calculated from time series measured at different heights across the boundary-layer depth, are compared with those from field measurements (Counihan, 1975) over very rough terrain in Fig. 6.5. The theoretical values of L_{ux} for appropriate roughness length z_0 are also plotted. It is seen that the measured approach boundary layer at position 4 (open circles) has integral length scales within the theoretical values for very rough terrain (between solid and dashed lines), and in good accordance with field measurements (filled circles) for heights $z_{FS} < 50$ m.

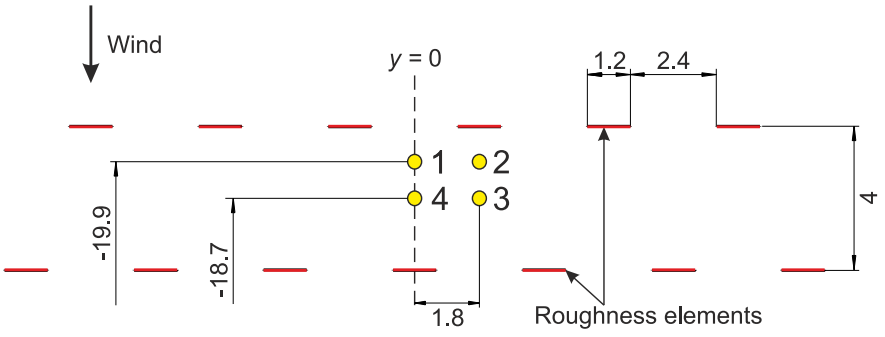

Figure 6.3: Top view of the positions where the measurements of the approach boundary layer vertical profiles were measured. The positions are related to the origin of the measurement coordinate system (x, y, z) and are normalized by the constant building height H of reference canyon model M1.

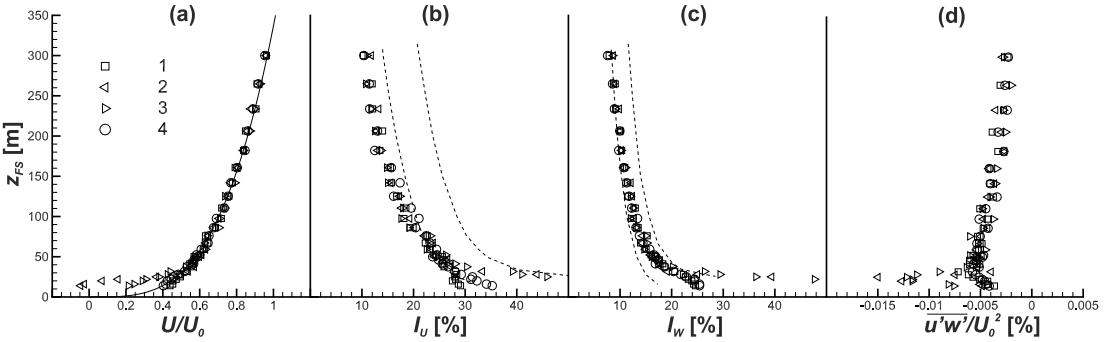

Figure 6.4: Approach boundary-layer vertical profiles at full scale (1:400 wind-tunnel scale) of (**a**) the dimensionless longitudinal velocity component, (**b**) the longitudinal turbulent intensity, (**c**) the vertical turbulent intensity and (**d**) the dimensionless momentum flux at four positions among the roughness elements. *Solid line* power fit of the velocity profile for position 4; *dashed lines* upper and lower bounds of the turbulent intensity for very rough terrain recommended by VDI (2000).

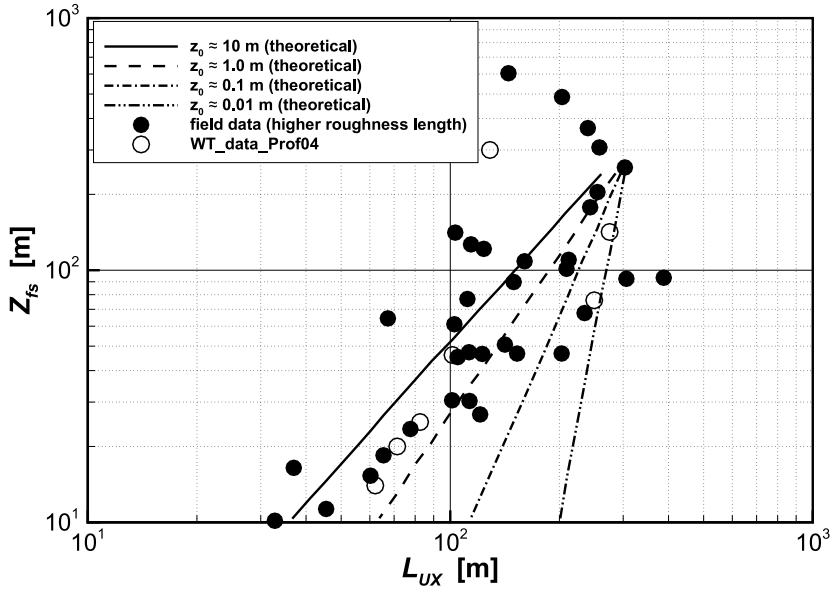

Figure 6.5: Comparison of integral length scales, L_{ux}, between the present study (*open circles*) and field data for very rough terrain (*filled circles*) according to Counihan (1975) at different heights. The lines represent theoretical values of L_{ux} for appropriate roughness length z_0.

Measurement techniques

Ventilation processes within the street canyons were investigated by making simultaneous point measurements of the two velocity components (longitudinal and vertical) and concentration employing an LDA probe and an HFR400 fast-response flame ionization detector (FFID) manufactured by Cambustion Ltd., respectively. This simultaneous use of an LDA probe and FFID probe and was introduced by Carpentieri et al. (2012) and Kukacka et al. (2012). However, the experimental principle of the simultaneous point measurement of the velocity component and concentration was applied earlier by, e.g., Fackrell and Robins (1982), using thermo-anemometry instead of the optical method for velocity measurements.

The LDA and FFID probes were assembled together on a 3D traverser system that allowed the measuring volume of the LDA to be close to the intake of the FFID sampling tube, the latter being placed 1 mm above, 1 mm behind and 1 mm beside the centre of the LDA measuring volume. We performed several test measurements with different positions of both probes and confirmed a negligible effect of the FFID sampling tube on the LDA measurement. The LDA sampling frequency, depending on the investigated flow region, was maintained between 1 and 2 kHz during the whole measuring campaign. The FFID sampling frequency was set to 0.5 kHz, corresponding to its tested response time of 2 ms. Because the FFID sample tube had a diameter of 1.2 mm and length of 200 mm, the mean delay in the physical sampling time relative to LDA was approximately 12 ms. This time delay varied with air density and dynamic pressure at the measuring point. We thus used the maximum coefficient of correlation between the time series of the velocity component and concentration to obtain a more precise individual FFID time delay (ranging from 10 to 13 ms). The effect of LDA seeding particles (approximately 1 μm in diameter) on the FFID concentration measurements was corrected in the application of the FFID calibration method. For this, we measured separately the background concentration of LDA seeding particles and subtracted it from the measured concentration of the calibration gas (all without the running of the line source).

6.3 Results

Because the dominant pollutant exchange between the street canyon and external flow takes place in the vertical direction, in the case of perpendicular flow, we performed the simultaneous point measurements of each canyon model ($M1_R$, $M1_L$, M2 and M3) in two horizontal planes. The first plane was chosen at a dimensionless height $z/H = 0.6$ according to the lowest canyon wall (where the pitched roofs were not considered). This measurement area thus encloses each canyon from the top. The second plane at $z/H = 1$ was chosen as the reference height, where stronger effects of the variability of building height of models M2 and M3 on ventilation processes can be observed (Fig.6.1b). Each plane had the

same measuring grid of 5×13 points in the $x \times y$ directions (i.e., streamwise $\times$ spanwise). At $z/H = 0.1$, we measured only the concentration in the windward and leeward wall regions, each consisting of 2×13 points, owing to LDA measuring constraints. Each canyon therefore had $(5 \times 13 \times 2) + (2 \times 13 \times 2) = 182$ measuring points. Consequently, the whole experiment consisted of $182 \times 4 \times 2 = 1456$ points (*number of points for each canyon* $\times$ *number of canyons* $\times$ *number of wind directions*) in total. According to the results of velocity and concentration central moment independence tests, the sampling time for each measuring point was set to 120 s. The overall measurement error of pollution fluxes (considering the errors of velocity (1%) and concentration measurements (4%) and the positioning error of the 3D traverser system (1%)) was estimated using ensemble statistics as 4.5%.

6.3.1 Mean flow and concentration

Although the local differences between the flows and concentrations are hidden by means of their line averaging (Fig. 6.6), they are presented at first to compare the models from an integral point of view. The line averaging of the given variable V (denoted by angular brackets) was performed along the spanwise direction of the street canyon y (index j) for each streamwise position x (index i) and height of the measured plane z (index k) as

$$\langle V \rangle_{i,k} = \frac{\sum_{j=1}^{N} V_j}{N}, \tag{6.1}$$

where $N = 13$ is the number of points measured in the spanwise direction.

To present the variance of the variable along the spanwise direction of the canyon, vertical bars indicating the standard error of line averaging, $\sigma_{\overline{V}i}$, are also plotted; these were computed as

$$\sigma_{\overline{V}i,k} = \sqrt{\frac{\sum_{j=1}^{N} (V_j - \langle V \rangle_{i,k})^2}{N(N-1)}}. \tag{6.2}$$

The dimensionless concentration was obtained according to VDI (2000) guidelines as

$$C^* = \frac{C L_s U_{ref} H}{Q}, \tag{6.3}$$

where C is the measured mean concentration, L_s is the length of the line source unit, U_{ref} is the reference velocity magnitude measured above the model centre at $z/H = 6$ and Q is the volume rate of ethane flow from the line source.

From a qualitative perspective, we observed very high similarity between the contour plots of the mean dimensionless streamwise and vertical velocity components, and dimensionless concentration fields of the right ($M1_R$) and left ($M1_L$)

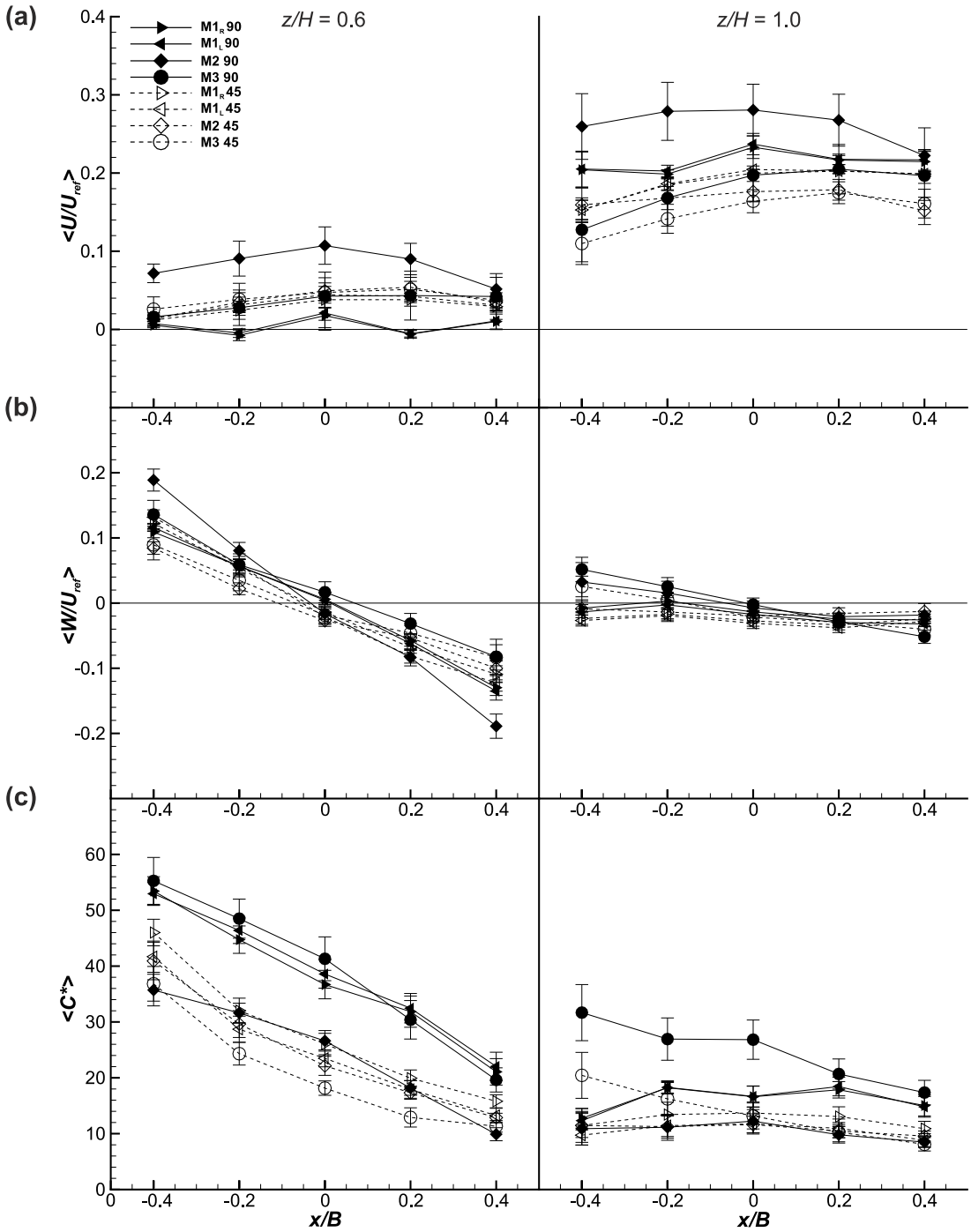

Figure 6.6: Streamwise distribution of the mean dimensionless (**a**) longitudinal and (**b**) vertical velocity components and (**c**) concentration, line-averaged along the spanwise direction of the canyon. *Right triangles* model $M1_R$; *left triangles* model $M1_L$; *diamonds* model M2; *circles* model M3; *filled symbols* perpendicular wind direction; *open symbols* oblique wind direction; *left column* $z/H = 0.6$; *right column* $z/H = 1$. The vertical bars indicate standard error of the averaged variable and the line source is positioned at $x/B = 0$.

Table 6.2: Similarity between models $M1_R$ and $M1_L$ expressed as the mean percentage of difference between the mean dimensionless variables for the perpendicular wind direction and two investigated heights (where zero refers to ideal similarity).

Height	$\Delta U/U_{ref}$	$\Delta W/U_{ref}$	ΔC^*
$z/H = 0.6$	11.5	30.3	2.0
$z/H = 1$	0.8	25.8	0.3

canyons (not shown here). However, to quantify the similarity, we calculated the mean percentage of the difference between the variables of $M1_R$ and $M1_L$ as

$$\Delta V = 100\frac{1}{N}\sum_{i=1}^{N}\frac{|V_{R,i} - V_{L,i}|}{\frac{|V_{R,i}+V_{L,i}|}{2}}, \tag{6.4}$$

where $V_{R,i}$ and $V_{L,i}$ are the particular mean values of the dimensionless variable corresponding to position i of $M1_R$ and $M1_L$ measurement grids, respectively, and N is the number of positions across the measured horizontal plane for the given case. $\Delta V = 0$ implies that the models are in ideal agreement for a given variable and case.

The mean percentages of the differences for each variable and perpendicular wind direction are listed in Table 6.2. For both heights, the agreement is very good except in the case of the vertical velocity ($\Delta W/U_{ref}$). The overall higher values of $\Delta W/U_{ref}$, are due to small average values (on the order of 0.001) in comparison with the absolute differences in Eq. 6.4. The streamwise distributions of the line-averaged dimensionless longitudinal velocity component $\langle U/U_{ref}\rangle$, vertical velocity $\langle W/U_{ref}\rangle$ and concentration $\langle C^*\rangle$ across each canyon model are compared in Fig. 6.6a, b and c, respectively.

Model M3 (circles), representing on average the step-down canyon, has similar line-averaged values (velocities and concentration) as the symmetrical model M1 (triangles) in the case of the perpendicular wind direction at height $z/H = 0.6$. The results for canyon M2 (diamonds), representing on average the step-down canyon, differ from those of M1 and M3 appreciably. The line-averaged concentrations of M2 are lower than those of M3 and M1 by a factor of approximately 1.5 across the entire canyon width at height $z/H = 0.6$ (Fig. 6.6c). This is in agreement with the results of previous wind-tunnel and CFD studies (Hoydysh and Daeberdt, 1988; Xiaomin et al., 2006). However, the presented concentration levels do not support the finding of Hoydysh and Daeberdt (1988) that the concentration on the windward ($x/B = 0.4$) side of the step-down canyon is higher than that on the leeward side ($x/B = -0.4$). The main explanation is that there are different local roof-height arrangements along each canyon wall, as will be later demonstrated for concentration and pollution flux fields. The main effect of the roof-height arrangement of model M2 is that it produces the

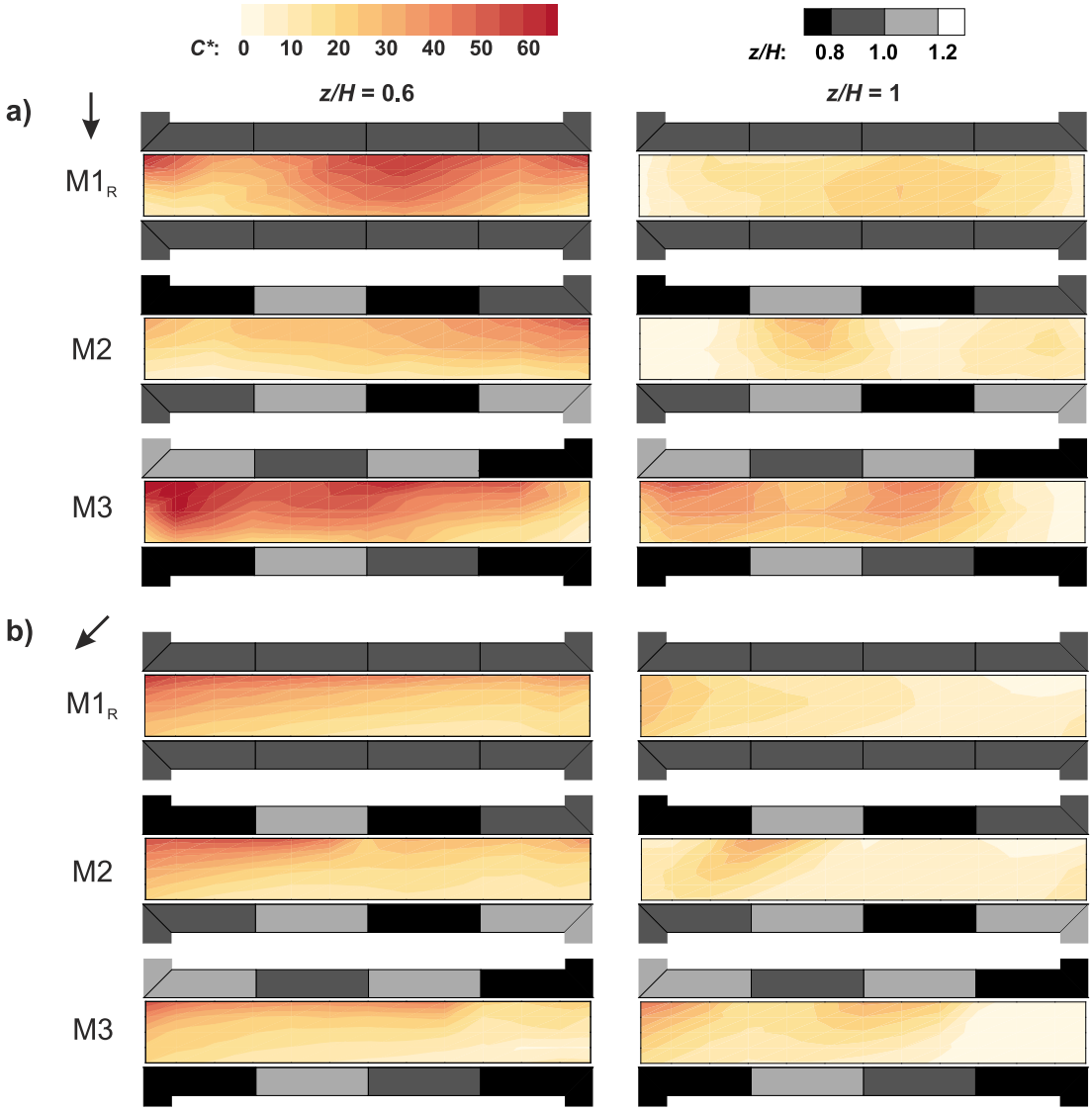

Figure 6.7: Mean dimensionless concentration fields C^* (coloured contours) for **a)** perpendicular, and **b)** oblique wind directions, all canyon models (rows) and dimensionless heights (columns). The roof height along the appropriate canyon wall is represented by dimensionless height z/H (grey contours).

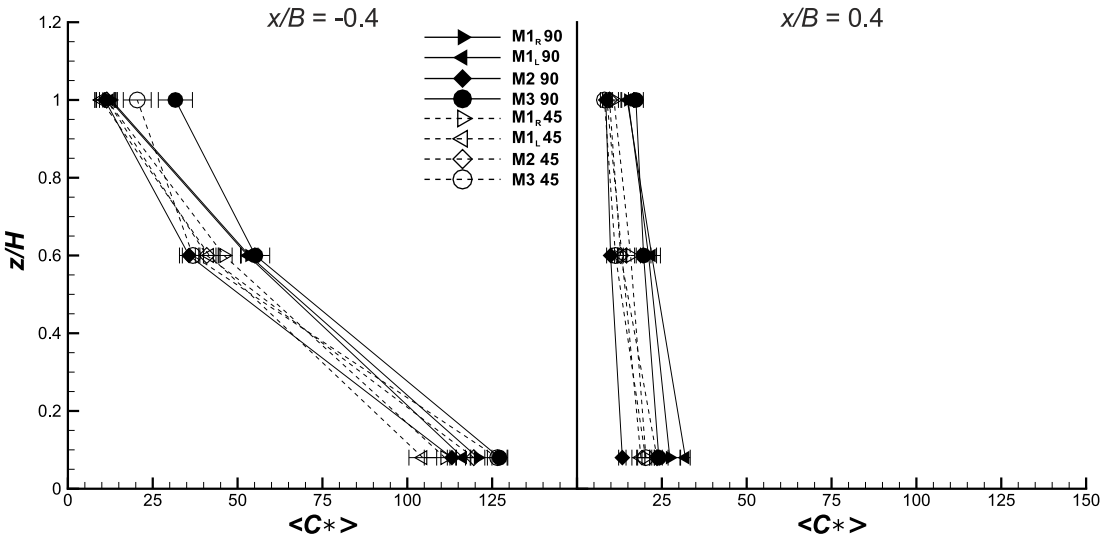

Figure 6.8: Mean dimensionless concentration vertical profiles line-averaged along the spanwise direction of the canyon at $x/B = -0.4$ (left column) and $x/B = 0.4$ (right column) walls. The symbols have the same meaning as those in Fig. 6.6. The horizontal bars indicate the standard error of the spatially averaged concentration.

highest line-averaged velocities (both streamwise and vertical) and the lowest concentration levels across the whole canyon width for each investigated height. The line-averaged vertical concentration profiles along the leeward and windward walls (Fig. 6.8) have appreciably lower values for model M2 also at the pedestrian level ($z/H = 0.1$).

For the oblique wind direction (open symbols in Fig. 6.6), there are negligible variations of line-averaged velocities ($\langle U/U_{ref} \rangle$, $\langle W/U_{ref} \rangle$) among all compared street canyon models ($M1_R$, $M1_L$, M2 and M3). This might be attributed to the channelling effects producing more uniform flow within all canyons. A weaker but still strong recirculation vortex can be seen at $z/H = 0.6$ (open symbols in Fig. 6.6b). The centre of the vortex with respect to the streamwise coordinates coincidences with the canyon centre ($x/B = 0$) as demonstrated for all investigated heights and flow directions. The strongest line-averaged upward and downward air motions along the leeward ($x/B = -0.4$) and windward ($x/B = 0.4$) walls, respectively, arise in the case of model M2 at $z/H = 0.6$ for the oblique wind direction (open diamonds in Fig. 6.6b). This suggests that the averaged step-up canyon configuration produces a stronger vortex inside the street canyon. At $z/H = 1$, the upward and downward motion is weaker for canyon models with varying roof height (M2 and M3) compared with the case when $z/H = 0.6$. In the case of the model with constant roof height ($M1_R$ and $M1_L$), where $z/H = 1$ for the roof level along the entire canyon, this air motion practically diminishes.

A strong effect of the wind direction on the mean concentration, $\langle C^* \rangle$, is observed for all canyon models in Fig. 6.6c and can be more clearly seen in mean

dimensionless concentration fields presented in Fig. 6.7. If the flow direction changes from perpendicular to oblique, the concentration field levels decrease appreciably for each canyon model. While the concentration contours for model $M1_R$ have a symmetrical spatial distribution at both heights in the case of the perpendicular wind direction (Fig. 6.7a, first row), models M2 and M3 produce asymmetrical concentration fields (second and third rows in Fig. 6.7a). These are strongly affected by local roof-height arrangements along both canyon walls of models M2 and M3. The line-averaged concentrations for the oblique wind direction show that the averaged step-down model (M3) has the lowest values among all canyon models across the whole canyon width at $z/H = 0.6$ (open circles in Fig. 6.6c, left column). This is in contrast with the case of the perpendicular wind direction for which the highest concentration levels within model M3 are presented by means of line-averaged values (filled circles in Fig. 6.6c) and concentration fields (Fig. 6.7a, third row). Owing to the locally lowest roof ($z/H = 0.8$) along the leeward and windward walls being positioned at the right margin of the model M3, cleaner air penetrates the canyon in the case of the oblique wind direction (Fig. 6.7b, third row). Hence, for a proper investigation of the spatial concentration distribution within a fully 3D canyon, the spanwise distribution of the roof height along both canyon walls needs to be taken into account. This stresses the importance of the street-canyon three-dimensionality (geometrical variability in all directions) in realistic dispersion studies.

6.3.2 Analysis of ventilation processes

Pollution fluxes

Analysis of the vertical pollution fluxes provides insight into the ventilation processes occurring within the street canyons. We computed the mean turbulent pollution flux from synchronized time series of the vertical velocity and concentration using the eddy-correlation method defined by Stull (1988) as

$$\overline{c^{*\prime}w^{\prime}} = \frac{1}{N}\sum_{i=1}^{n} {c^{*\prime}}_i {w^{\prime}}_i, \tag{6.5}$$

where $c^{*\prime}$ and ${w^{\prime}}_i$ are the fluctuations of the dimensionless concentration and vertical velocity at a particular time, respectively, and N is the length of the discrete time series. The mean total pollution flux was calculated as the sum of its turbulent and advective parts,

$$\overline{c^{*}w} = \overline{c^{*\prime}w^{\prime}} + C^{*}W, \tag{6.6}$$

where C^{*} and W are the temporally averaged dimensionless concentration and vertical velocity, respectively. The relative contribution of the turbulent pollution flux to the total vertical pollution flux was computed as

$$\overline{c^{*\prime}w^{\prime}}_{rel} = \frac{|\overline{c^{*\prime}w^{\prime}}|}{|\overline{c^{*\prime}w^{\prime}}| + |C^{*}W|}. \tag{6.7}$$

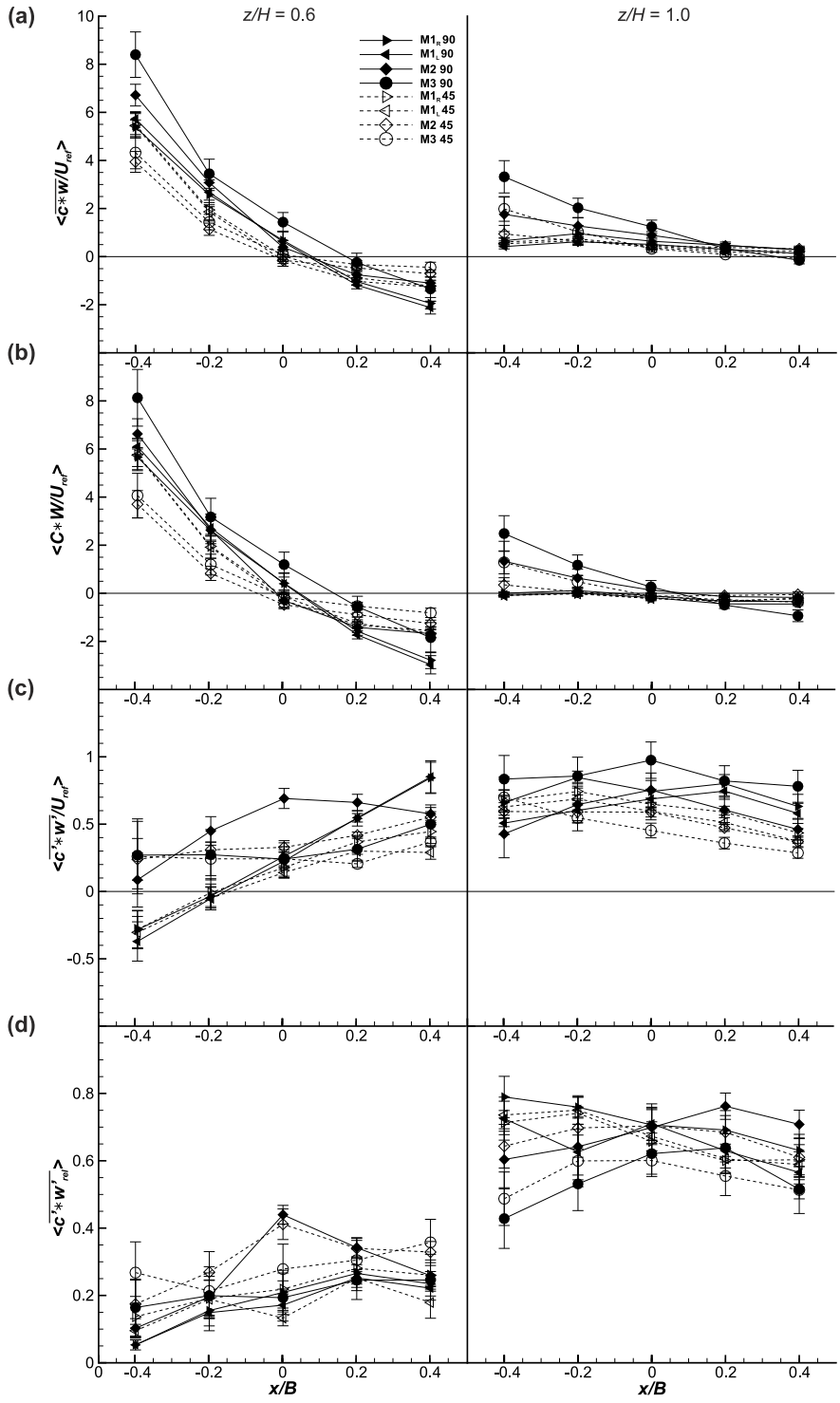

Figure 6.9: Streamwise distributions of the pollution fluxes line-averaged along the spanwise direction of the canyon: (**a**) total, (**b**) advective and (**c**) turbulent; (**d**) relative contribution of the turbulent pollution flux to total pollution flux. The symbols have the same meaning as in Fig. 6.6.

If $\overline{c^{*\prime}w'}_{rel} = 1$, all pollution transport is produced by the turbulent contribution. We applied line averaging (Eq. 6.1) and computed the standard error estimation (Eq. 6.2) for pollution fluxes and we present them in dimensionless form (by dividing them by reference velocity U_{ref}).

The line-averaged values of the dimensionless total pollution flux, $\langle \overline{c^*w}/U_{ref} \rangle$, show very strong upward and not so strong downward (re-emission) total pollutant transport at the leeward and windward walls, respectively, for the perpendicular wind direction at $z/H = 0.6$ of all canyon models (Fig. 6.9a, left column). At $z/H = 1$, $\langle \overline{c^*w}/U_{ref} \rangle$ points upward across the whole canyon width of each canyon model (Fig. 6.9a, right column). No appreciable effect of the wind direction on total pollutant transport is observed in the case of the model with constant roof height ($M1_R$ and $M1_L$), while there is an appreciable decrease in total pollutant transport for models with varying roof height if the wind direction changes from perpendicular to oblique. The strongest upward pollutant transport was observed for model M3 at both heights in the case of the perpendicular wind direction (filled circles in Fig. 6.9a, first column). In the case of the oblique wind direction, the strongest upward pollutant transport and re-emission were achieved with the model having constant roof height at $z/H = 0.6$ (open triangles in Fig. 6.9a, first column).

As for the mean velocity and concentration fields, the local variability of the total pollution flux is lost in the line-average horizontal profiles. While model M2 shows similar symmetry of the $\overline{c^*w}/U_{ref}$ field as model $M1_R$ at $z/H = 0.6$ (Fig. 6.10a, left column), the effect of different building heights on the field can be clearly seen for $z/H = 1$ (Fig. 6.10a, right column). Owing to the presence of only one highest building on the canyon leeward side, higher pollution fluxes are produced by model M2 than by $M1_R$. Especially, in the case of model M3, the strongest upward total pollution fluxes at both investigated heights (Fig. 6.10a, third row) are enhanced by the presence of the two highest buildings along the leeward side. The spatial variability of the total pollution flux for all models is more complex in the case of the oblique wind direction (Fig. 6.10a) and remains hidden when looking only at the line-averaged horizontal profiles.

The effects of the type of street canyon on the line-averaged advective pollution flux, $\langle C^*W/U_{ref} \rangle$, and turbulent pollution flux, $\langle \overline{c^{*\prime}w'}/U_{ref} \rangle$, are shown in Fig. 6.9b and Fig. 6.9c, respectively. Within ($z/H = 0.6$) canyons of constant roof height ($M1_R$ and $M1_L$), the turbulent pollution transport opposes the advective pollution transport as reported in our previous study (Kukacka et al., 2014). The same cannot be stated for the models with varying roof height (M2 and M3), where the line-averaged turbulent pollution fluxes are positive across the whole canyon width, irrespective of height (Fig. 6.9b, left and right columns). This is again the consequence of line averaging, while the contour plots show the interchanging of negative and positive turbulent fluxes along the leeward walls of both canyon models M2 and M3 at both investigated heights (Fig. 6.11a). This confirms that the roof-height variability along the canyon walls needs to be considered in studying local pollutant transport patterns within realistic 3D

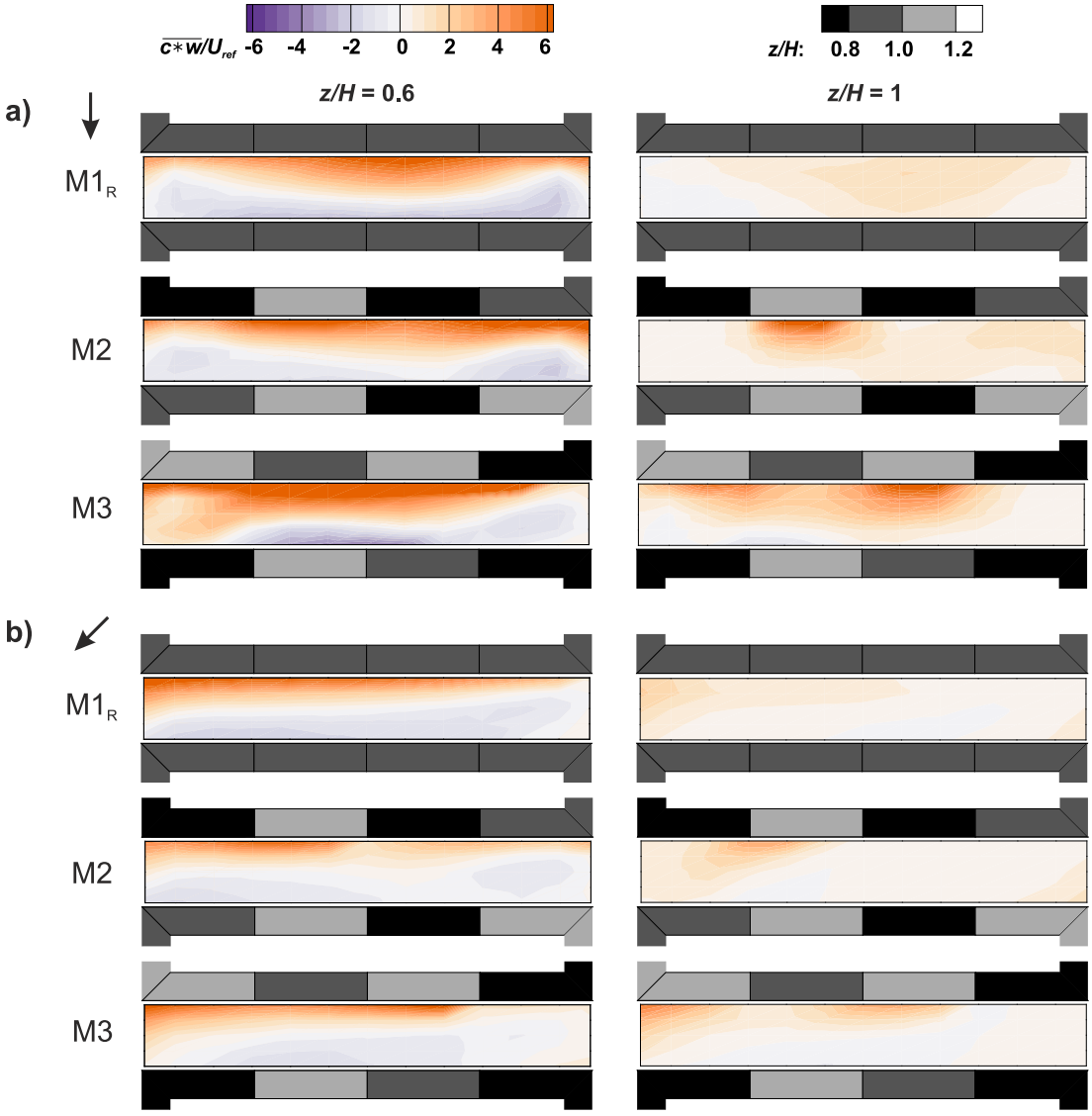

Figure 6.10: Mean dimensionless total pollution flux fields $\langle c^* w \rangle / U_{ref}$ (coloured contours) for, **a)** perpendicular, and **b)** oblique wind directions, all canyon models (rows) and dimensionless heights (columns). The roof height along the appropriate canyon wall is represented by dimensionless height z/H (grey contour).

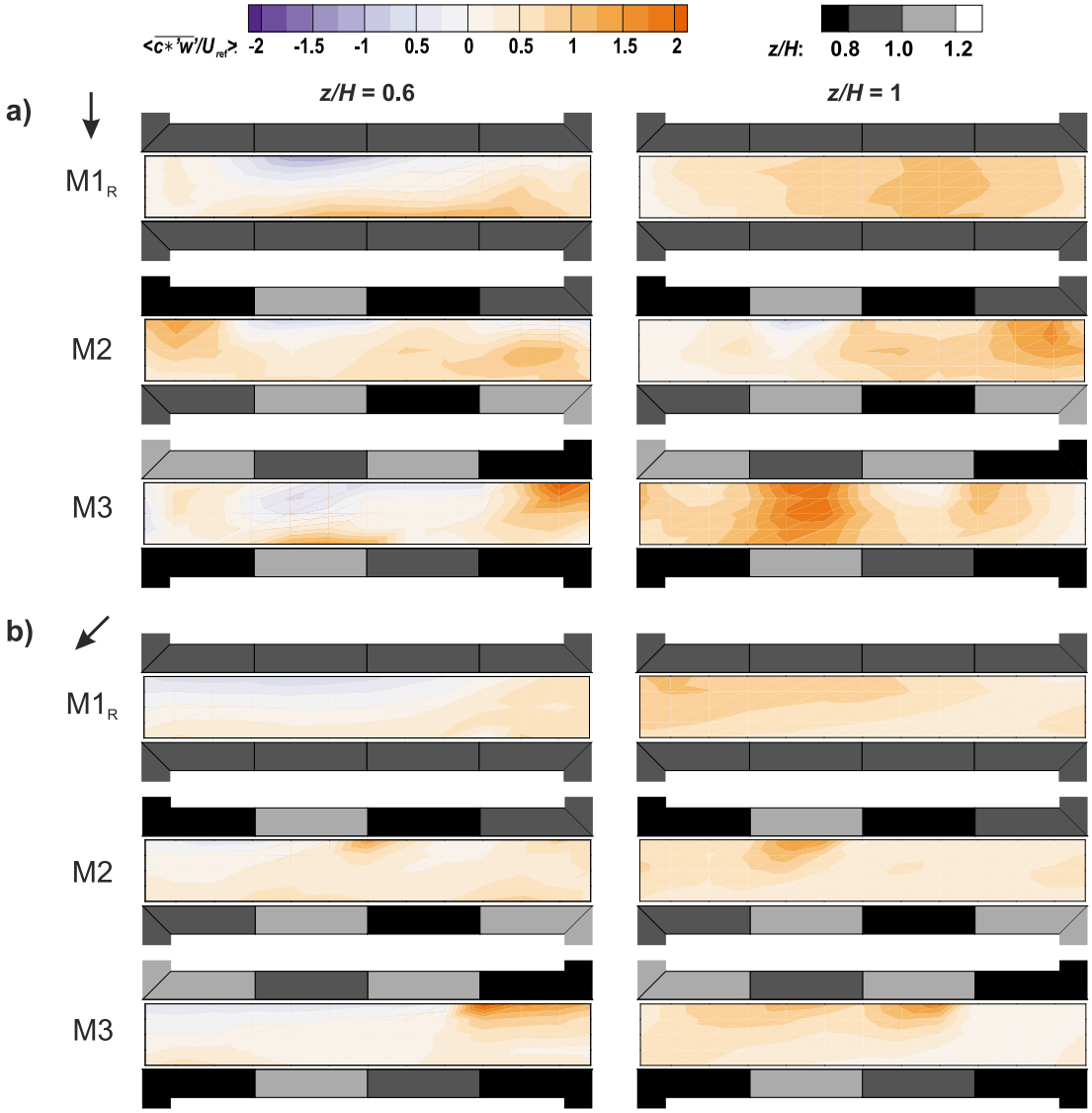

Figure 6.11: Mean dimensionless turbulent flux fields $\overline{c^{*\prime}w^{\prime}}/U_{ref}$ (coloured contours) for, **a)** perpendicular, and **b)** oblique wind directions, all canyon models (rows) and dimensionless heights (columns). The roof height along the appropriate canyon wall is represented by dimensionless height z/H (grey contour).

Table 6.3: Relative pollutant removal, E_{rel}, and spatially-averaged dimensionless concentration, $\langle C^* \rangle$, for each canyon model at height $z/H = 0.6$ and for the perpendicular wind direction

	$M1_R$	M2	M3
E_{rel}	0.63	0.84	1.31
$\langle C^* \rangle$	37.5	24.4	40.3

canyons.

The contribution of the turbulent pollution flux to the total pollution flux, $\langle \overline{c^{*\prime} w^{\prime}}_{rel} \rangle$, is dominant at $z/H = 1$ for all canyon models and is strongly affected by the model type and is independent of the wind direction even if the line averaging is taken into account (Fig. 6.9d, right column). The spatial averaging of the turbulent flux contribution fields (not shown here) at $z/H = 1$ for each type of model, $M1_R$, M2 and M3, results in contributions of 72%, 69% and 57%, respectively, in the case of the perpendicular wind direction. Michioka et al. (2014), using an LES model, computed almost the same value of $\langle \overline{c^{*\prime} w^{\prime}}_{rel} \rangle = 75\%$ at the roof level of a 3D canyon with flat roofs and $L/B = 4$ as in our case of model $M1_R$ (72%).

Relative pollutant removal

To better understand the mechanisms of pollutant removal acting within the street canyons, we calculated the relative pollutant removal from the mean total pollution flux fields as

$$E_{rel} = \frac{1}{Q} \int_{-0.4B}^{0.4B} \int_{0.02L}^{0.98L} \overline{cw} \mathrm{d}y \mathrm{d}x, \tag{6.8}$$

where $\overline{cw}$ is the total vertical pollution flux and Q is the rate of emission from the source presented in the canyon of the same length (L). Owing to the complexity of the three-dimensionality of the flow within the canyons, together with the finite length of the line source, we performed the integration only in the case of the perpendicular wind direction at height $z/H = 0.6$. This height ensures that all canyon models are enclosed by the measurement plane from the top. Of course, that area did not cover the entire horizontal area owing to spatiality constraints of the measurement (integral limits in Eq. 6.8). Therefore, the integrated (measurement) plane corresponded to 77% of the total area enclosed by the canyon geometry in the case of the height $z/H = 0.6$; $E_{rel} = 1$ implies that all emissions from the source are removed through the measurement plane to the flow aloft.

Integrating the mean dimensionless concentration pollution field, C^* (Fig. 6.7), across the measurement plane and dividing it by its area, A, we obtain the

spatially-averaged dimensionless concentration at a given height:

$$\langle C^* \rangle = \frac{1}{A} \int_{-0.4B}^{0.4B} \int_{0.02L}^{0.98L} C^* \mathrm{d}y\mathrm{d}x. \tag{6.9}$$

As in the case of E_{rel}, we integrate C^* only for the case of the perpendicular wind direction at height $z/H = 0.6$. Results for E_{rel} and $\langle C^* \rangle$ are presented in Table 6.3.

This shows that the pollutant removal ($E_{rel} = 0.63$) from the middle canyon height to the flow aloft in the case of the constant roof-height model ($\mathrm{M1}_R$) is similar to that in the case of the canyon with flat roofs ($E_{rel} = 0.65$) calculated by Michioka et al. (2014). Approximately 37% (35% in the case of Michioka et al. (2014)) of the pollutant is emitted laterally to the intersections, and pitched roofs of constant height do not appreciably affect pollutant removal from the canyon.

Canyons with variable roof heights (M2 and M3) have higher relative pollutant removals to the top and hence less removal laterally. Striking pollutant removal mechanisms occur in the case of model M3 ($E_{rel} = 1.31$), where not only all emission from the source is removed but another 31% of this emission is ventilated from the canyon surroundings. The dimensionless total pollution flux fields presented in Fig. 6.10a clearly show that this extra pollutant entrainment occurs at the left edge of canyon M3, where the biggest step-down local configuration is presented. This yields the highest spatially-averaged dimensionless concentration of model M3 ($\langle C^* \rangle = 40.3$) and cannot be attributed to the higher re-emission rates, in contrast to the case of the 2D street-canyon models as was demonstrated by, e.g., Liu et al. (2005). From the point of view of E_{rel} and $\langle C^* \rangle$, model M3 might be determined as the most unfavourable street-canyon arrangement according to the simulated line-source model. Meanwhile, if only the line source within the canyon is simulated, model M3 has better ventilation processes than model $\mathrm{M1}_R$ owing to the extra unpolluted air lateral entrainment from the intersections, hence reducing $\langle C^* \rangle$ from 40.3 to 28.2. This suggests that additional pollutant fluxes through the lateral areas of the canyon need to be experimentally investigated in future work to gain better insight into the mechanisms of pollutant removal from the 3D canyon. The best ventilation performance is, without any considerations, achieved by M2 with respect to the highest E_{rel} and the lowest $\langle C^*_{avg} \rangle$ among all investigated canyon models.

Relationship between the dominant momentum and scalar fluxes

For the atmospheric surface layer, it is widely accepted that coherent structures, referred to as the sweep and ejection of momentum, are responsible for the mass transport (Katul et al., 2006; Li and Bou-Zeid, 2011). We thus also focused on street canyon ventilation with respect to the relationships between the dominant events of the momentum and pollution fluxes. We used a simple conditional technique known as *quadrant analysis*, developed by Willmarth (1975), which is applied to scatter plots of two turbulent quantities. Here, we used instantaneous

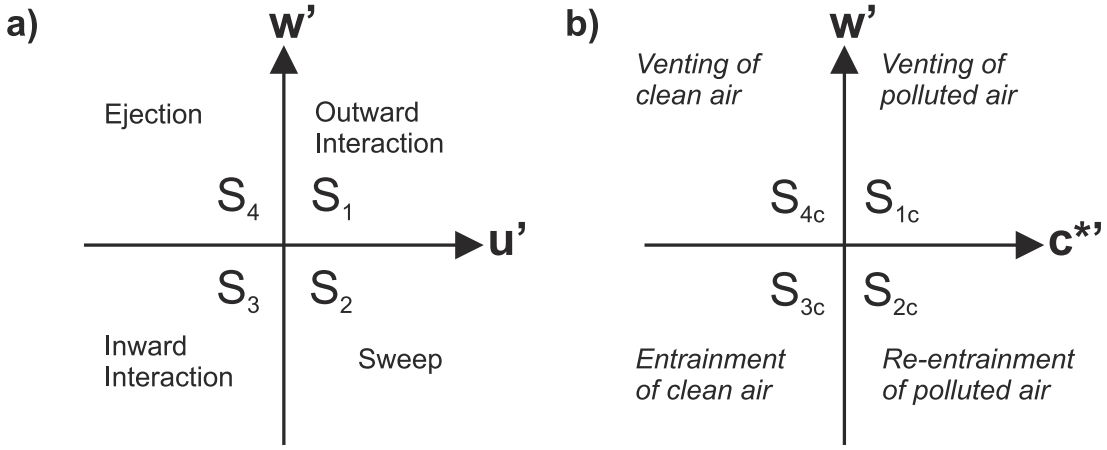

Figure 6.12: Schema of the quadrant nomenclature for, (**a**) momentum, and (**b**) scalar transport.

longitudinal (u') and vertical (w') velocity fluctuations for the momentum flux, and the dimensionless concentration ($c^{*\prime}$) and vertical (w') fluctuations for the scalar flux.

We follow Katul et al. (2006) and use the same quadrant nomenclature for the momentum transport (Fig. 6.12a). The meaning of physical processes of defined events are as follows: faster particles of air are transported downwards during sweep events. Meanwhile, ejection refers to the transport of slower particles upwards. Prevailing sweep and ejection events in a turbulent flow within the boundary layer are caused by the transport of momentum towards a surface. Outward and inward interactions transport faster moving particles upwards and slower particles downwards, respectively.

For scalar transport, we design the quadrant nomenclature according to the processes going on (Fig. 6.12b). The first and third quadrants, where the venting of polluted air ($c' > 0$ and $w' > 0$) and the entrainment of clean air ($c' < 0$ and $w' < 0$) take place, respectively, are considered as street-canyon ventilation processes. The remaining second and fourth quadrants represent the re-entrainment of polluted air ($c' > 0$ and $w' < 0$) and venting of clean air ($c' < 0$ and $w' > 0$), respectively, and are thus considered pollution processes.

We found that sweeps and ejections and ventilation processes are dominant in all simulated cases. Hence, we present only their fractional contributions, which we computed as

$$S_i = \frac{|\langle\overline{u'w'}\rangle_i|}{|\overline{u'w'}|}, S_{ic} = \frac{|\langle\overline{c'w'}\rangle_i|}{|\overline{c'w'}|}, \tag{6.10a}$$

$$\langle\overline{u'w'}\rangle_i = \frac{1}{T}\int_0^T u'(t)w'(t)I_i, \mathrm{d}t, \tag{6.10b}$$

$$\langle\overline{c'w'}\rangle_i = \frac{1}{T}\int_0^T w'(t)c'(t)I_i \mathrm{d}t, \tag{6.10c}$$

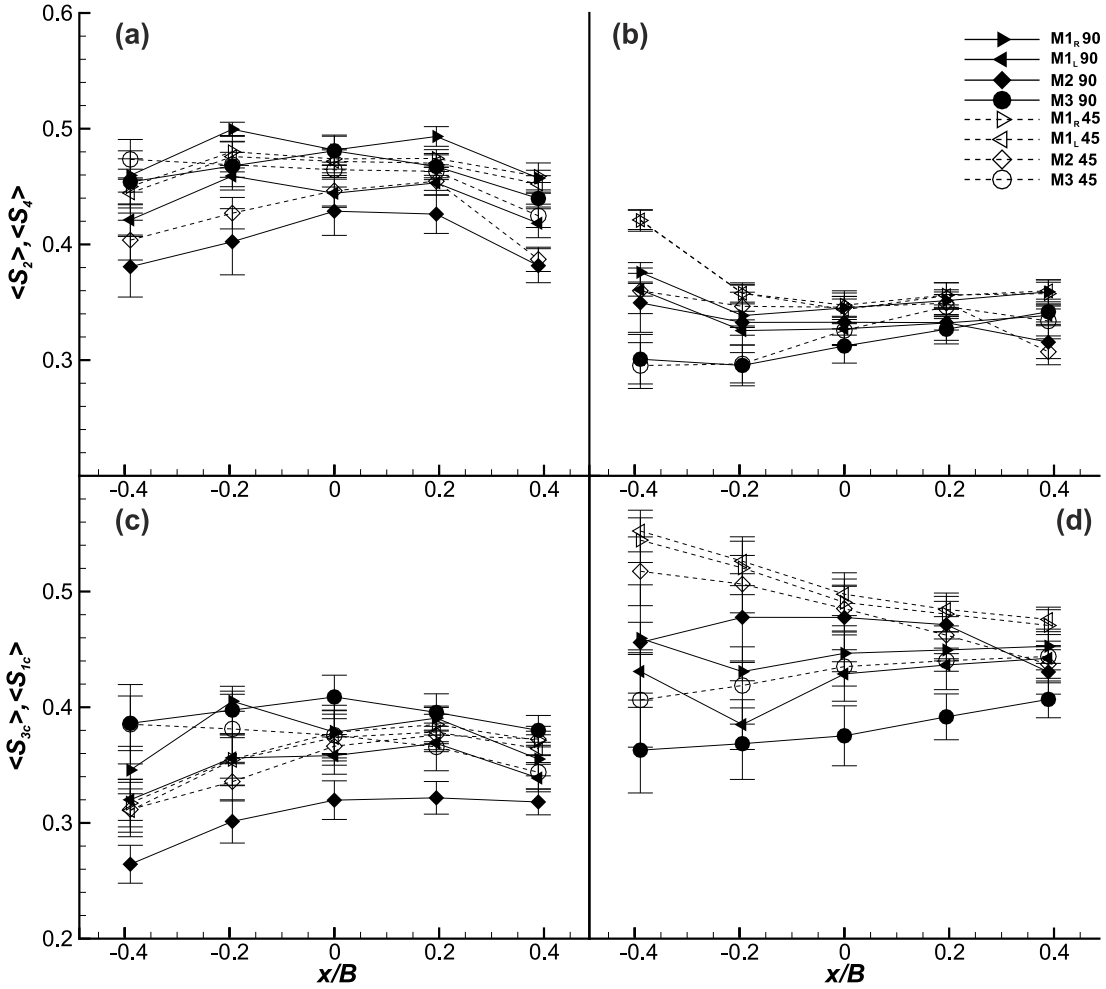

Figure 6.13: Fractional contributions of the, (**a**) sweep $\langle S_2 \rangle$, and (**b**) ejection $\langle S_4 \rangle$, and the (**c**) entrainment of clean air $\langle S_{3c} \rangle$, and (**d**) venting of the polluted air $\langle S_{1c} \rangle$, line-averaged along the spanwise direction at height $z/H = 1.0$. The symbols have the same meaning as in Fig. 6.6.

where $\langle\ \rangle$ is the conditional average, $\overline{u'w'}$ and $\overline{c'w'}$ are the momentum and scalar fluxes, respectively, and I is the indicator function. $I_i = 1$ if $u'w'$ (or $c'w'$) is within quadrant $i = 2, 4$ (or 1,3) and $I_i = 0$, otherwise.

The streamwise distributions of the line-averaged fractional contributions of sweeps $\langle S_2 \rangle$ and ejections $\langle S_4 \rangle$, and the entrainment of clean air $\langle S_{1c} \rangle$ and venting of polluted air $\langle S_{3c} \rangle$ at $z/H = 1$ are presented in Fig. 6.13a,b and Fig. 6.13c,d, respectively. The sweeps (Fig. 6.13a) contribute more than the ejections (Fig. 6.13b) across the whole canyon, irrespective of the street-canyon model. This shows that the prevailing mechanism of the momentum transport is a motion of faster moving air downwards into the canyon. Interestingly, there is no appreciable effect of the wind direction on sweep and ejection streamwise distributions for any canyon model.

If we look at the ventilation processes in the case of the perpendicular wind

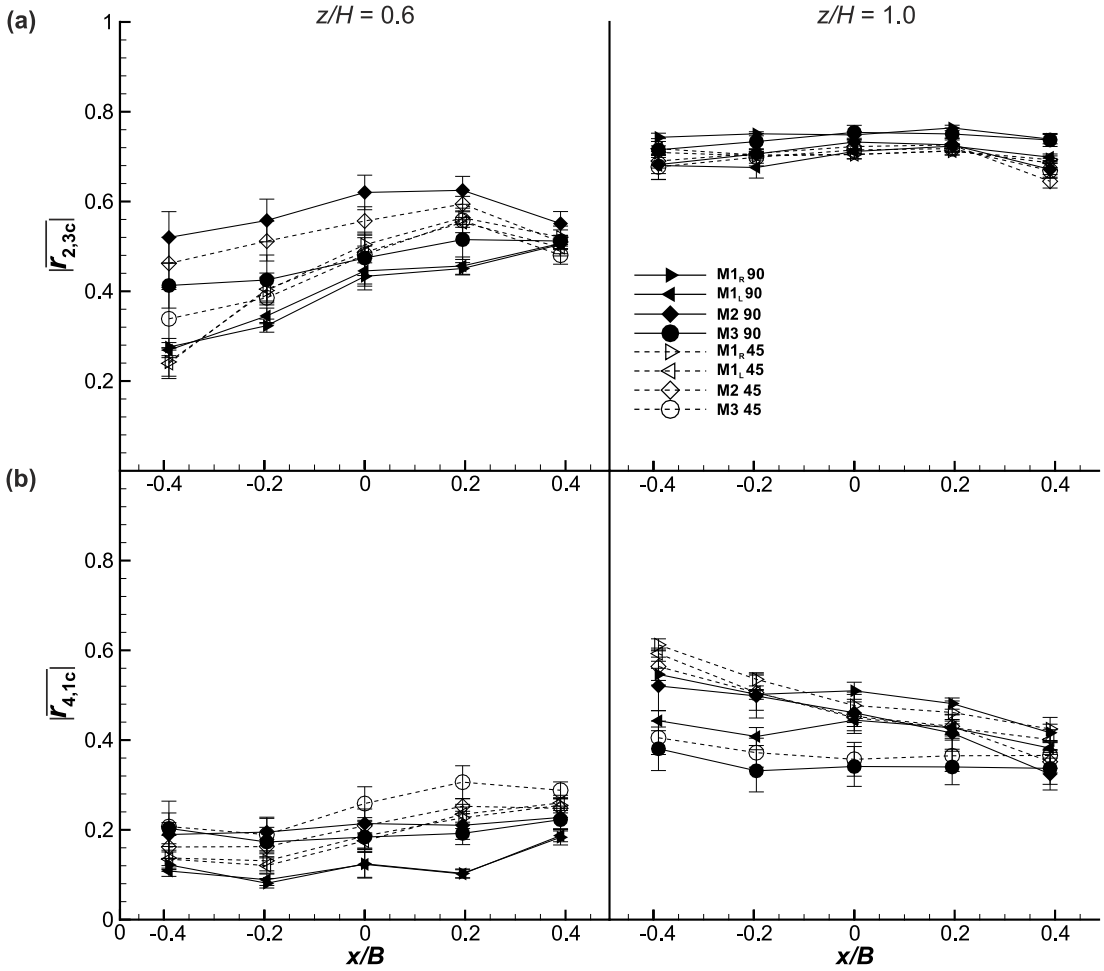

Figure 6.14: Streamwise distributions of the coefficients of correlation between the (**a**) sweep and clean air entrainment $|\overline{r_{2,3c}}|$, and between the (**b**) ejection and polluted air venting $|\overline{r_{4,1c}}|$, line-averaged along the spanwise direction of the canyon. The symbols have the same meaning as in Fig. 6.6.

direction, models M1 and M2 have higher contributions to polluted air ventilation (filled triangles and diamonds in Fig. 6.13d, respectively) than to the entrainment of the clean air (Fig. 6.13c). The ventilation processes are approximately equal for model M3 (filled circles in Fig. 6.13c and d). The highest polluted air ventilation and the lowest clean-air entrainment among all investigated canyons are observed for model M2, across the entire canyon width. If the wind direction becomes oblique, an appreciable increase in polluted air ventilation is observed for each canyon model (open symbols in Fig. 6.13d). The same cannot be stated for clean-air entrainment, where only one appreciable increase (model M2) occurs (open diamonds in Fig. 6.13d).

To quantify the relationship between the coherent structures and ventilation processes, we calculated the coefficients of correlation between the sweep and clean-air entrainment ($r_{2,3c}$) and between the ejection and polluted air ventilation

$(r_{4,1c})$ as

$$r_{2,3c} = \frac{\overline{(u'w')_2(w'c')_3}}{\sigma_{uw2}\sigma_{wc3}},\ r_{4,1c} = \frac{\overline{(u'w')_4(w'c')_1}}{\sigma_{uw4}\sigma_{wc1}}, \tag{6.11}$$

where $(u'w')_i$ and $(w'c')_j$ are the time series of the momentum $(i = 2, 4)$ and scalar events $(j = 3, 1)$, respectively, and σ_{uwi} and σ_{wcj} are their standard deviations. Similar coefficients of correlation between the momentum flux and two scalar fluxes (sensible and latent heat) were used by Li and Bou-Zeid (2011).

Because events are always negative and the scalar fluxes are always positive, the correlation coefficient is always negative. We thus present the absolute values of the correlation coefficients to stress that the investigated dominant momentum (sweeps and ejections) and scalar (inward and outward interactions) fluxes vary in the same direction.

The line-averaged streamwise distributions of $|\overline{r_{2,3c}}|$ and $|\overline{r_{4,1c}}|$ at both investigated heights are presented in Fig. 6.14a and Fig. 6.14b, respectively. First, there is little effect of the wind direction on either correlation coefficient in all investigated cases. Very high correlations (ranging from 0.7 to 0.75) between sweeps and clean-air entrainment ($|\overline{r_{2,3c}}|$) are seen across all canyon model widths at $z/H = 1.0$ for both wind directions (Fig. 6.14a, right column). This finding supports the idea that the sweep events "sweep" the clean air into the canyon at roof level. At $z/H = 0.6$, lower but still appreciable correlations between sweeps and clean-air entrainment are observed for canyons with varying roof height.

The correlations between the ejection and polluted air ventilation ($|\overline{r_{4,1c}}|$) are weak at both heights. However, they are still appreciable at $z/H = 1.0$ (Fig. 6.14b, right column). This supports the results of CFD studies (e.g., Michioka et al. (2014); Liu et al. (2013)), where the low momentum fluid ($u' < 0$) was related to pollutant removal at roof level ($z/H = 1$).

6.4 Conclusions

According to topical knowledge of street-canyon ventilation obtained in previous wind-tunnel and CFD studies, we designed a wind-tunnel experiment that addressed ground-level line-source ventilation processes within 3D street canyons. The three-dimensionality refers to roof-height non-uniformity along both leeward and windward canyon walls. We simulated two approach flow directions over three different types of street-canyon models arranged in an urban-like array and formed by courtyard-type buildings.

Detailed analysis of the mean velocity, concentration and pollution flux fields shows that roof-height variability along both canyon walls cannot be treated as that of an averaged step-up, step-down or uniform street canyon if one needs to study the ventilation processes within the canyon locally or for non-perpendicular approach wind directions. However, the studied non-uniform street canyons, represented as averaged step-up and step-down canyons, produce lower and higher

concentration levels than the uniform canyon, respectively, in the case of a perpendicular wind direction.

We demonstrated the complexity of the flow three-dimensionality within non-uniform canyons by analyzing the pollutant removal for the perpendicular wind direction. Generally, more pollutant is removed to the flow aloft from the non-uniform canyons than from the uniform canyon. In the case of the averaged step-down canyon, not only were all the emissions from the line source positioned within the canyon removed but also another 31% of this emission amount was ventilated from the canyon surroundings. Hence, the resulting highest spatially-averaged concentration cannot be attributed to the higher pollutant re-emission as was demonstrated in many CFD studies on 2D canyons.

If only the line source within the canyon is taken into account, the averaged step-down canyon will have better ventilation than the uniform canyon owing to the extra lateral entrainment of unpolluted air from the intersections. The best ventilation performance with respect to the highest pollutant removal and the lowest spatially-averaged concentrations, and hence the lowest reemission, was achieved by the averaged step-up canyon. To gain better insight into the mechanisms of pollutant removal from 3D canyons, additional experimental and numerical studies are needed.

We introduced nomenclature for the ventilation processes according to quadrant analysis of the pollutant flux. We observed that the venting of polluted air from a canyon increases if the wind direction changes from perpendicular to oblique, irrespective of the studied canyon model. Furthermore, we found strong correlations between the turbulent coherent structures and ventilation processes at roof level, irrespective of the canyon model and wind direction. The sweeps and ejections were highly correlated (> 0.5) with clean air entrainment and polluted air venting, respectively.

Acknowledgements
This work was supported by the Charles University in Prague (project GAUK No. 535412), the Czech Science Foundation GACR (project GAP15-18964S) and the institutional support RVO: 61388998.

6.5 References

B. Addepalli and E. R. Pardyjak. A study of flow fields in step-down street canyons. *Environmental Fluid Mechanics*, 15(2):439–481, 2015. ISSN 15677419. doi: 10.1007/s10652-014-9366-z.

J. J. Baik and J. J. Kim. On the escape of pollutants from urban street canyons. *Atmospheric Environment*, 36(3):527–536, 2002. ISSN 13522310. doi: 10.1016/S1352-2310(01)00438-1.

J.-J. Baik, R.-S. Park, H.-Y. Chun, and J.-J. Kim. A Laboratory Model of Urban Street-Canyon Flows. *Journal of Applied Meteorology*, 39(9):1592–1600,

2000. ISSN 0894-8763. doi: 10.1175/1520-0450(2000)039⟨1592:ALMOUS⟩2.0.CO;2. URL http://journals.ametsoc.org/doi/abs/10.1175/1520-0450%282000%29039%3C1592%3AALMOUS%3E2.0.CO%3B2.

J. F. Barlow, I. N. Harman, and S. E. Belcher. Scalar fluxes from urban street canyons. Part I: Laboratory simulation. *Boundary-Layer Meteorology*, 113(3): 369–385, dec 2004. ISSN 00068314. doi: 10.1023/B:BOUN.0000045525.70731.ff. URL http://link.springer.com/10.1007/s10546-004-6204-8.

S. E. Belcher. Mixing and transport in urban areas. *Philosophical Transactions of the Royal Society A: Mathematical, Physical and Engineering Sciences*, 363(1837):2947–2968, 2005. ISSN 1364-503X. doi: 10.1098/rsta.2005.1673. URL http://rsta.royalsocietypublishing.org/cgi/doi/10.1098/rsta.2005.1673.

K. Bezpalcova. *Physical Modelling of Flow and Diffusion in Urban Canopy*. PhD thesis, Charles University in Prague, 2006.

K. Blackman, L. Perret, and E. Savory. Effect of upstream flow regime on street canyon flow mean turbulence statistics. *Environmental Fluid Mechanics*, 15 (4):823–849, 2015. ISSN 15731510. doi: 10.1007/s10652-014-9386-8.

B. Blocken. Computational Fluid Dynamics for urban physics: Importance, scales, possibilities, limitations and ten tips and tricks towards accurate and reliable simulations. *Building and Environment*, 91:219–245, 2015. ISSN 03601323. doi: 10.1016/j.buildenv.2015.02.015.

R. E. Britter and S. R. Hanna. Flow and Dispersion in Urban Areas. *Annual Review of Fluid Mechanics*, 35(1):469–496, jan 2003. ISSN 0066-4189. doi: 10.1146/annurev.fluid.35.101101.161147. URL http://www.annualreviews.org/doi/10.1146/annurev.fluid.35.101101.161147.

X. M. Cai, J. F. Barlow, and S. E. Belcher. Dispersion and transfer of passive scalars in and above street canyons-Large-eddy simulations. *Atmospheric Environment*, 42(23):5885–5895, 2008. ISSN 13522310. doi: 10.1016/j.atmosenv.2008.03.040.

M. Carpentieri and A. G. Robins. Influence of urban morphology on air flow over building arrays. *Journal of Wind Engineering and Industrial Aerodynamics*, 145:61–74, 2015. ISSN 01676105. doi: 10.1016/j.jweia.2015.06.001.

M. Carpentieri, P. Hayden, and A. G. Robins. Wind tunnel measurements of pollutant turbulent fluxes in urban intersections. *Atmospheric Environment*, 46: 669–674, jan 2012. ISSN 13522310. doi: 10.1016/j.atmosenv.2011.09.083. URL http://linkinghub.elsevier.com/retrieve/pii/S1352231011010909.

H. Cheng and I. P. Castro. Near-wall flow development after a step change in surface roughness. *Boundary-Layer Meteorology*, 105(3):411–432, 2002. ISSN 00068314. doi: 10.1023/A:1020355306788.

J. Counihan. Adiabatic atmospheric boundary layers: A review and analysis of data from the period 1880–1972. *Atmospheric Environment (1967)*, 9(10): 871–905, oct 1975. ISSN 00046981. doi: 10.1016/0004-6981(75)90088-8. URL `http://linkinghub.elsevier.com/retrieve/pii/0004698175900888`.

W. F. Dabberdt and W. G. Hoydysh. Street canyon dispersion: Sensitivity to block shape and entrainment. *Atmospheric Environment Part A, General Topics*, 25(7):1143–1153, 1991. ISSN 09601686. doi: 10.1016/0960-1686(91)90225-V.

Y. dong Huang, W. rong He, and C. N. Kim. Impacts of shape and height of upstream roof on airflow and pollutant dispersion inside an urban street canyon. *Environmental Science and Pollution Research*, 22(3):2117–2137, 2015. ISSN 16147499. doi: 10.1007/s11356-014-3422-6.

J. E. Fackrell and A. G. Robins. The effects of source size on concentration fluctuations in plumes. *Boundary-Layer Meteorology*, 22(3):335–350, mar 1982. ISSN 0006-8314. doi: 10.1007/BF00120014. URL `http://link.springer.com/10.1007/BF00120014`.

C. S. B. Grimmond and T. R. Oke. Aerodynamic Properties of Urban Areas Derived from Analysis of Surface Form. *Journal of Applied Meteorology*, 38(9):1262–1292, 1999. ISSN 0894-8763. doi: 10.1175/1520-0450(1999)038⟨1262:APOUAD⟩2.0.CO;2. URL `http://journals.ametsoc.org/doi/abs/10.1175/1520-0450%281999%29038%3C1262%3AAPOUAD%3E2.0.CO%3B2`.

Z. L. Gu, Y. W. Zhang, Y. Cheng, and S. C. Lee. Effect of uneven building layout on air flow and pollutant dispersion in non-uniform street canyons. *Building and Environment*, 46(12):2657–2665, 2011. ISSN 03601323. doi: 10.1016/j.buildenv.2011.06.028.

W. G. Hoydysh, Y. Ogawa, and R. A. Griffiths. A scale model study of dispersion of pollution in street canyons. In *Annual Meeting of the Air Pollution Control Association, Denver, Colorado*, 1974.

W. G. Hoydysh and W. F. Daeberdt. Kin ∼ Mati ∼ S and Dispersion C ∼ Ara ∼ Eristics Flows in Asymmetric Street Canyons of. *Environment*, 22(12): 2677–2689, 1988.

P. Kastner-Klein and E. J. Plate. Wind-tunnel study of concentration fields in street canyons. *Atmospheric Environment*, 33(24-25):3973–3979, 1999. ISSN 13522310. doi: 10.1016/S1352-2310(99)00139-9.

P. Kastner-Klein, R. Berkowicz, and R. Britter. The influence of street architecture on flow and dispersion in street canyons. *Meteorology and Atmospheric Physics*, 87(1-3):121–131, jun 2004. ISSN 01777971. doi: 10.1007/s00703-003-0065-4. URL http://link.springer.com/10.1007/s00703-003-0065-4.

G. Katul, D. Poggi, D. Cava, and J. Finnigan. The relative importance of ejections and sweeps to momentum transfer in the atmospheric boundary layer. *Boundary-Layer Meteorology*, 120(3):367–375, sep 2006. ISSN 0006-8314. doi: 10.1007/s10546-006-9064-6. URL http://link.springer.com/10.1007/s10546-006-9064-6.

P. Klein, B. Leitl, and M. Schatzmann. Driving physical mechanisms of flow and dispersion in urban canopies. *International Journal of Climatology*, 27(14): 1887–1907, 2007. ISSN 08998418. doi: 10.1002/joc.1581.

L. Kukacka, S. Nosek, R. Kellnerova, K. Jurcakova, and Z. Janour. Wind Tunnel Measurement of Turbulent and Advective Scalar Fluxes: A Case Study on Intersection Ventilation. *The Scientific World Journal*, 2012:1–13, 2012. ISSN 1537-744X. doi: 10.1100/2012/381357. URL http://www.hindawi.com/journals/tswj/2012/381357/.

L. Kukacka, S. Nosek, R. Kellnerova, K. Jurcakova, and Z. Janour. Contribution of Advective and Turbulent Contaminant Transport to the Intersection Ventilation. In D. G. Steyn and S. T. Castelli, editors, *NATO Science for Peace and Security Series C: Environmental Security*, volume 137, pages 665–668. Springer, Dordrecht, 2013. ISBN 9789400755765. doi: 10.1007/978-94-007-5577-2_113. URL http://link.springer.com/10.1007/978-94-007-5577-2_113.

L. Kukacka, V. Fuka, S. Nosek, R. Kellnerova, and Z. Janour. Ventilation of idealised urban area, LES and wind tunnel experiment. *EPJ Web of ...*, 62:1–10, 2014. ISSN 2100-014X. doi: 10.1051/epjconf/20146702062. URL http://www.epj-conferences.org/articles/epjconf/abs/2014/04/epjconf_efm-13_02062/epjconf_efm-13_02062.html.

B. Leitl and R. Meroney. Car exhaust dispersion in a street canyon. Numerical critique of a wind tunnel experiment. *Journal of Wind Engineering and Industrial Aerodynamics*, 67-68:293–304, 1997. ISSN 01676105. doi: 10.1016/S0167-6105(97)00080-9.

D. Li and E. Bou-Zeid. Coherent Structures and the Dissimilarity of Turbulent Transport of Momentum and Scalars in the Unstable Atmospheric Surface Layer. *Boundary-Layer Meteorology*, 140(2):243–262, aug 2011. ISSN 0006-8314. doi: 10.1007/s10546-011-9613-5. URL http://link.springer.com/10.1007/s10546-011-9613-5.

C. H. Liu, D. Y. C. Leung, and M. C. Barth. On the prediction of air and pollutant exchange rates in street canyons of different aspect ratios using large-eddy simulation. *Atmospheric Environment*, 39(9):1567–1574, 2005. ISSN 13522310. doi: 10.1016/j.atmosenv.2004.08.036.

C.-h. Liu, C.-t. Ng, and C. C. C. Wong. A Theory on the Ventilation over Hypothetical Urban Areas. *J Hazard Mater*, 15:2013, 2013. ISSN 03043894.

P. Louka, S. E. Belcher, and R. G. Harrison. Coupling between air flow in streets and the well-developed boundary layer aloft. *Atmospheric Environment*, 34 (16):2613–2621, 2000. ISSN 13522310. doi: 10.1016/S1352-2310(99)00477-X.

D. M. S. Madalozzo, A. L. Braun, A. M. Awruch, and I. B. Morsch. Numerical simulation of pollutant dispersion in street canyons: Geometric and thermal effects. *Applied Mathematical Modelling*, 38(24):5883–5909, 2014. ISSN 0307904X. doi: 10.1016/j.apm.2014.04.041.

R. N. Meroney, M. Pavageau, S. Rafailidis, and M. Schatzmann. Study of line source characteristics for 2-D physical modelling of pollutant dispersion in street canyons. *Journal of Wind Engineering and Industrial Aerodynamics*, 62(1):37–56, aug 1996. ISSN 01676105. doi: 10.1016/S0167-6105(96)00057-8. URL `http://linkinghub.elsevier.com/retrieve/pii/S0167610596000578`.

T. Michioka, H. Takimoto, and A. Sato. Large-Eddy Simulation of Pollutant Removal from a Three-Dimensional Street Canyon. *Boundary-Layer Meteorology*, 150(2):259–275, feb 2014. ISSN 0006-8314. doi: 10.1007/s10546-013-9870-6. URL `http://link.springer.com/10.1007/s10546-013-9870-6`.

K. Moon, J.-M. Hwang, B.-G. Kim, C. Lee, and J.-i. Choi. Large-eddy simulation of turbulent flow and dispersion over a complex urban street canyon. *Environmental Fluid Mechanics*, 14(6):1381–1403, dec 2014. ISSN 1567-7419. doi: 10.1007/s10652-013-9331-2. URL `http://link.springer.com/10.1007/s10652-013-9331-2`.

M. A. Nelson, E. R. Pardyjak, J. C. Klewicki, S. U. Pol, and M. J. Brown. Properties of the wind field within the Oklahoma City Park Avenue Street Canyon. Part I: Mean flow and turbulence statistics. *Journal of Applied Meteorology and Climatology*, 46(12):2038–2054, 2007. ISSN 15588424. doi: 10.1175/2006JAMC1427.1.

T. Nozu and T. Tamura. LES of turbulent wind and gas dispersion in a city. *Journal of Wind Engineering and Industrial Aerodynamics*, 104-106: 492–499, may 2012. ISSN 01676105. doi: 10.1016/j.jweia.2012.02.024. URL `https://www-sciencedirect-com.ezproxy.is.cuni.cz/science/article/pii/S0167610512000487http://linkinghub.elsevier.com/retrieve/pii/S0167610512000487`.

L. Perret and E. Savory. Large-Scale Structures over a Single Street Canyon Immersed in an Urban-Type Boundary Layer. *Boundary-Layer Meteorology*, 148(1):111–131, 2013. ISSN 00068314. doi: 10.1007/s10546-013-9808-z.

S. Rafailidis. Influence of Building Areal Density and Roof Shape on the Wind Characteristics Above a Town. *Boundary-Layer Meteorology*, 85(2):255–271, 1997. ISSN 0006-8314. doi: 10.1023/A:1000426316328. URL http://dx.doi.org/10.1023/A:1000426316328%5Cnhttp://www.springerlink.com/content/tv75403656835135/?p=5642ba0733db479e96ff9921362c6ae6&pi=2%5Cnhttp://www.springerlink.com/content/tv75403656835135/fulltext.pdf.

S. Rafailidis and M. Shatzmann. Concentration measurements with different roof patterns in street canyons with aspect ratios B/H=1/2 and B/H=1. Technical report, Meteorology Institute, University of Hamburg, 1995.

A. Robins, A. Scaperdas, E. Savory, E. Savory, D. Grigoriadis, A. Scaperdas, A. Robins, and D. Grigoriadis. Spatial variability and source-receptor relations at a street intersection. *Water, Air, and Soil Pollution: Focus*, 2(5):381–393, 2002. ISSN 1567-7230. doi: 10.1023/A:1021360007010. URL http://dx.doi.org/10.1023/A:1021360007010.

P. Salizzoni, M. Marro, L. Soulhac, N. Grosjean, and R. J. Perkins. Turbulent Transfer Between Street Canyons and the Overlying Atmospheric Boundary Layer. *Boundary-Layer Meteorology*, 141(3):393–414, 2011. ISSN 00068314. doi: 10.1007/s10546-011-9641-1.

E. Savory, L. Perret, and C. Rivet. Modelling considerations for examining the mean and unsteady flow in a simple urban-type street canyon. *Meteorology and Atmospheric Physics*, 121(1-2):1–16, 2013. ISSN 01777971. doi: 10.1007/s00703-013-0254-8.

M. Schatzmann and B. Leitl. Issues with validation of urban flow and dispersion CFD models. *Journal of Wind Engineering and Industrial Aerodynamics*, 99 (4):169–186, apr 2011. ISSN 01676105. doi: 10.1016/j.jweia.2011.01.005. URL http://linkinghub.elsevier.com/retrieve/pii/S0167610511000079.

W. Snyder. Guideline for fluid modeling of atmospheric diffusion, jun 1979. URL https://www.osti.gov/biblio/5521001.

R. B. Stull. *An Introduction to Boundary Layer Meteorology*. Kluwer Aademic Publishers, Dordrecht, 1988. ISBN 978-90-277-2769-5. doi: 10.1007/978-94-009-3027-8. URL http://link.springer.com/10.1007/978-94-009-3027-8.

H. Takimoto, A. Inagaki, M. Kanda, A. Sato, and T. Michioka. Length-Scale Similarity of Turbulent Organized Structures over Surfaces with Different

Roughness Types. *Boundary-Layer Meteorology*, 147(2):217–236, 2013. ISSN 00068314. doi: 10.1007/s10546-012-9790-x.

W. Theurer. Typical building arrangements for urban air pollution modelling. *Atmospheric Environment*, 33(24-25):4057–4066, 1999. ISSN 13522310. doi: 10.1016/S1352-2310(99)00147-8.

VDI. *Environmental meteorology – Physical modelling of flow and dispersion processes in the atmospheric boundary layer – Application of wind tunnels*. Verein Deutscher Ingenieure, Dusseldorf, Dusseldorf, 2000.

W. W. Willmarth. Structure of turbulence in boundary layers. *Arch Appl Mech*, 15:159–254, 1975.

X. Xiaomin, H. Zhen, and W. Jiasong. The impact of urban street layout on local atmospheric environment. *Building and Environment*, 41(10):1352–1363, oct 2006. ISSN 03601323. doi: 10.1016/j.buildenv.2005.05.028. URL `http://linkinghub.elsevier.com/retrieve/pii/S0360132305002003`.

X. Xie, Z. Huang, and J.-s. Wang. Impact of building configuration on air quality in street canyon. *Atmospheric Environment*, 39(25):4519–4530, aug 2005. ISSN 13522310. doi: 10.1016/j.atmosenv.2005.03.043. URL `http://linkinghub.elsevier.com/retrieve/pii/S1352231005003596`.

Y. Yang and Y. Shao. Numerical simulations of flow and pollution dispersion in urban atmospheric boundary layers. *Environmental Modelling and Software*, 23(7):906–921, 2008. ISSN 13648152. doi: 10.1016/j.envsoft.2007.10.005.

D. Zajic, H. J. Fernando, M. J. Brown, and E. R. Pardyjak. On flows in simulated urban canopies. *Environmental Fluid Mechanics*, 15(2):275–303, 2015. ISSN 15677419. doi: 10.1007/s10652-013-9311-6.

7. Impact of roof height non-uniformity on pollutant transport between a street canyon and intersections

Environmental Pollution, 2017, Volume 227, p. 125-138. ISSN 0269-7491. doi: 10.1016/J.ENVPOL.2017.03.073

Štěpán Nosek[2], Libor Kukačka[1,2], Klára Jurčáková[2], Radka Kellnerová[2], Zbyněk Jaňour[2]

[1] Charles University in Prague, Faculty of Mathematics and Physics, Prague, Czech Republic
[2] Institute of Thermomechanics, Academy of Sciences of the Czech Republic, Prague, Czech Republic

Abstract
This paper presents an extension of our previous wind-tunnel study (Nosek et al., 2016) in which we highlighted the need for investigation of the removal mechanisms of traffic pollution from all openings of a 3D street canyon. The extension represents the pollution flux (turbulent and advective) measurements at the lateral openings of three different 3D street canyons for the winds perpendicular and oblique to the along-canyon axis. The pollution was simulated by emitting a passive gas (ethane) from a homogeneous ground-level line source positioned along the centreline of the investigated street canyons. The street canyons were formed by courtyard-type buildings of two different regular urban-array models. The first model has a uniform building roof height, while the second model has a non-uniform roof height along each building's wall. The mean flow and concentration fields at the canyons' lateral openings confirm the findings of other studies that the buildings' roof-height variability at the intersections plays an important role in the dispersion of the traffic pollutants within the canyons. For the perpendicular wind, the non-uniform roof-height canyon appreciably removes or entrains the pollutant through its lateral openings, contrary to the uniform canyon, where the pollutant was removed primarily through the top. The analysis of the turbulent mass transport revealed that the coherent flow structures of the lateral momentum transport correlate with the ventilation processes at the lateral openings of all studied canyons. These flow structures coincide at the same areas and hence simultaneously transport the pollutant in opposite directions.

Keywords
Urban array, 3D street canyon, pollution flux measurement, wind tunnel, coherent structures.

7.1 Introduction

The street network formed by buildings is an inherent part of a city. While the buildings have favourable effects on the well-being of city dwellers, e.g., offering shade from the sun during warm seasons, they have also unfavourable effects, e.g., preventing the ventilation of pollutants from traffic (Oke, 1988). The air quality then deteriorates not only in pedestrian zones but also inside the buildings that line the streets and intersections (Jin et al., 2016; Yang et al., 2016). Another health-related issue is the accidental or deliberate release of harmful substances within a local spot of a street network, and this is becoming more serious as most of the world's population lives in cities (Barlow, 2014).

Owing primarily to these health-related issues, extensive research on identifying and understanding the physical processes that drive and influence the near-field pollutant dispersion in urban environments has experienced substantial progress over the last three decades. While earlier studies relied on wind-tunnel (Hoydysh et al., 1974; Klein et al., 2007; Brixey et al., 2009; Carpentieri et al., 2012) or field (Allwine et al., 2002; Longley et al., 2004; Pol and Brown, 2008; Balogun et al., 2010) experiments, recent studies are focused more on numerical approaches, mostly using computational fluid dynamics (CFD) (Hamlyn and Britter, 2005; Gu et al., 2011; Michioka et al., 2014; Buccolieri et al., 2015) and, to some extent, semi-empirical models (Brown et al., 2015; Soulhac et al., 2016). Each of these approaches and their advantages and limitations have been recently reviewed by several studies (Lateb et al., 2016; Tominaga and Stathopoulos, 2016; Blocken et al., 2016). Lateb et al. (2016) clearly concluded that "the topic of micro-scale dispersion still requires further investigation to understand the effect of all parameters on wind flow and pollutant dispersion in urban areas" and that there "is a clear need for the development of computational methods for wind engineering applications utilising 3D numerical modelling of flow and dispersion fields around buildings." However, all these reviews also concluded that the main limitation of CFD or semi-empirical models is that they still require validation against experimental tests. Due to the recent increase in CFD studies, it is essential that the performance of quality experiments go hand in hand.

Although field experiments have the important advantage, in comparison to physical and numerical modelling, that they are conducted under real atmospheric conditions, these conditions are uncontrollable, and hence a repeat of the experiment under identical conditions is impossible (Schatzmann and Leitl, 2011). In addition, the number of measurement points is limited owing to financial or technical constraints. While the first disadvantage can be solved by wind-tunnel tests

(providing an appropriately modelled atmospheric boundary-layer flow approaching a reduced-scale model), the latter is recently solved only by the CFD models (Lateb et al., 2016) since they compute the flow and concentration fields over the entire computational domain.

While several wind-tunnel studies, focused on pollutant dispersion within 3D urban-like arrays formed by blocks of uniform (Davidson et al., 1996; Brown et al., 2001; Garbero et al., 2010; Castro et al., 2017) or variable (Hoydysh et al., 1974; Klein et al., 2007; Heist et al., 2009) height, gave insight into the pollutant dispersion within such street networks, they lack the full urban three-dimensionality (variability of the obstacle geometry in all directions) at the cost of the highest possible geometrical simplification. The study of Nosek et al. (2016) showed by means of even and uneven roof height along each courtyard building's wall of a regular urban array that the pollutant fluxes and pollutant removal capabilities through the street-canyon roof top are strongly affected by those roof-height arrangements. That study confirmed the observations from the CFD study of Gu et al. (2011) and highlighted that the roof-height non-uniformities along both street-canyon walls are able to improve or worsen the street-canyon air quality with regard to the source position and above-roof wind direction. Interestingly, Nosek et al. (2016) also concluded that the 'vertical' turbulent coherent structures (known as sweeps and ejections) are highly correlated with ventilation processes (introduced by that study as entraining of clean air and venting of polluted air), irrespective of the canyons' roof-height arrangements and wind direction.

Conclusions drawn from two field campaigns, Joint Urban in Oklahoma city, Oklahoma, US (Pol and Brown, 2008) and DAPPLE in London, UK (Balogun et al., 2010), indicate that both the direction of the above-roof winds and the buildings' roof-height non-uniformity at the intersections play an important role in developing complex flow structures at the lateral ends of the canyons. These structures were found to be a combination of individual flow structures, such as horizontally rotating "corner" vortices at the canyon ends and converging or diverging flows from/into the adjoining canyons and intersections. Because these structures drive the pollutant exchange processes between the street canyon and intersections principally in the horizontal direction (Klein et al., 2007; Carpentieri et al., 2012), there is a clear need for additional experimental studies that will give better insight into these processes in that direction with respect to buildings' roof-height non-uniformity at these intersections. This will help to better understand the near-field pollutant dispersion phenomena for real cases of urban environments and provide the lacking experimental data for validation of CFD models.

The present paper is, therefore, principally an extension of the study of Nosek et al. (2016), and the aims are the following: (i) investigate the horizontal pollutant exchange processes at the lateral openings of the same uniform and non-uniform canyons with respect to the wind direction; (iii) find the correlations between the 'lateral' coherent structures and ventilation processes, similar to those for vertical pollutant transport; and (iii) observe the effect of the roof-height non-

uniformity on the street-canyon pollutant exchange processes with respect to the regularity of the urban-array layout. To accomplish these aims, we performed additional wind-tunnel runs where both the turbulent and advective pollution fluxes were measured at each canyon's lateral openings for two wind directions, perpendicular and oblique (i.e., 45°) to the along-canyon axis. The pollution was simulated by homogeneously emitted passive gas (ethane) from a ground-level line source. The line source was positioned along the centreline of the investigated street canyons, crossing the adjoining intersection, and hence represented the pollution from idealised homogenous traffic.

7.2 Methods

7.2.1 Experimental setup

The experiments were conducted under neutrally stratified conditions in the Environmental wind tunnel of the Institute of Thermomechanics of the Czech Academy of Sciences. This is an open low-speed wind tunnel with cross dimensions of 1.5 × 1.5 m, and the lengths of the development and test sections are 20.5 m and 2 m, respectively. The freestream velocity can be maintained within a range of 0.1–10 m.s^{-1} by means of a frequency convertor of the fan with an accuracy of 0.05 m.s^{-1}. Because the pollutant dispersion in urban areas is related to the atmospheric boundary layer developed above terrain of such considerable roughness, the corresponding approaching boundary layer, with a scale of 1:400, was initiated by turbulence generators (a set of three spires, 1.4 m in height) and subsequently developed by a staggered array of roughness elements (thin plates of 50 mm in width and height) along the remaining part of the development section in the wind tunnel. The characteristics of the boundary layer were measured at the wind-tunnel freestream velocity $U_0 = 6.2$ m.s^{-1} (measured using a Prandtl tube at a fixed position, 1m above the wind-tunnel bottom and 4 m upwind from the test section) by 2D Laser Doppler Anemometry (LDA) at four positions between the roughness elements at the end of the development section. The position and characteristics of the best-fitted vertical profile are described in detail in Nosek et al. (2016), together with the aerodynamic parameters (roughness length, $z_0 = 1.87$ m; displacement height, $z_0 = 3$ m; and friction velocity, $u_* = 0.43$ m.s^{-1}, all at full scale) and characteristics of turbulence. The mean near-surface streamwise and vertical intensities of turbulence were $I_u = 35\%$ and $I_w = 25\%$, respectively, and in good accordance with VDI (2000) guidelines. We also computed the integral length scales of the streamwise velocity component, L_{ux}, from time series measured at 7 different heights across the boundary-layer depth. For the heights $z_{FS} < 50$ m (full scale), these integral length scales were within the theoretical values for very rough terrain and in good accordance with the filed measurements (Counihan, 1975).

To study the effect of urban array three-dimensionality and wind direction on pollutant transport from traffic while keeping the configuration as simple as pos-

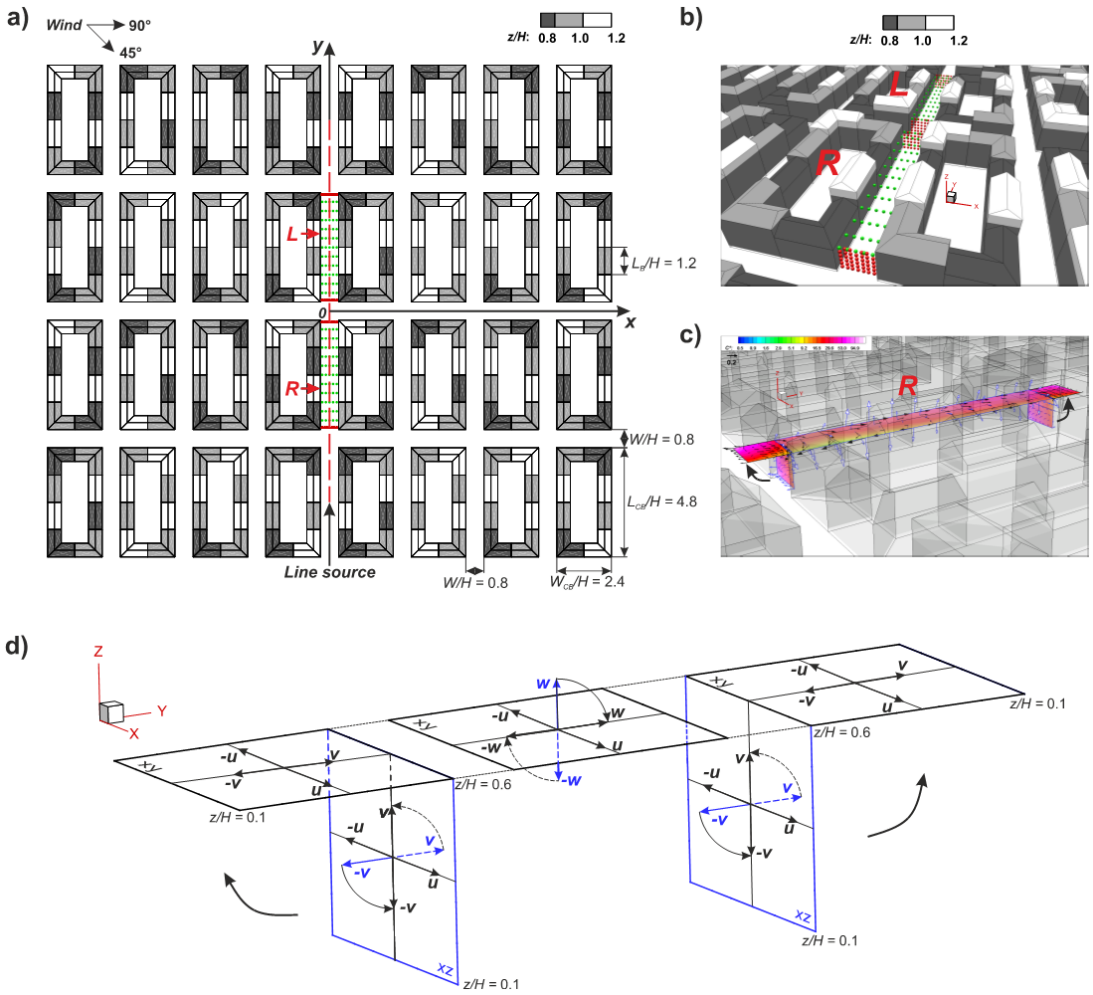

Figure 7.1: Schemas of the urban-array model A2 with respect to the wind-tunnel coordinates x, y and z: **a**) top and **b**) 3D view. The grey contour represents the dimensionless height (z/H) of the courtyard building's segment; the green and red points represent the measuring points at the horizontal (xy) and vertical planes (xz), respectively; the labels 'R' and 'L' denote the 'right' and 'left' street canyon; **c**) 3D view of the lateral plane transformation from the vertical to the horizontal plane, and **d**) schema of that transformation where the measured velocity components (u, v, w, blue arrows) normal to the measured planes (blue) were rotated to these planes.

sible, we designed two urban array models according to the typical pattern of the centres of Central European cities (Fig. 7.1). Both idealised models were formed by evenly spaced 8 x 4 courtyard-type buildings of constant length (L_{CB} = 300 mm) and width (W_{CB} = 150 mm). The difference between the modelled urban arrays consisted of the heights of the pitched roofs of the courtyard buildings. While the reference urban model (A1) had a constant roof height (H = 62.5 mm, i.e., 25 m at full scale) for each building, the second urban model (A2) had

arbitrarily distributed roof heights along each building's wall (Fig. 7.1). The roof-height non-uniformity of model A2 was distributed such that each of the courtyard buildings had four and two segments (all of 75 mm in length, L_B in Fig. 7.1a) of different roof heights ($z/H = 0.8$, 1 or 1.2) along its longer (L_{CB}) and shorter (W_{CB}) wall, respectively. Meanwhile, the average height ($H_m = H$), plan ($\lambda_p = A_b/A_t = 0.28$, where A_b is the area occupied by the buildings and A_t is the total ground area) and frontal ($\lambda_f = A_f/A_t = 0.27$, where A_f is the frontal area of the buildings viewed from the approach direction of flow) densities of both urban arrays were the same. The flow was fully independent of the Reynolds number based on the building's height and freestream velocity (i.e., $Re_B = HU_0/\nu \approx 24.400$, where ν is the kinematic viscosity of the air) or based on the friction velocity and roughness length (i.e., $Re^* = z_0 u^*/\nu \approx 240$) according to Snyder (1979).

We simulated the pollution from traffic by means of a ground-level line source that emitted the passive gas (ethane) homogenously. Although in real cases, the traffic within the streets is not homogenous due to the acceleration and deceleration at the intersections (Gokhale, 2011), we aimed to decrease the input parameters, which would affect the observation of the near-field pollutant dispersion, to a minimum. The line source was formed by 504 equally spaced tubes made of stainless steel placed flat side-by-side continuously at the bottom of the centreline of the investigated street canyons and adjoining intersections (see the red dashed line in Fig. 7.1a). The tubes had an inner diameter of 0.3 mm and length of 100 mm, and they were incorporated into the plenum chamber, which was positioned below the wind-tunnel bottom. Thus, the entire lengths of the tubes were positioned below the ground level of the urban-array models with outlets facing that level. The pressure drop between the plenum chamber and the wind-tunnel bottom was substantial to make the gas flow rate of 18 ml s^{-1} insensitive to the local pressure fluctuations of the street-canyon flow (Meroney et al., 1996). We tested the homogeneity of the line source and the influence of its ethane discharge velocity on the street-canyon flow by several measurement and visualization tests prior to the measurement campaign.

For both urban-array models, we simulated two wind directions: perpendicular and oblique (i.e., 45°) to the line source. Further details regarding the line source and above-urban-array flow homogeneity are reported in Nosek et al. (2016)

7.2.2 Measurement techniques

For the measurement of the pollutant transport through the lateral openings of the street canyons (red points in Figs. 7.1a and 7.1b), we followed the method used by Nosek et al. (2016), where the ventilation processes through their tops were investigated (green points in Figs. 7.1a and 7.1b). This method comprises simultaneous point measurements of two velocity components and concentration using a Dantec LDA probe and a probe of a Cambustion HFR400 fast-response

flame ionization detector (FFID), respectively. The LDA and FFID probes were assembled together on a 3D traverser system such that the end of the FFID sampling tube with an outer diameter of 0.5 mm was placed 1 mm above, 1 mm behind and 1 mm beside the centre of the LDA measuring volume. Different positions of the FFID sampling tube, conducted during several measurement tests, did not affect the LDA measurement. The seeding particles (glycerine droplets of approx. 1 μm in diameter) for the LDA were produced by a commercial haze generator Smoke Factory, Tour Hazer II, at the beginning of the wind-tunnel development section, approx. 0.5 m in front of the Irwin spires. Owing to the air flow equally filled by these seeding particles and a high-power Argon-Ion laser from Spectra Physics (model 165) used for the LDA, a data rate of approximately 0.5 kHz was attained at the bottom levels (i.e., $z/H = 0.1$) and up to 1 kHz within the street canyons (i.e., $z/H = 0.6$). The sampling time (120 s) for each measuring point was set according to the results of velocity and concentration central moment independence tests. Because the FFID sampling frequency (0.5 kHz) was lower than that of the LDA, the measured 120-s-long time series of the instantaneous concentration and velocities were reconstructed using linear interpolation at the constant frequency of 0.5 kHz. Due to the length (200 mm) of the FFID sample tube, the mean delay in the physical sampling time relative to that of LDA was approximately 12 ms. This delay varied such that the air density and dynamic pressure varied with the time and position. To synchronize the time series from the LDA with those from the FFID, a maximum coefficient of correlation (time lag) was computed between these two time series. A correction of the effect of the LDA seeding particles on the FFID concentration measurements was achieved by subtracting the background concentration of the LDA seeding particles from the concentration of the calibration gas.

Fig. 7.1b) shows the positions of the measurement points (red) at the lateral openings of the non-uniform street canyons (hereafter, the street canyons are labelled according to the downstream view as 'R' and 'L' for the right and left canyon, respectively). Based on previous studies (Carpentieri et al., 2012; Kukacka et al., 2012), it is assumed that the prevailing pollutant exchange between these openings and intersections occurs in a horizontal direction for both simulated wind directions, and hence we measured in the present study the lateral (v, blue arrows normal to xz planes in Fig. 7.1d) and longitudinal (u, blue arrows parallel with xz planes in Fig. 7.1d) velocity components at these openings for all investigated canyons. Analogically, the dominant pollutant exchange between the canyon and the flow aloft occurs in the vertical direction through the canyon's top, and hence we measured in our previous study Nosek et al. (2016) the vertical (w, blue arrows normal to xy planes in Fig. 7.1d) and longitudinal (u, blue arrows parallel with xy planes in Fig. 7.1d) velocity components at these openings. Regarding the height of the lowest canyon wall of the investigated non-uniform canyons (i.e., $z/H = 0.6$, dark grey contour in Fig. 7.1b), the top openings were measured at that height to compare the investigated canyons among themselves. The overall measurement error of pollution fluxes, considering the errors of ve-

locity (1%), concentration measurements (4%) and the positioning error of the 3D traverser system (1%), was estimated using ensemble statistics as 4%.

7.3 Results and discussions

7.3.1 Mean flow and dispersion in the street canyons

Because we observed that the roof-height non-uniformity produces very complex flow structures at the investigated planes, we present these planes in a compact manner to gain better insight into these structures. For this, we used the transformation of the lateral planes (xz, labelled blue in Fig. 7.1d) to the horizontal plane (xy, labelled black in Fig. 7.1d) according to the right-hand Cartesian coordinate system. Thus, the transformation represents the rotation of the right and left lateral plane along the x-axis by an angle of 90° and −90°, respectively, hence folding their bottom ($z/H = 0.1$) up to the horizontal plane at the dimensionless height $z/H = 0.6$. The mean flow field is presented by means of the mean dimensionless velocity vectors $\boldsymbol{U_{lat}} = (U/U_0, V/U_0)$ for the lateral planes and $\boldsymbol{U_{ver}} = (U/U_0, W/U_0)$ for the horizontal planes, where U, V and W are the mean longitudinal, lateral and vertical velocities. Because the measured lateral (v) and vertical (w) velocity components were normal to the measured horizontal planes (blue arrows in Fig. 7.1d), they were transformed into these planes (black arrows in Fig. 7.1d) to observe their orientation.

The top views of the mean flow and concentration fields for the investigated planes and canyons are presented in Figs. 7.2 and 7.3 for the perpendicular and oblique wind directions, respectively. For the concentration fields, we used the dimensionless form according to VDI (2000) guidelines as

$$C^* = \frac{C L_s U_0 H}{Q}, \tag{7.1}$$

where C is the measured mean volume concentration, L_s is the length of the line source, and Q is the ethane volume flow rate from the line source.

Perpendicular wind

Fig. 7.2a) confirms several flow and concentration field patterns observed in numerous wind-tunnel (Soulhac et al., 2009; Heist et al., 2009; Brixey et al., 2009) and numerical (Hamlyn and Britter, 2005; Michioka et al., 2014) studies for 3D street canyons of uniform height and perpendicular winds. The presented horizontal plane in Fig. 7.2a) gives evidence of the symmetrical in-canyon flow structures driven by the shear layers, which are twofold: one emerging from the upstream roof, and the second emerging from the upstream side corners of that uniform canyon. The first drives the vertically recirculating vortex with the along-canyon axis and is represented by the downward flow at the downstream wall ($x/H = 0.4$, where the $\boldsymbol{U_{ver}}$ vectors are aligned with the direction of the

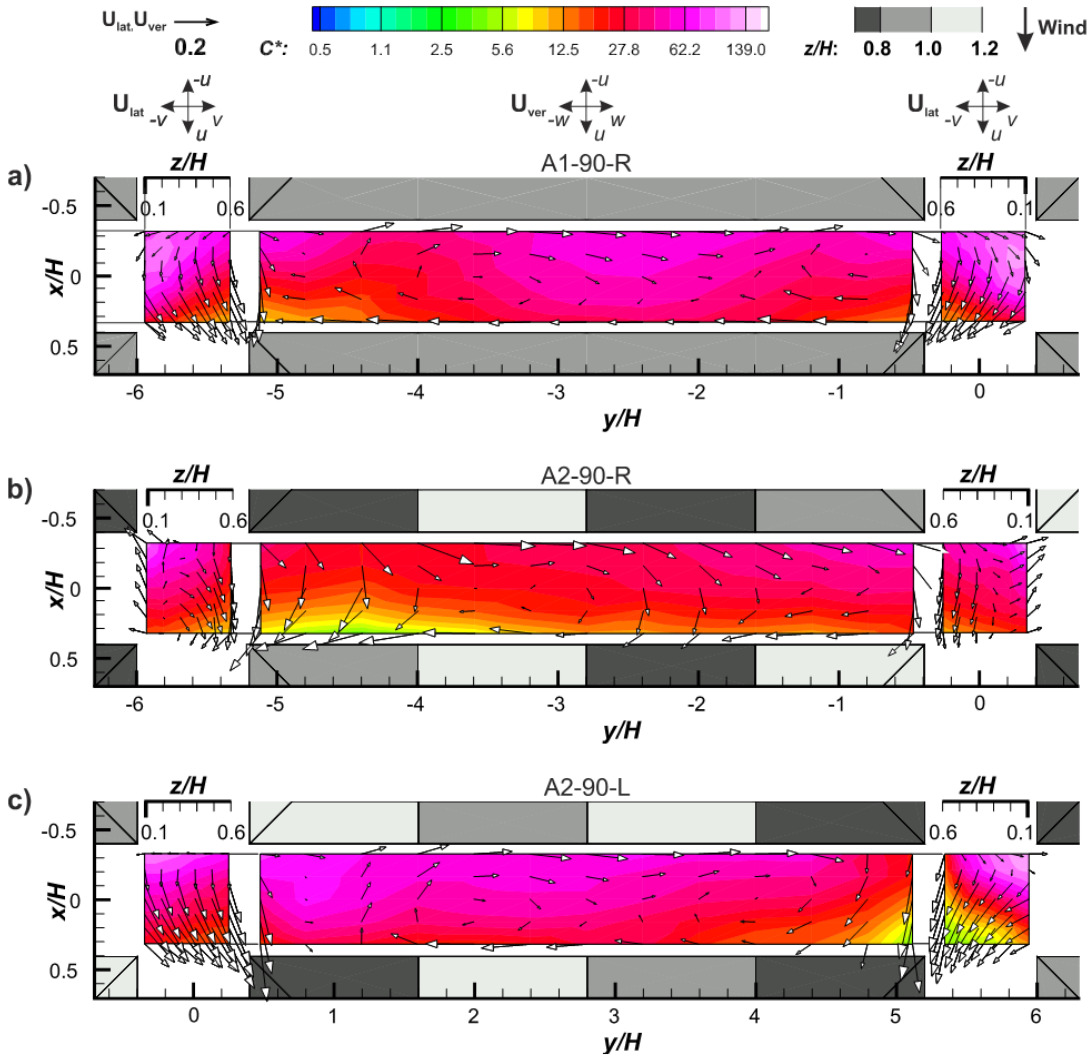

Figure 7.2: Top view of the mean dimensionless 2D vector and concentration C^* (coloured contours) fields for the **a**) uniform canyon (A1-R), and the non-uniform **b**) right (A2-R) and **c**) left (A2-L) canyons od the model A2, all for the perpendicular wind direction. The transformed lateral fields are presented apart the lateral sides of the horizontal field in order to avoid the vectors overlaying. The direction of the velocity components, (u, v) and (u, w), is illustrated by the arrows above the corresponding field. The arrow at the top-left corner indicates the same scale for both mean dimensionless velocity vectors $(\boldsymbol{U_{lat}}, \boldsymbol{U_{ver}})$. The grey contour represents the dimensionless height (z/H) of the buildings.

$-w$ velocity component in Fig. 7.2a) and the upward flow at the upstream wall ($x/H = -0.4$, where the $\boldsymbol{U_{ver}}$ vectors are aligned with the direction of the w velocity component) at the mid-point of the canyon ($y/H = -2.8$, Fig. 7.2a). This mechanism transports the pollutants from the line source to the upstream wall and then raises the pollutants along this wall to the roof-top shear layer

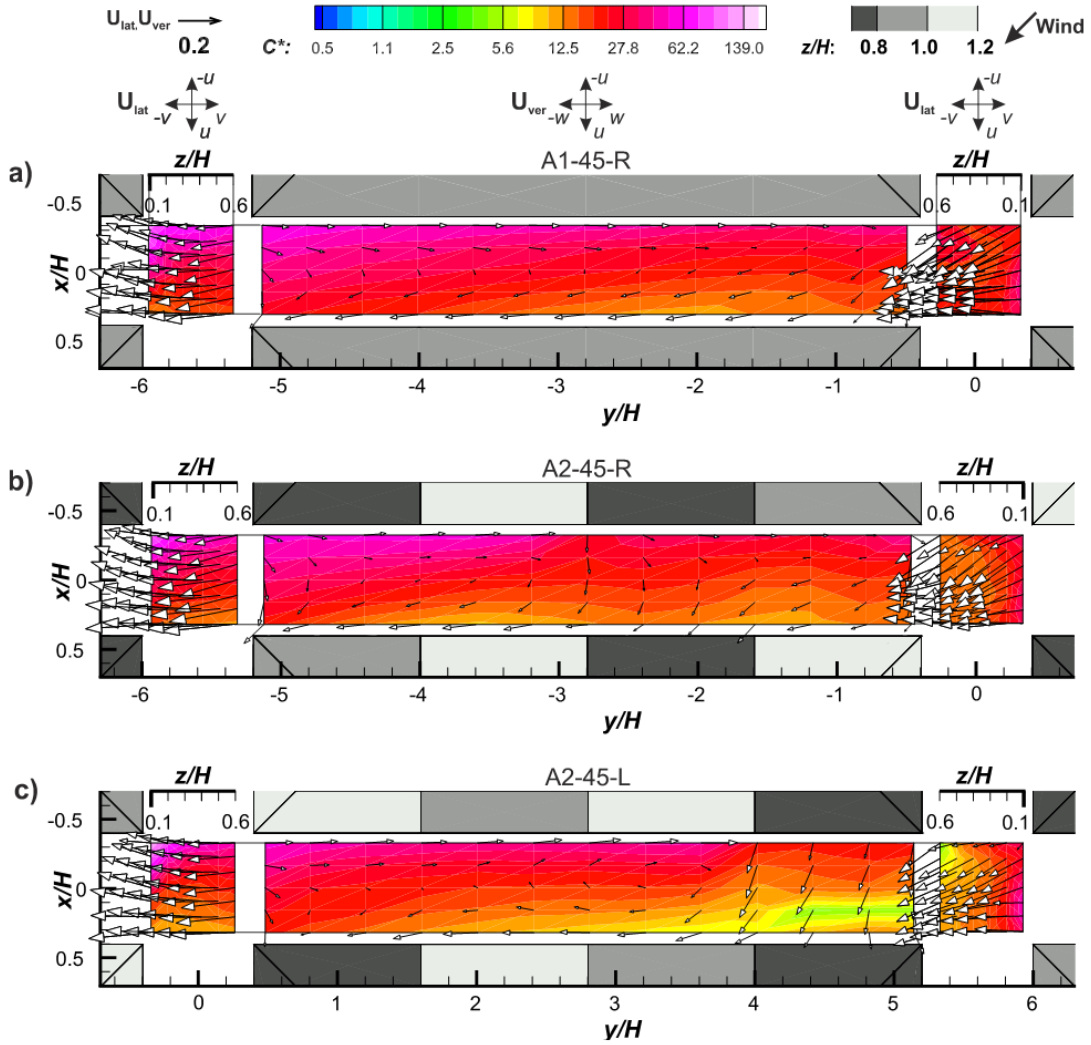

Figure 7.3: The same as in Fig. 7.2, but for the oblique wind direction.

where they are intermittently flapped to the flow aloft or back to the canyon, as has also been observed for 2D street canyons (Liu et al., 2005; Salizzoni et al., 2011). Contrary to the 2D street canyon, this vortex is not present along the entire length of the 3D uniform canyon, as the second shear flows emerge symmetrically from the upstream side corners and drive the horizontally rotating vortices at the canyon's ends. These corner vortices have the time-averaged footprint of the vertical axis positioned more or less symmetrically about $0.5H$ inward from those ends and can also be evidenced from the concentration and 2D velocity vector ($\boldsymbol{U_{ver}}$) fields of the lateral planes, displayed apart from the lateral sides of the horizontal plane in Fig. 7.2a).

Both the lateral and horizontal fields in 7.2a) suggest that these unsteady corner vortices have a helical structure (Hamlyn and Britter, 2005; Soulhac et al., 2009) as they transport partly polluted air from the adjoining intersections into the canyon nearby its downstream-wall bottom (note the appreciable $\boldsymbol{U_{lat}}$ vectors

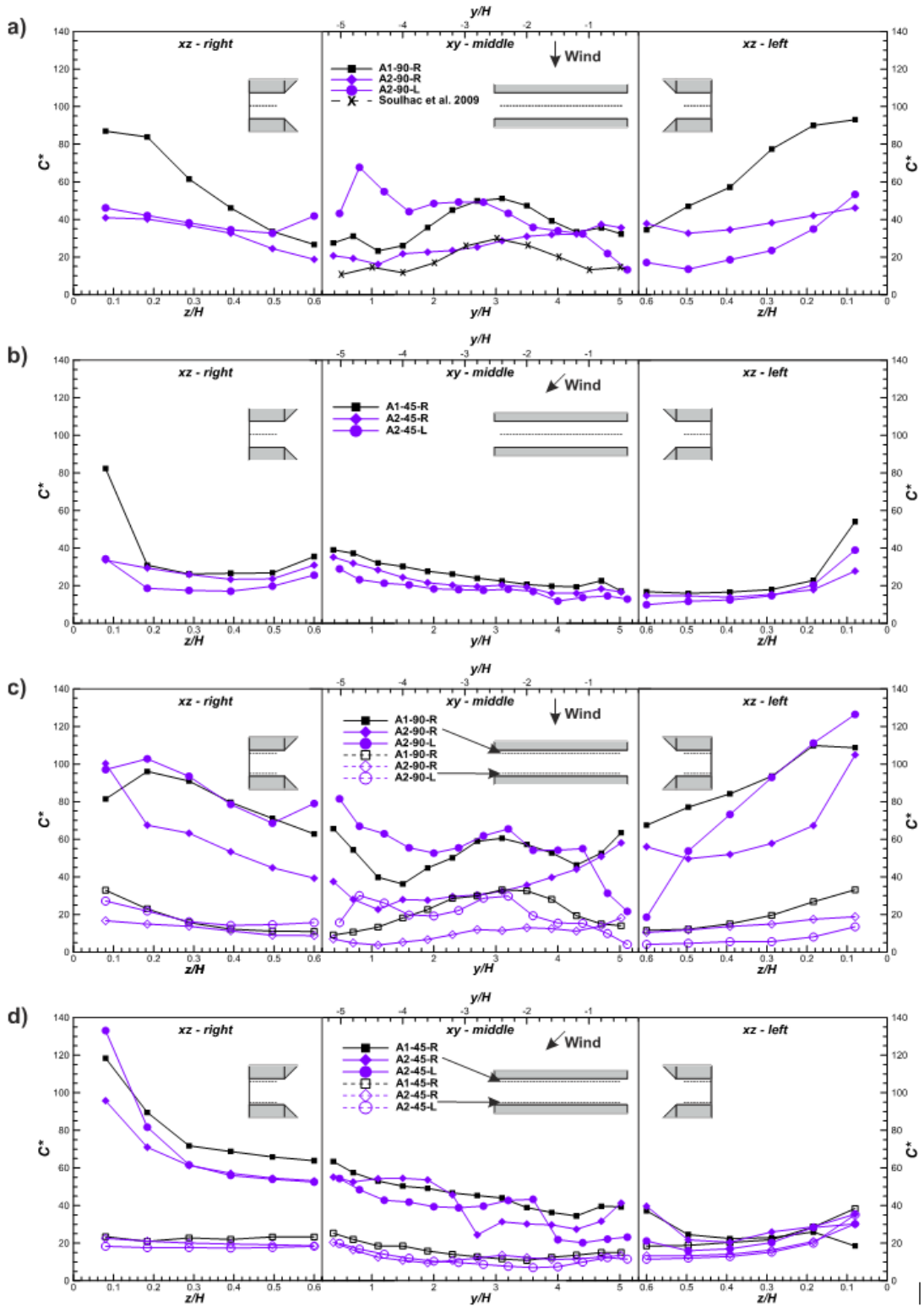

Figure 7.4: Horizontal (middle column) and vertical (left and right column) dimensionless concentration (C*) profiles at $x/H = 0$ (**a, b**), $x/H = -0.4$ (filled symbols in **c** and **d**) and $x/H = 0.4$ (empty symbols in **c** and **d**), for the perpendicular (**a**, **c**) and oblique wind direction (**b**, **d**), and for all canyons. The horizontal profiles are at $z/H = 0.6$. The crosses in **a**) are from the wind-tunnel study of Soulhac et al. (2009) at $z/H = 0.5$.

at $z/H = 0.1$, at the lateral planes in Fig. 7.2a) and spiral it upwards to the canyon upstream wall, where it is transported back into the intersections or to the flow aloft. This transport mechanism can also be deduced from the horizontal and vertical concentration profiles obtained in the middle ($x/H = 0$, black squares in Fig. 7.4a) and nearby the upstream ($x/H = -0.4$, black squares in Fig. 7.4c) and downstream wall ($x/H = 0.4$, empty squares in Fig. 7.4c) of that canyon (A1-R). It is important to note that these horizontal and vertical profiles are slightly asymmetrical along the mid-point of the canyon ($y/H = -2.8$ in Fig. 7.4a), middle column), but within the uncertainties of the measurement (4%). The mid-point peak and two smaller lateral peaks observed for the horizontal concentration profile along the centreline of the uniform canyon (middle column in Fig. 7.4a) illustrate the positions of the above-mentioned vortices. For comparison with previous studies, we present the horizontal concentration profile from the wind-tunnel study of Soulhac et al. (2009) (crosses in the middle column of Fig. 7.4a) obtained at the half height ($z/H = 0.5$) of a uniform street canyon with similar aspect ratios ($H/W = 1, L/H = 5$) but formed by blocks with flatted roofs. Although the concentrations from the present study are greater than those from the study of Soulhac et al. (2009), by a factor of two, they follow the same profile. The explanation for the higher concentration values of the present study might be, basically, twofold: first, the concentration in the present study was normalized (Eq. 7.1) by the freestream velocity, which is certainly higher than the velocity at the canyon height that was used in the study of Soulhac et al. (2009); and second, the geometry of the blocks of the urban array of the present study (courtyard buildings with pitched roofs) differ obviously from those of the study of Soulhac et al. (2009) (solid blocks with flatted roofs).

For the non-uniform canyons (Figs. 7.2b and 7.4c), the flow and concentration fields of both investigated canyons vary from the uniform canyon appreciably at both the horizontal and lateral planes. The first point to note is that the right (A2-R, Fig. 7.2b and left (A2-L, Fig. 7.2c) canyons represent, on average, step-up and step-down types of canyons, respectively, as was already introduced in Nosek et al. (2016). That study also concluded that the averaged step-up and step-down canyons have lower and higher concentrations than the uniform canyon, respectively, in the case of the perpendicular wind direction. Indeed, from the lateral planes, it can clearly be seen that the averaged step-up canyon (A2-R) has a dominant outflow at the lower parts (i.e., $z/H < 0.2$ in Fig. 7.2b) across the entire street width of both lateral planes, whereas the averaged step-down canyon (A2-L) has dominant inflow throughout both lateral planes (Fig. 7.2c). While the outflows transport the pollutant from the A2-R canyon, and hence reduce the concentrations within that canyon (see, e.g., the diamonds in the middle column of Figs. 7.4a) and 7.4c), the inflows at the lateral ends of the A2-L canyon transport the pollutants or clean air into that canyon and hence elevate or reduce the mean concentrations within that canyon (see, e.g., the circles in the middle column of Figs. 7.4a) and 7.4c). The vertical vectors (U_{ver}) at the local step-up notch at the right end of the canyon A2-R ($y/H < -4$, Fig. 2b) indicate a

strong sweep of the upcoming above-roof flow, which in turn is diverged along the downstream wall into the intersections and that canyon. This causes the reduced mean concentrations at those regions as the upcoming above-roof flow comprises non-polluted air, and this can be more clearly seen from the concentration fields (Fig. 2a) and profiles (circles in Fig. 7.4a and 7.4c) at the left end ($y/H > 4$) of the A2-L canyon. The opposite is true for the step-down notches, e.g., for the right end of the A2-L canyon ($y/H < 1.3$, Fig. 7.2c), where the horizontal convergence of the flow together with the strong corner vortex appreciably raises the concentrations in that region (see, e.g., the circles in the middle column at $y/H < 1.3$ in Figs. 7.4a) and 7.4c).

The lateral penetrations of either the polluted air or the clean air into the canyon are also influenced by the roof-height non-uniformities at the adjoining intersections. Both Figs. 7.2 and 7.4 suggest that, if the downstream-corner roofs across the intersection are higher than those of the canyon (e.g., both downstream roofs at the ends of the canyon A2-L in Fig. 7.2c), the flow is swept inward to the canyon with ease due to the horizontally converged flow at the bottom, which is supported by the presence of those higher buildings across the intersection. The opposite phenomena, outward flow from the canyon through the lateral openings, can be observed for the lower downstream-corner roofs across the intersection than those of the canyon. This confirms and extends the results from the wind-tunnel study of Klein et al. (2007), where the significant lateral flow component in the intersection was observed for the higher building at one of the four blocks forming that intersection.

Oblique wind (45°)

It is well known that, for oblique winds, the helical vortex with the along-canyon rotation axis dominates within a uniform street-canyon (Soulhac et al., 2008; Moonen et al., 2011). Such a flow structure can be observed in the present study for the uniform canyon and 45° wind to the along-canyon axis (Fig. 7.3a). The flow enters at the left lateral opening of the canyon (from the downstream view) by means of complex flow structures (see the overlaying $\boldsymbol{U_{lat}}$ vectors in that plane in Fig. 7.3a). These structures are aligned at this canyon's lateral entrance, and the helical vortex starts to develop, having the counter-rotating sense, if observed from downstream. This sense of the rotation can be indicated from the velocity vectors in the horizontal plane where they point upwards (aligned with the direction of the w velocity component in Fig. 7.3a) along the entire upstream wall or downwards (aligned with the direction of the $-w$ velocity component) along the entire downstream wall. In conjunction with strong advection, this produces a 'washing-out' effect, which can be observed to have, on average, two times lower concentrations compared to those from the perpendicular wind direction (e.g., compare the black and empty squares in Figs. 7.4a and 7.4c with those in Figs. 7.4b and 7.4d, respectively).

In the case of non-uniform canyons (Figs. 7.3b and 7.3c), the flow and concentration fields again differ appreciably from those of the uniform canyon. The

helical flow structure of the uniform canyon can also be observed for the non-uniform canyons, but its along-canyon length is governed by the position of the highest upstream wall, which shelters that flow structure downstream. While the helical vortex starts to develop in the middle ($y/H = -3$, Fig. 7.3b) for the case of the averaged step-up canyon (A2-R), in the case of the averaged step-down canyon (A2-L), a similar flow structure already starts to develop behind the first quarter of the canyon length ($y/H = 4$, Fig. 7.3c) and persists downstream from the canyon's end due to the higher buildings ($z/H > 1$) at the upstream wall. Interestingly, there is no appreciable difference in the flow and concentration fields at the right (outflow) ends of all investigated canyons (see also the left column in Figs. 7.4b) and 7.4d). As Nosek et al. (2016) concluded, the averaged step-down canyon (A2-L) has, on average, the lowest concentrations in the horizontal plane among all investigated cases (canyons and wind directions) owing to the lowest roof at the upstream wall at the left margin of that canyon, where the clean air penetrates the canyon with ease if the above-roof wind blows in that oblique direction (see the left lateral end of that canyon, $y/H > 4$, Fig. 7.3c). The same is also true for the lateral openings (circles in Figs. 7.4b and 7.4d) and is in contrast with the case of the perpendicular wind, for which the averaged step-down canyon (A2-L) was the most polluted street canyon considering all investigated openings.

7.3.2 Driving processes for the pollutant transport

It has been observed (Liu et al., 2005; Michioka et al., 2014) that, for the winds perpendicular to the street canyon, the pollutant transport occurs mainly in the vertical direction, between the canyon's roof top and the above-roof flow, and that this vertical transport is mainly governed by its turbulent part. In our previous study (Nosek et al., 2016), we have shown that the dominance of the turbulent part is independent of the wind direction, while it strongly depends on the canyon's roof geometry. In that study, we found that turbulent coherent structures (known as the sweeps and ejections of momentum) are highly correlated with ventilation processes, irrespective of the canyons' roof-height arrangements and wind direction. For an explanation of the meaning of these ventilation processes and their correlations with the structures of the turbulent flow, we recall the nomenclature for the momentum (Katul et al., 1997) and scalar (Nosek et al., 2016) transport. Both nomenclatures are based on the conditional technique known as quadrant analysis (Willmarth, 1975), which is applied to scatter plots of two turbulent quantities (herein, u' and w' (v') for the momentum and c' and w' (v') for the scalar transport).

These nomenclatures are presented for each canyon opening separately in Fig. 7.5 in the Appendix. Of course, the momentum and scalar transport for the right opening of the canyon presented in Figs. 7.5a and 7.5d), respectively, are mirrored from those of the left opening (Figs. 7.5a and 7.5b). According to these nomenclatures, the positive correlation coefficients mean that the momentum pro-

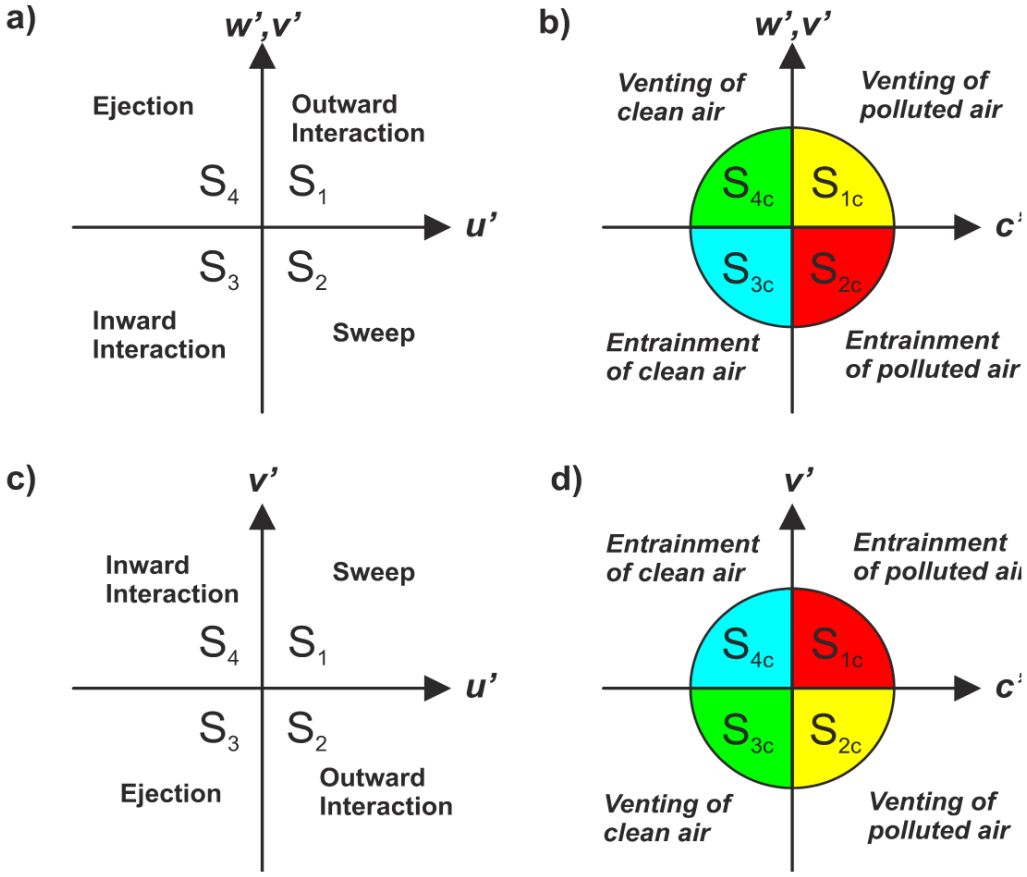

Figure 7.5: Nomenclature for the momentum (**a**, **c**) and scalar (**b**, **d**) transport based on the quadrant analysis: **a**) vertical ($u'w'$) and lateral ($u'v'$) momentum transport through the top and left lateral openings of the canyon, respectively; **b**) vertical ($c'w'$) and lateral ($c'v'$) scalar transport through the top and left lateral openings of the canyon, respectively; the lateral **c**) momentum ($u'v'$) and **d**) scalar ($c'v'$) transport through the right lateral opening of the canyon.

cesses at given quadrants (events) correlate with those for the scalar transport (ventilation processes). Thus, for instance, the ejection and sweep events detrain clean air from and bring polluted air into the canyon through the given opening, respectively. Similarly, the negative correlation coefficients mean that the momentum events have opposite signs of those from the scalar transport processes, and hence, e.g., ejection and sweep events detrain polluted air from and bring clean air into the canyon, respectively. In the study of Nosek et al. (2016), it was shown, with regard to the ventilation performance of the street canyon through the canyon's roof top, that only these negative correlations are appreciable and that they are independent on the roof morphology and wind direction.

The above-mentioned findings, however, may not be true for the canyon's lateral openings. To verify this, we, firstly, calculated the relative contribution of

the turbulent pollution flux to the total pollution flux as

$$\overline{c^{*\prime}v^{\prime}}_{rel} = \frac{|\overline{c^{*\prime}v^{\prime}}|}{|\overline{c^{*\prime}v^{\prime}}| + |C^{*}V|}, \tag{7.2}$$

for the lateral openings and

$$\overline{c^{*\prime}w^{\prime}}_{rel} = \frac{|\overline{c^{*\prime}w^{\prime}}|}{|\overline{c^{*\prime}w^{\prime}}| + |C^{*}W|}, \tag{7.3}$$

for the top openings of the canyons, where $\overline{c^{*\prime}v^{\prime}}$ and $\overline{c^{*\prime}w^{\prime}}$ are the time-averaged lateral and vertical turbulent pollution fluxes, and $C^{*}V$ and $C^{*}W$ are the lateral and vertical advective pollution fluxes, respectively.

From Figs. 7.6 and 7.7 can be observed that the contribution of the turbulent part to the total pollution flux at the lateral and top openings of the canyons depends on the street-canyon geometry and wind direction. While there are appreciable contributions of the turbulent parts to the total pollutant transports at both the lateral and top openings of all investigated canyons in the case of the perpendicular wind (Fig. 7.6), the pollutant is mainly advected through the all lateral openings of all investigated canyons in the case of the oblique wind (light-blue contours at lateral openings in Fig. 7.7). This is in contrast with the observations for the top opening at the roof top ($z/H = 1$) where the pollutant transport is governed mainly by its turbulent part, irrespective of the wind direction (Nosek et al., 2016).

Because there are non-legible turbulent transports at the canyons' lateral openings only at the perpendicular wind, we performed the calculation of the correlations between the lateral coherent structures and ventilation processes only for that wind direction. For this, we followed the method used in Nosek et al. (2016):

$$r_{(2,3c)v} = \frac{\overline{(u^{\prime}v^{\prime})_2(v^{\prime}c^{\prime})_3}}{\sigma_{uv_2}\sigma_{vc_3}}, r_{(4,1c)v} = \frac{\overline{(u^{\prime}v^{\prime})_4(v^{\prime}c^{\prime})_1}}{\sigma_{uv_4}\sigma_{vc_1}}, \tag{7.4}$$

for the lateral turbulent transport through the left opening and

$$r_{(1,4c)v} = \frac{\overline{(u^{\prime}v^{\prime})_1(v^{\prime}c^{\prime})_4}}{\sigma_{uv_1}\sigma_{vc_4}}, r_{(3,2c)v} = \frac{\overline{(u^{\prime}v^{\prime})_3(v^{\prime}c^{\prime})_2}}{\sigma_{uv_3}\sigma_{vc_2}}, \tag{7.5}$$

for the case of the lateral turbulent transport through the right opening of the canyon, where the indexes represent the quadrants for the corresponding transport and canyon opening as presented in Fig. 7.5. Thus, for instance, $r_{(2,3c)v}$ in Eq. 7.4 represents the correlation between the sweeps (second quadrant, Fig. 7.5a) and clean air entrainments (third quadrant, Fig. 7.5b).

In Figs. 7.8 and 7.9, the contour fields of the correlation coefficients between the sweeps and clean air entrainments and between the ejections and polluted air venting, respectively, are presented for both the lateral and vertical turbulent transport (the coefficients for the vertical turbulent transport have an index w,

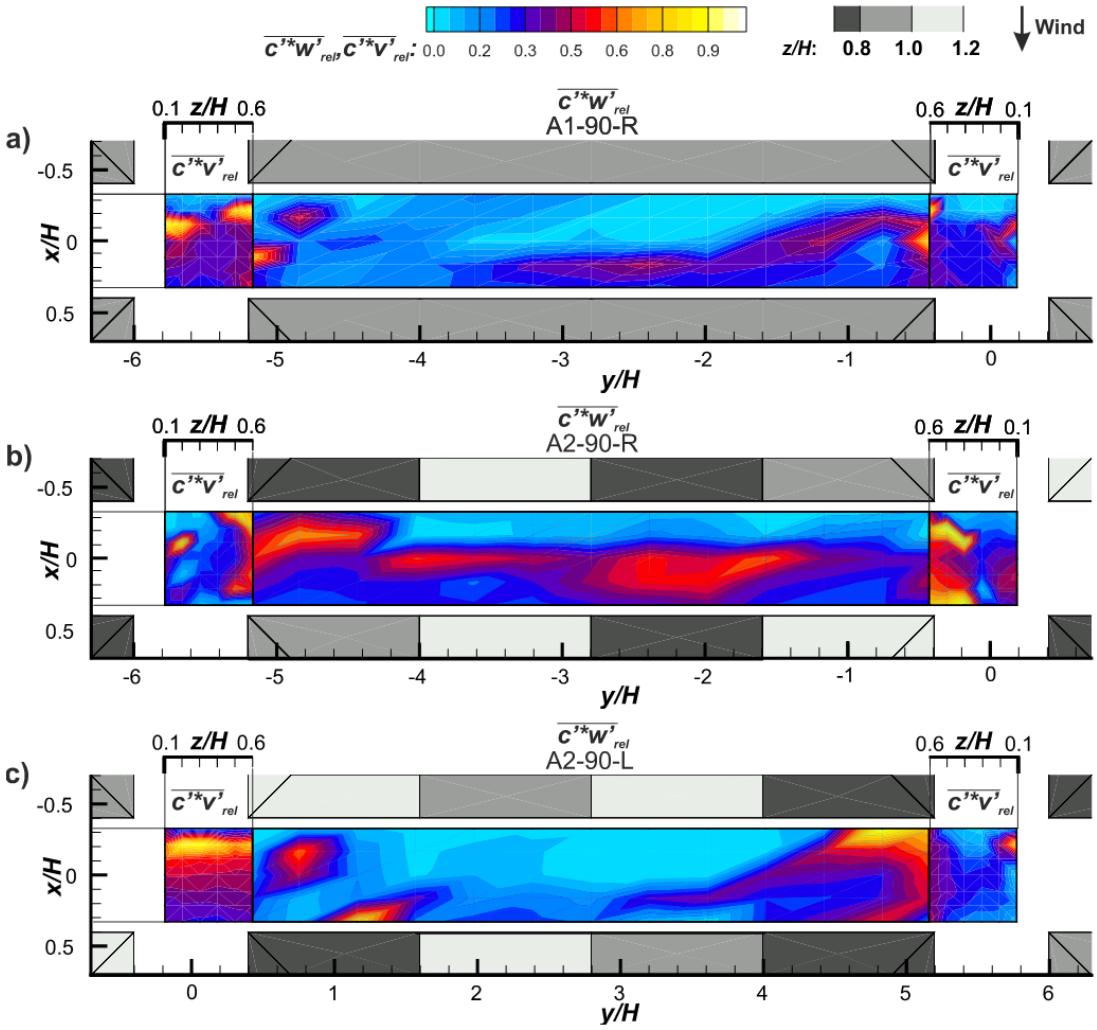

Figure 7.6: Contour fields of the relative contribution of the vertical turbulent pollution flux to the total vertical pollution flux ($\overline{c^{*\prime}w^{\prime}}_{rel}$) at the top opening and the relative contribution of the lateral turbulent pollution flux to the total lateral pollution flux ($\overline{c^{*\prime}w^{\prime}}_{rel}$) at the lateral openings of the canyons **a**) uniform canyon A1-90-R and non-uniform canyons **b**) A2-90-R and **c**) A2-90-L, all for the perpendicular wind.

i.e., $r_{(2,3c)w}$). The first point to note is that the areas of high correlations between the sweeps and clean air entrainments (Fig. 7.8) coincide with those of the correlations between the ejections and polluted air venting (Fig. 7.9) only for the lateral openings of the canyons. For these openings of all investigated canyons, there can be observed extensive areas of very high correlations (from 0.5 up to 0.8) between the sweeps and clean air entrainments (Fig. 7.8) and a substantial dependency of these areas on the buildings' roof height at the intersections. The sweeps of the momentum are also highly correlated with the clean air entrainments in the areas of the horizontal planes, for the cases of the non-

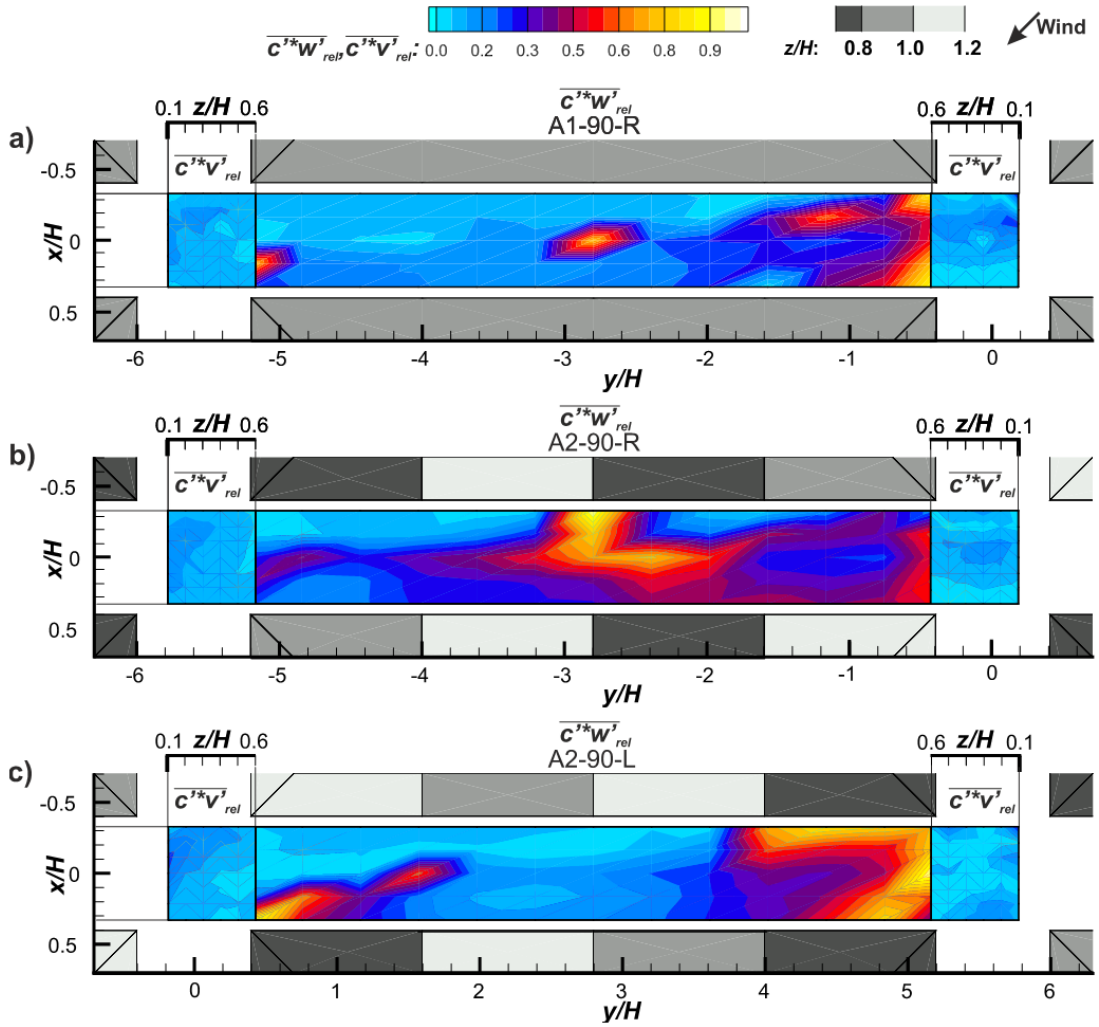

Figure 7.7: The same as in Fig. 7.6, but for the oblique wind direction.

uniform canyons, where the upstream roofs are the lowest, and, indeed, represent the roof-top opening (Fig. 7.8b and Fig. 7.8c). Conversely, there are negligible correlations between both the ejections and polluted air ventilation and the sweeps and clean air entrainment at the entire upstream wall in the case of the uniform canyon (Figs. 7.8a and Fig. 7.9a). This confirms the findings of other studies (Kukacka et al., 2014; Michioka et al., 2014), which observed that the advection of the pollutant is dominant along the upstream wall within the uniform 3D canyon. The advection may be inferred similarly for the lateral openings from the fields of negligible correlations between the events and ventilation processes (Figs. 7.8 and 7.9) in conjunction with the fields of negligible contribution of the turbulent pollution flux to the total pollution flux (Fig. 7.6) and mean flow fields (Fig. 7.2). While the only advective transport of the pollutant occurs nearby the upstream wall in the case uniform canyon (Fig. 7.6a), there are advective transports also near the bottom at the lateral ends of the non-uniform canyons

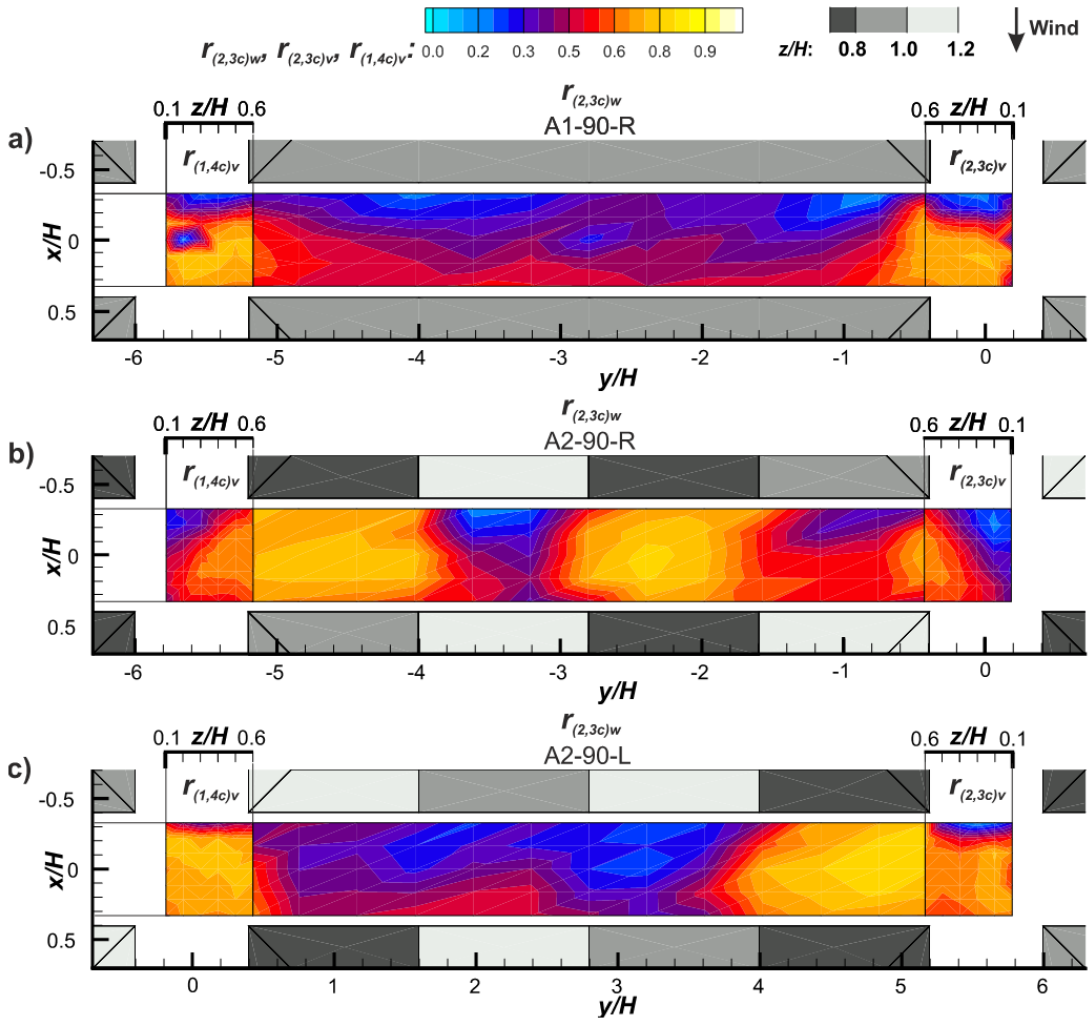

Figure 7.8: Contour fields of the correlation coefficient between the lateral sweeps and clean air entrainments at the right $r_{(1,4c)v}$ and left $r_{(2,3c)v}$ transformed lateral openings, and between the vertical sweeps and clean air entrainments at the top opening $r_{(2,3c)w}$ of the **a**) uniform canyon A1-90-R and non-uniform canyons, **b**) A2-90-R and **c**) A2-90-L, all for the perpendicular wind.

(Figs. 7.6b and 7.6c). Owing to the local step-up roof notches at the sides of the non-uniform step-up canyon (A2-R), which causes the divergence of the flow (already described in Sec. 7.3.1), the pollutant is primarily advected from the canyon through the lateral openings near the bottom (Figs. 7.2b and 7.6b). An appreciable advective pollutant transport also occurs at the left lateral opening of the non-uniform step-down canyon (Fig. 7.6c). In contrast, both lateral openings of the uniform canyon (Fig. 7.6a) and the right lateral opening of the non-uniform step-down canyon (Fig. 7.6c) negligibly advects pollutants through these openings due to the presence of the horizontally rotating corner vortex. For these openings the transport of the pollutant is governed by the turbulent coherent structures, the 'lateral' sweeps (Figs. 8a and 8c) and ejections (Figs. 7.9a

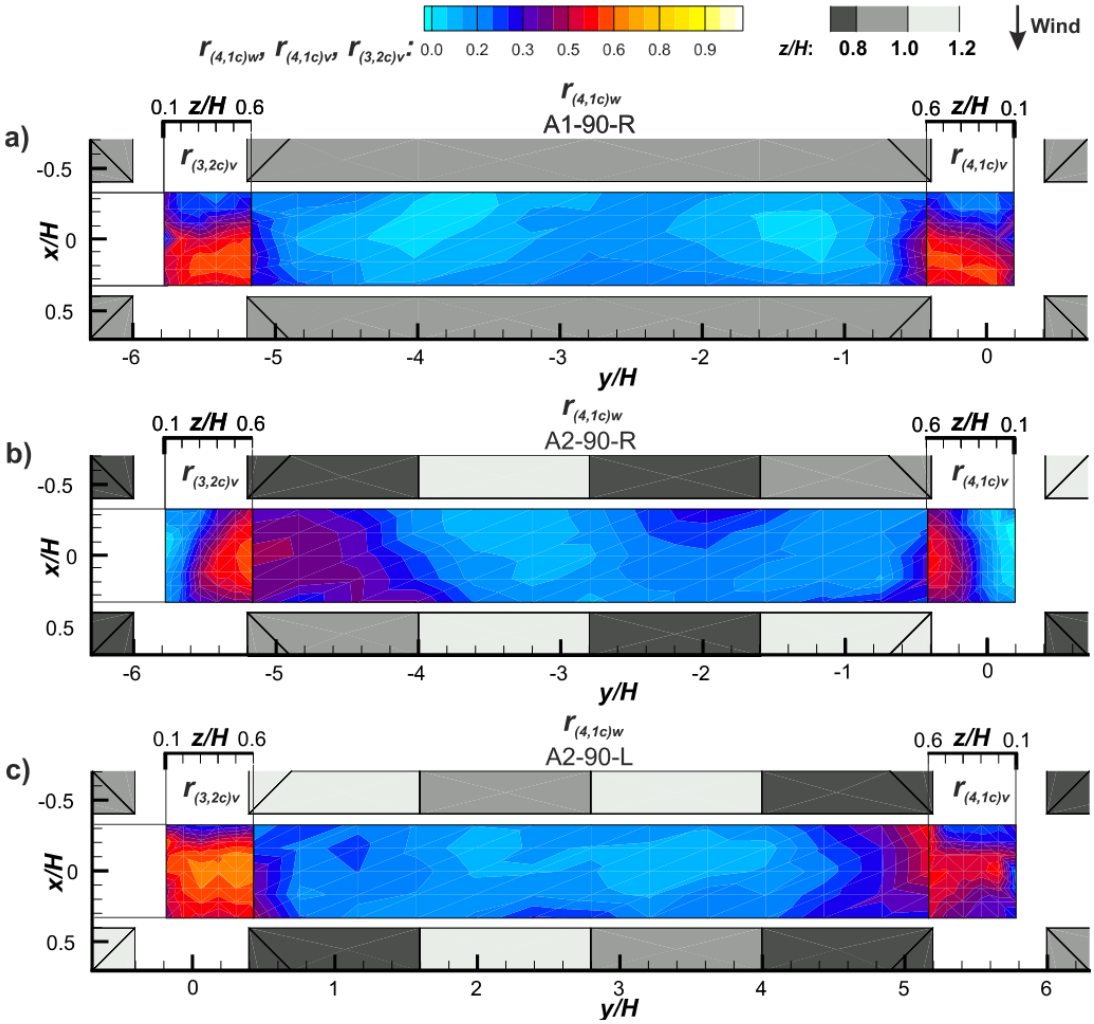

Figure 7.9: Contour fields of the correlation coefficient between the lateral ejections and polluted air venting at the right $r_{(3,2c)v}$ and left $r_{(4,1c)v}$ transformed lateral openings and between the vertical ejections and clean air entrainments at the top opening $r_{(4,1c)w}$ of the **a**) uniform canyon A1-90-R and non-uniform canyons, **b**) A2-90-R and **c**) A2-90-L, all for the perpendicular wind.

and 7.9c). These findings clearly show that even for the regular urban-array layout the type of the pollutant transport (advective, turbulent) between the street canyon and intersections strongly depends on the roof-height non-uniformity and wind direction.

7.4 Final discussions and conclusions

While the presented urban-array models were, with respect to the defined three-dimensionality, as simple as possible, we demonstrated that, for better understanding of the near-field pollutant dispersion in urban environments, it is of primary concern to take into account the full three-dimensionality of the buildings and the approaching wind direction. The results of the mean flow and concentration fields of the present study confirm the findings from other wind-tunnel (Klein et al., 2007; Michioka et al., 2014) and field (Pol and Brown, 2008; Balogun et al., 2010) studies that the buildings' roof-height variability at the intersections plays an important role in dispersion of the traffic pollutants within the canyon. Despite the same solidities being used in the present study ($\lambda_p = 0.28$, $\lambda_f = 0.27$) for both urban-array models, the flow patterns for the non-uniform canyons differed significantly from those for the uniform canyon. These flow patterns were responsible for the higher pollutant removal capability compared to that of the uniform canyon. Indeed, in the case of the perpendicular wind, the local step-down notches at the ends of the non-uniform canyon produced the convergence of the flow, thus entraining potentially clean or polluted air from the adjoining intersections into that canyon at the bottom and venting it through the top to the flow aloft. Conversely, the local step-up roof notches at these canyon ends produced the divergence of the flow, thus entraining clean air from the above-roof flow coming upstream and venting polluted air from the canyon to the adjoining intersections through the lateral ends near the bottom. Thus, for a non-uniform canyon and perpendicular wind, it is not necessarily true that pollutants will be removed only through the top, as was observed for uniform canyons (Liu et al., 2005; Soulhac et al., 2009).

We also observed the impact of the canyon non-uniformity on the near-field pollutant dispersion for oblique winds. The helical vortex with the along-canyon axis, well known for uniform canyons, was also observed for non-uniform canyons, but its along-canyon length was governed by the position of the highest upstream wall, which shelters that vortex downstream. The higher the upstream walls of the non-uniform canyon were, the more pollutants were removed through the top, and hence less pollutants were removed through the canyon's end to the intersection downstream for that wind direction.

Furthermore, we performed analysis of the turbulent mass transport with respect to the turbulent coherent structures for all canyons' openings. This analysis revealed that the coherent structures of the lateral turbulent transport act at the lateral openings as appreciably as those of the vertical transport observed at the roof-top opening of the uniform (Michioka et al., 2014) or non-uniform (Nosek et al., 2016) canyons. The 'lateral' sweeps and ejections were correlated with the entrainment of clean air and venting of polluted air from the canyon, respectively, at the lateral openings of all studied canyons. Thus, for the canyon's lateral openings, it may also be stated that these 'lateral' sweeps and ejections bring clean air into and detrain polluted air from the canyon, respectively. However, we ob-

served that the type of the mechanism for the pollutant transport (advective or turbulent) between the street canyon and intersection strongly depends on the roof-height non-uniformity and wind direction. In the case of the oblique wind, the pollutant is mainly advected through the lateral openings of all investigated canyons, and hence the 'lateral' sweeps and ejections are negligible for the pollutant transport.

Acknowledgements
The authors gratefully acknowledge funding from the Czech Science Foundation GACR (GAP15-18964S) and from the institutional support RVO: 61388998. Authors also would like to thank Dr. Petr Bauer for his discussions and Jan Kozohorsky for his valuable support during the experiments. We also would like to express our thanks to the anonymous reviewers whose constructive comments and helpful suggestions improve the presented paper substantially.

7.5 References

K. J. Allwine, J. H. Shinn, G. E. Streit, K. L. Clawson, and M. Brown. Overview of URBAN 2000: A Multiscale Field Study of Dispersion through an Urban Environment. *Bulletin of the American Meteorological Society*, 83(4):521–536, apr 2002. ISSN 0003-0007. doi: 10.1175/1520-0477(2002)083⟨0521:OOUAMF⟩2.3.CO;2. URL http://journals.ametsoc.org/doi/abs/10.1175/1520-0477%282002%29083%3C0521%3AOOUAMF%3E2.3.CO%3B2.

A. A. Balogun, A. S. Tomlin, C. R. Wood, J. F. Barlow, S. E. Belcher, R. J. Smalley, J. J. N. Lingard, S. J. Arnold, A. Dobre, A. G. Robins, D. Martin, and D. E. Shallcross. In-Street Wind Direction Variability in the Vicinity of a Busy Intersection in Central London. *Boundary-Layer Meteorology*, 136(3): 489–513, sep 2010. ISSN 0006-8314. doi: 10.1007/s10546-010-9515-y. URL http://link.springer.com/10.1007/s10546-010-9515-y.

J. F. Barlow. Progress in observing and modelling the urban boundary layer. *Urban Climate*, 10(P2):216–240, dec 2014. ISSN 22120955. doi: 10.1016/j.uclim.2014.03.011. URL http://linkinghub.elsevier.com/retrieve/pii/S2212095514000558.

B. Blocken, T. Stathopoulos, and J. P. van Beeck. Pedestrian-level wind conditions around buildings: Review of wind-tunnel and CFD techniques and their accuracy for wind comfort assessment. *Building and Environment*, 100: 50–81, 2016. ISSN 03601323. doi: 10.1016/j.buildenv.2016.02.004. URL http://dx.doi.org/10.1016/j.buildenv.2016.02.004.

L. A. Brixey, D. K. Heist, J. Richmond-Bryant, G. E. Bowker, S. G. Perry, and R. W. Wiener. The effect of a tall tower on flow and dispersion through a model urban neighborhood : Part 2. Pollutant dispersion. *Journal of Environmental*

Monitoring, 11(12):2171, dec 2009. ISSN 1464-0325. doi: 10.1039/b907137g. URL http://xlink.rsc.org/?DOI=b907137g.

M. Brown, R. Lawson, D. S. DeCroix, and R. Lee. Comparison of centerline velocity measurements obtained around 2D and 3D building arrays in wind tunnel. In *International Society of Environmental Hydraulics Conference*, number December 2001, Tempe, AZ, 2001.

M. J. Brown, M. D. Williams, M. A. Nelson, and K. A. Werley. QUIC Transport and Dispersion Modeling of Vehicle Emissions in Cities for Better Public Health Assessments. *Environmental health insights*, 9(Suppl 1):55–65, jan 2015. ISSN 1178-6302. doi: 10.4137/EHI.S15662.Received. URL http://ovidsp.ovid.com/ovidweb.cgi?T=JS&PAGE=reference&D=prem&NEWS=N&AN=27867300.

R. Buccolieri, P. Salizzoni, L. Soulhac, V. Garbero, and S. Di Sabatino. The breathability of compact cities. *Urban Climate*, 13:73–93, sep 2015. ISSN 22120955. doi: 10.1016/j.uclim.2015.06.002. URL http://linkinghub.elsevier.com/retrieve/pii/S2212095515000243.

M. Carpentieri, P. Hayden, and A. G. Robins. Wind tunnel measurements of pollutant turbulent fluxes in urban intersections. *Atmospheric Environment*, 46: 669–674, jan 2012. ISSN 13522310. doi: 10.1016/j.atmosenv.2011.09.083. URL http://linkinghub.elsevier.com/retrieve/pii/S1352231011010909.

I. P. Castro, Z.-T. Xie, V. Fuka, A. G. Robins, M. Carpentieri, P. Hayden, D. Hertwig, and O. Coceal. Measurements and Computations of Flow in an Urban Street System. *Boundary-Layer Meteorology*, 162(2):207–230, feb 2017. ISSN 0006-8314. doi: 10.1007/s10546-016-0200-7. URL http://link.springer.com/10.1007/s10546-016-0200-7.

J. Counihan. Adiabatic atmospheric boundary layers: A review and analysis of data from the period 1880–1972. *Atmospheric Environment (1967)*, 9(10): 871–905, oct 1975. ISSN 00046981. doi: 10.1016/0004-6981(75)90088-8. URL http://linkinghub.elsevier.com/retrieve/pii/0004698175900888.

M. Davidson, W. Snyder, R. Lawson, and J. Hunt. Wind tunnel simulations of plume dispersion through groups of obstacles. *Atmospheric Environment*, 30(22):3715–3731, nov 1996. ISSN 13522310. doi: 10.1016/1352-2310(96)00103-3. URL http://linkinghub.elsevier.com/retrieve/pii/1352231096001033.

V. Garbero, P. Salizzoni, and L. Soulhac. Experimental Study of Pollutant Dispersion Within a Network of Streets. *Boundary-Layer Meteorology*, 136(3): 457–487, sep 2010. ISSN 0006-8314. doi: 10.1007/s10546-010-9511-2. URL http://link.springer.com/10.1007/s10546-010-9511-2.

S. Gokhale. Traffic flow pattern and meteorology at two distinct urban junctions with impacts on air quality. *Atmospheric Environment*, 45(10):1830–1840, mar 2011. ISSN 13522310. doi: 10.1016/j.atmosenv.2011.01.015. URL http://linkinghub.elsevier.com/retrieve/pii/S1352231011000227.

Z. L. Gu, Y. W. Zhang, Y. Cheng, and S. C. Lee. Effect of uneven building layout on air flow and pollutant dispersion in non-uniform street canyons. *Building and Environment*, 46(12):2657–2665, 2011. ISSN 03601323. doi: 10.1016/j.buildenv.2011.06.028.

D. Hamlyn and R. Britter. A numerical study of the flow field and exchange processes within a canopy of urban-type roughness. *Atmospheric Environment*, 39(18):3243–3254, jun 2005. ISSN 13522310. doi: 10.1016/j.atmosenv.2005.02.020. URL http://linkinghub.elsevier.com/retrieve/pii/S1352231005001718.

D. K. Heist, L. A. Brixey, J. Richmond-Bryant, G. E. Bowker, S. G. Perry, and R. W. Wiener. The effect of a tall tower on flow and dispersion through a model urban neighborhood : Part 1. Flow characteristics. *Journal of Environmental Monitoring*, 11(12):2163, dec 2009. ISSN 1464-0325. doi: 10.1039/b907135k. URL http://xlink.rsc.org/?DOI=b907135k.

W. G. Hoydysh, Y. Ogawa, and R. A. Griffiths. A scale model study of dispersion of pollution in street canyons. In *Annual Meeting of the Air Pollution Control Association, Denver, Colorado*, 1974.

X. Jin, L. Yang, X. Du, and Y. Yang. Particle transport characteristics in the micro-environment near the roadway. *Building and Environment*, 102:138–158, jun 2016. ISSN 03601323. doi: 10.1016/j.buildenv.2016.03.023. URL http://linkinghub.elsevier.com/retrieve/pii/S0360132316301068.

G. Katul, G. Kuhn, J. Schieldge, and C.-I. Hsieh. THE EJECTION-SWEEP CHARACTER OF SCALAR FLUXES IN THE UNSTABLE SURFACE LAYER. *Boundary-Layer Meteorology*, 83(1):1–26, apr 1997. ISSN 0006-8314. doi: 10.1023/A:1000293516830. URL http://link.springer.com/10.1023/A:1000293516830.

P. Klein, B. Leitl, and M. Schatzmann. Driving physical mechanisms of flow and dispersion in urban canopies. *International Journal of Climatology*, 27(14):1887–1907, 2007. ISSN 08998418. doi: 10.1002/joc.1581.

L. Kukacka, S. Nosek, R. Kellnerova, K. Jurcakova, and Z. Janour. Wind Tunnel Measurement of Turbulent and Advective Scalar Fluxes: A Case Study on Intersection Ventilation. *The Scientific World Journal*, 2012:1–13, 2012. ISSN 1537-744X. doi: 10.1100/2012/381357. URL http://www.hindawi.com/journals/tswj/2012/381357/.

L. Kukacka, V. Fuka, S. Nosek, R. Kellnerova, and Z. Janour. Ventilation of idealised urban area, LES and wind tunnel experiment. *EPJ Web of ...*, 62:1–10, 2014. ISSN 2100-014X. doi: 10.1051/epjconf/20146702062. URL http://www.epj-conferences.org/articles/epjconf/abs/2014/04/epjconf_efm-13_02062/epjconf_efm-13_02062.html.

M. Lateb, R. Meroney, M. Yataghene, H. Fellouah, F. Saleh, and M. Boufadel. On the use of numerical modelling for near-field pollutant dispersion in urban environments - A review. *Environmental Pollution*, 208:271–283, jan 2016. ISSN 02697491. doi: 10.1016/j.envpol.2015.07.039. URL http://linkinghub.elsevier.com/retrieve/pii/S0269749115003723.

C. H. Liu, D. Y. C. Leung, and M. C. Barth. On the prediction of air and pollutant exchange rates in street canyons of different aspect ratios using large-eddy simulation. *Atmospheric Environment*, 39(9):1567–1574, 2005. ISSN 13522310. doi: 10.1016/j.atmosenv.2004.08.036.

I. Longley, M. Gallagher, J. Dorsey, M. Flynn, and J. Barlow. Short-term measurements of airflow and turbulence in two street canyons in Manchester. *Atmospheric Environment*, 38(1):69–79, jan 2004. ISSN 13522310. doi: 10.1016/j.atmosenv.2003.09.060. URL http://linkinghub.elsevier.com/retrieve/pii/S1352231003007970.

R. N. Meroney, M. Pavageau, S. Rafailidis, and M. Schatzmann. Study of line source characteristics for 2-D physical modelling of pollutant dispersion in street canyons. *Journal of Wind Engineering and Industrial Aerodynamics*, 62(1):37–56, aug 1996. ISSN 01676105. doi: 10.1016/S0167-6105(96)00057-8. URL http://linkinghub.elsevier.com/retrieve/pii/S0167610596000578.

T. Michioka, H. Takimoto, and A. Sato. Large-Eddy Simulation of Pollutant Removal from a Three-Dimensional Street Canyon. *Boundary-Layer Meteorology*, 150(2):259–275, feb 2014. ISSN 0006-8314. doi: 10.1007/s10546-013-9870-6. URL http://link.springer.com/10.1007/s10546-013-9870-6.

P. Moonen, V. Dorer, and J. Carmeliet. Evaluation of the ventilation potential of courtyards and urban street canyons using RANS and LES. *Journal of Wind Engineering and Industrial Aerodynamics*, 99(4):414–423, apr 2011. ISSN 01676105. doi: 10.1016/j.jweia.2010.12.012. URL http://linkinghub.elsevier.com/retrieve/pii/S0167610510001455.

S. Nosek, L. Kukacka, R. Kellnerova, K. Jurcakova, and Z. Janour. Ventilation Processes in a Three-Dimensional Street Canyon. *Boundary-Layer Meteorology*, 159(2):259–284, may 2016. ISSN 15731472. doi: 10.1007/s10546-016-0132-2. URL http://link.springer.com/10.1007/s10546-016-0132-2.

T. Oke. Street design and urban canopy layer climate. *Energy and Buildings*, 11(1-3):103–113, mar 1988. ISSN 03787788. doi: 10.1016/0378-7788(88)90026-6. URL https://www.sciencedirect.com/science/article/pii/0378778888900266.

S. U. Pol and M. J. Brown. Flow patterns at the ends of a street canyon: Measurements from the joint urban 2003 field experiment. *Journal of Applied Meteorology and Climatology*, 47(5):1413–1426, may 2008. ISSN 15588424. doi: 10.1175/2007JAMC1562.1. URL http://journals.ametsoc.org/doi/abs/10.1175/2007JAMC1562.1.

P. Salizzoni, M. Marro, L. Soulhac, N. Grosjean, and R. J. Perkins. Turbulent Transfer Between Street Canyons and the Overlying Atmospheric Boundary Layer. *Boundary-Layer Meteorology*, 141(3):393–414, 2011. ISSN 00068314. doi: 10.1007/s10546-011-9641-1.

M. Schatzmann and B. Leitl. Issues with validation of urban flow and dispersion CFD models. *Journal of Wind Engineering and Industrial Aerodynamics*, 99 (4):169–186, apr 2011. ISSN 01676105. doi: 10.1016/j.jweia.2011.01.005. URL http://linkinghub.elsevier.com/retrieve/pii/S0167610511000079.

W. Snyder. Guideline for fluid modeling of atmospheric diffusion, jun 1979. URL https://www.osti.gov/biblio/5521001.

L. Soulhac, V. Garbero, P. Salizzoni, P. Mejean, and R. J. Perkins. Flow and dispersion in street intersections. *Atmospheric Environment*, 43(18):2981–2996, jun 2009. ISSN 13522310. doi: 10.1016/j.atmosenv.2009.02.061. URL http://linkinghub.elsevier.com/retrieve/pii/S1352231009001186.

L. Soulhac, G. Lamaison, F. X. Cierco, N. Ben Salem, P. Salizzoni, P. Mejean, P. Armand, and L. Patryl. SIRANERISK: Modelling dispersion of steady and unsteady pollutant releases in the urban canopy. *Atmospheric Environment*, 140:242–260, 2016. ISSN 18732844. doi: 10.1016/j.atmosenv.2016.04.027. URL http://dx.doi.org/10.1016/j.atmosenv.2016.04.027.

L. Soulhac, R. J. Perkins, and P. Salizzoni. Flow in a street canyon for any external wind direction. *Boundary-Layer Meteorology*, 126(3):365–388, mar 2008. ISSN 00068314. doi: 10.1007/s10546-007-9238-x. URL http://link.springer.com/10.1007/s10546-007-9238-x.

Y. Tominaga and T. Stathopoulos. Ten questions concerning modeling of near-field pollutant dispersion in the built environment. *Building and Environment*, 105:390–402, 2016. ISSN 03601323. doi: 10.1016/j.buildenv.2016.06.027. URL http://dx.doi.org/10.1016/j.buildenv.2016.06.027.

VDI. *Environmental meteorology – Physical modelling of flow and dispersion processes in the atmospheric boundary layer – Application of wind tunnels*. Verein Deutscher Ingenieure, Dusseldorf, Dusseldorf, 2000.

W. W. Willmarth. Structure of turbulence in boundary layers. *Arch Appl Mech*, 15:159–254, 1975.

F. Yang, Y. Gao, K. Zhong, and Y. Kang. Impacts of cross-ventilation on the air quality in street canyons with different building arrangements. *Building and Environment*, 104:1–12, 2016. ISSN 03601323. doi: 10.1016/j.buildenv.2016.04.013. URL `http://dx.doi.org/10.1016/j.buildenv.2016.04.013`.

Part III

OVERVIEW LISTS

List of Figures

List of Tables

List of the Major Symbols and Abbreviations[1]

α	power exponent
B (L, S)	street canyons width
BL	boundary layer
C^*	dimensionless concentration - mean value
$c^{*\prime}$	dimensionless concentration - fluctuation
d_0	displacement height
FS	full scale
φ	wind direction
H	building height
I_u, I_v, I_w	turbulence intensity
ν	kinematic viscosity
L	street canyons length, line source length
L_{ux}	integral length scales of the streamwise velocity component
$\mathrm{MX_{L,\,R}}$	street canyon model number X positioned on the right and left of the streamwise avenue
Δp	pressure drop across the tubes of the line source
Q	flow rate of pollution source
r	correlation coefficient
R_i	relative contribution from i^{th} quadrant to the total momentum / pollution flux
Re	Reynolds number
Re_B	Reynolds building number
Re_{crit}	critical Reynolds number

[1]Symbols and abbreviations may differ across the thesis due to various nomenclature used in each individual publication.

ρ	density
S_i	particular contribution from i^{th} quadrant to the total momentum / pollution flux
S_max	particular contribution from the dominant event to the total momentum / pollution flux
σ	standard error
U, V, W	velocity components - mean values
u', v', w'	velocity components - fluctuations
U_0, U_{ref}	reference free stream velocity
U_{2H}	stream velocity at height $2H$
u_*	friction velocity
x, y, z	coordinates
z_0	roughness length

List of Author's Publications

H. Chaloupecka, Z. Janour, K. Jurcakova, L. Kukacka, and S. Nosek. Sudden releases of gases. *EPJ Web of Conferences*, 67:02045, mar 2014. ISSN 2100-014X. doi: 10.1051/epjconf/20146702045. URL http://www.epj-conferences.org/10.1051/epjconf/20146702045.

R. Kellnerova, L. Kukacka, K. Jurcakova, V. Uruba, and Z. Janour. Comparison of wavelet analysis with velocity derivatives for detection of shear layer and vortices inside a turbulent boundary layer. *Journal of Physics: Conference Series*, 318(6):062012, dec 2011. ISSN 1742-6596. doi: 10.1088/1742-6596/318/6/062012. URL http://stacks.iop.org/1742-6596/318/i=6/a=062012?key=crossref.d03c1e8ba275576ba7e4c50cf3bd64f6.

R. Kellnerova, L. Kukacka, K. Jurcakova, V. Uruba, and Z. Janour. PIV measurement of turbulent flow within a street canyon: Detection of coherent motion. *Journal of Wind Engineering and Industrial Aerodynamics*, 104-106: 302–313, may 2012a. ISSN 01676105. doi: 10.1016/j.jweia.2012.02.017. URL http://linkinghub.elsevier.com/retrieve/pii/S0167610512000414.

R. Kellnerova, L. Kukacka, V. Uruba, K. Jurcakova, and Z. Janour. Detailed analysis of POD method applied on turbulent flow. *EPJ Web of Conferences*, 25:01038, apr 2012b. ISSN 2100-014X. doi: 10.1051/epjconf/20122501038. URL http://www.epj-conferences.org/10.1051/epjconf/20122501038.

R. Kellnerova, L. Kukacka, S. Nosek, V. Uruba, K. Jurcakova, and Z. Janour. Wavelet analysis of the turbulent flow over the very rough surface. *EPJ Web of Conferences*, 67:02051, mar 2014a. ISSN 2100-014X. doi: 10.1051/epjconf/20146702051. URL http://www.epj-conferences.org/articles/epjconf/abs/2014/04/epjconf_efm-13_02051/epjconf_efm-13_02051.html%5Cnhttp://www.epj-conferences.org/10.1051/epjconf/20146702051.

R. Kellnerova, F. Vladimir, L. Kukacka, and Z. Janour. Street Canyon Ventilation of Traffic Pollution : Comparison Between Experiment and LES. (August), 2014b. doi: 10.13140/2.1.1153.8883.

L. Kukacka, R. Kellnerova, K. Jurcakova, and J. Zbynek. Analysis of scalar fluxes and flow within modelled intersection depending on the approach flow direction. In D. G. Steyn and S. T. Castelli, editors, *Proceeding of the 31st NATO/SPS International technical meeting on air pollution modelling and its application Air Pollution Modeling and its Application XXI*, pages 113–118. Springer, Dordrecht, Netherlands, 2011. ISBN 978-94-007-1361-1.

L. Kukacka, S. Nosek, R. Kellnerova, K. Jurcakova, and Z. Janour. Wind Tunnel Measurement of Turbulent and Advective Scalar Fluxes: A Case Study on Intersection Ventilation. *The Scientific World Journal*, 2012:1–13, 2012. ISSN 1537-744X. doi: 10.1100/2012/381357. URL http://www.hindawi.com/journals/tswj/2012/381357/.

L. Kukacka, S. Nosek, R. Kellnerova, K. Jurcakova, and Z. Janour. Quadrant analysis of turbulent pollution flux above the modelled street intersection. *EPJ Web of Conferences*, 45:01053, apr 2013a. ISSN 2100-014X. doi: 10.1051/epjconf/20134501053. URL http://www.epj-conferences.org/articles/epjconf/abs/2013/06/epjconf_efm2013_01053/epjconf_efm2013_01053.htmlhttp://www.epj-conferences.org/10.1051/epjconf/20134501053.

L. Kukacka, S. Nosek, R. Kellnerova, K. Jurcakova, and Z. Janour. Contribution of Advective and Turbulent Contaminant Transport to the Intersection Ventilation. In D. G. Steyn and S. T. Castelli, editors, *NATO Science for Peace and Security Series C: Environmental Security*, volume 137, pages 665–668. Springer, Dordrecht, 2013b. ISBN 9789400755765. doi: 10.1007/978-94-007-5577-2_113. URL http://link.springer.com/10.1007/978-94-007-5577-2_113.

L. Kukacka, V. Fuka, S. Nosek, R. Kellnerova, and Z. Janour. Ventilation of idealised urban area, LES and wind tunnel experiment. *EPJ Web of ...*, 62:1–10, 2014. ISSN 2100-014X. doi: 10.1051/epjconf/20146702062. URL http://www.epj-conferences.org/articles/epjconf/abs/2014/04/epjconf_efm-13_02062/epjconf_efm-13_02062.html.

S. Nosek, Z. Janour, K. Jurcakova, R. Kellnerova, and L. Kukacka. Neutrally stratified flow modelling over complex terrain at meso-scale: open-cut coal mine study. *EPJ Web of Conferences*, 45:01070, apr 2013. ISSN 2100-014X. doi: 10.1051/epjconf/20134501070. URL http://www.epj-conferences.org/10.1051/epjconf/20134501070.

S. Nosek, Z. Janour, L. Kukacka, K. Jurcakova, R. Kellnerova, and E. Gulikova. Atmospheric dispersion modelling over complex terrain at small scale. *EPJ Web of Conferences*, 67:02084, mar 2014a. ISSN 2100-014X. doi: 10.1051/epjconf/20146702084. URL http://www.epj-conferences.org/10.1051/epjconf/20146702084.

S. Nosek, Z. Janour, L. Kukacka, K. Jurcakova, and R. Kellnerova. Atmospheric dispersion modelling over complex terrain at small scale. *EPJ Web of Conferences*, 67:1–6, mar 2014b. ISSN 2100-014X. doi: 10.1051/epjconf/20146702084. URL http://www.epj-conferences.org/articles/epjconf/abs/2014/04/epjconf_efm-13_02084/epjconf_efm-13_02084.htmlhttp://www.epj-conferences.org/10.1051/epjconf/20146702084.

S. Nosek, L. Kukacka, R. Kellnerova, K. Jurcakova, and Z. Janour. Ventilation Processes in a Three-Dimensional Street Canyon. *Boundary-Layer Meteorology*, 159(2):259–284, may 2016. ISSN 15731472. doi: 10.1007/s10546-016-0132-2. URL http://link.springer.com/10.1007/s10546-016-0132-2.

S. Nosek, L. Kukacka, K. Jurcakova, R. Kellnerova, and Z. Janour. Impact of roof height non-uniformity on pollutant transport between a street canyon and intersections. *Environmental Pollution*, 227:125–138, aug 2017. ISSN 02697491. doi: 10.1016/j.envpol.2017.03.073. URL http://linkinghub.elsevier.com/retrieve/pii/S0269749116313380.

S. Nosek, V. Fuka, L. Kukacka, Z. Klukova, and Z. Janour. Street-canyon pollution with respect to urban-array complexity: The role of lateral and mean pollution fluxes. *Building and Environment*, 138:221–234, jun 2018. ISSN 03601323. doi: 10.1016/j.buildenv.2018.04.036. URL http://linkinghub.elsevier.com/retrieve/pii/S0360132318302452.